BIBLIOGRAPHIC INFORMATION

PB94-164605

Report Nos: UCB/EERC-94/02

Title: Energy Dissipation with Slotted Bolted Connections.

Date: Feb 94

Authors: C. E. Grigorian and E. P. Popov.

NTIS Field/Group Codes: 89D (Structural Analyses), 89G (Construction Materials, Components, & Equipment)

Price: PC A11/MF A03

Availability: Available from the National Technical Information Service, Springfield, VA. 22161

Number of Pages: 247p

Keywords: *Energy dissipation, *Bolted joints, *Vibration isolators, *Earthquake resistant structures, Structural analysis, Displacement, Loads(Forces), Earthquake engineering, Test facilities, Friction, Dynamic response, Steel structures, Buildings.

Abstract: Slotted Bolted Connections (SBCs) are modified bolted, butt jointed, shear splice connections. The modification consists primarily of slotting or elongating the holes in one of the plates of the connection. These connections dissipate energy by means of friction between sliding surfaces. Presented in this document are the experimental and analytical results of the testing of individual SBCs and the testing of a large test structure, equipped with twelve SBCs, on the shake table.

:72-101

REPORT DOCUMENTATION PAGE	1. REPORT NO. NSF/ENG-94002	2.	3. Recipie PB94-164605

Title and Subtitle "Energy Dissipation with Slotted Bolted Connections"		5. Report Date February 1994
		6.
Author(s) Carl E. Grigorian and Egor P. Popov		8. Performing Organization Rept. No. UCB/EERC-94/02
Performing Organization Name and Address Earthquake Engineering Research Center University of California, Berkeley 1301 So. 46th Street Richmond, Calif. 94804		10. Project/Task/Work Unit No.
		11. Contract(C) or Grant(G) No. (C) (G) BCS-9016781 and BCS-9222110
12. Sponsoring Organization Name and Address National Science Foundation 1800 G Street, N.W. Washington, D.C. 20550 American Iron & Steel Inst 1101 17th St NW, Ste 1300 Washingtion, DC 20036 American Iust of Steel Construc One East Wacker Dr, Ste 3100 Chicago, IL 60601-2001		13. Type of Report & Period Covered
		14.

15. Supplementary Notes

16. Abstract (Limit: 200 words)

Slotted Bolted Connections (SBCs) are modified bolted, butt jointed, shear splice connections. The modification consists primarily of slotting or elongating the holes in one of the plates of the connection. These connections dissipate energy by means of friction between sliding surfaces. Presented in this document are the experimental and analytical results of the testing of individual SBCs and the testing of a large test structure, equipped with twelve SBCs, on the shake table.

17. Document Analysis   a. Descriptors

b. Identifiers/Open-Ended Terms

c. COSATI Field/Group

18. Availability Statement Release Unlimited	19. Security Class (This Report) unclassified	21. No. of Pages 248
	20. Security Class (This Page) unclassified	22. Price

(See ANSI–Z39.18)   See Instructions on Reverse   OPTIONAL FORM 272 (4–77) (Formerly NTIS–35) Department of Commerce
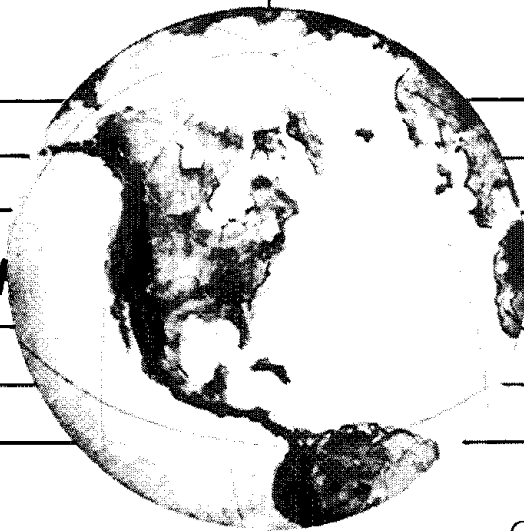
REPORT NO.
UCB/EERC-94/02
FEBRUARY 1994

EARTHQUAKE ENGINEERING RESEARCH CENTER

ENERGY DISSIPATION WITH SLOTTED BOLTED CONNECTIONS

by

CARL E. GRIGORIAN
EGOR P. POPOV

COLLEGE OF ENGINEERING

UNIVERSITY OF CALIFORNIA AT BERKELEY

Energy Dissipation with Slotted Bolted Connections

by

Carl E. Grigorian

and

Egor P. Popov

Report No. UCB/EERC-94/02

Earthquake Engineering Research Center

College of Engineering

University of California at Berkeley

February, 1994

Abstract

Slotted Bolted Connections (SBCs) are modified bolted, butt jointed, shear splice connections. The modification consists primarily of slotting or elongating the holes in one of the plates of the connection. These connections dissipate energy by means of friction between sliding surfaces. Presented in this document are the experimental and analytical results of the testing of individual SBCs and the testing of a large test structure, equipped with twelve SBCs, on the shake table.

The testing of individual SBCs involved, mainly, two types of SBCs. These were SBCs with steel-steel sliding surfaces and SBCs with steel-brass sliding surfaces. It is found that SBCs with steel-steel surfaces exhibit undesirable behavior characteristics. The undesirable behavior characteristics are shown to be eliminated by use of simple brass shim plates.

Results are presented for steel-brass SBCs tested under both sinusoidal and simulated seismic imposed displacements. Data are presented for such steel-brass SBCs with $\frac{1}{2}$ and $\frac{3}{4}$ inch diameter A325 bolts. Effects of using a number of different bolt assemblies including combinations of Belleville and Direct Tension Indicator washers are considered.

An existing frame structure was retrofitted with a system of chevron braces incorporating twelve SBCs. This 96,000 pound structure was tested on the shake table with three different SBC slip force configurations. The structure was subjected to a variety of prerecorded earthquake acceleration histories as well as a number of harmonic acceleration records. The SBCs of the test structure are shown to have performed as predicted by the results of tests of individual SBCs. Experimental results are presented detailing the responses of the test structure to the shake table accelerations and the effects of the SBCs on the behavior of the structure. Finally, it is shown that numerical simulations, with readily available analytical tools, of the structure's response to recorded acceleration histories of the shake table can produce results in excellent correlation with the experimental behavior.

Acknowledgements

Contents

List of Figures

List of Tables

Chapter 1

Introduction

1.1 The Role of Energy Dissipation in Seismic Design

The performance of a structural system in response to severe seismic loading is intimately related to the structural system's ability to dissipate, or shed, its kinetic and strain energies through hysteretic and viscous energy dissipation mechanisms. Conventional seismic design practice permits the use of lateral design forces significantly below levels necessary to maintain the structure in the elastic deformation range. Such reductions are allowed on the premise that inelastic deformations of a well designed structure will provide mechanisms for hysteretic energy dissipation.

The quantification of the energy quantities involved in the response of a structural system to severe seismic loading is accomplished through the absolute energy balance equation [28, 3], given as:

$$E_i = E_k + E_s + E_v + E_h$$

In this equation, E_i is the absolute input energy. This quantity represents the work done by the sum of the inertial forces acting on the structure in resisting the displacements of the ground under the base of the structure. E_k is the absolute kinetic energy.

This value is a measure of the instantaneous kinetic energy of the masses of structural system. This kinetic energy is calculated by using velocities as measured with respect to a fixed reference frame in relation to the ground. E_s is the strain energy. This value is a measure of the instantaneous energy stored elastically in the deformed members of the structure. E_v is the quantity of energy dissipated viscously, and E_h is the quantity of energy dissipated hysteretically. The distinction between hysteretic and viscous dissipation is in that hysteretic dissipation is achieved by elements whose resistance to deformation is entirely dependent on the magnitudes of deformation, while viscous energy dissipation is achieved by elements whose resistance to deformation is entirely dependent on the rate, with respect to time, of deformation. In words, the energy balance equation states that at any instant, the total work done by the ground on the structure is equal to the sum of the instantaneous values of the kinetic and strain energies of the structure and the total energy dissipated by the structure through viscous and hysteretic means.

The quantity E_h has been described as a measure of damage to the system [3, 27, 17]. This notion is based on the fact that in conventional structures, hysteretic energy dissipation is accompanied by accumulated damage. Such damage can be said to occur in two modes: controlled and uncontrolled. Damage occurs in a controlled mode when it occurs in elements which have been specifically designed to dissipate energy while accruing damage. Properly designed beam-column connections, eccentric link beams, column panel zones, double angle connections as well as properly detailed ductile reinforced concrete shear walls and columns and reinforced masonry walls may be said to fall in this category. Damage occurs in these members by yielding and work hardening of steel and crushing of concrete and masonry. Damage may be said to occur in an uncontrolled manner when structural and non-structural elements, not designed with dissipation of energy in mind, suffer damage and incidentally dissipate energy. All non-structural damage, such as damage to wall panels and windows, as well as structural damage to non-seismically designed structural elements, such as unreinforced masonry walls, fall in this category of damage.

The advent of the use of hysteretic energy dissipation mechanisms and devices, capable of dissipating energy without suffering irreversible damage, causes the

notion of using E_h as a damage index to be less acceptable. A modified point of view is to consider E_h to be be the sum of two components, one destructive and one non-destructive. That is, in equation form, $E_h = E_{hd} + E_{hnd}$, where the additional subscript letters d and nd indicate, respectively, the destructive and non-destructive natures of the hysteretic energy dissipation components. From this point of view, the energy balance equation can be rewritten as;

$$E_i = E_k + E_s + E_v + E_{hd} + E_{hnd}.$$

The Source-Sink Analogy

The Source-Sink analogy, due to T.S. Yang [17], is a convenient tool for the presentation of the intuitive concepts behind the energy balance equation. Figure 1.1 shows a graphical display of this analogy. Shown in the figure are a pipe, with a faucet and volume of flow gage, carrying a liquid into a sink with a drain and an overflow tube. Three buckets collect, respectively, the fluid leaving the sink through the overflow tube, through the drain and through spill over the sink. In this analogy, the pipe or the source represents the earthquake, while the fluid represents energy. Volumes of fluid represent quantities of energy. The volume of flow gage indicates the absolute input energy, E_i, input to the system. A faucet, the state of which is a function of the ground motion and the instantaneous properties of the structural system, determines the instantaneous rate of flow of the fluid into the system. The state of the faucet represents the complex dynamic response of the non-linear structure to the seismic excitations. The sink itself represents the reactive masses and the elements of the structure capable of storing strain energy. The overflow tube and the overspill edge of the sink represent the mechanisms, respectively, for non-destructive and destructive hysteretic energy dissipation. The conventional drain at the bottom of the sink represents the mechanisms for viscous energy dissipation. The total volume of fluid in the sink represents the sum of the instantaneous kinetic and strain energies. The main objectives in seismic design of a structure can roughly be equated with either limiting this volume or causing the overspilled volume to be of the controlled type.

Seismic Design Strategies

Several seismic design strategies may be, simplistically, described with the use of the Source-Sink analogy. In conventional seismic structural design, emphasis is placed on increasing the structures' capacity to absorb strain energy and to provide for controlled, albeit generally destructive, means for hysteretic energy dissipation. In the Source-Analogy, this strategy is associated with increasing the size of the sink, and at the same time relying on controlled overspill over the edge of the sink. The strategy of base isolation, in which the structure is separated from its foundation by relatively flexible or low-strength elements, can be described in the analogy by either moving the entire basin of the sink away from the source pipe or by manipulating the faucet to achieve low rates of flow. In conventional analysis of structures, some viscous energy dissipation capacity is always assumed to be inherently present in structural systems. This is generally done to account for unknown mechanisms of energy dissipation in a mathematically feasible manner. This is represented in the analogy by the presence of a conventional drain at the bottom of the sink. However, a number of truly viscous energy dissipation devices are now marketed for structural use. The practice of including such viscous energy dissipation devices in structural systems can be described in the analogy as enlargening the size of the conventional drain pipe. Finally, the strategy most intimately related to the subject of this document, the provision of non-destructive hysteretic energy dissipation mechanisms can be described in the analogy by adding or enlargening the overflow tube.

Of the strategies mentioned above, it is rare that any single one is used exclusively in any design. As an example, most base isolated structures rely on either viscous or hysteretic energy dissipation mechanisms, linked with the isolation systems. The isolated structures themselves are designed as conventional structures with capacity for strain energy absorption and controlled destructive hysteretic energy dissipation.

Structural Systems with Rigid-Perfectly-Plastic Elements

An element is said to be ideally rigid-perfectly-plastic (RPP) if it remains rigid, e.g. does not deform, for applied forces below a certain threshold force and deforms plastically, e.g. deforms continuously without any increase in applied force, for an applied force equal to threshold force. Such ideal RPP element models are often used for numerical modeling of elements exhibiting material yield at a given yield force. The RPP element model is also suited, ideally, for representation of elements in which slip occurs due to an applied force overcoming a friction induced resistance to slip. The RPP model suits both type of systems well as long as the forces necessary to cause slip or yield in the modelled system do not vary significantly with slip or yield distance. An RPP element model, intended for use under cyclic loading, requires two parameters for precise definition. These are a positive and a negative force threshold.

Figure 1.2 shows a mechanical, and a structural, representation of a single-degree-of-freedom (SDOF) system. The two representations describe identically the same SDOF system. In both representations, v_g represents displacements of the ground with respect to some fixed reference frame, and v represents horizontal displacements of the mass, m, with respect to the ground. The upper, mechanical, representation is shown with mass, m, viscous damper with coefficient, c, linear elastic springs of stiffnesses Kc and Kb and an RPP element, in series with the spring of stiffness Kb. The RPP element has equal negative and positive threshold forces of magnitude, F_{slip}. This threshold force magnitude could just as well have been named "F_{yield}," as often is done for similar representations. But, as the subject of this document relates to friction, F_{slip} is the more descriptive notation. The structural SDOF representation is shown below the mechanical representation. This representation can be thought of as that of a single story shear structure. The two linear elastic columns have flexural stiffnesses, with respect to v, of $\frac{Kc}{2}$. A diagonal linear elastic brace of axial stiffness $\frac{Kb}{\cos^2\theta}$, where θ is the angle of the brace with brace with the horizon, is in series with an RPP element. The RPP element has equal negative and positive threshold forces of magnitude $\frac{F_{slip}}{\cos\theta}$. As in the mechanical representation, the

mass has magnitude m. The inherent damping of the structure is represented by a viscous dash-pot of coefficient c. The brace axial stiffness and the RPP element threshold forces of the structural representation are chosen so as to result in force-deformation characteristics, with respect to v, identical to the one of the mechanical representation.

Figure 1.3(a) shows force-deformation curve of the RPP element of the mechanical representation in response to nearly a full cycle (say, sinusoidal) of applied displacements at v with equal negative and positive amplitudes large enough to cause slip in the RPP element. If such a curve were to be drawn for the RPP element of the structural representation, due to the same cycle of applied displacements at v, the rectangular "hysteresis loop" would be larger in height by a factor of $\frac{1}{\cos\theta}$. The loop would be narrower in width by a factor of $\cos\theta$. The relations governing these transformations are based on small angle geometry. It is noted that non-conservative work is performed on the RPP elements in imposing such displacements on them. The non-conservative work done on the elements is converted to heat. The energy input, through work done on them, to the RPP elements may be said to have been dissipated as heat since, even though the heat may be stored in the elements, it does not effect the characteristics of the SDOF systems. Furthermore, the energy has been dissipated hysteretically as the RPP element is a hysteretic element. The quantity of energy dissipated in a full cycle of displacements is equal to the area enclosed by the force-deformation curves of the RPP elements. Clearly, the energy quantities dissipated by the RPP elements of the two representations are identical for identical applied displacements at v. Figure 1.3(b) shows the the force-deformation curve for the two equivalent SDOF systems. Given that the linear elastic springs can only store recoverable elastic energy, it is seen that the area enclosed by the force-deformation curve of the SDOF system is identical to the area enclosed by the force-deformation curves of either of the RPP elements in the two representations.

Quantification of Seismic Hysteretic Energy Dissipation Demands

Most seismic design codes, in specifying seismic design forces, implicitly rely on structural force-deformation behaviors similar to that shown in Figure 1.3(b). To relate Figure 1.3(b) to code design forces, consider a simpler SDOF model in which $Kc = 0$. This model is known as the linearly-elastic-perfectly-plastic (LEPP) SDOF model. The natural period, T of such an SDOF is based on the initial stiffness of the force-deformation curve and is given by $T = 2\pi\sqrt{\frac{m}{Kb}}$. For a typical steel structure, c can be taken to represent 5 % of critical damping. Seismic code design forces can be interpreted as yield or slip force for the simplified SDOF model.

The design base shear ratio (with respect reactive weight), C_w, specified by UBC-1988 [12], has been interpreted [26, 17] as a base shear ratio at yield, C_y, given as:

$$C_y = C_w \Omega Y.$$

In this relation, Y represents the magnification ratio for increasing design forces from an allowable stress level to the first significant yield level. The value of Y for the 1989 AISC ASD Specifications [6], can conservatively be taken as 1.4 [26]. The factor Ω is the overstrength factor. This is the factor by which the system's yield force exceeds the force level at first significant yield. Shake table tests of large steel structures have shown that overstrength factors in excess of 2.0 can be attained [29, 32]. Given the above interpretation, a C_y versus T curve can be calculated based on the UBC-1988 specification of C_w. The parameters governing C_w are chosen as $Z = 0.4$, $I = 1.0$, $S = 1.2$ and $R_w = 8$ (see UBC-1988). Such C_y curves are shown in Figure 1.4. The solid curve in this figure represents the UBC-1988 C_w. The two curves above this curve are C_y curves interpreted from the C_w curve based on Ω values of 1.0 and 2.0.

Given a C_y value, the F_{slip} value of the SDOF system can be determined simply as $F_{slip} = C_y mg$, where g is the gravitational constant. With knowledge of an LEPP system's period, T, mass, m, viscous damping coefficient, c and "yield force" F_{slip}, the total quantity of hysteretic energy, E_h, dissipated due to a given

seismic input can be numerically calculated. T.S. Yang [17] has generated spectra for such E_h values for several recorded acceleration histories. Figure 1.5 shows one such hysteretic energy spectrum in terms of C_y and T given for the Llolleo record of the 1985 Chilean earthquake. The hysteresis energy axis is given in units of fractions of mg^2sec^2. Each point in the C_y-T plain represents a single SDOF system, similar to the simplified SDOF system in discussion. The hysteretic energy dissipation demanded by the Llolleo record from UBC-1988 designed structures, with the specified C_ws can be found by tracing the curves of Figure 1.4 on the C_y-T plain of Figure 1.5 and finding the associated E_h values.

Table 1.1 lists the maxima of such E_h values for the C_y curve, with $\Omega = 2$ and shown in Figure 1.4, due to a number of unamplified and amplified acceleration history records. Table 1.2 describes the origins of the records in Table 1.1. In addition to the maxima of E_h, Table 1.1 also indicates the C_y and T values associated with each E_{max}. Given E_{max} and C_y values, the total cumulative slip or travel distance of the RPP elements of the SDOF models can be calculated. For the mechanical and structural SDOF models, shown in Figure 1.2, these cumulative travel distances are calculated by multiplying the E_{hmax} values by $\frac{1}{C_ymg}$ and $\frac{\cos\theta}{C_ymg}$, respectively. The two values are given respectively in Table 1.1 as δ_h and δ_b, where the subscripts h and b stand for horizontal and brace components, respectively, of total cumulative travel. The δ_b value is calculated by assuming the brace to be at 45 degrees with respect to the horizon. The values tabulated in the extreme right column represent the number of full cycles of slip as calculated by accounting for the number of yield returns (NYR) encountered in the analyses. Two yield returns are accounted for as one cycle of deformation involving yield or slip.

Satisfying the Seismic Hysteretic Energy Demand

Table 1.1, discussed above, presents seismic hysteretic energy dissipation demands on a typical class of code designed structures based on representation of these structures as SDOF systems with LEPP force deformation characteristics. The RPP element in these SDOF systems is entirely responsible for the dissipation of

the hysteretic energy. In the terminology of the earlier discussion of the Source-Sink analogy, energy dissipation by RPP elements can be thought to be accomplished either destructively or non-destructively, assuming that the sustained damage does not deteriorate the capacity of the structural elements represented by the RPP element. The focus of this document is on the development and exposition of a structural element which, indeed, nearly approximates RPP behavior and suffers no structural damage in the course of energy dissipation within the ranges of cumulative travel and cycles of yield, or slip, described in Table 1.1.

1.2 Slotted Bolted Connections

Figure 1.6 (a) shows the schematic diagram of a bolted, butt-jointed, shear splice connection. The splice consists of two outer plates "sandwiching" a third main plate. The plates are clamped together through bolts in standard holes going through all three plates. Standard holes refer, in general practice, to holes of diameter $\frac{1}{16}$-th inch larger than the bolt diameter which they are to accommodate. The splice is shown with the outer plates fixed in place. The dashed curve in Figure 1.6 (b) shows a schematic representation of the axial force-deformation characteristics of such a splice connection. Four stages of load-deformation, encountered in monotonic loading, are identified [13]. Stages 1 and 3 indicate elastic stretch of the plates. Stage 4 designates inelastic behavior of the plates and/or bolts. Stage 4 ends with the rupture of the bolts or plates. This last event is marked with an "X." Of interest to the present discussion is Stage 2. In this stage, the frictional forces, which are due to the clamping forces of the bolts, are overcome by the axial applied force, and the main plate slips relative to the outer plates. The slippage continues until the bolts come into direct bearing against the bolt holes. Further loading causes the deformations seen in Stage 3. Necessarily, the slip distance can not be more than $\frac{1}{8}$-th inch.

Traditionally, the slip forces, F_{slip}, of such connections are calculated by using the laws of Coulomb friction. That is, the slip force is calculated as the product of the normal force per bolt, the number of bolts, the number of surfaces in friction and the friction coefficient for the surfaces in contact. Application of a full cycle of

force of positive and negative amplitudes equal to the slip force of the connection would, under ideal conditions, result in a hysteresis curve as shown by the solid curve in Figure 1.6 (b). It is seen that this curve exhibits LEPP behavior. By ideal conditions, it is meant that the frictional force required to cause sliding remains constant throughout the distances of slip. The elastic portion of this LEPP behavior is due to elastic stretch in the plates. The splice can be thought of as an elastic spring, representing the length of the plates, in series with an RPP element representing the bolted portion of the plates. That is, the bolted segment of the splice is generally stiff enough axially, due to its short length, that in can be considered to be rigid.

The bolted segment of the shear splice, then, ideally has RPP behavior within the displacement range of twice the tolerance of the bolt holes over the diameter of the bolts. Given the need for structural elements with RPP behavior, it is natural to ask whether by elongating the holes of the main plate advantage can be taken of the inherent behavior of such a shear splice to result in a RPP element with displacement ranges suitable for seismic applications. In this document, such shear splices, with elongated or slotted holes in the main plates, are termed Slotted Bolted Connections (SBCs).

Ideal Conditions Versus Real Conditions

For applications in structural engineering, it is of particular interest to investigate the behavior of SBCs of structural steel, bolted with high strength bolts. The discussion above focused on the behavior of SBCs under the assumption of the presence of ideal constant Coulomb frictional forces. However the restrictions of using structural steel, as a frictional material, and high strength bolts, for the provision of normal or clamping forces, create adverse conditions for the maintenance of stable frictional forces during slippage. An SBC with like structural steel frictional surfaces, clamped together with high strength bolts, with the surfaces sliding against each other over a number of cycles and large cumulative travel violates some of the most basic conditions necessary for the existence of stable frictional forces. Namely, basic principles of friction dictate that, for the existence of stable frictional conditions, the

normal forces between the friction surface must be kept as low as possible and that unlike materials of high hardness must be used. High strength bolts are designed, in particular, to provide large clamping forces. Structural steel has rather low surface hardness values and a rather strong affinity for galling against like structural steel surfaces.

Yet, the inherent simplicity of SBCs and the possibly tremendous economic advantage gained by using SBCs for energy dissipation, rather than relying on proprietary and often complex energy dissipation devices, has made the use of SBCs for energy dissipation an irresistible concept.

1.3 Objectives and Scope

It has been the objective of the investigation, the results of which are summarized in this document, to investigate the possibility of the use of the concept of SBCs for energy dissipation purposes. The investigation has been focused on both the development of functional and efficient individual SBC designs and the experimental investigation of the incorporation of SBCs into real structural systems and their effect on the systems.

The scope of the experimental work, geared at development of SBC designs with functional and efficient behavior, has been limited by the types of modifications, of the original SBC concept, considered reasonable. The modifications deemed reasonable have been those involving only readily available materials, and components, and fabrication technique within the capability of conventional steel fabrication shops.

The scope of the experimental and analytical work on the inclusion of SBCs into real structural systems, has been limited to experimental and analytical studies of a single test structure. The investigation has included the retrofit of test structure with a bracing system with SBCs, the testing of the structure on the shake table and the analysis of the results. Further, the analytical investigation has included confirmation of the feasibility, for design purposes, of analytical simulations of the behavior of the test structure with SBCs.

1.4 Literature Review

The investigation conducted at the University of California at Berkeley has been strongly motivated by experimental pilot studies at the San Jose State University (SJSU). The earliest known tests, conducted on SBC type connections, were done at SJSU by Professor W.J. Venuti in 1976 [30]. Further tests were conducted at SJSU in 1984, and again in 1986, by Professor T. Zsutti. The results of the experimental work conducted under the direction of T. Zsutti were presented by T.F. Fitzgerald, et al., in 1989 [9]. This last citation is responsible for the coining of the term Slotted Bolted Connection (SBC), adopted in this investigation. The concepts of using Direct Tension Indicator and Belleville washers (These will be described in the next chapter) are due to the last two citations.

The first publications, coauthored by the author, of samples of the results presented in this document appeared in 1992 [11]. A second publication followed in 1993 [10]. Interestingly, this second publication, which appeared in the proceedings of a conference, was published side by side with an article by R. Tremblay and S. F. Steimer [25] in which results were presented for SBC connections which were similar, albeit different in design, than those presented by the author.

Indirect experimental investigations of frictional connections similar to SBCs have also be conducted by several researchers. Of note are A. Pall, et. al, [14, 15, 16, 1] and K. Roik, et al. [22]. A. Pall, et. al, have presented results for "limited slip" bolted connections, used in large panel construction, and a proprietary frictional device where the normal force is provided by a bolt. K. Roik, et al. have presented results for the testing of a number of structural configurations, using SBC type connections, under pseudo-dynamic testing conditions. The main focus of this last investigation has been the pseudo-dynamic testing method and the complex structural configurations, rather the the central element, the SBC type connections.

Record	E_{hmax}	T	C_y	δ_h	δ_b	$\frac{NYR}{2}$
-	(mg^{2}sec^2)	(sec)	-	(inches)	(inches)	(cycles)
Pacoima Dam	.018	.8	.24	28.51	20.16	5
Taft	.0004	.7	.27	.58	.41	3
El Centro	.0045	.8	.24	7.13	5.04	6
Miyagi-Ken-Oki	.017	.85	.23	28.04	19.83	11
1.5× El Centro	.015	.75	.25	22.76	16.09	6
Corralitos	.009	.7	.27	13.04	9.22	7
4× Taft	.025	.65	.28	34.48	24.38	15
Llolleo	.030	.5	.33	34.74	24.56	35
SCT	.0533	1.8	.14	144.97	102.51	15

Table 1.1: Seismic demand on code-designed SDOF systems.

Record	Earthquake	Date	Components	PGA (Gs)
Pacoima Dam	San Fernando	2/9/71	S16E	1.17
Taft	Kern County	7/21/52	N21E	0.16
El Centro	Imperial Valley	5/18/40	N00E	0.35
Miyagi-Ken-Oki	Tohuku Sendai	6/12/78	N00E	0.26
Corralitos	Loma Prieta	10/17/89	Ch. 1, 90 Degrees	0.63
Llolleo	Chile	3/3/85	N10E	0.67
SCT	Mexico City	9/19/85	N90W	0.17

Table 1.2: Description of records used for tabulation of seismic demands.

Volume of Flow = Ei

Overspill = Destructive Hysteretic Energy Dissipation (Damage)

Overflow Tube = Mechanism for Non-Destructive Hysteretic Energy Dissipation

Volume of Fluid in Sink = Es + Ek

Volume= Ehd

Conventional Drain= Mechanism for Viscous Energy Dissipation

Volume = Ehnd

Volume = Ev
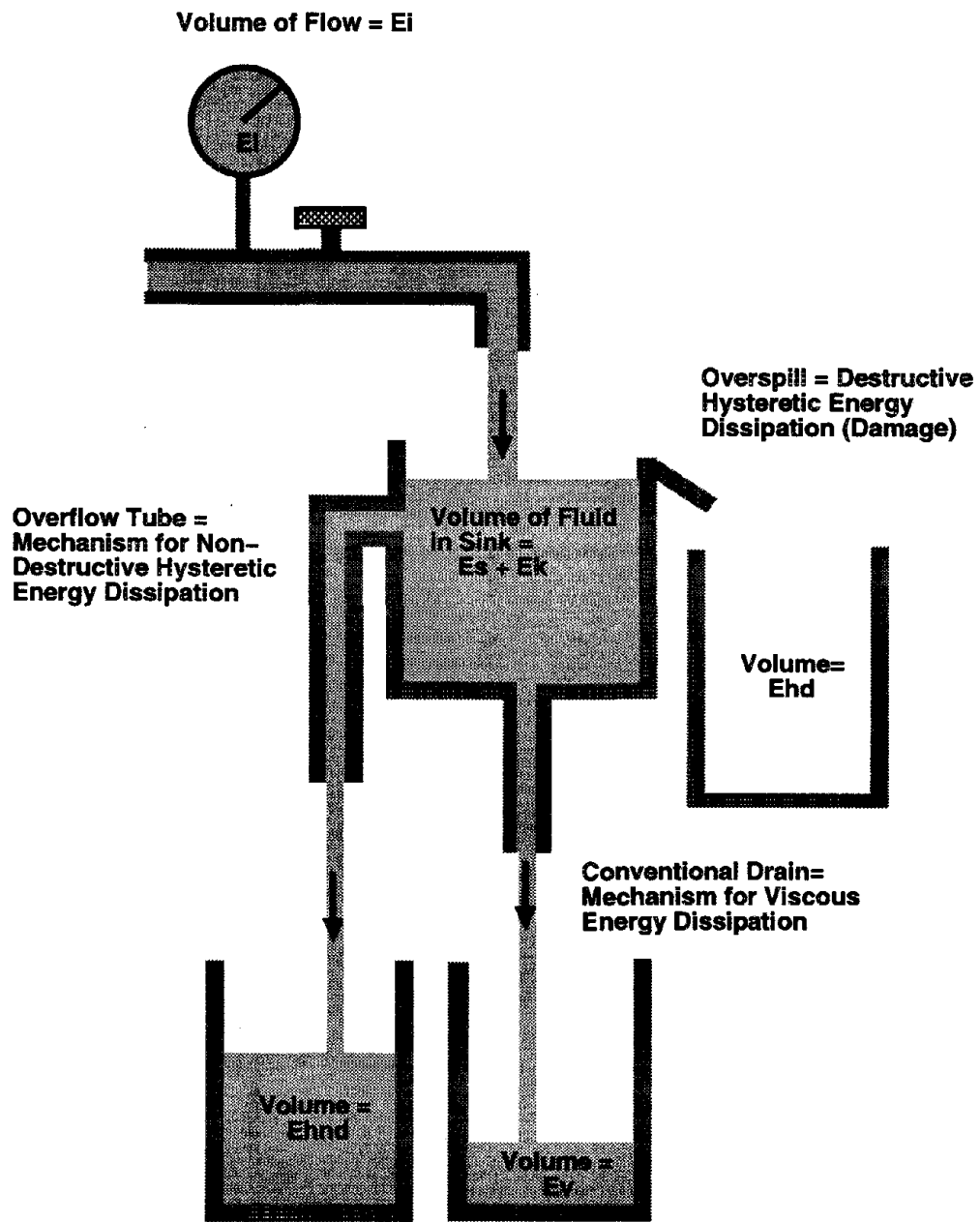
Figure 1.1: The Source-Sink Analogy
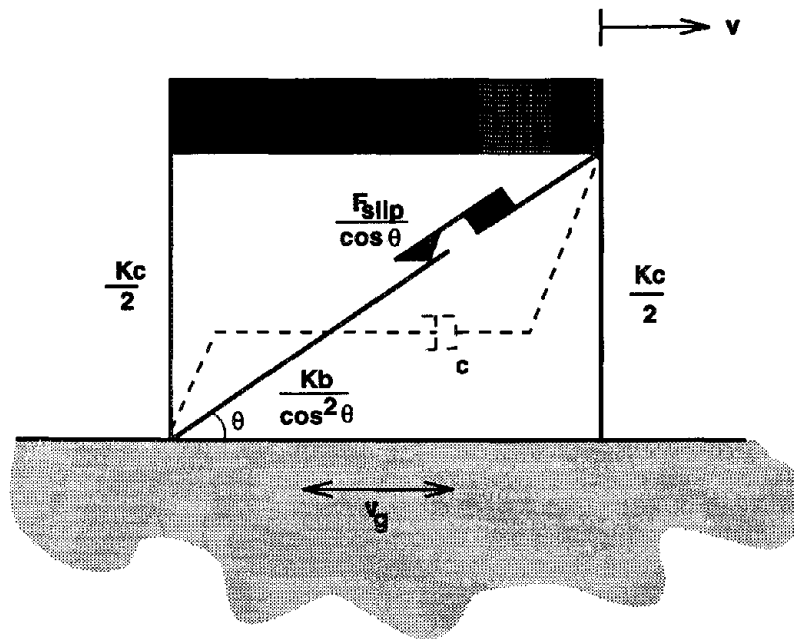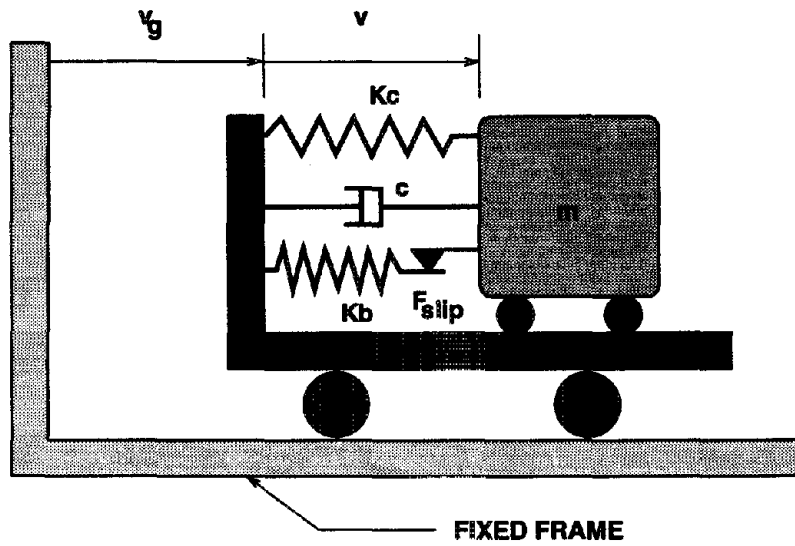
Figure 1.2: Equivalent mechanical and structural SDOF system representations.
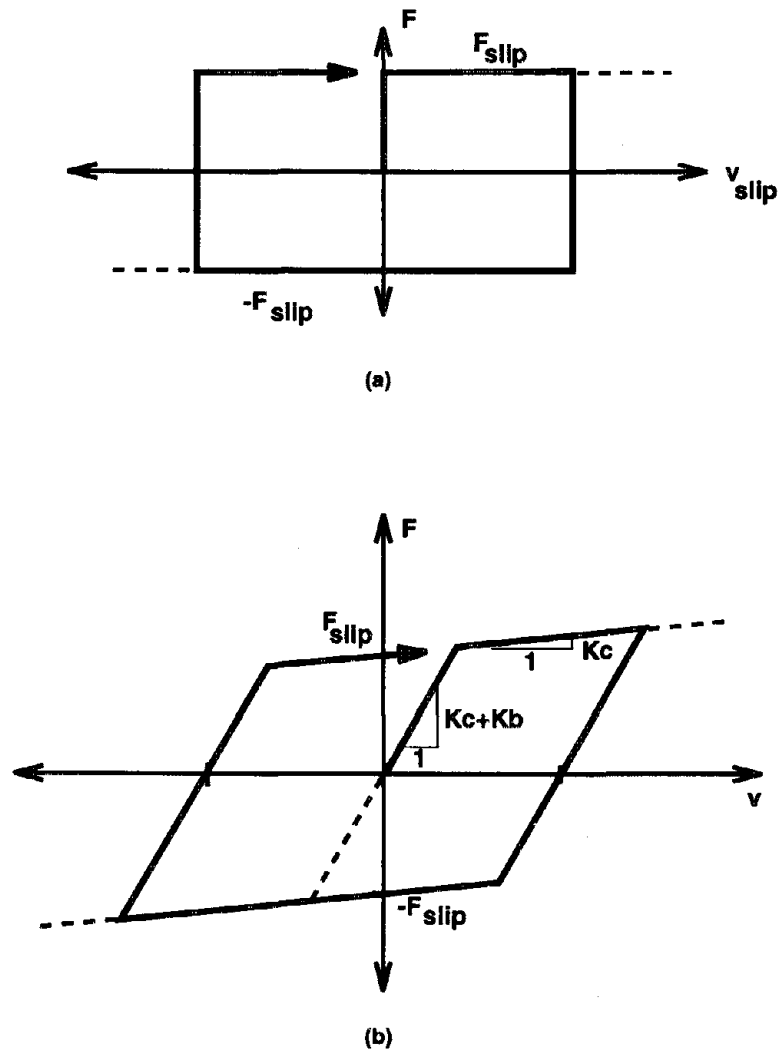
Figure 1.3: Force-deformation curve of rigid-perfectly plastic element and its effect on the-force deformation curve of the SDOF system.

CODE FORCE SPECTRA
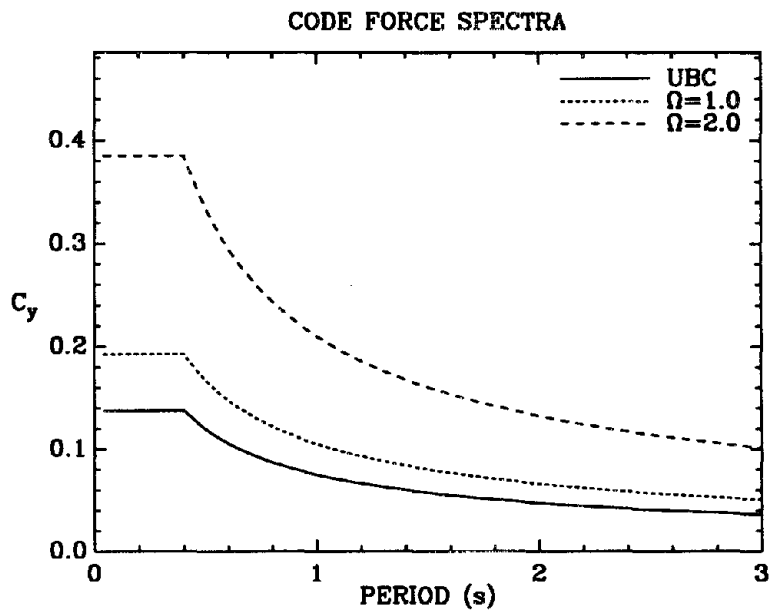
Figure 1.4: Base shear at yield ratios based on UBC specifications.

HYSTERESIS ENERGY (CHILE 1985) (mg^2s^2)
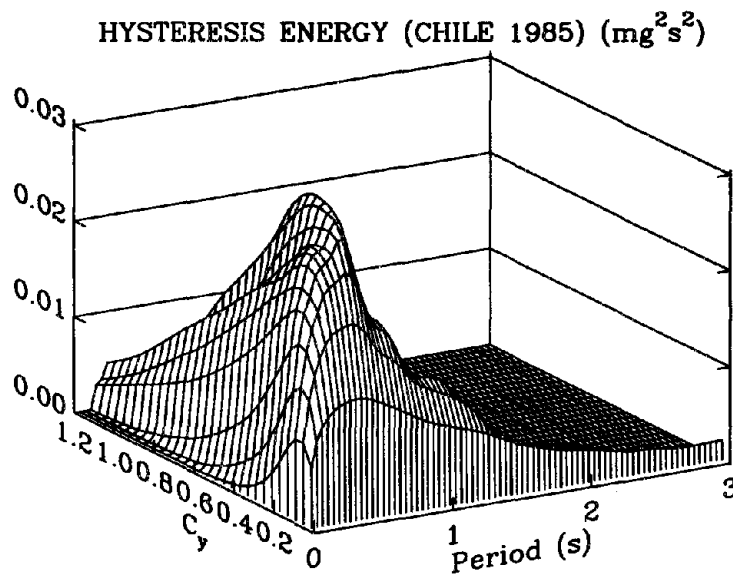
Figure 1.5: Hysteretic energy spectrum for the Llolleo record.

BOLT IN STANDARD HOLE

F, v

MAIN PLATE

OUTER PLATE

(a)

F

Stage 2

X

Stage 4

Stage 3

F_{slip}

Stage 1

v

$-F_{slip}$

(b)
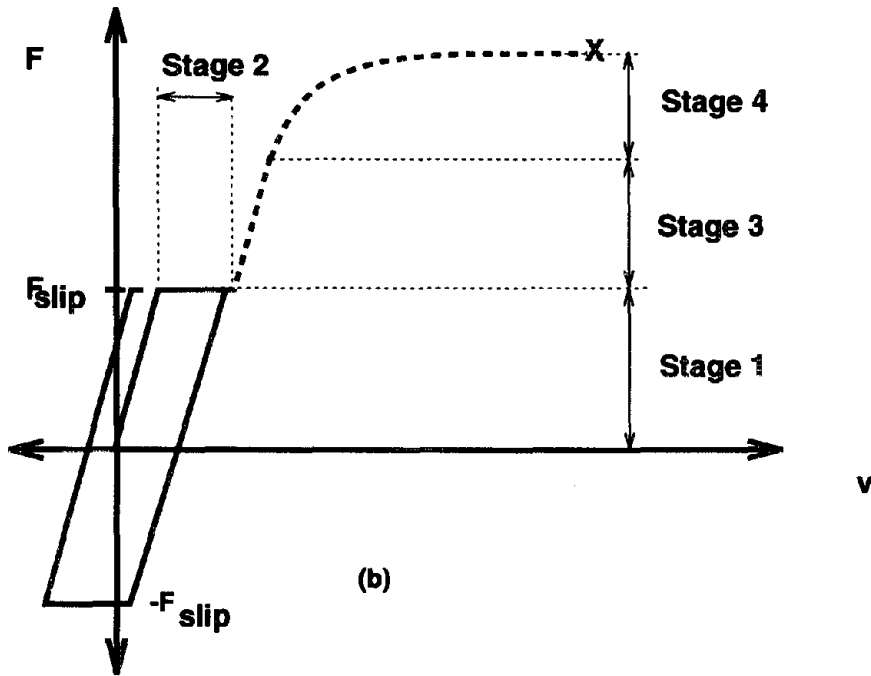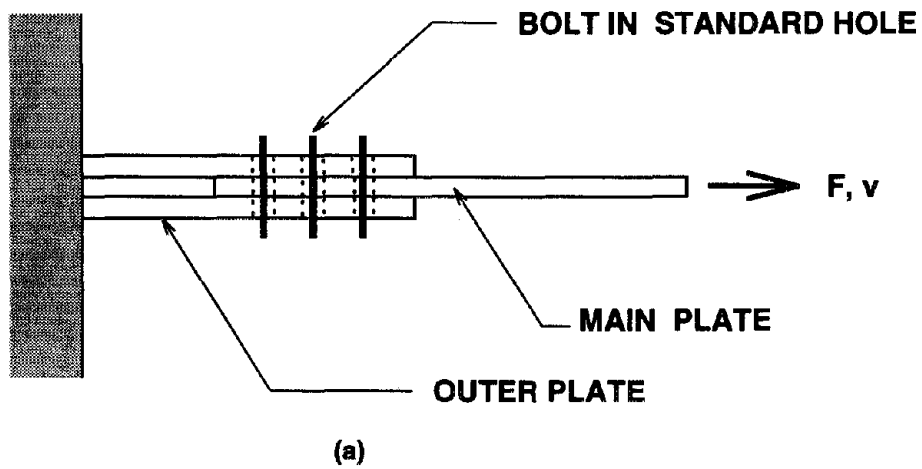
Figure 1.6: Shear-splice with typical force-deformation characteristics.

Chapter 2

SBCs with Steel-Steel Sliding Surfaces

2.1 Purpose

The experimental investigation of the behavior of SBCs conducted at the University of California, Berkeley (UCB), can be said, for clarity of presentation, to consist of four, not necessarily sequentially spaced in time, phases. In the first phase, individual SBCs with like mill scale steel surfaces were tested in an MTS testing frame where they were subjected to imposed sinusoidal displacements. These connections were shown to have undesirable behavior characteristics. It was found that by modifying these connections with the addition of simple brass shim plates the undesirable characteristics could be eliminated. The second phase of the experimental program consisted of testing, in the MTS testing frame, of individual SBCs with steel on brass frictional surfaces by subjecting the connections, as in the case of the first phase, to sinusoidal imposed displacements. In the third phase similar connections to those tested in second phase were tested in the MTS frame by subjecting them to analytically derived simulated seismic imposed displacements. A part of the third phase of experimental work was done in preparation for inclusion of SBCs into a test structure which was tested on UCB's shake table located at the university's Richmond facility which includes the Earthquake Engineering Research Center (EERC). The

fourth phase of the experimental program involve the instrumentation, assembly and testing of the test structure on the shake table. The ordering of the phases described above do not exactly correspond to their ordering in time. The sequencing of the four phases in time was different from the order given in that phase two continued after the completion fourth phase, that is more individual connection were tested in the MTS frame, subjected to sinusoidal imposed displacements, after the completion of the shake table testing of the test structure. However, the ordering of the phases, as given, lends itself to a logical development of the of the presentation of results in this document. The presentation of experimental results in this document follows the order of the numbering of the phases.

The present chapter deals with the above mentioned phase one. Chapters 3 and 4, respectively, describe phases two and three. Phase four is described in Chapters 5 through 7. Chapter 8 deals with analytical simulations of the test structure subjected to acceleration histories used in shake table tests of the test structure. This chapter first describes typical test specimens, the experimental set-up and the nomenclature used in naming the specimens. Then, results for typical SBCs where friction occurs between steel-on-steel surfaces are presented. The deficiencies in the behaviors of these specimens are pointed out, and a solution, in the form of the addition of shim plates, is presented. A drastic improvement in the behavior of the SBCs is shown to occur with this addition. Short background material is provided on the subject of Tribology, the body of knowledge dealing with the study of friction, wear and lubrication. The improved behavior of the SBCs, due to the addition of brass shims, is explained in terms of concepts of tribology.

2.2   Specimens and Experimental Set-Up

A typical one bolt SBC test specimen is shown in Figure 2.1. Two steel plates with standard holes to match $\frac{1}{2}$ inch diameter bolts "sandwich" a plate with a long slotted hole. The three plates are fastened together with a $\frac{1}{2}$ inch diameter A325 bolt with special washers, to be described later, under the bolt head and nut. The term "standard hole" here refers to the standard practice of drilling or punching

holes of diameter $\frac{1}{16}$-th inch larger than the diameter of the bolt which the hole is to accommodate. In this chapter and throughout the text, the two plates with standard holes will be referred to as "outer plates," while the plate with long slot, or slots, will be referred to as the "main plate." All dimensions given in figures describing test specimens are for center to center dimensions. For all specimens described in this document the steel sliding surfaces are in clean mill scale condition. That is, loose debris has been removed from the surfaces with a wire-brush and the surface has been degreased with a generic degreaser.

A typical bolt assembly for such a SBC test specimen is shown in Figure 2.2. In this type of bolt assembly, referred to here as "Method 1," a Direct Tension Indicator (DTI) washer is placed under the head of the bolt, while Belleville spring washers, if any are used, are placed under the nut, separated from the nut with a standard hardened washer. There is also a "Method 2" of bolt assembly which will be discussed in Chapter 3.

Belleville Washers

Belleville washers, also known as conical compression washers or spring washers or disk springs, are truncated-cone shaped disks of spring material. These annular disk springs are ideally suited for applications involving bolts. The springs, hereafter referred to as Belleville washers, can be stacked in parallel or series arrangement to achieve a variety of force deformation characteristics. All washers used in this experimental program were manufactured by the Solon Manufacturing Company, although they are also produced by a number of other manufacturers. All Belleville washers used were of AISI 6150 alloy steel. Only parallel stacking of the washers was used. In such stacking arrangement, the load required to flatten the washers is equal to the load required to flatten a single washer multiplied by the number of washers in the stack. The deformation which the stack can undergo remains roughly equal to the deformation required to flatten single washer.

Figure 2.3 shows experimentally arrived at force-displacement curves for a single and stack of three in parallel 8-EH-112 Solon compression washers as a bolt

compresses them. The manufacturer's specifications for this type of washer indicates a load at the flat position of 6 kips, and a flat position displacement of 0.04 inches. Each of the two curves shown represent loading and unloading of the washers. For each case, the top curve in the upper portion of the loop represents loading up to a peak force and then unloading along a curve below the loading curve. The change of stiffness, seen at roughly 0.045 inches of displacement, in the loading curves corresponds to the washer approaching its flat configuration. The vertical portions of the unloading curves correspond to the friction forces restraining the edges of the outer diameters of the washers from slipping back into their unloaded position. With reduction of the loading of the washer, the friction force is reduced and the washer begins to slip. The unloading curves for the washers are below the loading curves due to the differences in the friction mechanisms between the case of loading and the case of unloading. When loading, the sharp circular rim of the washer is, in effect, pushed into the bearing material. While unloading, the rim is dragged over the bearing material. The differences in the two mechanism produce the hysteretic behavior seen. For the case of the three washers in parallel, part of the area within the the force-displacement curve also represents the energy dissipated in friction between the washers as they slide against each other. Indeed this hysteretic behavior of stacks of Belleville washers is taken advantage of in mechanical engineering applications to create damping mechanisms. Further information on force-deformation characteristics of Belleville washers can be found in [5].

It is seen from the figure that the curve for the single washer indeed comes very close to the manufacturer's claimed behavior. The curve for the three washers in parallel appears to indicate somewhat more flexible behavior than what theory would suggest if the springs were considered to be in ideal parallel configuration. This extra flexibility is probably due to the fact that the washer holes are somewhat larger than diameter of the bolts that go through them, and therefore there is some room for slippage of the washers over each other.

DTI Washers

DTI washers (ASTM designation F959) are special washers with projections arranged circumferentially on one flat face. When the surface of a bolt head or standard hardened washer bears down on these projections, the projections are deformed. These deformations decrease the gap between the bolt head or standard hardened washer surface and the base of the projections on the DTI washer. The gaps can be measured with a feeler gage. When the average widths of the gaps are below a specified value, set by the manufacturer, the desired preload in the bolt is indicated to have been reached. Of the three methods of use suggested by the manufacturer, two were used in this study. These were "Method 1" and "Method 2." In this document, the entire assembly of bolt, nut, Belleville washer, standard hardened washer and DTI washer is referred to as "Method 1" or "Method 2" type assembly depending on whether the DTI was installed according to "Method 1" or "Method 2" of the manufacturer. The Manufacturer's "Method 1" and "Method 2" require that the gaps between the bolt head or standard hardened washer surface and the base of the projections on the DTI washer be less than or equal to, respectively, .015 or .005 inches. Two sizes of DTI washers were used in this study; one for each of $\frac{1}{2}$ inch and $\frac{3}{4}$ inch diameter A325 bolts. For these bolts the Research Council on Structural Connections (RCSC) specifies bolt preloads of, respectively 12 and 28 kips [13]. The DTIs used are designed to indicate bolt loads in the range of 12 to 14 and 28 to 34 kips respectively.

The MTS Testing Frame

All testing of individual SBC connections was carried out on an MTS testing frame. The MTS frame, hereafter referred to as the Compression/Tension (C/T) machine, is built around an MTS series 252 servoram. The servoram is supplied with oil at 2700 psi through a 60 gpm valve. A 120 hp electric pump, in conjunction with accumulators, supply the pressure and flow. With this arrangement the C/T machine can produce, statically, forces of up to 300 kips. The C/T machine can also be operated dynamically with maximum applied forces of up to 250 kips. The velocity of

the applied displacements are limited to 1 to 1.5 inches per second. Displacements of up to $+/-$ 3 inches can be applied by the C/T machine. The control system allows for both displacement and force control. Given a displacement history within the velocity and displacement limitations of the C/T machine, the control system can reproduce the displacement history on the C/T machine. A Linear Variable Displacement Transducer and a load cell are built into the C/T machine. The instruments report analog signals indicating the displacement undergone by the servoram and the force it transmits through a test specimen. A PC based data acquisition system was used for the recording of these data during testing.

The machine was originally used for compression tests of concrete. In order to be able to test specimens, such as SBC specimens, cyclically, a set of special clevices was designed to fit the MTS machine. The clevices were designed to withstand tensile forces of up to 300 kips. The clevices can grab plates up to two inches thickness. For large SBC specimens, such as will be discussed in the next two chapters, the specimens fitted directly into the clevices. The clevice to specimen attachment was accomplished through a set of $\frac{3}{4}$ inch diameter A325 bolts. For the testing of smaller lap joint type SBCs, such as the one shown in Figure 2.1, a set of adaptor plates were designed which were fitted into the clevices and to which the SBC specimens were bolted. The upper plate in Figure 2.4 shows an SBC specimen of the type shown in Figure 2.1 bolted to the said adaptor plates which are, in turn, secured to the upper and lower set of clevices. The instrumentation shown on the SBC bolt, the close up of which is shown in the lower plate of Figure 2.4, is for measuring the deflections of the stack of Belleville washers. The use of this measurement will be discussed in the coming sections.

Sinusoidal Imposed Displacements

Figure 2.5 shows a typical history of the displacements imposed on SBC specimens tested with sinusoidal displacements. All specimen test results presented in this and the next chapter, unless indicated, correspond to, essentially, the imposed displacement history shown in Figure 2.5. The amplitudes of the displacements were

chosen based on what may be realistically expected to occur in the brace of a structure. The frequencies of the sine waves of displacement were based on the velocity limitations of the C/T machine. As seen in Figure 2.5, the signal is composed of seven segments of ten sinusoidal cycles each. The frequencies of the segments are, in order from first to last, 1.0, 0.67, 0.5, 0.25, 0.5. 0.67 and 1.0 Hertz. The amplitudes of the seventh segments are, roughly, 0.4, 0.7, 1.1, 1.6, 1.1, 0.7 and 0.4 inches.

Figure 2.6 shows the cumulative travel history due to the cyclic imposed displacements shown in Figure 2.5. It will be recalled from Chapter 1 that even under severe earthquakes, a code designed structure, the lateral force resisting system of which consists entirely of SBC type systems, will experience cumulative travel in typical braces of no more than 25 inches. It is seen then that the sinusoidal imposed displacement history used in the testing of the SBCs results in a cumulative travel distance of nearly 10 times the magnitude expected in a sever earthquake.

2.3   Experimental Results

Figure 2.7 shows typical test results for three specimens similar to that shown in Figures 2.1 and 2.4. Plots on the left in the figure are force histories experienced by the specimens in response to imposed displacement histories similar to that shown in Figure 2.5. Plots on right show curves of the force responses versus the imposed displacement history for the given specimen. These curves are also known as hysteresis curves. Specimen designations such as 1B2W3 indicate the number and type of bolts, the number of Belleville washers and the order of the testing of identical specimens. The first integer value in the designation indicates the number of bolts in the connection. The letters "B" and "A", to be encountered in the next chapter, indicate respectively that $\frac{1}{2}$ and $\frac{3}{4}$ inch diameter A325 bolts were used in the SBC. The integer between this letter and the letter "W" indicates the number of Belleville washers in the bolt assembly. The last integer in the designation indicates the sequence of the specimen where a number of identical specimens are tested. As will be seen later, a "BR" between the "W" and the last integer in the designation indicates that friction was between brass and steel surfaces. Where this "BR" is

lacking, friction occurs between like clean mill scale surfaces. Given this designation scheme, it is seen that the results in Figure 2.7 are for SBCs with one $\frac{1}{2}$ inch diameter A325 bolt each and that friction in the specimens occurs between steel surfaces. Also gathered is that the specimen at the top of the figure has no Belleville washer, the one in the middle has one and that the one at the bottom has two.

General Remarks

Certain features are common to all SBCs tested, regardless of whether friction is between steel and steel or steel and brass. These can be described in terms of three general notions in the study of frictional systems. These are the concepts of static frictional force, kinetic frictional force and velocity dependence of the kinetic frictional force. The static frictional force is, perhaps, the more familiar concept in structural engineering. Static frictional force is the force necessary to overcome frictional forces keeping a system at rest. For friction between structural steel clean mill scale surfaces this force is defined in terms an average static slip coefficient of 0.33 [13] with standard deviation of 0.07. Given this, the nominal static slip force for the SBCs shown in Figure 2.7 is calculated to be $12 \times 0.33 \times 2 = 7.92$ kips, where the values 12.0 reflects the nominal normal force on the surfaces provided by the $\frac{1}{2}$ inch diameter A325 bolt. It is seen that near time 0.0 for specimen 1B0W the value on the force axis is indeed very close to the above calculated value. It should be emphasized here that the referenced static slip coefficient is for unworn or "virgin" surfaces. Any sliding of the surfaces, such as occurs in SBCs, may, and indeed more often than not does, alter the static slip force.

The kinetic frictional force is the force necessary to keep a frictional system in sliding. Often, mechanical engineering reference books tabulate, side by side, friction coefficients labeled as "static" and "kinetic." This may be interpreted to imply that kinetic friction may be treated analogous to the treatment of static friction. That is, to obtain a kinetic slip force one simply multiplies the tabulated kinetic slip coefficient by the normal force on the surfaces. This would be a gross oversimplification. It has been shown that the kinetic frictional coefficient is a function of the velocity

of the relative movement of the frictional surfaces [18]. The general is that the kinetic frictional force decreases with increasing velocity. In addition, whereas that treatment of the static slip coefficient as a constant value is applicable to structural engineering in the design of "slip critical" joints, it has been shown that the static friction coefficient is a function of the time of contact [18], that is the time for which the system has had zero velocity or is at "stick." The general trend here is for the static slip coefficient to increase with time of "stick." However, such variations are only significant at short time of static contact of below approximately 0.1 seconds. Restricting attention to the individual hysteresis loops of, for example, specimen 1B2W3, it will be noticed that force values near the horizontal portions of the loops are somewhat larger than the force values near the centers of the vertical portions of the loops. The loops exhibit behavior consistent with the concepts mentioned above. In the application of sinusoidal type displacements, the imposed velocities are greatest near the points of zero crossing of the displacements and the least near the maximum amplitude of the displacements. Therefore, as expected, the kinetic slip force is the least near the zero crossings of the displacements and increases as the maximum displacement amplitude is reached. In addition, the imposed velocities go to zero at peak displacement amplitudes. Although in theory this happens instantaneously, in practice there is a non-zero time period at which the system is at zero velocity or "stick." Such stick periods, are the longest for the middle segment of the applied sinusoidal displacements, where displacements are applied at frequency of 0.25 Hertz and amplitude of 1.6 inches. Given the explanation regarding the time dependence of the static slip force, it would be expected that this phenomenon would reveal itself more strongly in this segment. Examination of the force history plot for specimen 1B2W3, in roughly the time window between 50 and 90 seconds, shows force spikes near the points of force zero crossings, concurrent in time with peak displacements, that are, indeed, larger than those of the other six segments. The large force spikes apparent in the left lower corners of the hysteresis curves of specimens 1B0W and 1B1W are not due to the phenomenon discussed. These are due to the bolt coming close to the deformed edges of the punched 4 inch long slots. In a real structural brace, a slight flexure of the brace would realign the bolt in the slot, however the

C/T machine allows no lateral flex causing the bolt to bear against the deformed walls of the slots resulting in the force spike.

The mean kinetic slip force for the specimens shown in Figure 2.7 is seen to go through a sharp initial increase, followed by a quick drop and reaching a somewhat stable plateau toward the end of the record of the imposed displacements. This behavior is a typical shortcoming of the steel on steel SBCs tested. Although such behavior has not been observed for all steel on steel SBCs tested, it is has been present in most. The hysteresis plots for the specimens shown in Figure 2.7 have been described by some as "beautiful," however despite the aesthetic nature of the curves, they represent the typical deficiencies of steel on steel SBCs. Such large variations in the slip forces of the SBCs make the job of modeling of such connections rather difficult. Elements connected through such SBCs would need to be designed for the peak slip forces experienced by the connection, whereas most energy dissipation occurs at slip forces of roughly half the magnitude of the peak slip force. This would lead to inefficient and inefficient designs. Although data for this are not presented in this document, it has been observed that, for steel on steel SBCs, larger peak forces and steeper declines in time of the slip forces occur for specimens with the least surface impurities, i.e., the cleaner a specimen is, the worse the behavior. By "cleaner" it is meant here that the surfaces showed the least evidence of corrosion, scaling or contamination with foreign substances. Given, that contamination and corrosion can not realistically be specified by designers, this alone precludes successful designs with SBCs where sliding occurs between like steel surfaces. The worst behavior of steel on steel SBCs has been observed for specimens where friction occurred between sand-blasted surfaces.

Effect of Belleville Washers

Comparison of the test results for the three specimens shown in Figure 2.7 and the top pair of plots shown in Figure 2.8 demonstrates the effect of the use of Belleville washers on the response of the SBC specimens to the applied displacements. The comparison of the results of the four specimens, one without Belleville and three

with each having one, two and three Bellevilles, respectively, indicates that use of more than one 8-EH-112 washer does not effectively improve the ability of the SBCs to maintain a high constant slip force for the steel on steel SBCs. There is little difference in the behavior, for example, of specimens 1B2W3 in Figure 2.7 and 1B3W1 in Figure 2.8. However, it is seen that by going from using no Bellevilles in specimen 1B0W in Figure 2.7 to using one 8-EH-112 washer in specimen 1B1W, shown in the same figure, the slip forces are roughly doubled after the initial approximately ten seconds of the record. This behavior occurs in spite of the fact that a single 8-EH-112 washer flattens under 6 kips of force, whereas the nominal preload in the bolt is twice that value. Then, it can be concluded that a decrease in the tensile bolt force of magnitude large enough to cause the Belleville to have an effect must occur. This would mean that in steel on steel SBCs with no Belleville washers roughly half the bolt tensile force may be lost. Otherwise, the single washer would have remained fully flat, acting almost as a simple flat washer, and would not effect the behavior of the connection. The Belleville washers were first used in the experimental work at the San Jose State University (SJSU) [30, 9]. This was done to mitigate the observed loosening of the bolts after several cycles imposed displacements. It is seen from examination of the results here that the use of the washers has partial success in moderating the slip force, and this may be, perhaps, due to the effect of the washers in retaining of the tension in the bolts.

Lateral Movement of Outer Plates

In this section it will be shown that simultaneous with increase and then drop of the slip force of a SBC specimen the outer plates of the SBC first move laterally outward, in direction parallel to the axis of the bolt, and then move back inward. The instrumentation shown in Figures 2.4, was used to indirectly measure this effect. The small platform to which two LVDTs were attached was placed between the Belleville washer stack and the nut. The washer stack deformations could be measured by taking taking the average displacement readings reported by the two LVDTs. Figure 2.9 shows such readings as the bolt was tightened for specimen

1B3W1, the results for which were given in Figure 2.8. The non-horizontal portions of this curve corresponds to the turning of the nut by the author. The horizontal portions represent periods of respite. It is seen that the longest rest time was approximately 20 seconds. The last reading indicates that the compression of the three, in parallel, 8-EH-112 washers is about 0.032 inches with the bolt tightened according to the DTI. Reexamination of Figure 2.3 indicates that under this deformation, the washer stack must be experiencing nearly 12 kips, if the curve for the three washers in parallel is to be trusted and just over 12 kips, if an extrapolation from the curve of the single washer is used. Given that the washer stack is in series with the bolt, these values correspond identically to the tension in the bolt. This verifies the performance of the DTI for the case of this specimen. Figure 2.10 shows the deformations of the washer stack during the time of the testing of the specimen. Interestingly, it is seen that this curve roughly matches the profile of the force response history curve of the specimen shown in the top left plot of Figure 2.8. It is seen that simultaneous with increase of the slip force the washer stack is further compressed, and that with the drop of the slip force the washer stack is decompressed. Indeed, at the end of the record the washer stack is less compressed than it was originally. This curve then indicates that the bolt tension, and therefore the normal force between the frictional surfaces, initially increases and then drops. Given that the 12 kip bolt preload of a $\frac{1}{2}$ inch diameter A325 bolt is rather near the 13.5 kip initial tensile yield force of the bolt, it is likely that the bolt undergoes some permanent stretch. In addition, the increase in the force may have further deformed, again permanently, the protrusions on the DTI. It is noted that for the washer stack to be further compressed from their initial position, the outer plates of the SBC must have necessarily moved outward and away from each other, prying on the bolt head and nut by pressing against the DTI under the head and the washer stack under the nut. Further, in order for the decompression of the washer stack to have occurred the plates must have moved back inward. If the plates were to have moved back into their original positions, permanent deformation of the DTI protrusions and the possible permanent stretch of the bolt would indeed contribute to a loss of the original compression of the washer stack. However, the primary behavior of interest is that which causes the plates to push out and then fall

back inward. If the phenomenon causing this effect can be mitigated, then reasonably constant normal forces could be achieved leading to reasonably constant slip forces, given a not too wildly varying kinetic slip coefficient. A hypothesis attempting to explain the behavior observed and explaining the mechanism of the mitigation of this phenomenon is presented further ahead in this chapter.

Effect of Increasing Number of Bolts

It is shown in this section that doubling the number of bolts in an SBC doubles the amplitude of the force response of the connection. This notion appears intuitively obvious, yet some care needs to be taken in the design of such connections. In tests of multi-bolt SBC connections in this study, it has been found that bolt spacings of four bolt diameters produces successful replication of single bolt type behavior with force amplitudes increased by a factor equal to the number of bolts. This spacing has been used both in spacing bolts along shared slots and in the spacing of individual slots. Figure 2.11 shows a two bolt version of the one bolt specimen shown in Figure 2.1. Force response and hysteresis curves for such a specimen are shown in the middle two plots of Figure 2.8. The force axis for this specimen, i.e. specimen 2B1W1, is scaled to show twice the forces values as that for specimen 1B3W1 shown in plots above it. The force response and hysteresis curves for the two specimens appear very similar in size and behavior despite the doubling of the force scale for the two bolt specimen. This indicates that the force response values for the two bolt specimen are nearly double that of the one bolt specimen.

Effect of Addition of Brass Shims

As mentioned already, the rapid increase and drop in the slip force of the steel on steel SBC was considered an undesirable behavior. Indeed, this behavior was cause for much consternation. However, the problem of reducing this variation in the slip force was solved by the addition of two brass shims to the SBC assembly. The logic behind this solution will be discussed in the next section. Figure 2.12 shows the details of an SBC modified with this solution. The two simple brass shims, made of

the most widely available type of brass; the half-hard cartridge brass (UNS-260), with standard size holes are simply placed between the main and the outer plates, causing the significant portion of sliding to occur between the faces of the main plate and the faces of the brass shims. Very minor slips also occur between the outer plates and the brass shims. However these are very small, on the order of the bolt hole tolerance or oversize, that is about $\frac{1}{16}$-th of an inch.

Results for such a SBC specimen, the details of which were shown in Figure 2.12, are shown in the bottom two plots of Figure 2.8. Test specimen 2B1WBR1, the results for which are given in the two plots, is different from specimen 2B1W1, the results for which are presented directly above the two plots for 2B1WBR1, only in the presence of the two brass shim plates in. Comparison of the four plots indicates a dramatic change in behavior brought about by the addition of the brass shim plates. Except for the force spikes present for the large amplitude cyclic displacements, the fourth of the seven displacement segments, the force response history indicates that far smaller force fluctuations occur in steel-brass specimen than do in the steel-steel specimen. The behavior in the initial stages of slipping, between 0 and 30 seconds, in the force response history curve for 2B1WBR1 is characterized by gradual increase in the slip force followed by a relatively flat force plateau. It is also noticed that the upper left and lower right corners of some of the hysteresis loops appear somewhat distorted or "chewed off." These "chewed of" corners are due to the small slips, mentioned above occurring between the shims and the outer plates of the connections. This characteristic feature will be seen to repeat itself in practically all tests of steel-brass SBC connections.

It is of interest to examine the force responses of the two specimens, steel-steel and steel-brass, as a function of the cumulative imposed travel distance in the ranges of realistic seismically induced travels. Figures 2.13 and 2.14 show absolute values of the force responses of specimens 2B1W1 and 2B1WBR1, respectively, versus their respective cumulative travel distances. Typical imposed cumulative travel distances for the imposed displacements were shown in Figure 2.6. The force quantities are shown in the 0 to 50 inch cumulative travel distance. 50 inches is on the order of twice the demanded cumulative travel distance for a typical code designed steel

structure in response to a severe earthquake.

Given that the values plotted against the cumulative travel distances are the absolute values of the connection forces which necessarily go through zero during every reversal of sliding direction, it is understood that for every reversal of sliding direction the absolute value of the force must necessarily decrease to zero and return to the slip force again. As this zero force in the connection is experienced relatively instantaneously, the data acquisition system practically never registers actual zero values. This explains why the force curves do not quite touch the zero force values.

It is seen, from the comparison of the two figures, that the steel-brass specimen has a smaller static slip force than the steel-steel connection, and that the mean slip force for this connection reaches a plateau at roughly 10 inches of cumulative travel. Further it is seen that variations between static and kinetic slip forces encountered upon every reversal of slip direction are much smaller than that for the steel-steel SBC. The behavior exhibited by this specimen is rather remarkable given the simplicity of the connection and the large forces involved. The behavior of steel-brass SBC connections is further explored in the next chapter. However, before proceeding to the next chapter, it will be attempted to account for the change observed in the behavior of steel-steel specimens by the addition of the brass shim plates. A hypothesis will be presented in terms of tribological concepts.

2.4   On Tribology

A discussion involving experimental results involving frictional phenomenon must necessarily involve concepts of tribology. Tribology is the broad and interdisciplinary body of science dealing specifically with the phenomena of friction, wear and lubrication. It is not intended here to discuss at depth any tribological phenomenon associated with the presented test results of SBCs, but rather to present basic tribological concepts which, it is felt, will bring about insight into the possible mechanisms involved in the function of the SBCs. First, it is necessary to define the necessary tribological terminology to be used in the discussion. Terminology is a matter of strong controversy in this field [7], with as many as seven definitions for the same tri-

bological terms appearing in the ASTM Compilations of Standard Definitions. The terminology adopted in the discussion here is adopted from the works of Rabinowicz [18, 19] and Blau [7]. Within the scope of the discussion here, the definitions of the two sources are consistent with each other. Seven definition, four from Rabinowicz and three from Blau follow:

Friction - "The resistance to motion which exists when a solid object is moved tangentially with respect to the surface of another which it touches, or when an attempt is made to produce such motion [18]."

Wear - "Removal of materials from solid surfaces as a result of mechanical action [18]."

Adhesive wear - "Form of wear which occurs when two smooth bodies are slid over each other, and fragments are pulled off one surface to adhere to the other. Later, these fragments may come off the surface on which they are formed and be transferred back to the original surface, or else form loose wear particles [18]."

Abrasive wear - "Form of wear which occurs when a rough hard surface, or a soft surface containing hard particles, slides on a softer surface, and ploughs a series of grooves in it. The material displaced from the grooves is displaced in the form of wear particles, generally loose ones [18]."

Steady state - "Condition of a given tribosytem [tribological system] wherein the average kinetic friction coefficient, wear rate, and/or other specified parameters have reached and maintained a relatively constant level [7]."

Break-in - "Those processes which occur prior to steady state when two or more solid surfaces are brought together under load and moved relative to another. This process is usually accompanied by changes in macroscopic friction force and/or rates of wear [7]."

Break-in curve - "A graphical representation of the initial changes in friction force or friction coefficient with respect to time, number of cycles of counterface passage, or cumulative distance of tribological contact. It may reflect the complete transition to the initial steady state, or a specified portion of that period [7]."

Given that falling out of debris was observed during tests of SBCs, it is clear that wear does occur. The volume of loose debris was by far more for the steel-steel SBCs. Small volumes of debris, in the form of fine brass particles, was observed for the steel-brass SBCs. Given that the prior to the tests, the unworn surfaces were smooth and flat, it is reasonable to believe that the initial wear mechanism is characterized by adhesive wear. The examination of worn plates, removed from disassembled specimens after testing, reveals grooves in the worn surfaces characteristic of abrasive wear. For the case of steel-steel SBCs, both steel surfaces could be described as severely scratched or grooved. For the case of the steel brass SBCs, only the brass surfaces appeared scratched, while the steel surfaces appeared unworn but with smears of brass. It is hypothesized that both types of wear, adhesive and abrasive, are present in the SBCs while sliding occurs. Possibly, the initial adhesive wear gives rise to work hardened wear particles which then act as abrasive particles giving rise to a mechanism of combined adhesive and abrasive wear. Initially, the volume of the wear particles generated causes the outer plates of the SBCs to push outward prying on the bolt and causing a larger tension force in the bolt and, therefore, a larger normal compressive force between the frictional surfaces. This rise in the normal force causes the initial increase in the slip force. Thus far, this hypothesis explains the observed outward movement of the outer plates of the SBCs concurrent with increase of the slip forces.

It is thought that after this initial stage, the wear particles are either reabsorbed onto the original surface, remain adhered to the opposing surface or fall out as loose debris. The fall out and reabsorbtion of the particles has the effect of allowing the outer plates to move inward and lessen the prying force on the bolt, reducing the normal force, and therefore causing a drop in the slip forces. This explanation is thought to account for both steel-steel and steel-brass SBC behaviors. The difference

between the behaviors of the two types of SBCs lies in the volume of wear particles generated. For the steel-steel SBCs, a large volume of loose particles is generated, causing the slip force of the connection to increase rapidly. The fall out of this debris then results in the drop in the slip force. For the SBCs with steel-brass surfaces, the wear volumes generated are small. This together with the tendency of these particles to adhere and smear over the steel surfaces, rather than fall out, causes much smaller variations in the slip forces.

As a general rule, severity of wear is directly proportional to normal force and distance of travel, and inversely proportional to the hardness of the surfaces. And, as a general rule of thumb, sliding of identical materials against each other produces more severe wear than the sliding of very different materials. The most basic relation for the estimation of wear volume in a frictional system is the Holm equation [19]. This equation states that volume of wear, V, due to adhesive wear is given by $V = \frac{KNd_{travel}}{H}$, where K is the "coefficient of wear," N is the normal force in the connection, d_{travel} is the distance of travel or sliding and H is the penetration hardness of the softer material in terms of units of stress (usually measured by a Brinell, Knoop or Vickers test). Hardness test of clean mill scale surfaces and of the half-hard cartridge brass indicated nearly identical surface hardnesses of 70 on the Rockwell-C scale. For the steel however, this measurement indicates the hardness of the substratum under the surface. It may be that the thin layer of mill scale and the work hardened layer below it may have a larger hardness than that apparent. To test the hardness of this very thin layer, micro-indentation tests would be necessary [7]. Micro-indentation tests of the surfaces were beyond the scope of the experimental program and were not conducted. Assuming that the hardnesses of the two surfaces are of the same magnitude and that the bolt forces in the two systems, steel-steel and steel-brass, produce roughly identical normal forces, at least initially, that leaves two quantities in the equation to be considered, d_{travel} and K. As the same imposed displacements were applied to both types of SBCs, d_{travel} can also be ruled out as a factor causing any difference in the wear volume. The wear coefficient, K, is generally very difficult to estimate with any accuracy [18]. However, for qualitative estimation purposes, Rabinowicz in [18] gives a value K of 1.7×10^{-3} for unlubricated like metal

surfaces and a value K of 6.7×10^{-5} for unlubricated unlike metal surfaces. It is seen that by this consideration, the implication is made that by switching from a steel-steel to a steel-brass sliding system, the initial wear volume, V, is expected to be reduced by a factor of 25. This lends credence to the hypothesis presented above which accounts for the differences between the behaviors of steel-steel and steel-brass SBCs by claiming these differences to be due to different volumes of wear particle generated during sliding.

Lastly, attention is turned to the definitions of steady state, break-in and break-in curve. It is noticed that, according to the given definitions, the curves shown in Figures 2.13 and 2.14 are, indeed, the break-in curves for the two specimens. In particular for Figure 2.14, the break-in curve for the steel-brass specimen, the cumulative travel range of 0 to 10 inches represents the break-in phase of the sliding. Brake-in curves of the type shown in Figure 2.14 appear to be rather typical in frictional systems in general. Blau identifies this type of curve as "type (a)" in the classification of the eight most commonly occurring break-in curves [7].

2"
2"

9/16 " DIAMETER HOLE (TYP.)

FOR DETAIL OF
BOLT ASSEMBLY
REFER TO TEXT

5/8" TH. A36 PLATE (TYP.)

9/16"x4" LONG SLOT

2"
2"

1.5"   4"   6.5"

1/2" DIAMETER A325

2"
2"

10.5"   1.5"
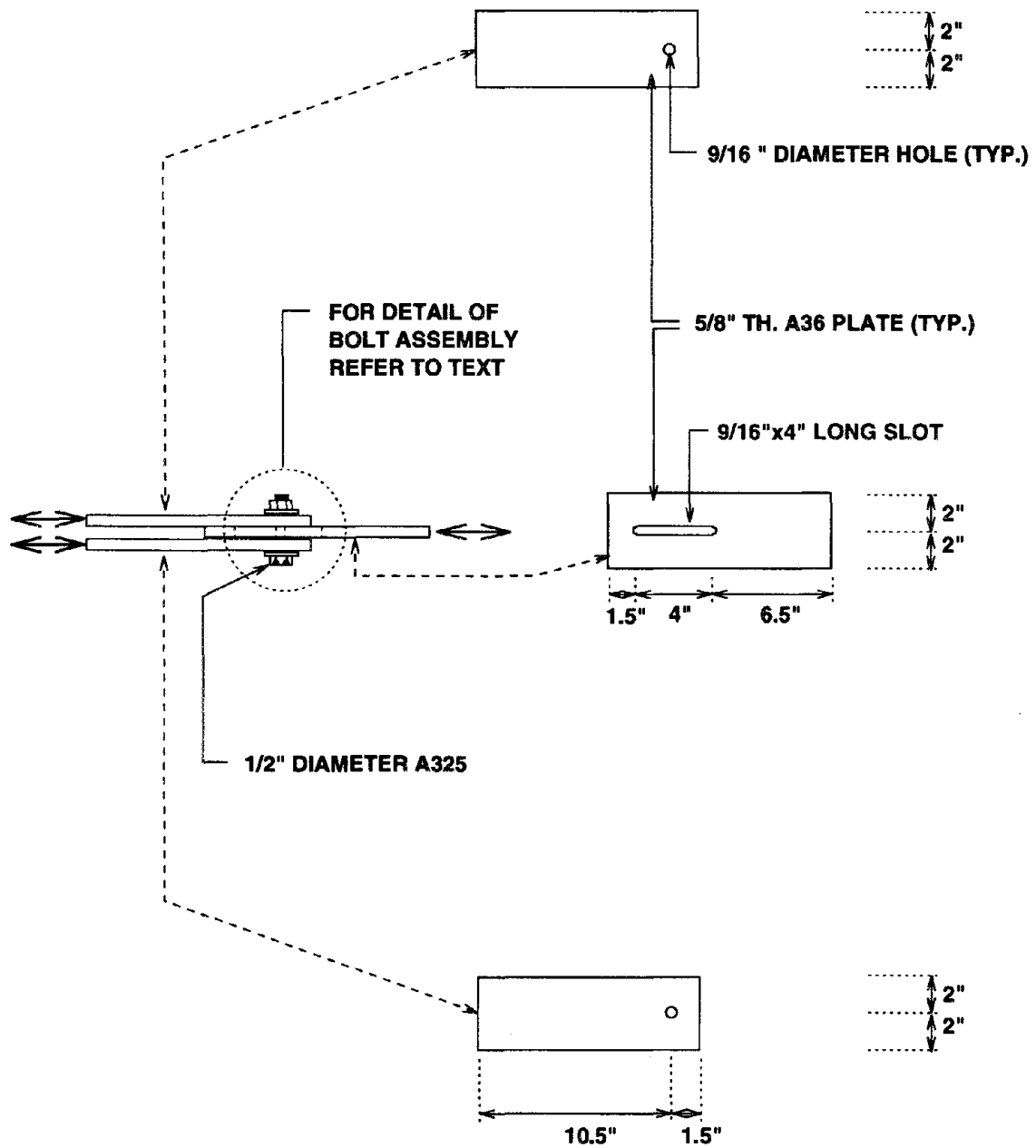
Figure 2.1: Typical detail of SBC test specimen with one $\frac{1}{2}$ inch diameter bolt.
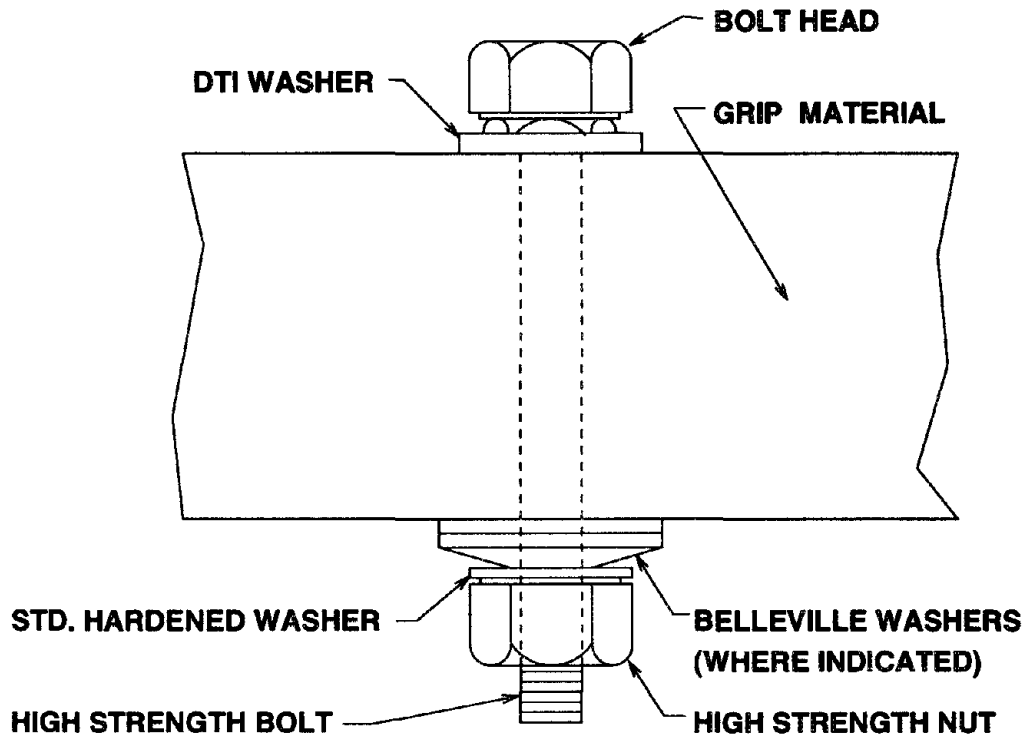
Figure 2.2: Method 1 of assembly of bolt, DTI and Belleville washers.
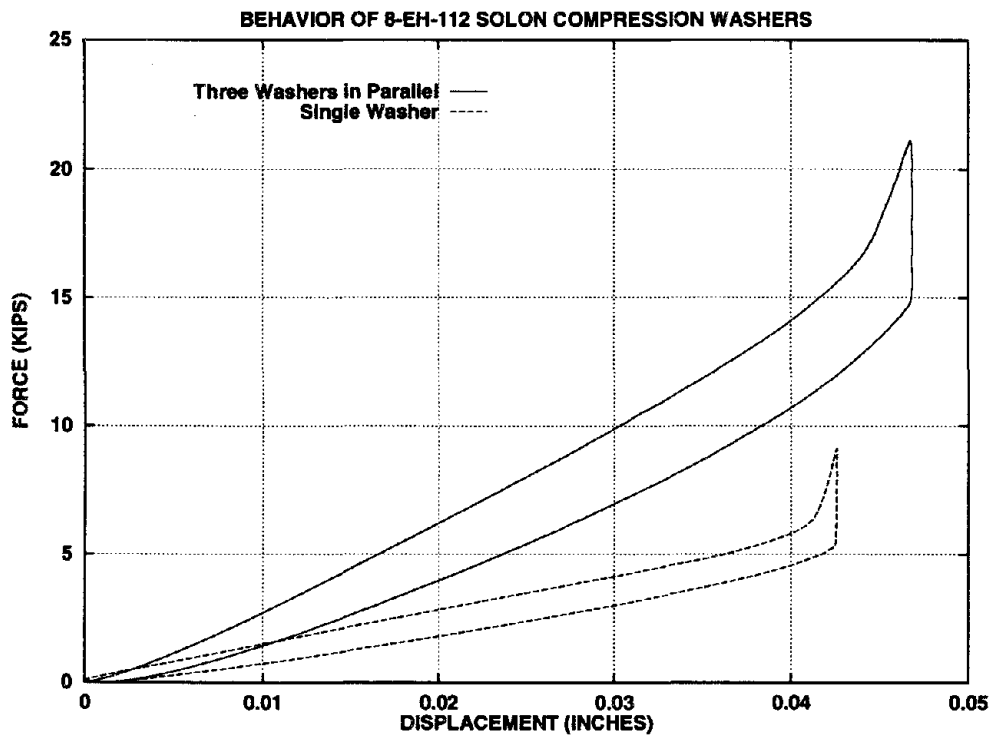
Figure 2.3: Behavior of single and three in parallel 8-EH-112 Solon compression washers.
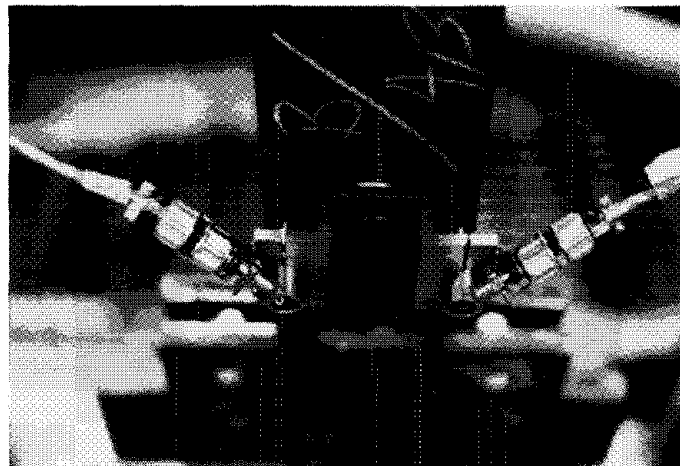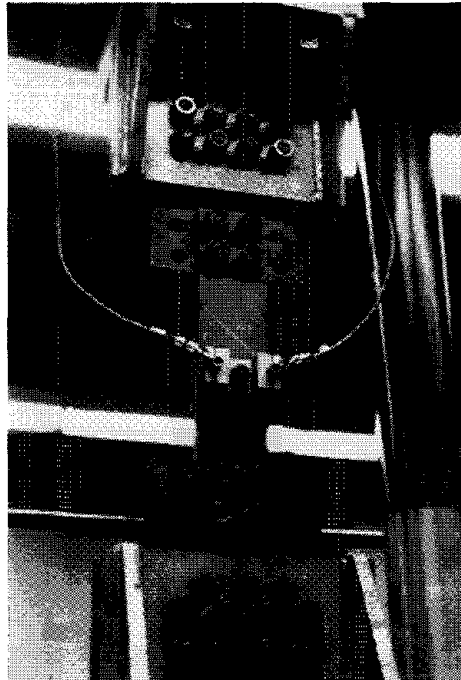
Figure 2.4: Photographs of one $\frac{1}{2}$inch bolt SBC with instrumentation.
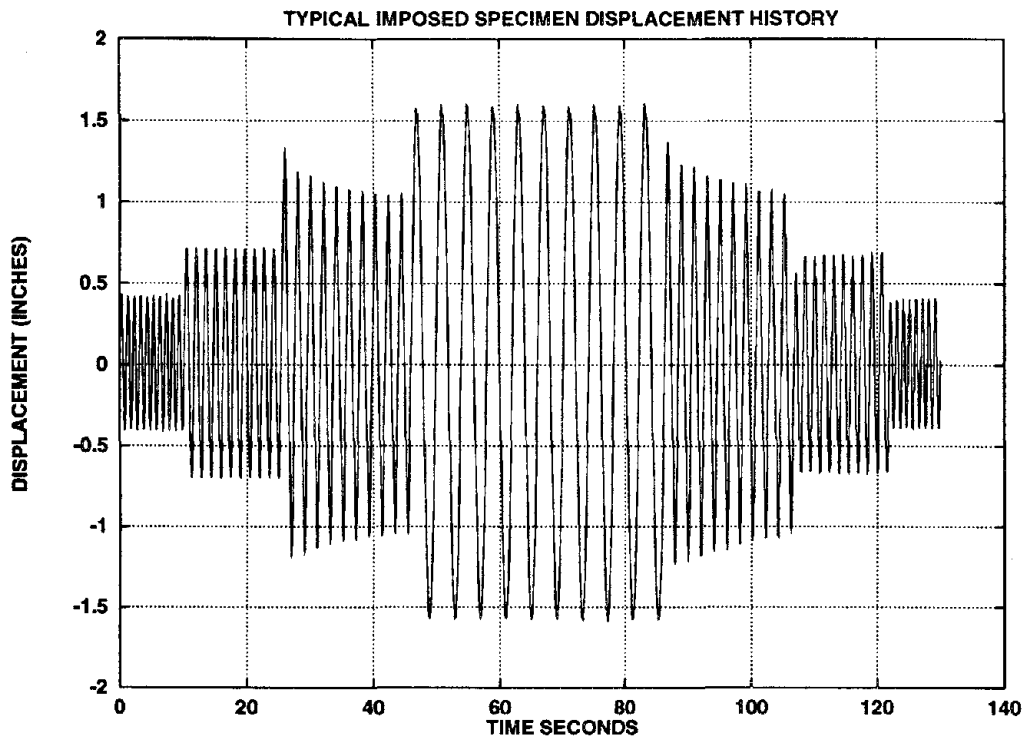
Figure 2.5: Typical C/T machine imposed displacements used in testing of SBCs.
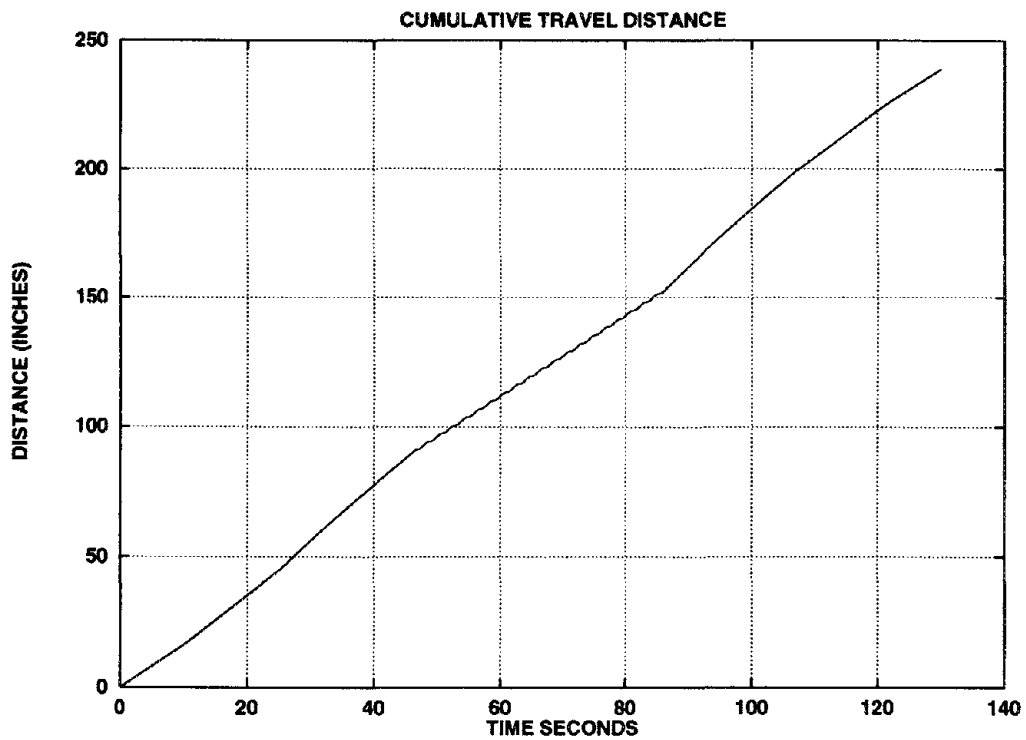
Figure 2.6: Cumulative distance traveled by bolt due to imposed displacements.
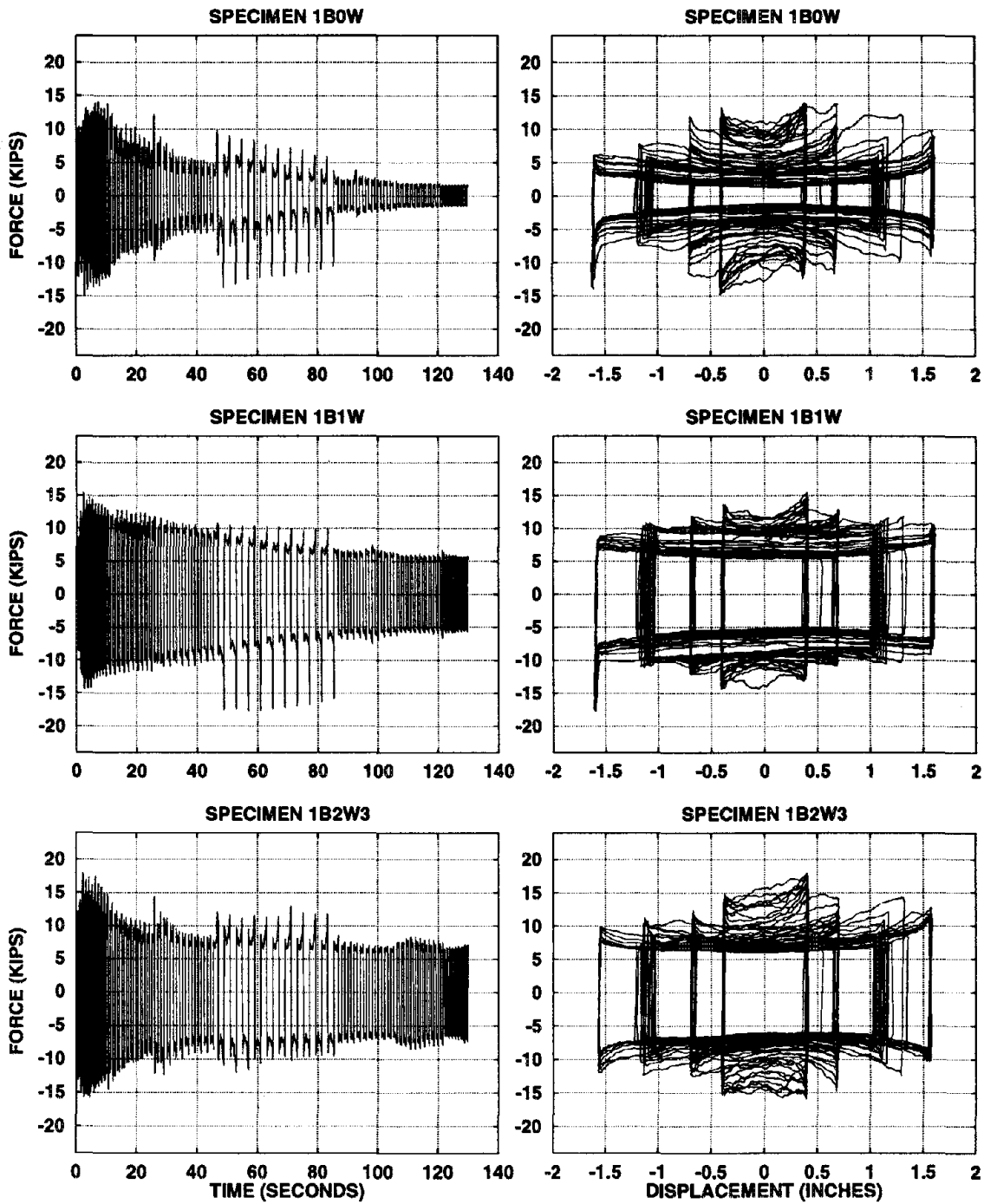
Figure 2.7: Results for steel-steel SBCs with 0, 1 and 2 Bellevile washers.
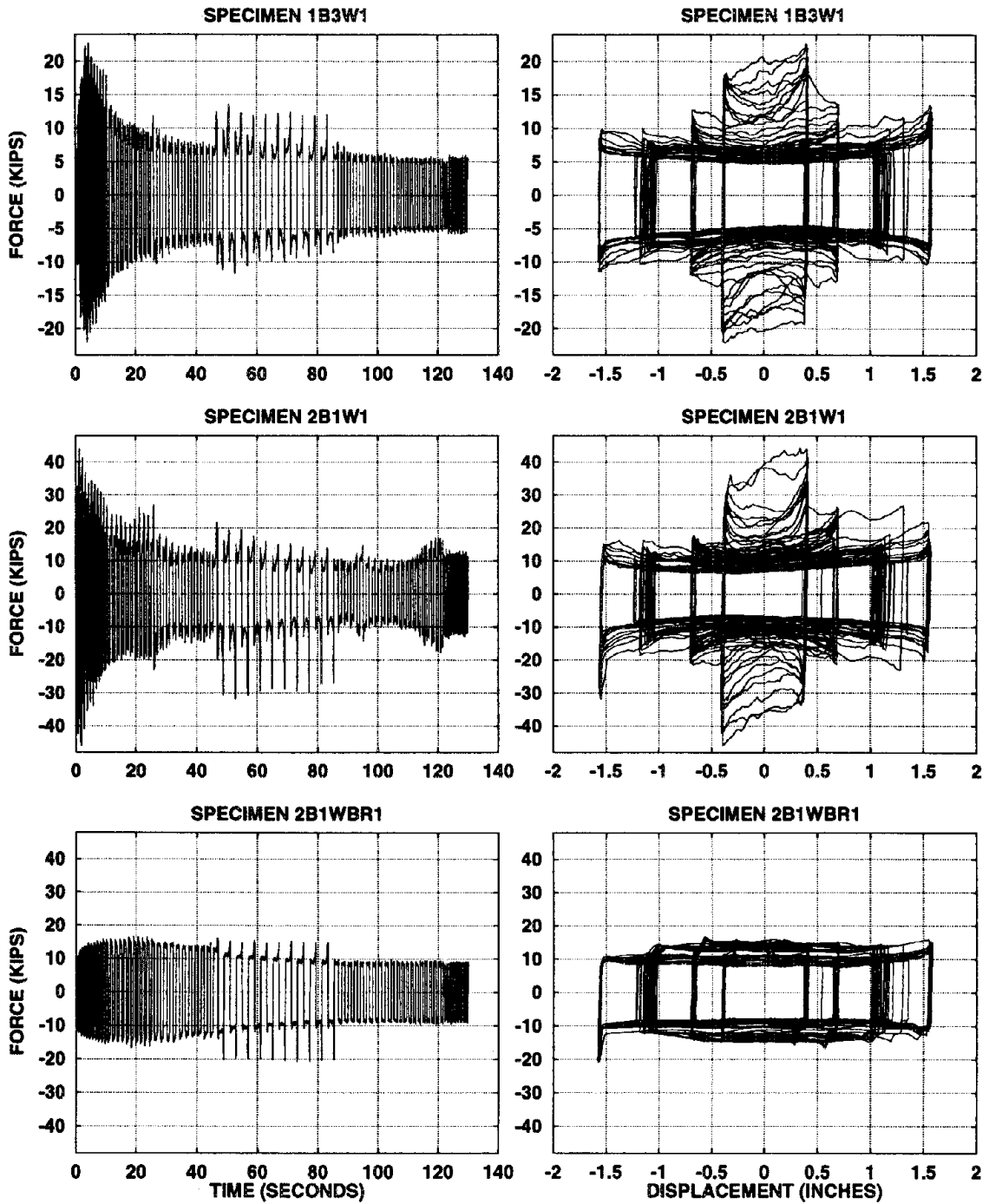
Figure 2.8: Effects of using 3 Bellevilles, doubling of bolts and using brass shims.

SPECIMEN 1B3W1
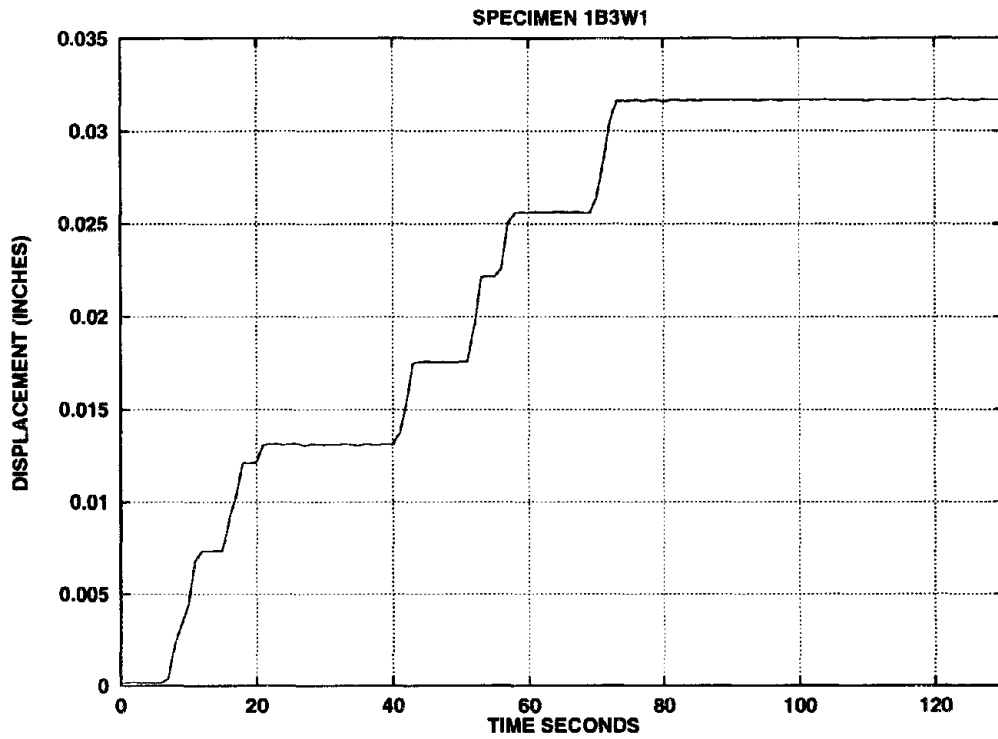
Figure 2.9: Compression of washer stack during tightening of bolt.

SPECIMEN 1B3W1
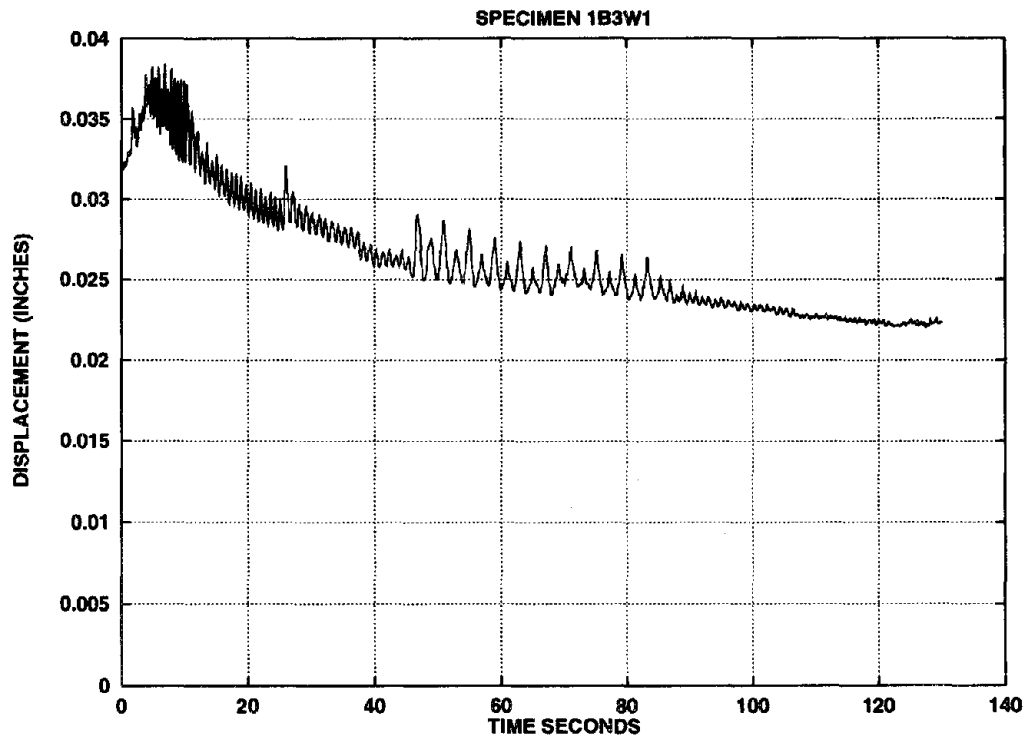
Figure 2.10: History of washer stack compression during test.
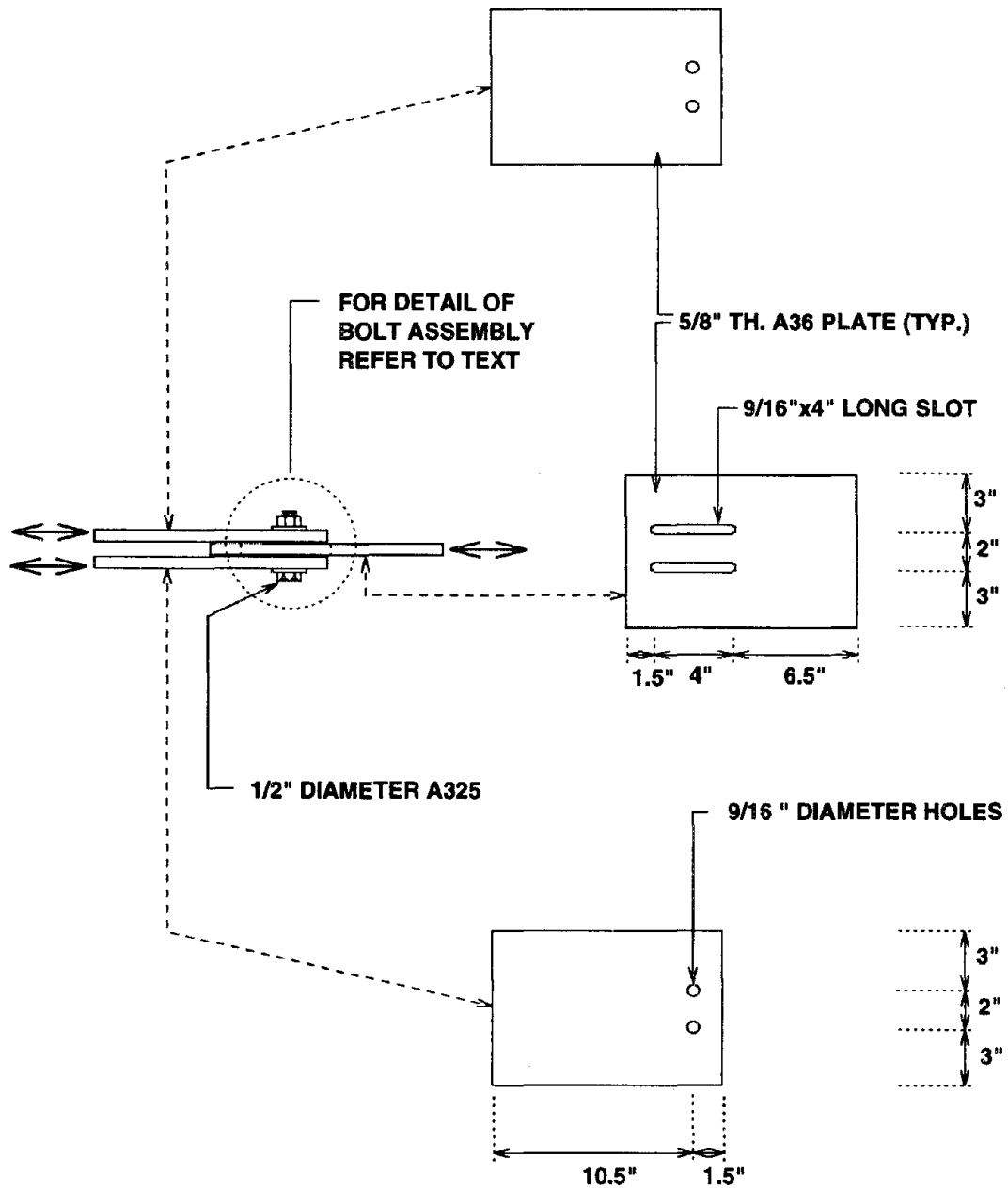
Figure 2.11: Typical detail of SBC test specimen with two $\frac{1}{2}$ inch diameter bolts.
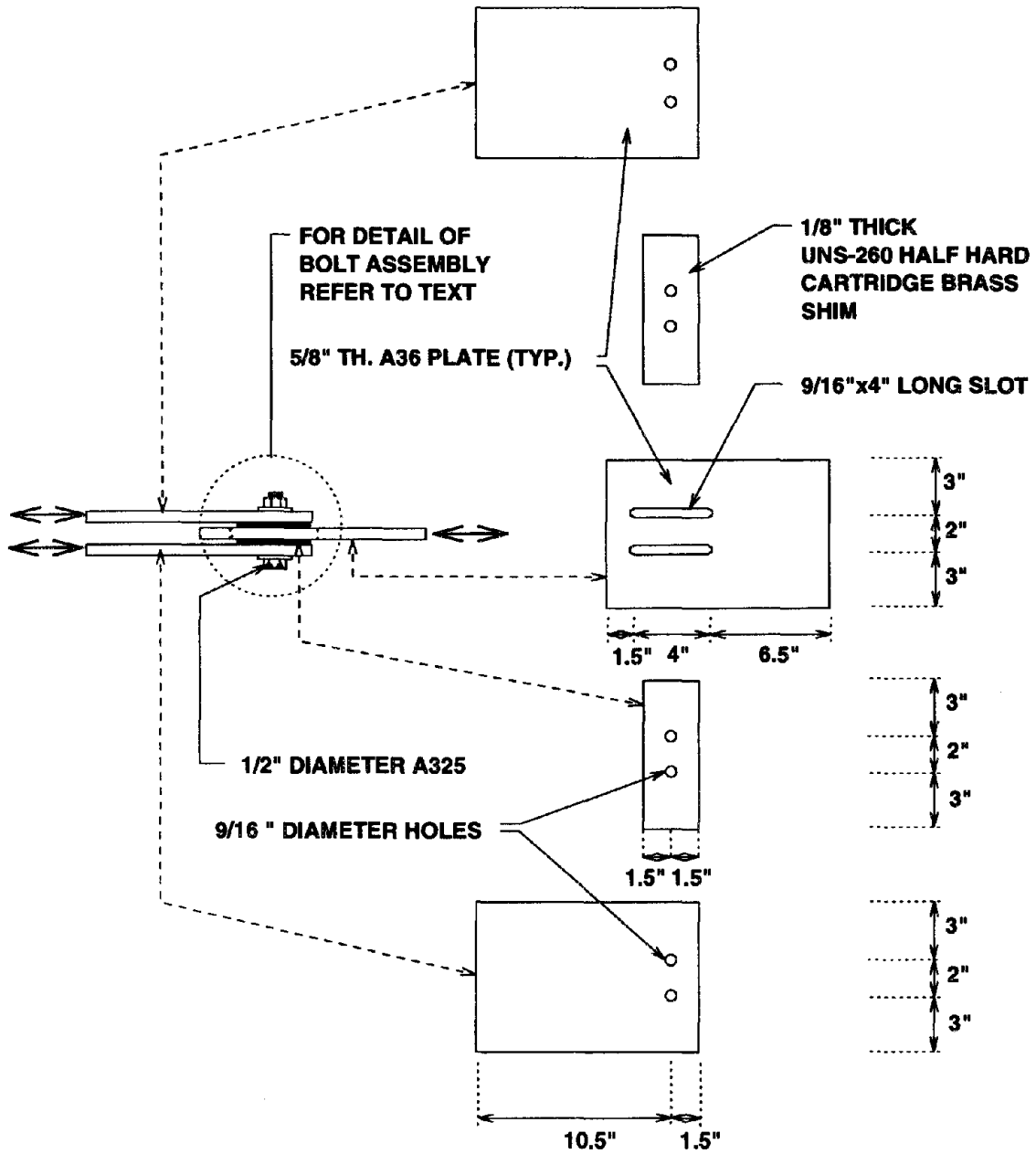
Figure 2.12: Typical detail of SBC test specimen with two $\frac{1}{2}$ inch diameter bolts and brass shims.

SPECIMEN 2B1W1
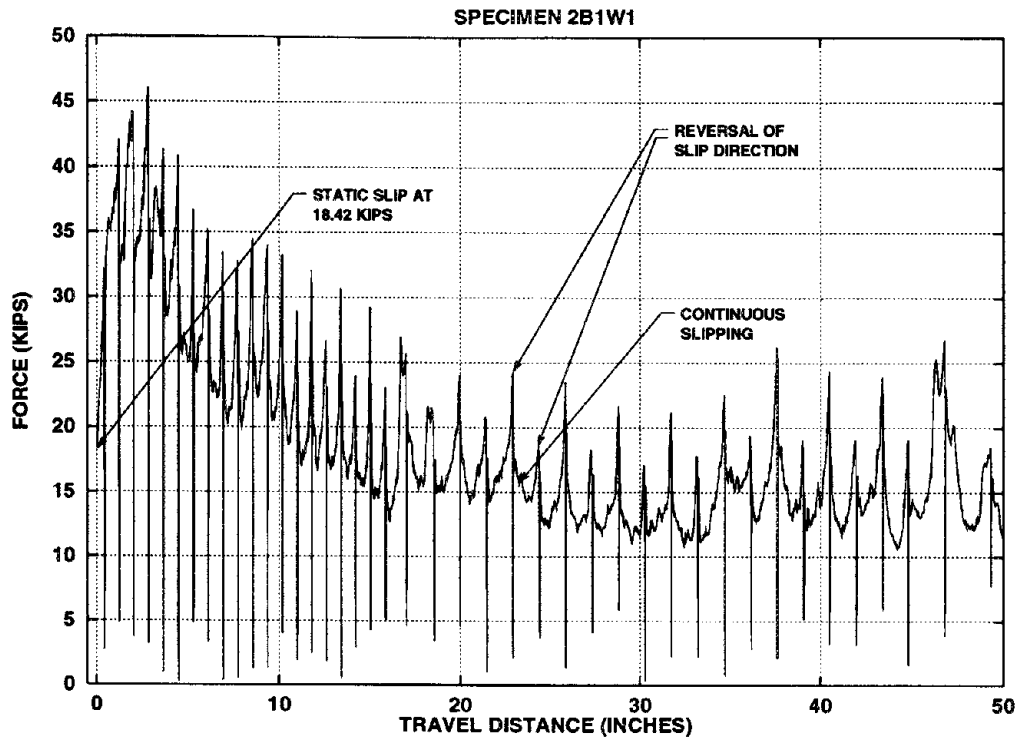
Figure 2.13: Cumulative travel vs. absolute value of SBC force for steel-steel SBC.

SPECIMEN 2B1WBR1
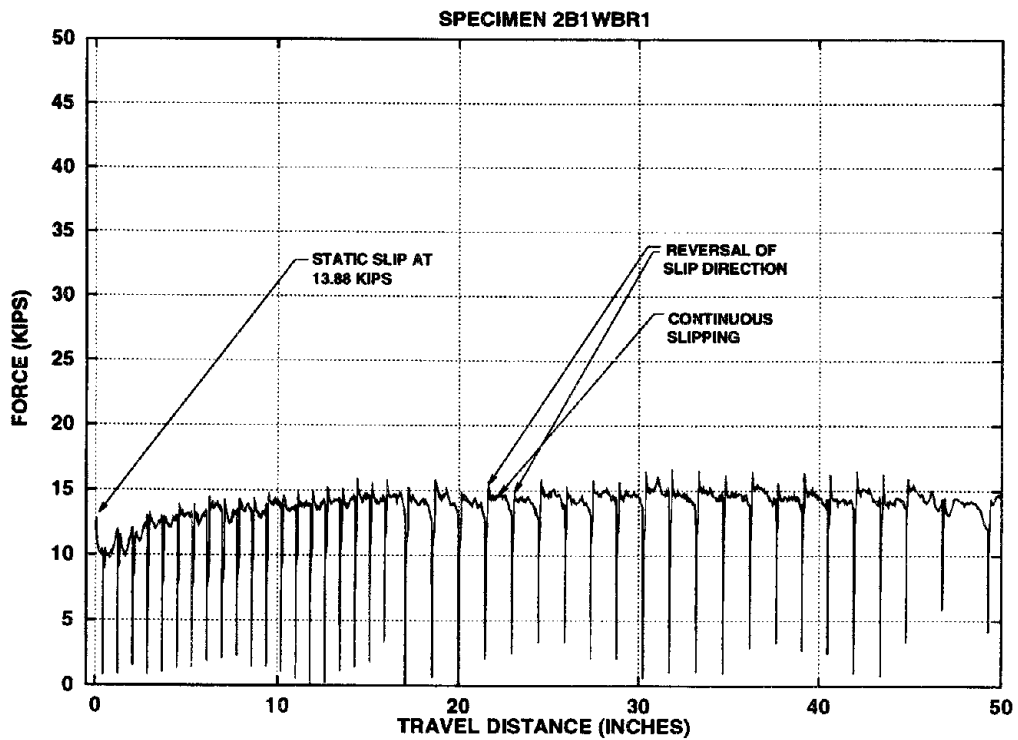
Figure 2.14: Cumulative travel vs. absolute value of SBC force for steel-brass SBC.

Chapter 3

SBCs with Steel-Brass Sliding Surfaces

3.1 General Remarks

A total of twenty three steel-brass SBCs were tested on the C/T machine. Of these, fifteen were tested under imposed sinusoidal displacements identical to those described in the last chapter and shown in Figure 2.5. These are the subject of this chapter. The remaining eight were tested under imposed simulated seismic displacements. The results for these will be presented in the next chapter. Table 3.1 gives a listing of the fifteen specimens tested under imposed sinusoidal displacements in the C/T machine. Specimen designations follow the naming conventions given in the previous chapter. A star ($\star$) to the left of the specimen designation indicates that results for the specimen are explicitly presented in this document. The results of these specimens represent typical behaviors. The column titled "Belleville Type" indicates the type of Solon Compression washer used in the bolt assembly. Force-deformation characteristics for 8-EH-112 washers were shown in Figure 2.3 in the previous chapter. Specifications for 12-EH-168 and 12-H-150 washers will be given further ahead in the discussion of the results of $\frac{3}{4}$ inch diameter A325 bolts. The column titled "DTI Method" indicates the method of bolt assembly. Method 1 of assembly was discussed in the previous chapter. "Method 2" will be described further ahead in this chapter.

3.2 Results for SBCs with $\frac{1}{2}$ inch A325 Bolts

Results for the test of specimen 2B1WBR1 were given in the previous chapter. The first six specimens to be discussed here have, with the exception of their bolt assemblies, the same identical general detail as specimen 2B1WBR1. The details of this specimen were given in Figure 2.12. The upper photographic plate of Figure 3.1 shows a close-up of the two bolts of a typical steel-brass SBC test specimen with two $\frac{1}{2}$ inch diameter A325 bolts. The particular specimen shown was tightened by "Method 1", as may be discerned from the upper photographic plate in which the light colored Belleville washer is apparent under a dark colored hardened washer topped with a high strength nut. Also apparent are the edges of the two slots in the main plate. Careful examination reveals vertical lines of brass smears visible just below the edge of the plate between the slots.

The lower photographic plate of the same figure shows typical specimens on the laboratory floor. The specimens to the right are seen as fully assembled, while the specimen to the left is shown disassembled. The two outer plates are seen near the upper edge of the photographic plate. The main plate is seen just below the outer plates. Two further views of typical SBCs with two $\frac{1}{2}$ diameter A325 bolts are shown in Figure 3.2. The upper photographic plate in this figure shows the specimen attached to adapter plates which are, in turn, secured to the clevices of the C/T machine. The lower photographic plate of the figure shows a close-up view of the specimen from the side. The $\frac{1}{8}$-th inch brass shim plates, and in particular the shim to the right of the main plate, are just visible.

Figure 3.3 shows results for tests of three specimens. As in Chapter 2, force response histories due to the sinusoidal imposed displacements are shown in the left column of plots, while the hysteresis curves for the specimens are shown in the right column of plots. The two plots at the top of the figure are for specimen 2B1WBR2, which was identical in every detail to specimen 2B1WBR1 the results for which where shown in the two bottom plots of Figure 2.8. Slightly smaller displacements were applied to specimen 2B1WBR2 in order to avoid the force spikes present in the results of specimen 2B1WBR1. As a comparison of the results for the two specimens shows, the

force spikes were successfully avoided. Otherwise, and in light of great scatter which is characteristic of kinetic friction data in general, the force response curves and the hysteresis curves appear to be, for practical purposes, identical. This is particularly evident from the comparison of Figure 3.4, showing the curve of the absolute value of force response plotted against cumulative travel distance for specimen 2B1WBR2, with a similar plot for specimen 2B1WBR1 shown in Figure 2.14 of the previous chapter.

Effect of Belleville Washers

The use of single 8-EH-112 washers in the bolt assemblies of 2B1WBR1 and 2B1WBR2 was influenced by the lessons learned from the tests of the steel-steel SBCs. As recalled from Chapter 2, the use of the single washer induced a pronounced improvement in the ability of the connections to retain a high slip force. The use of more than one such washer resulted in no further improvements. However, as in the case of steel-steel SBCs, it was of interest to investigate the effect of excluding and varying the number of Belleville washers for the steel-brass SBCs. The two plots in the middle and the two plots at the bottom of Figure 3.3 are for specimens similar to specimens 2B1WBR1 and 2B1WBR2, with the exception that these specimens had no Belleville washers in their bolt assemblies. That is, the hardened flat washers, under the nuts, rested directly against the faces of the outer plates. The most striking feature of the results for these two specimens, 2B0WBR1 and 2B0WBR2, is that the hysteresis curves appear skewed. That is, the heights of the hysteresis loops appear smaller in the negative displacements range (extension) than in the positive displacement range (compression). This effect is thought to be not due to any inherent property of the specimens, but to misalignment of the C/T machine clevices. After the testing of specimen 2B0WBR1 an attempt was made to realign the clevices. Upon the testing of the next specimen, specimen 2B0WBR2, a lesser degree of skewness resulted as can be seen in the hysteresis curves of the specimen as shown in the lower right plot of Figure 3.3.

Apart from the skewness of the hysteresis curves, the responses of specimens

2B0WBR1 and 2B0WBR2 appear to be similar, both qualitatively and quantitatively, to the results of specimens 2B1WBR1 and 2B1WBR2. Figure 3.5 shows the curve of the absolute value of force response against cumulative travel distance for specimen 2B0WBR2. The differences between this curve and that shown in Figure 3.4, for specimen 2B1WBR2, are not significantly different. This indicates that not much is gained by the use of the single 8-EH-112 washer. A single 8-EH-112 washer becomes flat under 6 kips of load, whereas the specified preload for a $\frac{1}{2}$ inch diameter bolt is 12 kips. Therefore, the single 8-EH-112 washer washer theoretically should not effect the flexibility of the Belleville-bolt-DTI clamping system. Because these single washers transfer the clamping force, which flattens them, through the outside diameter edge, they result in less concentrated stresses between the "sandwiched" plates. Unless the bolt force drops to near 6 kips, this is the only theoretically conceivable effect of a single washer on the SBCs.

While a single 8-EH-112 washer flattens under 6 kips of load, a stack of three in parallel of such washers is flattened under a nominal load of 18 kips. This value being larger than the 12 kips specified preload for a $\frac{1}{2}$ inch diameter A325 bolt, it would be expected that the use of such a stack of washers in the bolt assembly would result in a more flexible Belleville-bolt-DTI clamping system than that of a SBC with a single 8-EH-112 washer or no Belleville washers at all. Given that in Chapter 2 it was hypothesized that the reduction in the slip load of the connections was due to the inward movement of the outer plates which occurred due to the reabsorbtion and falling out and of the wear particles, it would be expected that given the same magnitude of the inward movement of the outer plates, a lesser drop in the slip force would be caused in the system with the more flexible clamping system. The top two plots of Figure 3.7 show the test results for a specimen, specimen 2B3WBR1, with the above mentioned stacks of three 8-EH-112 washers in parallel in its bolt assemblies. It is clearly evident that, as expected, less of a reduction in the slip forces occurs for this specimen than did for specimens 2B1WBR1, 2B1WBR2, 2B0WBR1 and 2B0WBR2. It is however noted that the initial increasing segment of the force response curve for specimen 2B3WBR1 is rather similar to those of the four mentioned above. This becomes evident upon the examination of Figure 3.8. For practical purposes, in the

given range of cumulative travel distance, this curve exhibits very similar behavior to the curves for the same quantities shown for specimens 2B1WBR1, 2B1WBR2 and 2B0WBR2 in Figures 2.14, 3.4 and 3.5, respectively. This indicates that in the range of cumulative travel distance relevant to a single severe seismic event, the effect of the stack of three 8-EH-112 washers in parallel is not significant.

However, apart from causing slightly higher slip forces in the later stages of sliding, the use of a stack of three 8-EH-112 washers is series in the bolts assembly of the SBCs of the type shown may have the additional benefit of reducing the loss of bolt preload. It has been shown that in a regular bolt assembly such losses of preload, which are due to creep, may be as large as 8% of the total bolt preload [13]. The addition to the bolt assembly of a washer stack with a flat load above that of the bolt preload has the effect of significantly increasing the flexibility of the the clamping system. A more flexible system is less prone to loss of load due to creep. However, this aspect of the benefit of using such washer stacks needs to be studied further as the washer stack itself may also be prone to creep.

Effect of Using Method 2 of Bolt Assembly

The arrangement of Method 2 of bolt assembly is shown in Figure 3.6. As shown in this figure, the DTI washer is topped with a hardened washer and placed under the nut, rather than being placed under the head of the bolt as in Method 1. Whereas the manufacturer's instructions for the tightening of bolts with Method 1 of DTI use require that the average gap between the DTI the flat portions (spaces between the protrusions) of the DTI and the opposing element be reduced to 0.015 inches or less, Method 2 requires the gaps to be reduced to 0.005 inches or less. This conservatism in Method 2 is apparently there to account for the fact that, by having the DTI protrusions against the turned element, the protrusions may become worn giving the appearance that the gaps have become smaller due to the increased bolt force.

Two specimens similar to the two bolt specimens thus far discussed, but with bolt assemblies of Method 2 type, and one such twelve bolt specimen, were tested. The

main plates for the two bolt specimens had been used as main plates for previously tested specimens, the result for which will be presented in Chapter 4. However, these plates had very minor smears of brass on them, and as will be mentioned in Chapter 4, results from the retesting of specimens with new brass shims indicated little to no difference from behavior of virgin plates.

Test results for the aforementioned two bolt specimens are shown in the middle and lower plots of Figure 3.7. Both specimens, 2B3WBR3 and 2B3WBR4, exhibited significantly larger slip forces and a distinctly different qualitative force response history than those of similar connection with Method 1 type of bolt assembly. The force magnitudes, in particular in the initial stage, were nearly 50% larger than the maximum force experienced for similar specimens with the Method 1 type of bolt assembly. The drastic difference in behavior between these specimens and comparable specimens tightened with Method 1 can be seen by comparing Figures 3.8 and 3.9. Figure 3.8 shows the curve of absolute value of force response versus cumulative travel distance for specimen 2B3WBR1, with bolt assembly of which was tightened by Method 1, and the same curve for specimen 2B3WBR4, with bolt assembly of which was tightened by Method 2.

It is believed that the differences in behaviors are due to the bolt preload being by far larger for bolt assemblies tightened by Method 2 than for their counterparts tightened by Method 1. The minimum tensile strength of a $\frac{1}{2}$ inch diameter A325 bolt is nominally 17.7 kips, while the minimal yield strength for the same bolt is nominally 13.3 kips. Supposing that the value of the bolt force, as tightened by Method 2, is near the nominal minimum tensile strength of the bolt and that Method 1 provides between 12 to 14 kips of bolt preload, this would imply that the normal force provided by a $\frac{1}{2}$ inch diameter A325 bolt tightened by Method 2 to the frictional surfaces would be larger than that provided by one such bolt tightened by Method 1 by a factor of between 1.3 and 1.5. This would partially explain the large differences in the magnitudes of slip force. In addition, if the bolts tightened by Method 2 are indeed at such a large preload compared to their nominal minimum yield strength, this would mean that they would have little stiffness as compared to bolts tightened by Method 1, where the bolt preloads would be just below or just

above the nominal minimum yield strength. This difference in stiffness would result in bolt force being comparatively less sensitive to any outward movement of the outer plates. This perhaps may explain, part way, the differences between the envelopes of the force response history curves of specimens with bolt assemblies tightened by Method 1 and those tightened by Method 2.

As mentioned, a twelve bolt specimen, 12B3WBR1 (not shown), with bolt assemblies tightened by Method 2 was also tested. The twelve bolts were configured into three rows of four bolts. The four bolts of each row shared a common long slot. That is, the main plate had three long slots each of which was shared by four bolts. The bolts were spaced on two inch by two inch grid lines. As with the two bolt specimens, the steel plates and brass shims were of $\frac{5}{8}$-th inch thick A36 plate material and $\frac{1}{8}$-th inch thick half hard cartridge brass, respectively. The slot lengths for this specimen were too short to accommodate the magnitudes of imposed displacements, shown in Figure 2.5, used for the testing of the two bolt connections. The imposed displacement history of Figure 2.5 was scaled in amplitude, but not in frequency, to suit the displacements allowed by the slot lengths of 12B3WBR1. This scaled imposed displacement history is shown in Figure 3.10. The imposition of the displacement history shown in Figure 3.10 resulted in the hysteresis curves shown in Figure 3.11. The horizontal segments of the hysteresis loops at roughly $+/-$ 50 kips are due to slips in the clevices and not due to slip at the SBC. The horizontal segments at near $+/-$ 75 kips are the effect of the slipping of the brass shims against the outer plates. These "chewed off" corners were mentioned in the previous chapter and are characteristic of the behavior of SBCs. The slip force achieved by this SBC was approximately 112 kips. This force value is a factor 1.24 larger than the value that would have been expected if the connection were tightened by Method 1. That is, the peak slip force for SBCs tightened by Method 1 appears to be roughly 15 kips per two bolt connection, or 7.5 kips per single $\frac{1}{2}$ inch diameter A325 bolt. Then for a twelve bolt connection one would have expected 7.5×12 or 90 kips. The common link between this specimen and specimens 2B3WBR3 and 2B3WBR4, which also exhibited uncommonly large slip forces, is that all three had bolt assemblies of Method 2 type. The curve of absolute force versus cumulative travel for this specimen is shown in

Figure 3.12. This curve, despite containing the extraneous slips of the clevices, has strong resemblance to the curve of the same quantities for specimen 2B3WBR4, shown in Figure 3.9. Again, the common link between theses specimens is that both used bolt assemblies tightened by Method 2.

3.3 Results for SBCs with $\frac{3}{4}$ inch A325 Bolts

Thus far in the presentation of the experimental results, only results for specimens with $\frac{1}{2}$ inch diameter A325 bolts have been presented. Results for specimen 12B3WBR1 demonstrated that SBCs with rather large slip forces could be designed by closely spacing a number of such $\frac{1}{2}$ inch diameter A325 bolts. Indeed, the twelve bolts of this connection fit into a rectangular area of only 4"×6", three rows of four bolts on two inch by two inch grid lines. However, it was of interest to investigate also the behavior of larger bolts. Given the nature of the wear equation, described in the previous chapter, the results for smaller bolts could not be assumed to extend automatically to larger size bolt by simply scaling slip force by the ratio of bolt preloads of the larger bolt to that of $\frac{1}{2}$ inch A325 bolts. That is, the wear equation would predict that for, say, doubling the bolt preload that the volume of wear particles would be doubled given the same imposed displacements. This doubling of the volume of the wear particles could, conceivably, significantly alter the behavior of the connection from that expected by assuming a linear extrapolation from results with smaller bolt preloads.

It was decided to investigate the behavior of SBCs with $\frac{3}{4}$ inch diameter A325 bolts. The preload specified by the RCSC for this size bolt is 28 kips, that is a factor of $\frac{28}{12}$, or 2.33, larger than the preload of $\frac{1}{2}$ inch diameter A325 bolt. Initially, two SBC specimens designed to accommodate $\frac{1}{2}$ inch diameter bolts were modified to accommodate $\frac{3}{4}$ inch diameter bolts. These modification consisted of enlargening the holes and slots in the outer plates, main plates and brass shims of the specimens. In imitation of the SBC specimens with $\frac{1}{2}$ inch diameter A325, where single 8-EH-112 washers having half the flat load of the bolt preload were used, a spring washer having roughly half the $\frac{3}{4}$ inch diameter A325 bolt preload as its flat load was used. This

was the 12-EH-168 washer indicated in Table 3.1. The manufacturer's specifications for this washer are that it becomes flat at 15 kips and that it deforms 0.062 inches under this load load. The first specimen tested with these washers was specimen 2A1WBR1, results for which are not shown here. The bolt assembly for the specimen was tightened by Method 1. The slip forces for this specimen were found to be much lower than expected. This was judged to be due to the bolt holes being too close to each other. The spacing was $2\frac{1}{4}$ inches center to center. Such close bolt spacing was due to the fact that the specimens were originally designed to accommodate $\frac{1}{2}$ inch diameter bolts. The close spacing may have possibly had two effects. First, it contributed to large compressive stresses between the sliding surfaces between the two bolts. Secondly, it is possible that the second bolt to have been tightened may have loosened the first tightened bolt as it further compressed the grip material in the vicinity of that bolt. The second specimen, 2A1WBR2, which was identical to 2A1WBR1 with exception that one bolt was left loose or "finger tight" was tested to investigate the behavior of the SBC while excluding the effects due to the closeness of the bolt holes. The results of testing of this specimen, not shown, indicated much larger slip forces, per single bolt, than was observed for the first specimen.

Subsequently, SBC specimens were designed with larger bolt hole separations. The details for a typical SBC specimen with two $\frac{3}{4}$ inch diameter A325 bolts are shown in Figure 3.13. As seen from a comparison of Figure 3.13 with Figure 2.12, the specimens with $\frac{3}{4}$ inch diameter A325 bolts are different from those with $\frac{1}{2}$ inch diameter A325 bolts mainly in that the bolt hole and slot separations are larger (three times the bolt diameter for both cases) and that the brass shims are wider. The thicknesses of the brass shims were the same in both types of specimens, that is $\frac{1}{8}$-th inch thick.

Figure 3.14 shows the test results for three such specimens. The plots of force response history and hysteresis curves are arranged as in the previous sections. The two plots at the top of the figure represent results for the test of specimen 2A0WBR1. The specimen was tightened by Method 1, as were all SBC specimens tested with $\frac{3}{4}$ inch diameter A325 bolts. No Belleville washers were included in the bolt assemblies of this specimen. The profile of the force response history curve for this specimen is

rather similar to those for specimens with $\frac{1}{2}$ inch diameter A325 bolts. Figure 3.15 shows the curve of absolute value of force response versus cumulative travel for specimen 2A0WBR1. Comparison of this figure with, say, Figure 2.14, showing the same curve for specimen 2B1WBR1, indicates similar behavior characteristics. The ratio of static slip forces between specimen 2A0WBR1 and 2B1WBR1, as can be discerned from the two figures, is $\frac{30.62}{13.88}$ or 2.21 which compares well with the ratio of the bolt preloads given above, that is 2.33. If the force plateaus for the two specimens are interpreted to be at 15 kips for 2B1WBR1 and at 35 kips for 2A0WBR1, the ratio of effective kinetic slip force for the two specimens is $\frac{35}{15}$ or 2.33, indicating linear increase in slip force with increase of bolt preloads. Again it must be emphasized, the in light of the wear equation given in the previous chapter, further linear extrapolation for large bolt preloads may not lead to linear increases in the slip forces.

The middle and bottom plots in Figure 3.14, for specimens 2A3WBR1 and 2A3WBR2, show result for the testing of two specimens with $\frac{3}{4}$ inch diameter A325 bolts and with washer stacks of three 12-H-150 spring washers in parallel. As in the case of the specimens with $\frac{1}{2}$ inch diameter A325 bolts, the stack was chosen to have a flat load larger than the bolt preload and, as such, to provide extra flexibility to the DTI-bolt-Bellevilles clamping system. According to the manufacturers specifications, a single 12-H-150 washer has a flat load of 12 kips. Then, a stack of three in parallel of such washers has a flat load of 36 kips, that is 8 kips larger than the preload of $\frac{3}{4}$ inch diameter A325 bolt. The deflection from the undeformed to the flat position of the washer is specified as 0.053 inches. The method of bolt assembly was again Method 1.

As in the case of the specimens with $\frac{1}{2}$ inch diameter A325 bolts, the effect of using washer stacks with flat loads larger than the bolt preload is most accentuated in the later stages of slipping. That is, the initial stages of force response history curves for specimens 2A3WBR1 and 2A3WBR2 are quite similar in magnitude to that of specimen 2A0WBR1 shown in the same figure. Figure 3.16 shows the curve of absolute value of force versus cumulative travel for specimen 2A3WBR2. Comparing this figure to Figure 3.15, showing the same curve for specimen 2A0WBR1, again indicates that no significant gains in slip force is achieved in the cumulative travel

range of interest by the use of the washer stacks. This result correlates well with lessons learned from the testing of specimens with $\frac{1}{2}$ inch diameter A325 bolts.

3.4 Discussion

Chronology of Testing

In order to put the results to be presented in the next chapters into perspective with the results presented in this chapter, a discussion of the chronology of the testing of the specimens is necessary. Specimen 2B1WBR1 was the first specimen tested with brass shims and the first specimen with results indicating not only acceptable, but excellent, behavior characteristics for an energy dissipation system. As explained in the previous sections of this chapter, this specimen utilized a single 8-EH-112 Solon compression washer in its bolt assembly. Later experiments, the results of which have been presented in this chapter, indicated that nearly the same behavior resulted from tests of similar SBCs without any Belleville washers. That is, the responses of specimens 2B0WBR1 and 2B0WBR2, apart from the skewness of the hysteresis loops attributed to the misalignment of the clevices, were quite similar to the responses of specimens 2B1WBR1. At the time of the testing of 2B1WBR1, a narrow time window of opportunity to use the shake table was present. In order to take advantage of this opportunity, attention was restricted to specimens of the 2B1WBR1 type. The experimental results presented in the next chapter are for specimens of same type as 2B1WBR1. That is, these specimens had bolt assemblies consisting of $\frac{1}{2}$ inch diameter A325 bolts, with their associated DTI and a single 8-EH-112 Solon compression washers, all assembled by Method 1. The SBCs of the shake table structure were also of this type. Indeed, they were identical to specimens 2B1WBR1 and 2B1WBR2, the result for which were presented in this chapter. All these connections performed excellently with very reliable behavior. The expansion of the experimental program to include steel-brass type SBCs with no Belleville, stacks of Bellevilles, with assemblies by Method 2 and with $\frac{3}{4}$ inch diameter A325 bolts came about after the completion of the shake table tests.

Relevance of Results to Practitioners

The above mentioned chronology and the wide scope of the experiments conducted after the completion of the shake table tests has resulted in there being a larger data-base for specimens of the type of 2B1WBR1 than any other type. Due to this, it is felt that while connections of the 2B1WBR1 type may be used with some confidence in the field, more experimental data need to be generated for the other types of SBCs that have been discussed in this chapter. It is felt that possible use in the field of the variants of SBCs discussed in this chapter other than the 2B1WBR1 types may be justified, however, if full scale as-designed connections of these types are tested in a C/T machine with realistic imposed displacements.

For design in the field with SBCs of the 2B1WBR1 type, two primary values are necessary. These are the initial static slip force and the kinetic slip force, each given per single bolt. It is emphasized that the values to be given are for the entire system of the $\frac{1}{2}$ inch diameter A325 bolt with the associated DTI, the single 8-EH-112 Solon compression washer and the hardened flat washer, all assembled by Method 1.

The average initial static slip force for 2B1WBR1 type specimens is calculated to be 7.2 kips per bolt based on tests of six virgin specimens. By virgin it is meant here that the elements of the specimen were not reused from another experiment. Of the six, results for two, 2B1WBR1 and 2B1WBR2, were presented in this chapter. The results for the remaining four are presented in the next chapter. If the DTI is to be supposed to provide, by Method 1, bolt preloads in the range of 12 to 14 kips, this then leads to a possible range of slip coefficients for clean mill scale A36 steel against half hard cartridge brass (UNS-260) of 0.30 to 0.26. These values are rather typical for such metallic couples. It was not possible to include in this data the results from twelve similar SBCs installed in the test structure that was tested on the shake table. As will be explained in chapter 6, due to the addition to the testing facility of a new and improved data acquisition system, the initial data, including the initial static slip forces of the SBCs, for the first few tests were lost.

Specification of an average kinetic slip force is not as clear-cut as the case of the initial static slip force. As has been demonstrated in the curves of absolute value

of force response versus cumulative travel for specimens 2B1WBR1 and 2B1WBR1, shown in Figures 2.14 and 3.4, the magnitude of slip forces of SBCs of this type are strongly dependent on cumulative travel distance. The variations of the slip forces with velocity are small enough to be ignored for design purposes. The trends seen for the six specimens above and the twelve SBCs of the test structure indicate that a force plateau of approximately 7.5 kips per bolt is consistently reached. For most of the specimens the initial kinetic slip force is approximately 5 kips. This value increases to 7.5 kips within a "break in" range of approximately 10 inches of cumulative travel. Again, if the DTI is assumed to provide between 12 and 14 kips of bolt preload for the $\frac{1}{2}$ inch diameter A325 bolt, the numbers above could be translated to initial kinetic friction coefficients of between 0.21 and 0.18 and kinetic friction coefficient plateau of between 0.31 and 0.27.

Specimen	Belleville Type	DTI Method	Comments
⋆2B1WBR1	8-EH-112	1	-
⋆2B1WBR2	8-EH-112	1	-
⋆2B0WBR1	-	1	-
⋆2B0WBR2	-	1	-
⋆2B3WBR1	8-EH-112	1	-
2B3WBR2	8-EH-112	1	-
⋆2B3WBR3	8-EH-112	2	Reused Main Plate
⋆2B3WBR4	8-EH-112	2	Reused Main Plate
⋆12B3WBR1	8-EH-112	2	-
2A1WBR1	12-EH-168	1	Small Bolt Hole Separation
2A1WBR2	12-EH-168	1	One Bolt "Finger Tight"
⋆2A0WBR1	-	1	-
⋆2A3WBR1	12-H-150	1	-
⋆2A3WBR2	12-H-150	1	-
2A3WBR3	12-H-150	1	-

Table 3.1: Steel-brass SBC specimens tested with sinusoidal displacements.
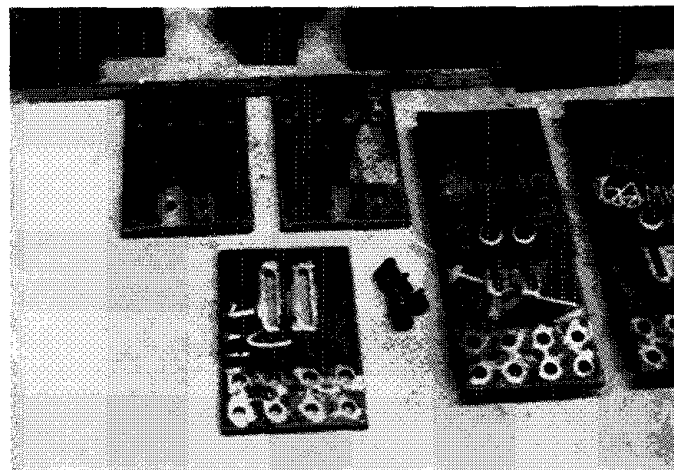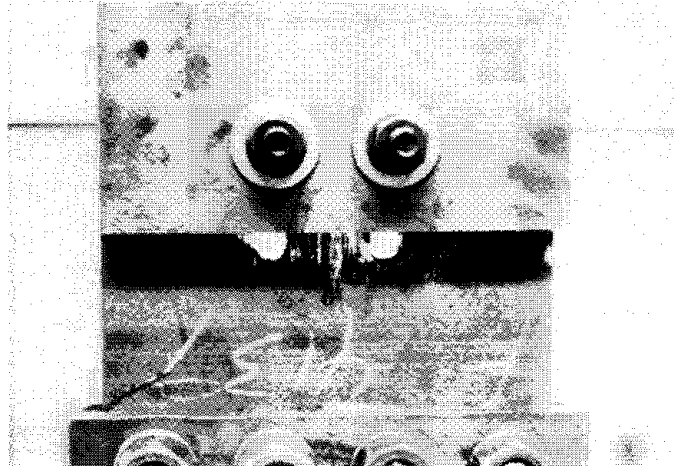
Figure 3.1: Two views of two $\frac{1}{2}$ inch bolt SBCs
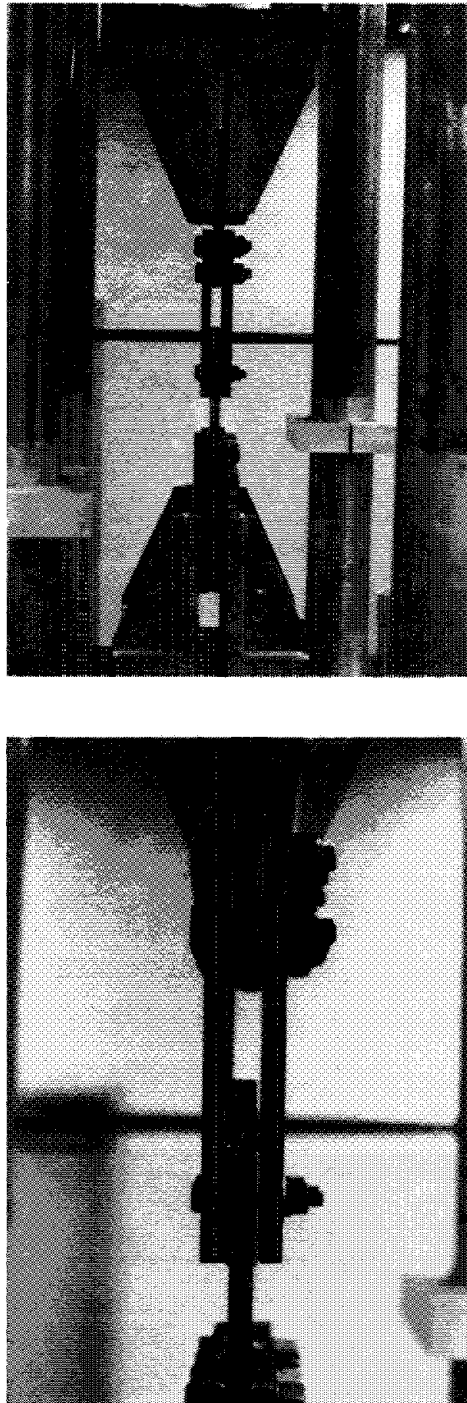
Figure 3.2: Two $\frac{1}{2}$ inch bolt SBC in MTS frame with close-up of shims.
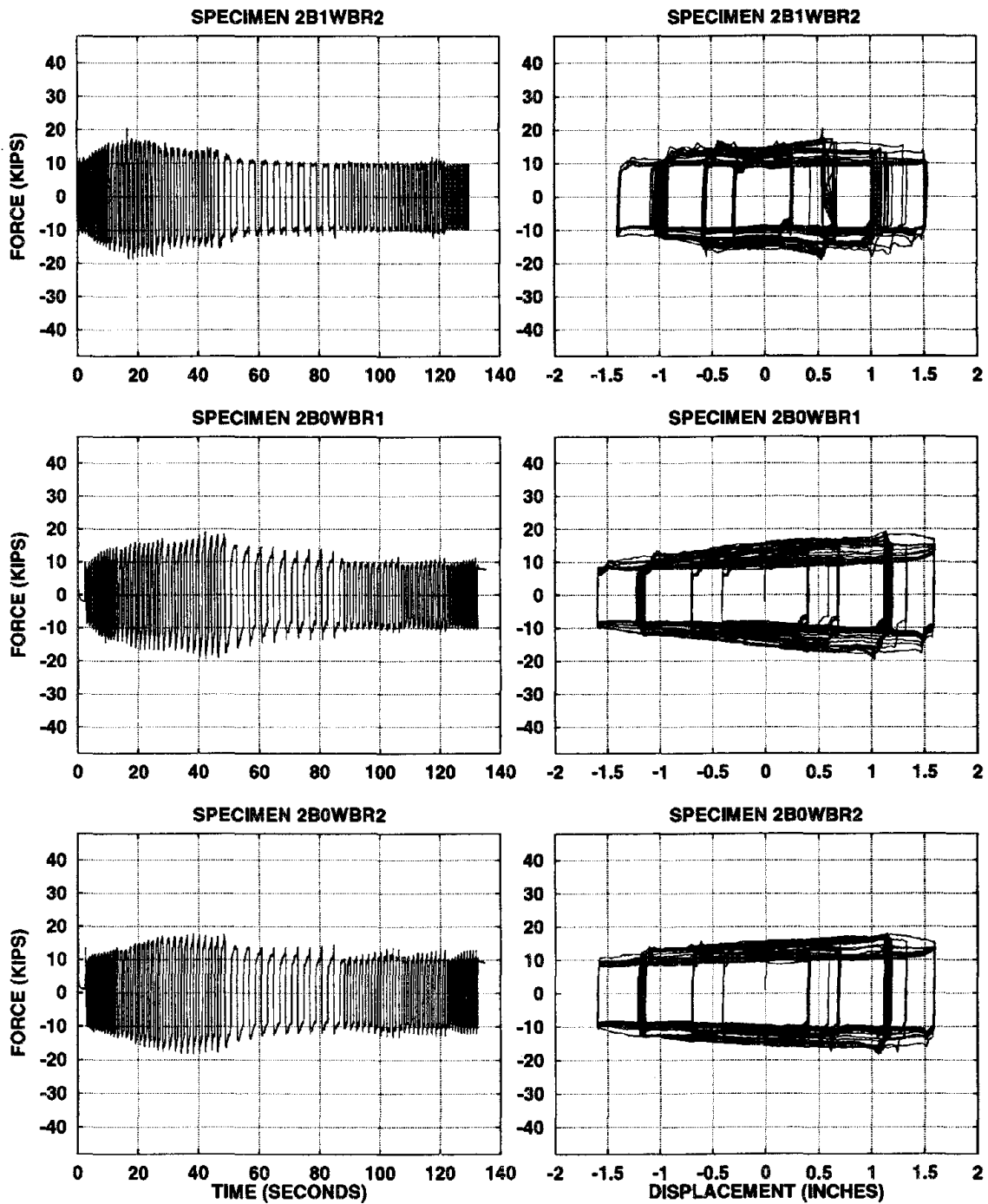
Figure 3.3: Force and hysteresis curves for 2B1WBR2, 2B0WBR1 and 2B0WBR2.
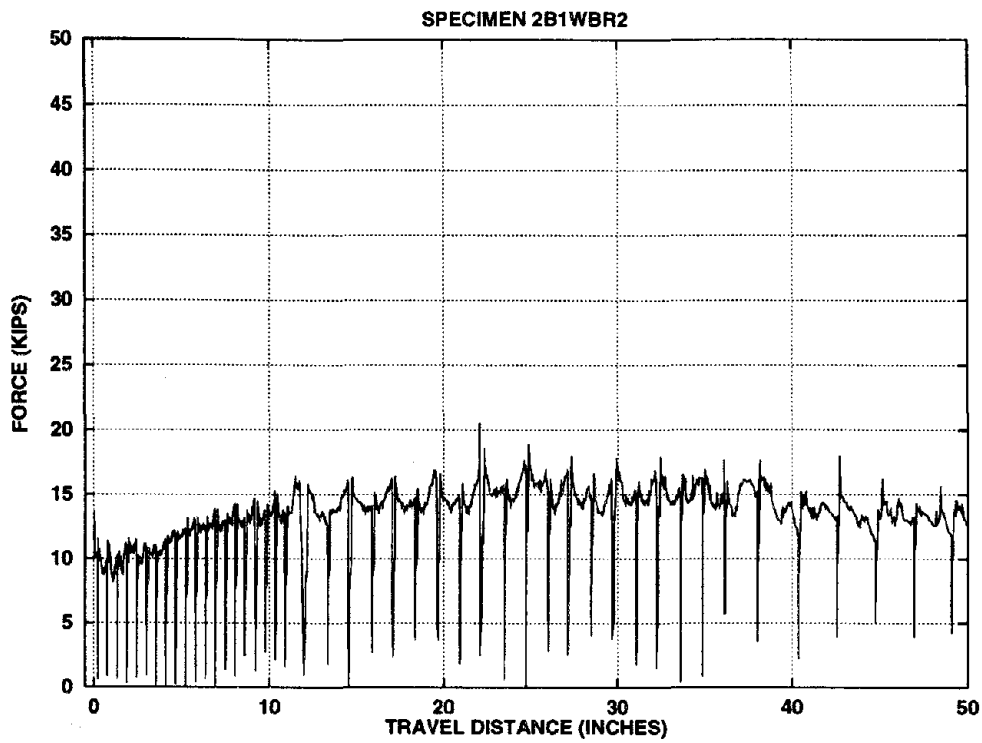
Figure 3.4: Cumulative travel versus SBC force for specimen 2B1WBR2.
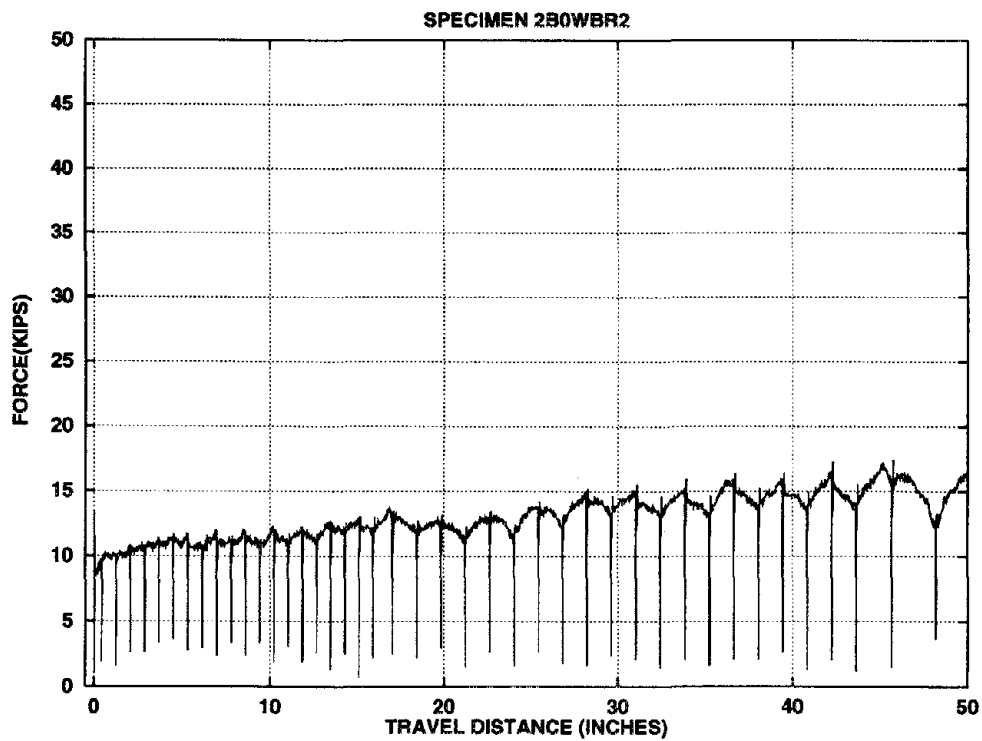
Figure 3.5: Cumulative travel versus SBC force for specimen 2B0WBR2.
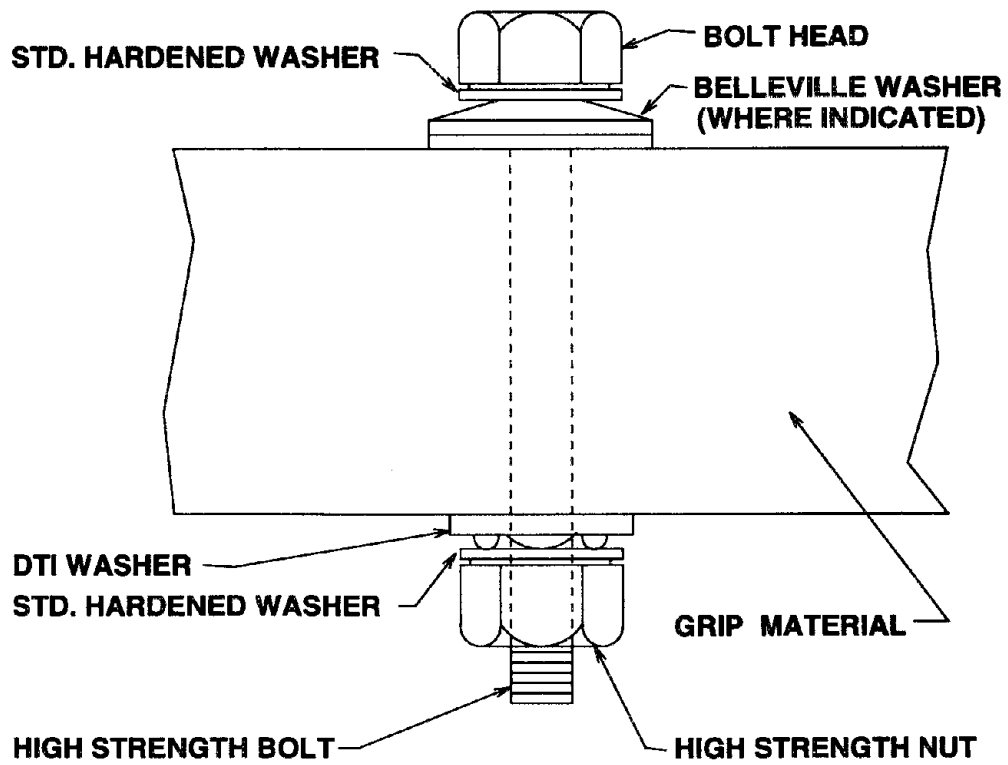
Figure 3.6: Method 2 of assembly of bolt, DTI and Belleville washers.
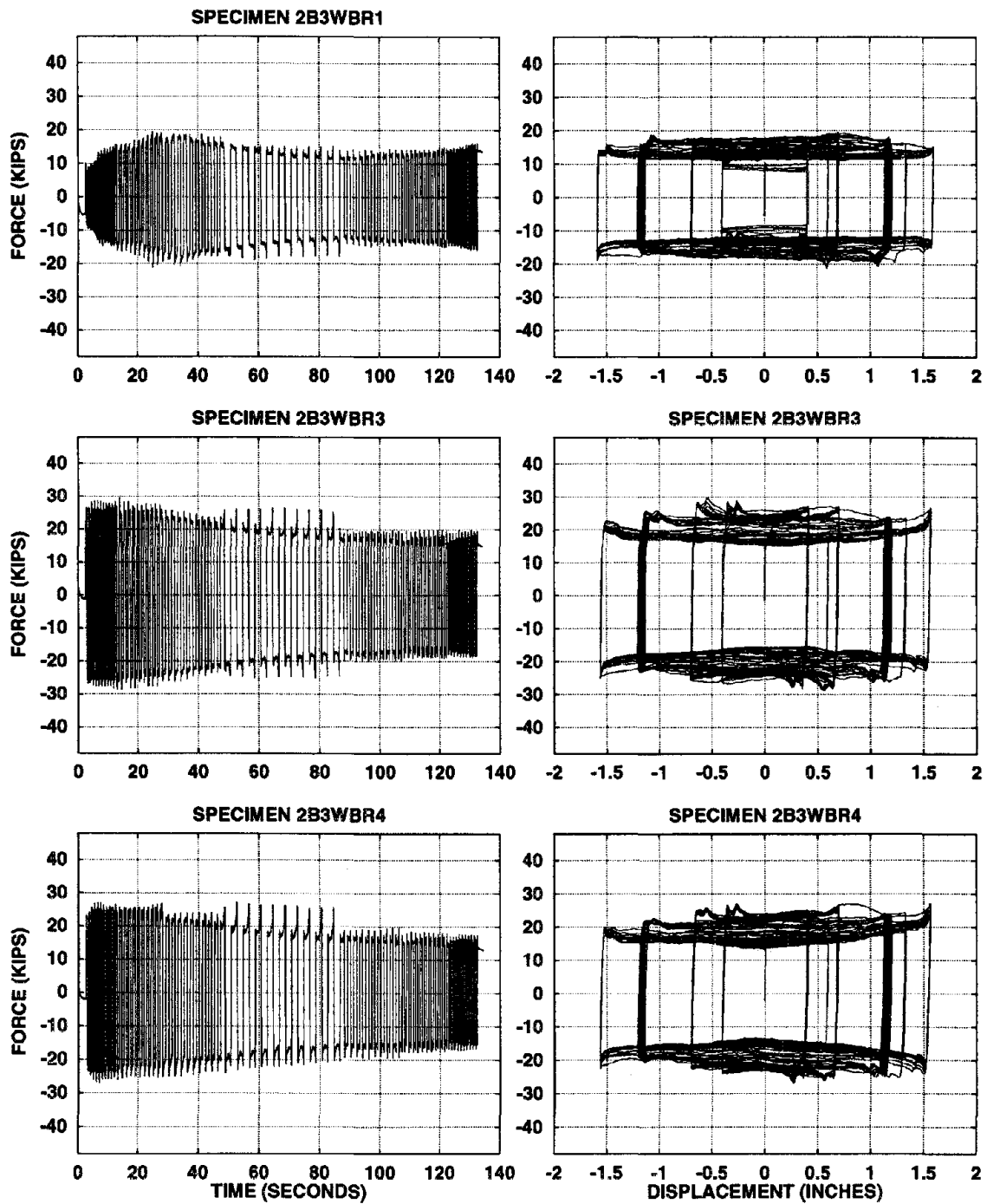
Figure 3.7: Force and hysteresis curves for 2B3WBR1, 2B0WBR3 and 2B0WBR4.
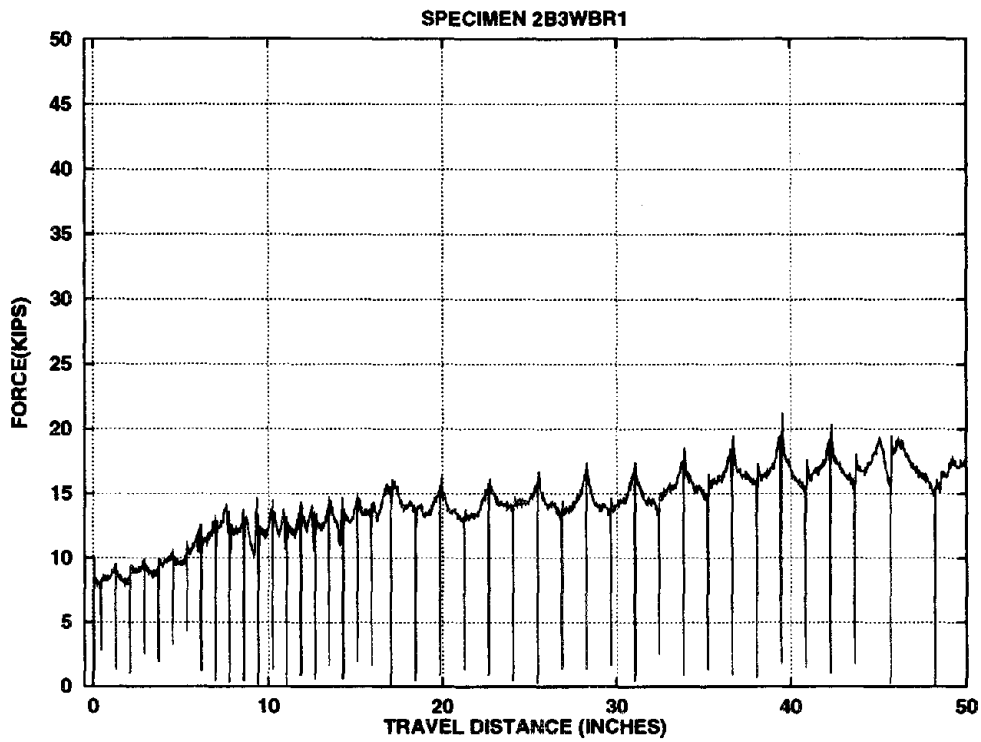
SPECIMEN 2B3WBR1

Figure 3.8: Cumulative travel versus SBC force for specimen 2B3WBR1.
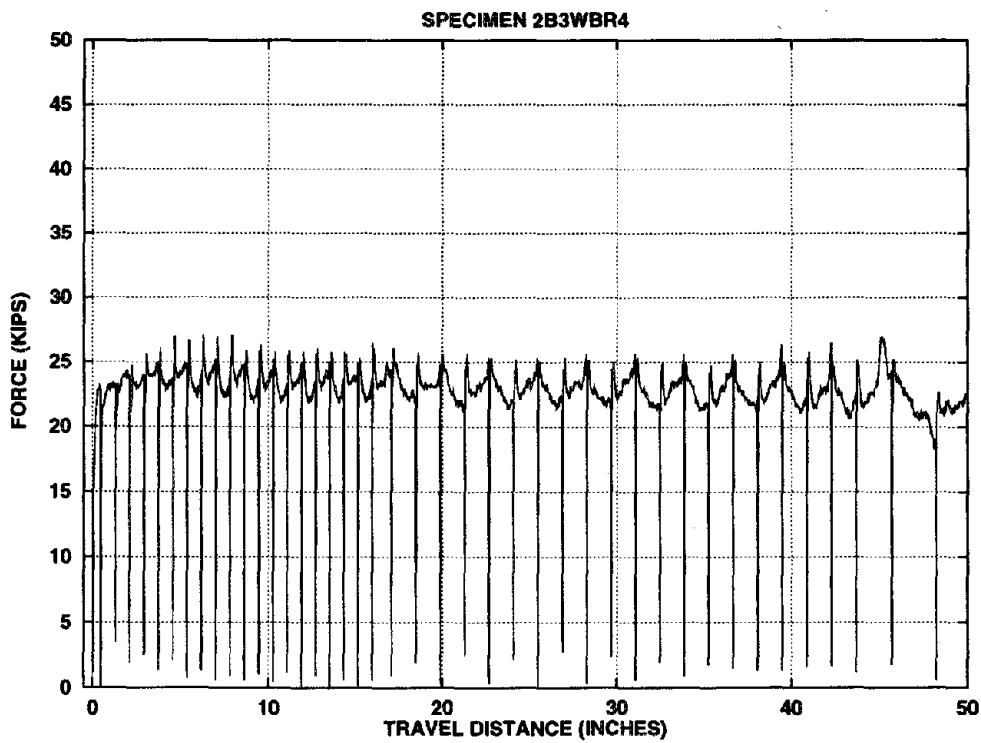
SPECIMEN 2B3WBR4

Figure 3.9: Cumulative travel versus SBC force for specimen 2B3WBR4.
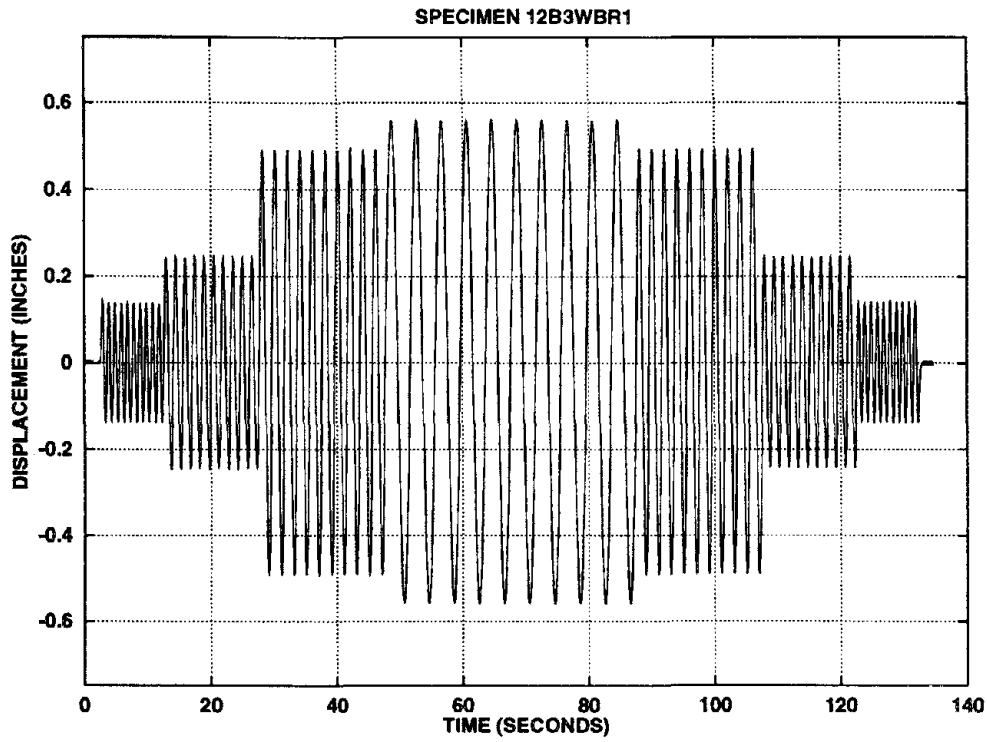
Figure 3.10: Imposed displacement history for testing of specimen 12B3WBR1.
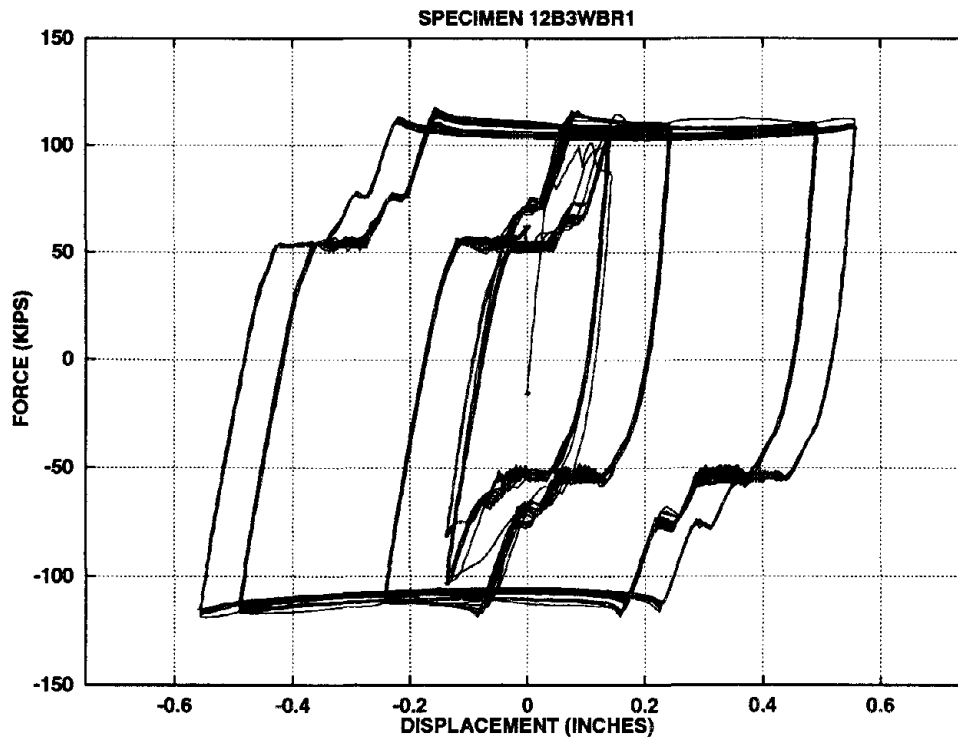
Figure 3.11: Hysteresis curves of specimen 12B3WBR1.
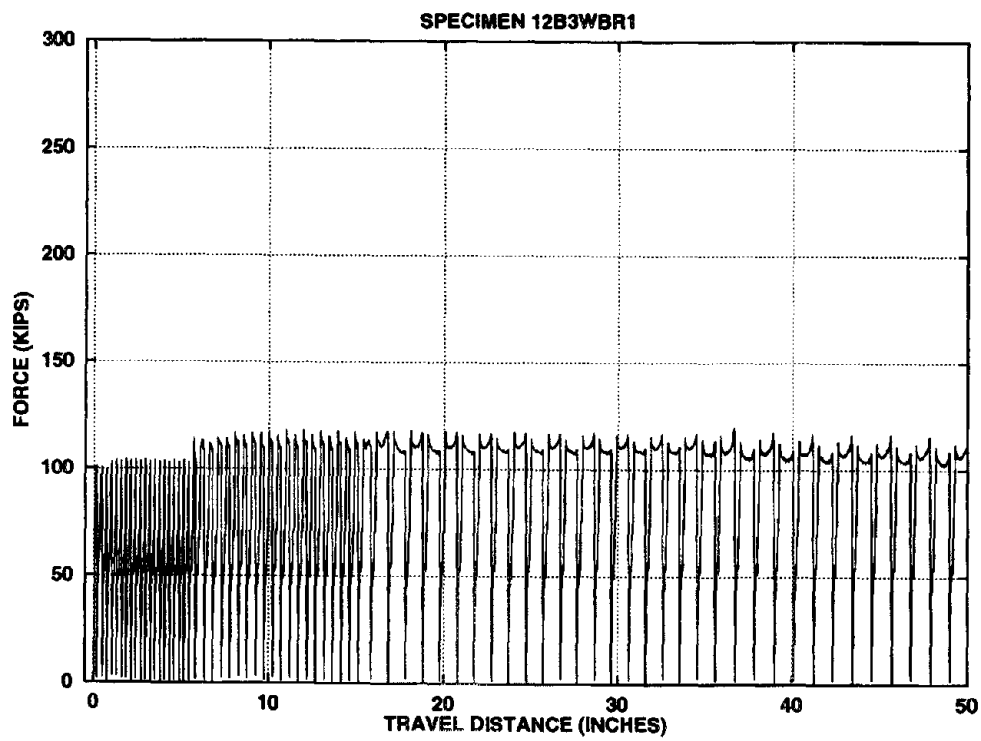
Figure 3.12: Cumulative travel versus SBC force for specimen 12B3WBR1.
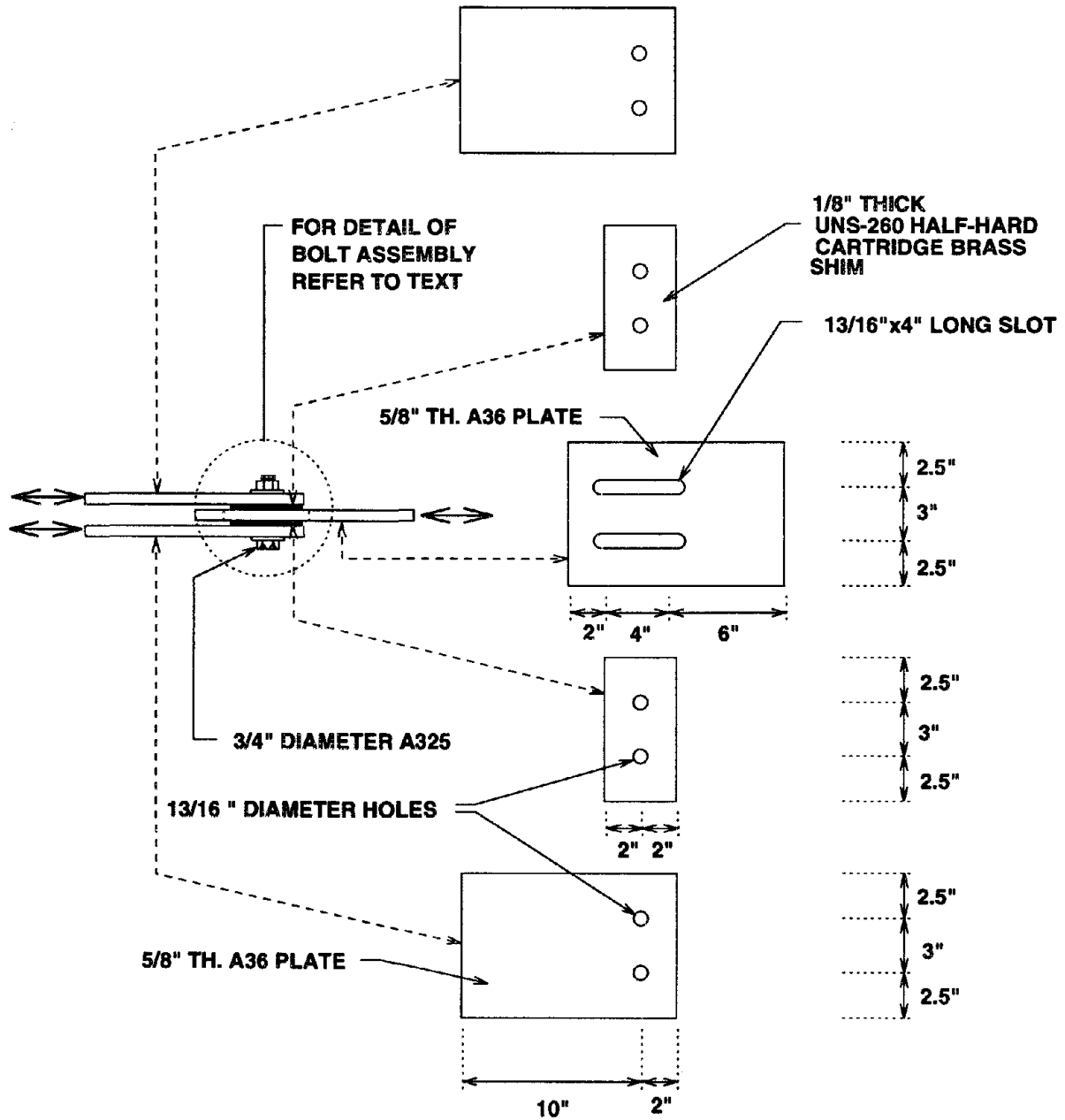
Figure 3.13: Typical detail of SBC test specimen with two $\frac{3}{4}$ inch diameter bolts.
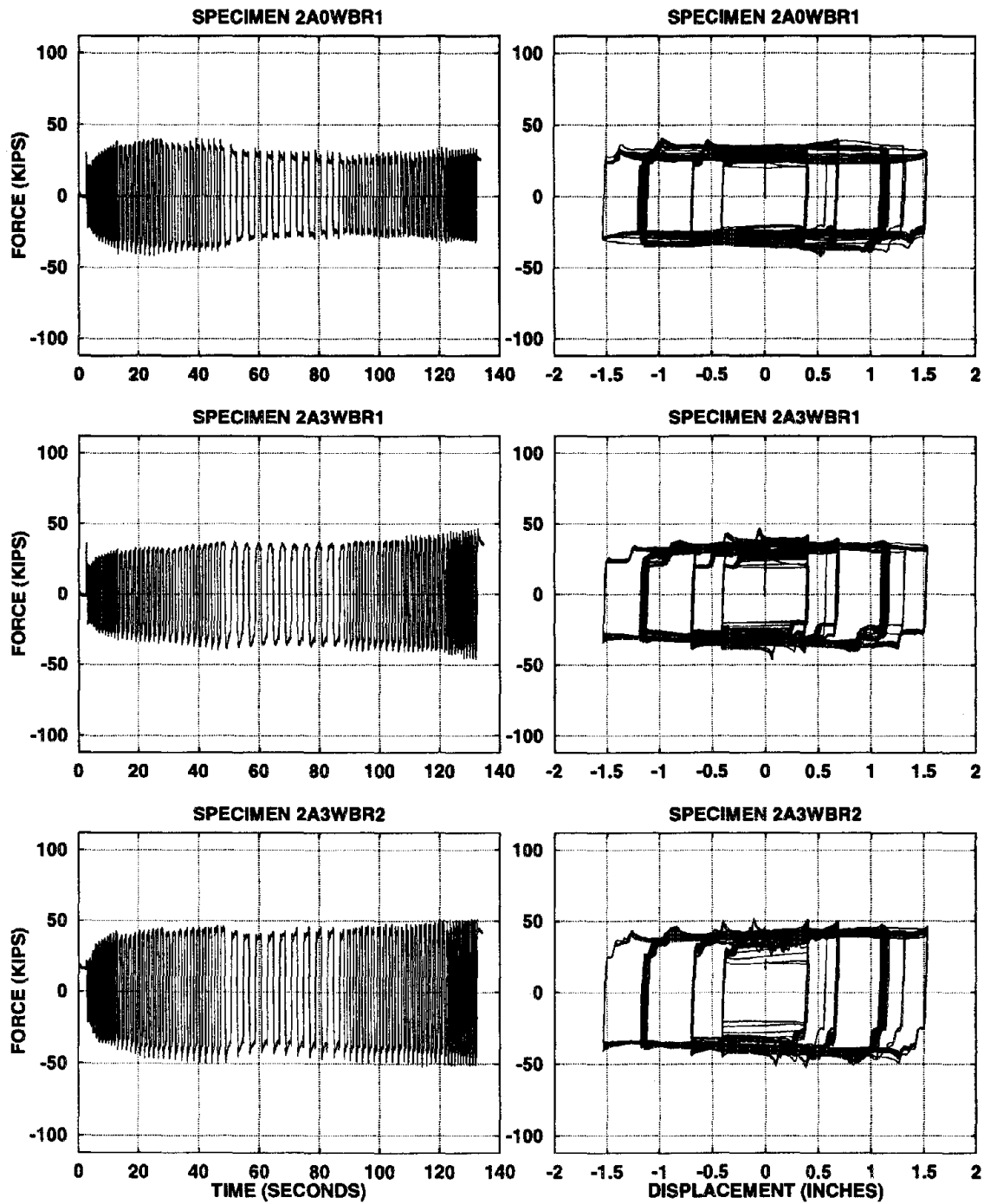
Figure 3.14: Force and hysteresis curves for 2A0WBR1, 2A3WBR1 and 2A3WBR2.
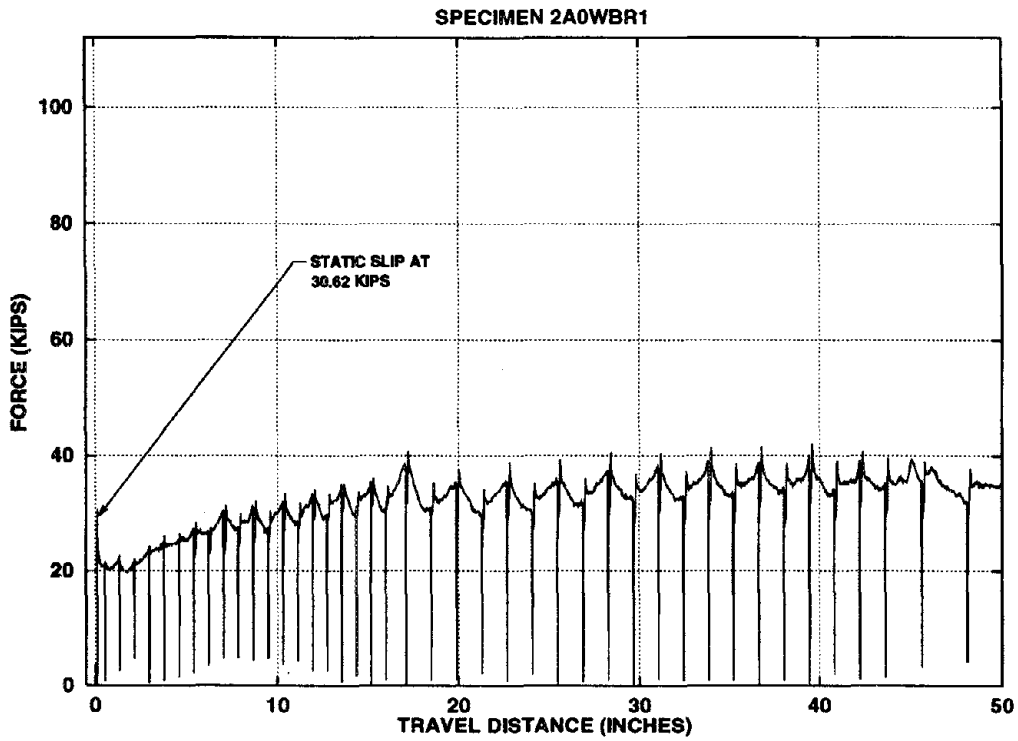
Figure 3.15: Cumulative travel versus SBC force for specimen 2A0WBR1.
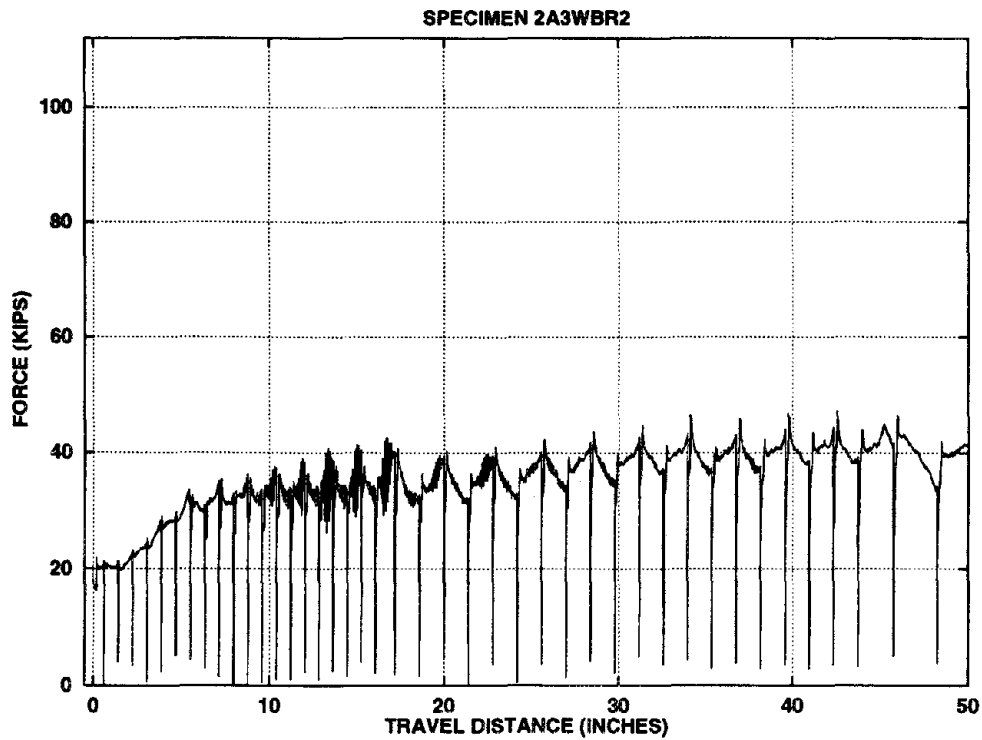
Figure 3.16: Cumulative travel versus SBC force for specimen 2A3WBR2.

Chapter 4

SBCs Under Seismic Imposed Displacements

4.1 General Remarks

SBC test results thus far presented in this document have been confined to SBC responses to imposed sinusoidal displacements. It was of interest to investigate the responses of SBCs to more realistic imposed displacements. Several steel-brass SBC specimens were tested with imposed simulated seismic displacements derived by non-linear dynamic analyses.

The testing procedure consisted of first deriving, analytically, the axial displacement histories of an SBC-type connection of a brace in a suitable mathematical structural model in response to a given acceleration history. This displacement history was then scaled, in time, to reduce velocities to within the limitations of the C/T machine. The last step in the procedure consisted of imposing these axial displacement histories onto an SBC specimen in the C/T machine and recording the results as in the tests of SBCs subjected to sinusoidal imposed displacements.

The testing of SBCs with imposed seismic displacements was done with two groups of specimens. For the first group, the analytical structural model was a hypothetical structure with a 60 kip SBC connecting its diagonal brace to the top of one the columns of the structure. For the second group, the analytical structural

model was that of the test structure to be tested on the shake table. The testing of the second group of specimens was done as a final verification of the behavior of SBCs before the implementation of twelve similar SBCs into the test structure.

Table 4.1 lists eight specimens tested under imposed simulated seismic displacements. The first four specimens listed comprised the first group mentioned, while the last four comprised the second group. The specimen designations, Belleville type and DTI method indicated in the table are to be interpreted as explained in Chapters 2 and 3. As in Chapter 3, a star ($\star$) next to the specimen designation indicates that results for the testing of the specimen are explicitly presented in this document. As was indicated in the last section of Chapter 3, all specimens discussed in this chapter have bolt assemblies identical to specimens 2B1WBR1 and 2B1WBR2, the results for which were presented in Chapters 2 and 3.

4.2 Results for SBCs of Hypothetical Structure

Figure 4.1 shows the hypothetical structure with a SBC in the diagonal brace. Member sections of the columns and the brace are indicated in this figure, together with the dimensions and the the dead load of the structure. For analysis, the SBC of the brace was assigned a 60 kip slip force. The structure was modeled as a single degree of freedom (SDOF) shear structure with a linear elastic spring, representing the horizontal stiffness contribution of the columns, and a linear-elastic-perfectly-plastic spring in parallel with the linear elastic spring, representing the horizontal stiffness and slip force contributions of the brace and SBC, respectively. A viscous damping ratio of 2% of critical damping was assigned to the structure. The DANS [33] computer analysis program, implementing a Newmark step-by-step integration method, was used for the dynamic analysis of the structure.

Four acceleration histories were used for the dynamic analyses. These were based on recorded acceleration histories from four earthquakes. The first three records were the El Centro, the Pacoima dam and the Taft records. The dates, component designations and earthquake names associated with these three records were given in Table 1.2 in Chapter 1. The fourth record used was from the Sylmar-Olive View

Medical Center record (Channel 2, 360 Degrees) for the 1/10/87 Whittier earthquake. The Taft, El Centro and Sylmar acceleration records were amplified by factors of 5, 2 and 40, respectively, to increase the response of the SBC.

Once the axial displacement histories, due to the above mentioned records, of the SBC of the hypothetical test structure were derived, these displacement histories were scaled in time by a factor of 20 to reduce the velocities to within range of the C/T machine's limitations. That is, the displacements were applied at a rate twenty times slower than the actual derived displacement history. These displacement histories were then applied, consecutively in the order of the records given above, as imposed displacements to two virgin specimens, 2B1WBR3 and 8B1WBR1. Specimen 2B1WBR3 was identical in every detail to specimens 2B1WBR1 and 2B1WBR3 discussed in previous chapters. Specimen 2B1WBR3 was tested in preparation for the testing of an eight $\frac{1}{2}$ inch diameter A325 bolt SBC, specimen 8B1WBR1. The eight bolt configuration was chosen to result in a slip force of 60 kips. The number of bolts was based on data from previous tests indicating a slip force plateau of 7.5 kips per bolt for this type of bolt assembly. Figure 4.2 shows two views of specimen 8B1WBR1. The upper photographic plate in this figure shows the specimen secured to the clevices of the C/T machine. The lower photographic plate in the figure shows a close up of the bolts assemblies. Seen in this photographic plate are the eight bolts of the connection viewed from side on which the nuts are tightened. The shiny 8-EH-112 washers are visible underneath darker appearing hardened washers, topped by high strength nuts. Three rows of bolts, with each row sharing a common slot, comprised the eight bolts of the connection. The two outer rows contained 3 bolts, while the middle row contained two bolts. As with specimen 12B3WBR1, discussed in the previous chapter, the bolt centers were positioned on two inch by two inch grid lines, and the steel plate and brass shims were, respectively, of $\frac{5}{8}$-th inch thick A36 plate material and $\frac{1}{8}$-th inch thick half hard cartridge brass.

Figures 4.3 and 4.4 show the the imposed displacements used for the testing of the two specimens, 2B1WBR3 and 8B1WBR1, and the resulting hysteresis curves for the specimens. The plots in the top rows of the two figures represent the time scaled derived SBC responses of the hypothetical structure due to the four mentioned

records. The middle and bottom rows of the two figures represent the hysteresis curves of specimens 2B1WBR3 and 8B1WBR1, respectively, due to the imposed displacement histories shown in the top plot of each column of plots in which the hysteresis curves are shown. It is seen that slip forces of very nearly 15 kips, for specimen 2B1WBR3, and 60 kips, for specimen 8B1WBR1, are reached due to the application of the imposed displacements due to the Pacoima record. With the application of next three displacement histories the slip forces in both specimens are seen to decrease, however not significantly.

Retrofits of Specimen 8B1WBR1

It was of interest to investigate the possibility of retrofitting the SBC connections. After the completion of the testing of specimen 8B1WBR1, the specimen was dismantled and reassembled with new brass shim plates and new DTIs. The bolts, nuts, hardened washers and the 8-EH-112 washers were reused. The reassembled specimen was designated 8B1WBR1A. This specimen was tested in an identical manner to the testing of 8B1WBR1. The results were, for practical purposes, identical. This specimen was also dismantled and reassembled this time not with new brass shims, but with the old brass shims turned so that the face previously facing the outer plates now faced the main plates. This specimen was designated 8B1WBR1B. Again, the specimen was tested as before. The only observable difference in the response of this second retrofit scheme was that the "chewed off corners" of the hysteresis loops had slightly exaggerated sizes due to the bolt holes in the shims having been deformed in the previous experiment.

4.3 Results for SBCs of Test Structure Model

The second group of SBC specimens tested under simulated seismic imposed displacements were tested as a part of the design process of the bracing system of the test structure to be tested on the shake table. These tests of SBCs served as a last verification step before the construction of the bracing system, with SBCs, of

the test structure. The test structure, to be discussed in the chapters ahead, was a three story one bay structure with chevron bracing with SBCs at all levels. A total of twelve SBCs, four per story, were included in the bracing system. Whereas in the case of the hypothetical structure, an SDOF model sufficed for the mathematical modelling of the structure, for the case of the test structure, the entire as-designed moment resisting frame and chevron bracing system with SBCs were modelled as a two dimensional frame with six SBCs. The nonlinear analysis program Drain-2DX [4] was used for the analysis. The details of the analytical model will be described in detail in Chapter 9.

The final design of the structure called for SBCs with 15 and 7.5 kip slip force plateaus to be used. Two specimens, 2B1WBR4 and 2B1WBR5, were tested with axial displacements derived from analyses of the as-designed test structure subjected to four ground acceleration history records. The two specimens were identical to specimens 2B1WBR1, 2B1WBR2 and 2B1WBR3 already discussed. Each of the two specimens, 2B1WBR4 and 2B1WBR5, were first subjected to two consecutive imposed displacement histories due to two acceleration histories. Each of the two specimens were then dismantled and reassembled with new brass shims, bolts, DTIs and 8-EH-112 washers but leaving one of the two bolts "finger tight" and with a second nut to have the effect of a lock nut. The reassembled specimens were then retested with the same imposed displacements as their virgin counterparts which had both bolts tightened. The reassembled specimens, each with one of two bolts "finger tightened," were designated 2B1WBR4B and 2B1WBR5B. The four ground acceleration record used were the Chile (Llolleo), the Taft, the El Centro and the Pacoima records. The dates, component designations and earthquake names associated with these records were given in Table 1.2 in Chapter 1. The four acceleration records were amplified by factors of 1.5, 6, 3 and 2, respectively following the order of the records given above. The derived displacement histories due to the Chile and Taft records were used, in the given order, for the testing of specimens 2B1WBR4 and 2B1WBR4B, while the histories due to the El Centro and Pacoima records were used, again in the given order, for the testing of specimens 2B1WBR5 and 2B1WBR5B. As in the case of the hypothetical structure, the derived displacement histories were

scaled in time by a factor of 20 to reduce the velocities to within the range of the limitations of the C/T machine.

The top two plots of Figure 4.5 show the time scaled imposed displacement histories due to the Chile and Taft records. The plots at middle and bottom of the left column represent the hysteresis curves for specimens 2B1WBR4B and 2B1WBR4, respectively due to the application of the displacement history due to the Chile record. The corresponding plots in the right hand column of the figure represent the hysteresis curves for 2B1WBR4B and 2B1WBR4 in response to derived imposed displacements due to the Taft record. Figure 4.6 shows plots, similarly arranged, for specimens 2B1WBR5B and 2B1WBR5B in response to derived imposed seismic displacements due to the El Centro and Pacoima records.

Again, it is seen that, as in the case of the results for specimens 2B1WBR3 and 8B1WBR1, the assumption that a slip force of 7.5 kips is provided by a single bolts assembled as described is verified by the results of the testing of 2B1WBR4, 2B1WBR4B, 2B1WBR5 and 2B1WBR5B. It seen that for specimens 2B1WBR4 and 2B1WBR5 slip forces of nearly 15 kips are achieved, while for specimens 2B1WBR4B and 2B1WBR5B, with one bolt only "finger tightened," the slip forces are nearly 7.5 kips. With such well behaved and predictable results, the verification process of the connections for use in the test structure, to be tested on the shake table, was considered a success. The next step in the experimental program was the construction of the bracing and supporting systems of the test structure, followed by instrumentation and testing on the shake table.

Specimen	Belleville Type	DTI Method	Comments
⋆2B1WBR3	8-EH-112	1	Prep. for 8B1WBR1 Testing
⋆8B1WBR1	8-EH-112	1	-
8B1WBR1A	8-EH-112	1	8B1WBR1 with New Shims
8B1WBR1B	8-EH-112	1	8B1WBR1A with Turned Shims
⋆2B1WBR4	8-EH-112	1	Prep. for Shake Table
⋆2B1WBR4B	8-EH-112	1	One Bolt "Finger Tight"
⋆2B1WBR5	8-EH-112	1	Prep. for Shake Table
⋆2B1WBR5B	8-EH-112	1	One Bolt "Finger Tight"

Table 4.1: Steel-brass SBC specimens tested with simulated seismic displacements.
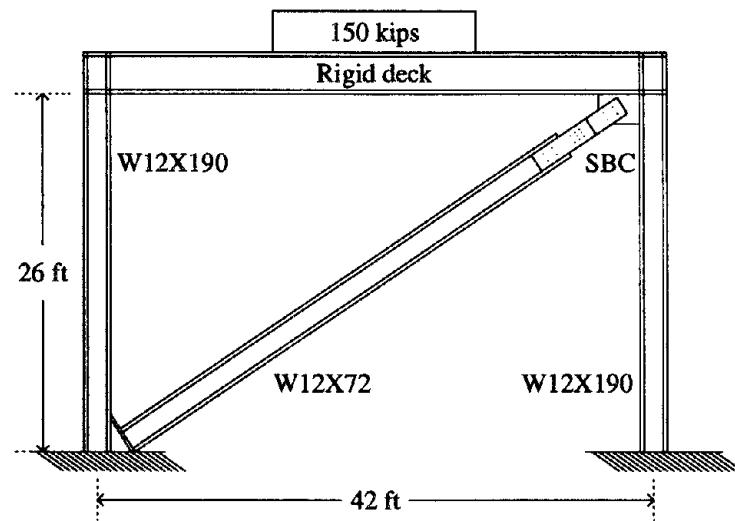
Figure 4.1: Hypothetical structure with 60 kip SBC in diagonal brace.
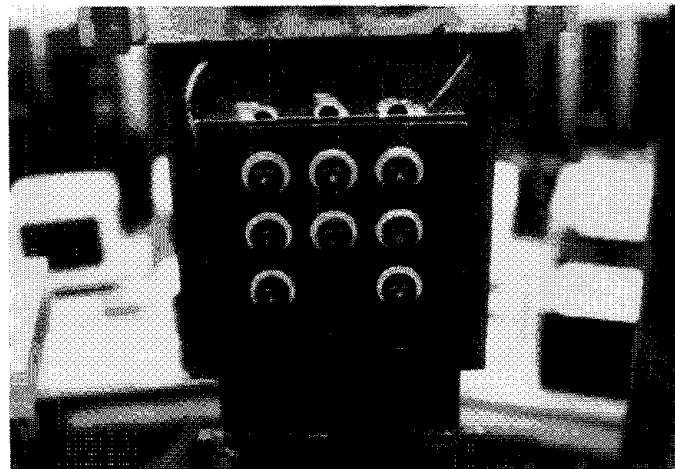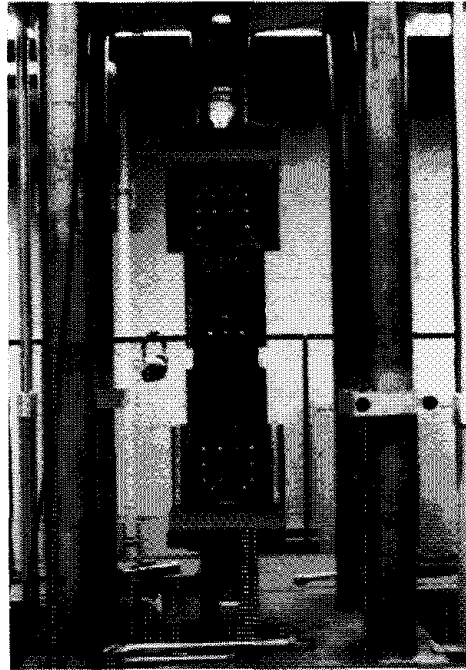
Figure 4.2: Photographs of eight $\frac{1}{2}$ inch diameter bolt SBC.
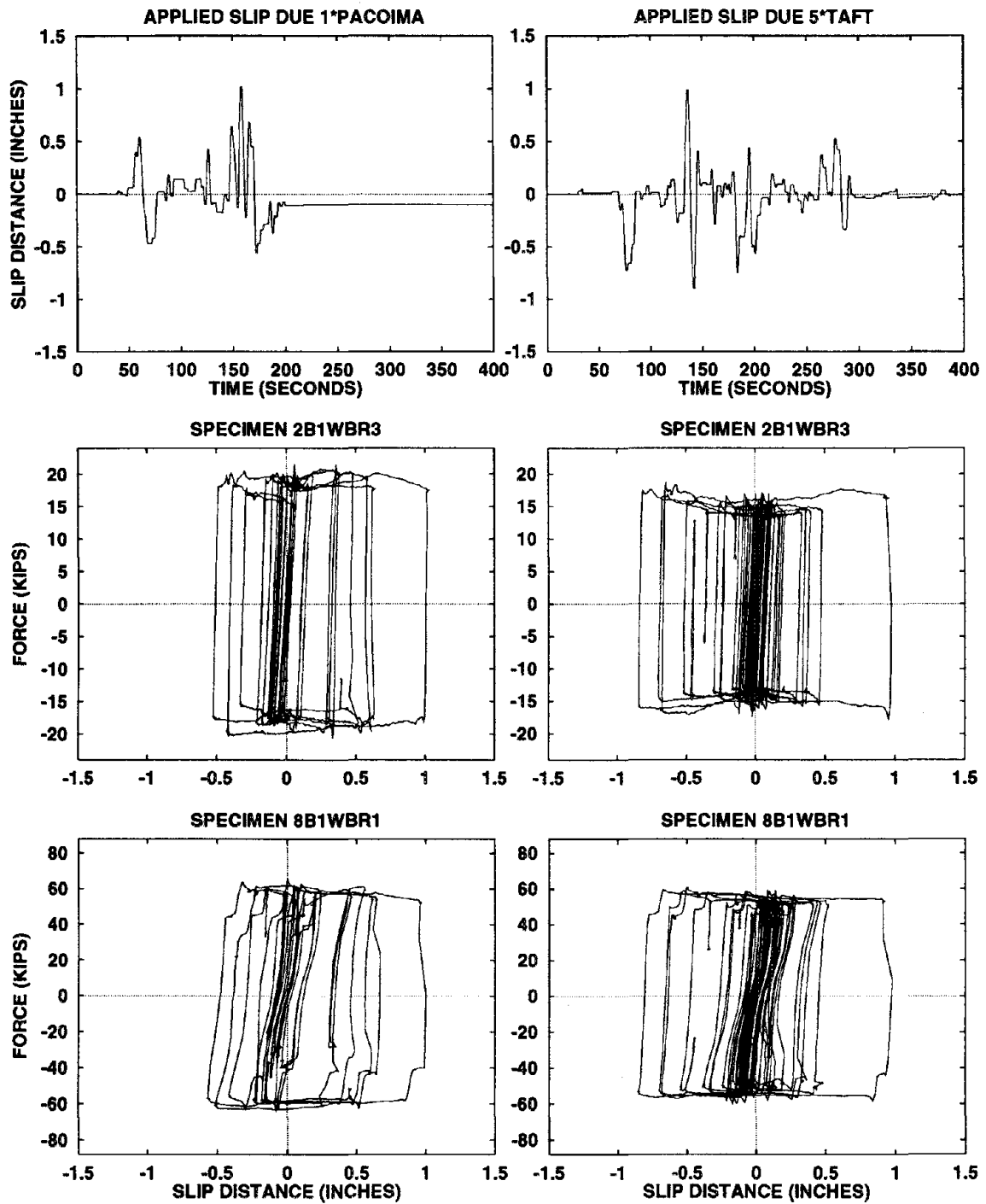
Figure 4.3: Hysteresis curves of 2B1WBR3 and 8B1WBR1 due to Pacoima and Taft.
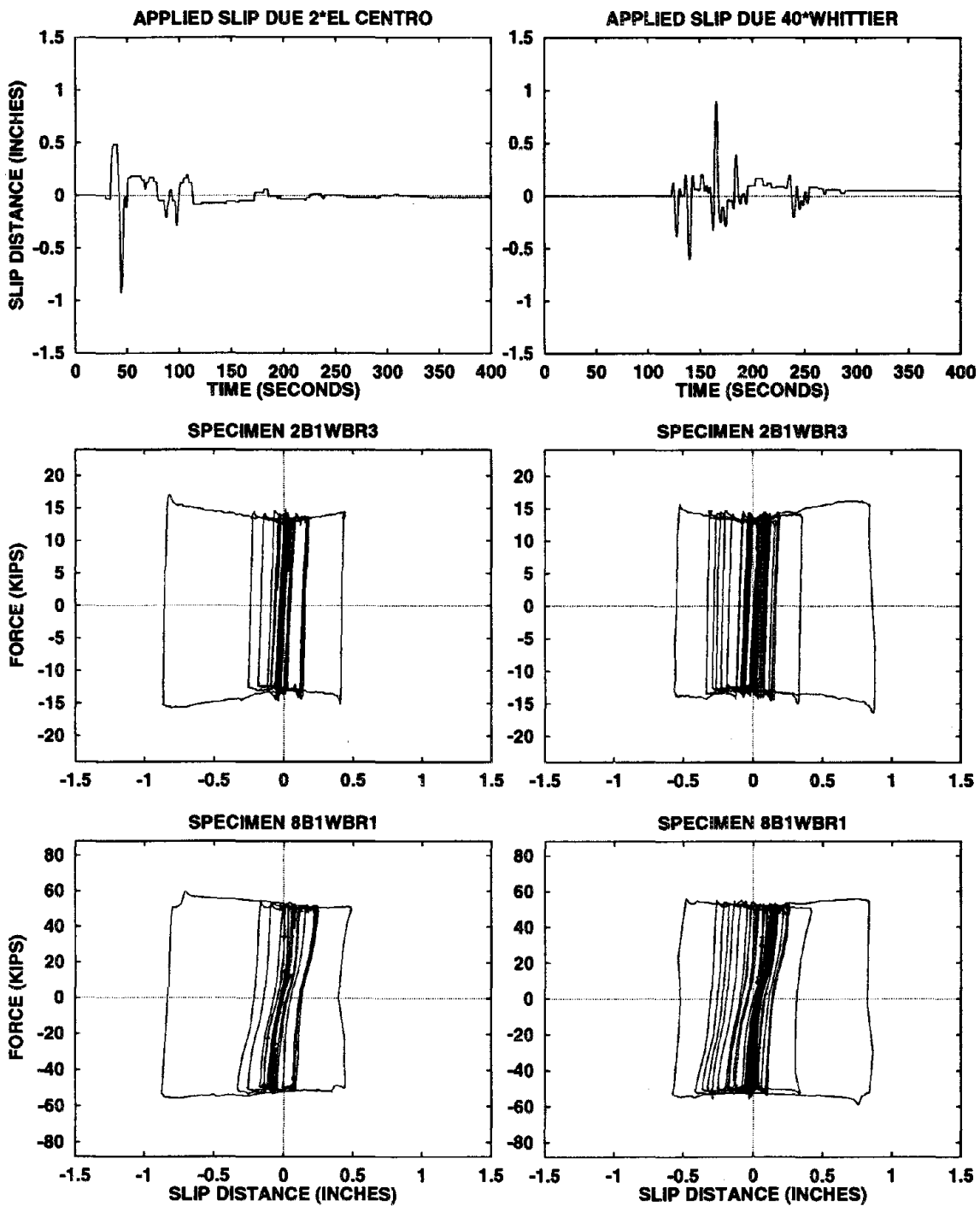
Figure 4.4: Hysteresis curves of 2B1WBR3 and 8B1WBR1 due to El Centro and Whittier.
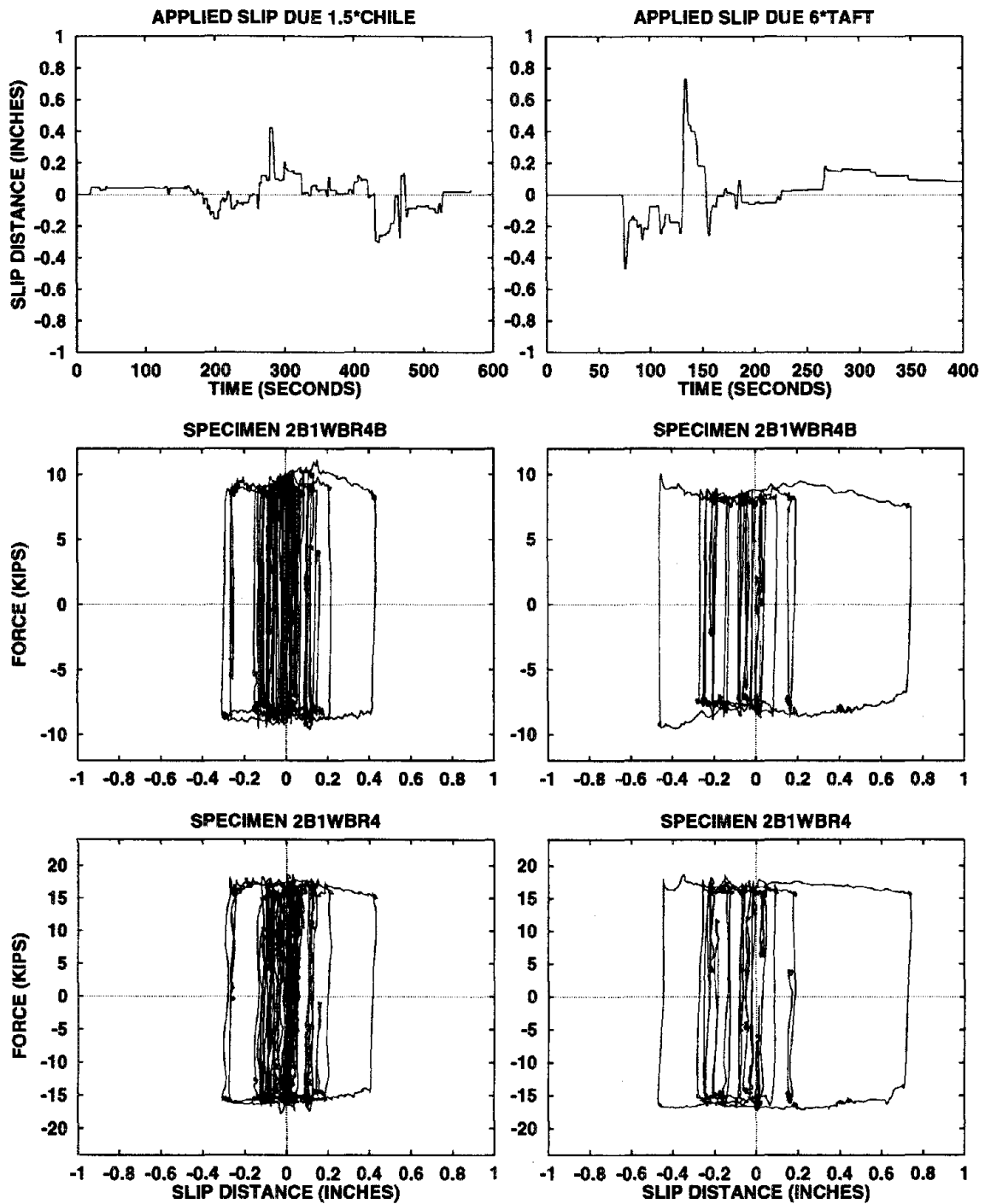
Figure 4.5: Hysteresis curves of 2B1WBR4 and 2B1WBR4B due to Chile and Taft.
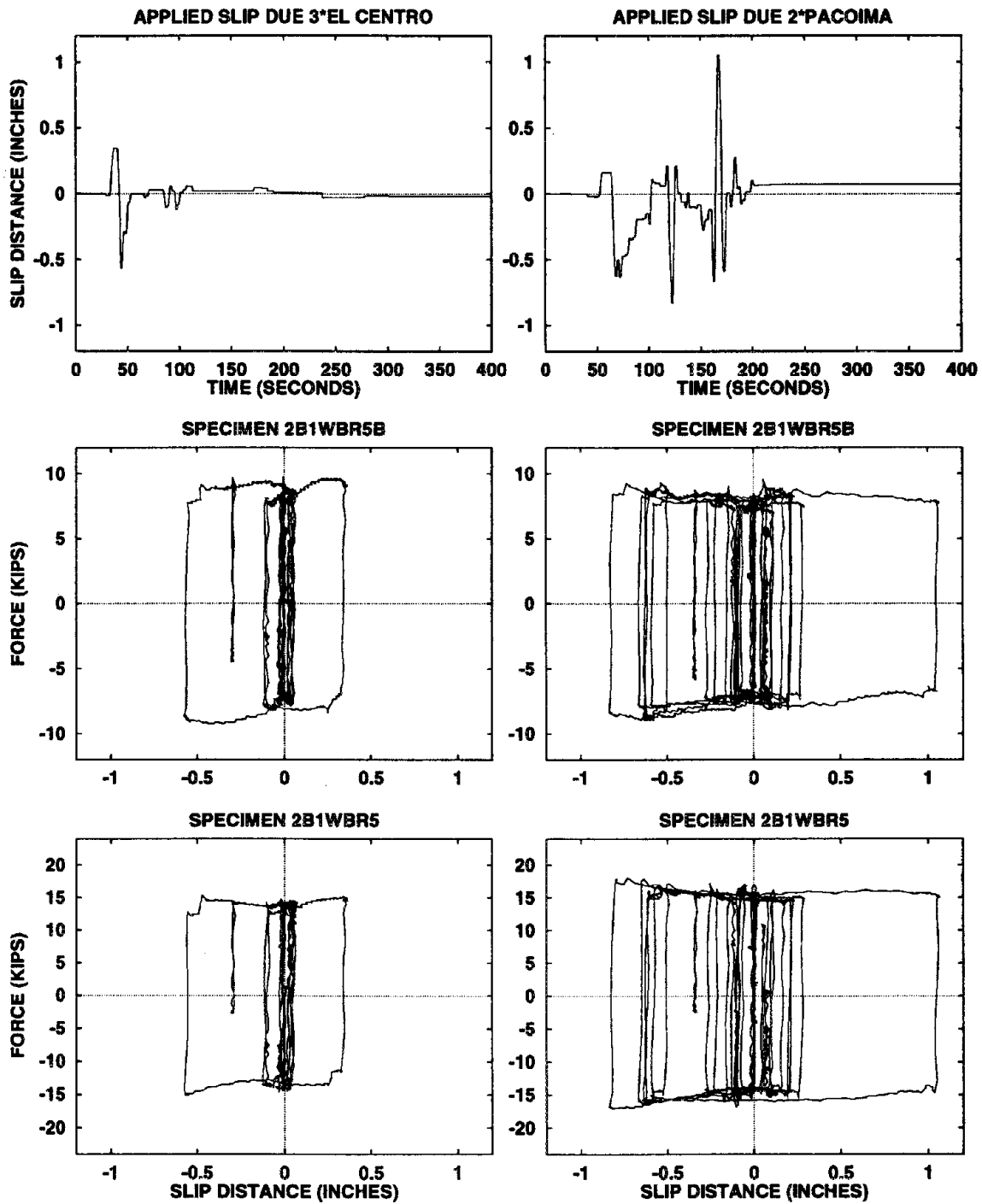
Figure 4.6: Hysteresis curves of 2B1WBR5 and 2B1WBR5B due to El Centro and Pacoima.

Chapter 5

Shake Table Tests

5.1 Purpose

The results of the experimental testing of SBCs on the C/T machine gave strong indication that the SBCs could provide an inexpensive and uncomplicated source for energy dissipation in a structural system subjected to strong seismic excitations. The simplicity, in behavior and physical assembly, of SBCs suggested that both analytical modeling of structural behavior and physical implementation of the connections into a real structure were feasible.

There were however certain issues that, despite analytical simulation and experiment on the C/T machine, begged verification through actual shake table testing of a structure fitted with SBCs. Simply put, the analytical simulations indicated performance that was "too good to be true." Simulations of the Clough and Tang structure [24, 8, 23] loaded with the masses used to load the said structure by Whittaker, et al. [31] indicated very small displacements and inter-story drifts in response to rather strong seismic excitations. This structure, with the said masses, was mentioned in the last chapter, where it was used as an analytical model to derive displacements to be imposed on SBCs in the C/T machine. Such good performance in reducing displacements was even more suspect as it was achieved, in one design case, by using only four $\frac{1}{2}$ inch bolts, one per SBC of brace, in the second and third levels and eight such bolts, two per SBC of brace, in the first level. In addition, while the

behavior of individual SBCs was well understood, their effect on and the interaction with a structure was only studied through analytical simulations. Experimental data, such as that from shake table tests of a structure, would be necessary to justify the soundness of the use of such simulations.

Moreover, for such a novel concept as the SBCs to gain the confidence of the professional community it was necessary to demonstrate conclusively that a real structure including SBCs could be designed and built using the knowledge gained from the testing of the connections in the C/T machine. Further, it would be needed to demonstrate that the structure could be designed using relatively widely available analytical tools and that the structure could be built using conventional fabrication techniques.

It was decided to test on the shake table the retrofitted Clough and Tang frame with chevron bracing connected with SBCs and based on the designs achieved by trial-and-error through simulations of the test structure. As mentioned above, histories of slip at representative braces for one of the designs were used to test several SBCs as a last verification of the performance of SBCs before the retrofit of the structure began. The results for these tests were presented in Chapter 4. The present and the next three chapters deal entirely with the shake table tests, their results, their implications and their comparison with analytical simulations. This chapter presents a description of the testing set-up, including the shake table, the test structure, the instrumentation and the schedule of the table input signals and their description.

5.2 The Shake Table

Detailed information on the characteristics and specifications of the Earthquake Engineering Research Center's (EERC) shake table can be found in [20, 21]. This section attempts to convey a general picture of the fundamental workings of the shake table.

Figure 5.1 shows a schematic representation of the test structure secured to the shake table. The table itself is a 20'×20' reinforced and post-tensioned concrete

platform weighing 100,000 lbs. When in operation, the sealed pit under the table is pressurized. The maximum allowable pressure in the pit is dictated by the strength of the nylon fabric seal. The usual operational pressure of the pit is between 2 and 3 psi over atmospheric pressure. This pressurization, combined with the action of four vertical 25 kip hydraulic actuators and four passive stabilizers, shown in Figures 5.1 and 5.2, supports the dead vertical load of the table and structure above. The pressurization can by itself support the shake table together with a 130 kip structure, however the actuators are needed to stabilize the the table when subjected to overturning moments imparted to it from structures tested. The vertical actuators and stabilizers are responsible also for controlling pitch and roll of the table. Three 70 kip horizontal hydraulic actuators, shown in Figures 5.1 and 5.2, produce horizontal motions in the table. The actuators are supplied with oil at 3000 psi of pressure generated by four 90 gpm pressure regulated pumps. Each pump is driven by a 120 hp electric motor. The actuators react against a reinforced concrete foundation encasing the sides and bottom of the pit and weighing 1,580,000 lbs. With this configuration the table can achieve a maximum horizontal displacement of 5 inches, a maximum horizontal velocity of 25 inches/second and a maximum horizontal acceleration of 1.5 Gs.

The positions of the actuators and the test structure in relation to the table are show in plan view in Figure 5.2. This figure also indicates the positions of some of the table instrumentation. These will be described in the next sections. Heavy dots marked "V" and "P" indicate the locations of the vertical actuators and passive stabilizers respectively. Arrows denoted "H" indicate the positions of the horizontal actuators. The positions, on the table, of the Eastern and Western longitudinal frames of the test structure are also indicated in this figure. The test structure was bolted to steel, I-sectioned, foundation beams which were, in turn, post-tensioned to the table.

5.3 The Test Structure

The ductile moment resisting space frame, chosen to be retrofitted with SBC and tested on the shake table, was that constructed for the original experi-

mental work by Clough and Tang [24, 8, 23] in 1973. The main purpose of that study was to define and verify mathematical modeling procedures used at the time for predicting earthquake response of steel moment-resisting frames. The structure was not designed as a similitude-scaled model of a larger structure, but rather as a "small structure". The Clough and Tang structure consisted of two identical three story, single bay, moment-resisting steel frames. The frames were connected by floor diaphragms consisting of transverse beams and trusses. The columns and beams of the structure were W5×16 and W6×12 rolled sections. The moment connections were typical all-welded connections. Total panel zone thickness of the columns in the connections, after reinforcement, was one inch. The frame was originally loaded with roughly 8,000 pounds per floor. References [24, 8, 23] provide further detailed information on the design and construction of the structure.

Clough and Tang Structure Braced with SBCs

In order to produce significant slips in SBCs of a bracing system installed in the Clough and Tang structure, it would be necessary that large inertial forces be generated at the story levels of the structure. Following the work of Whittaker, et al. [31], in which the Clough and Tang frame was retrofitted with the ADAS energy dissipation system, it was decided to load the structure with roughly 30,000 pounds per floor. Whittaker, et al., tested the structure as a "small structural system and not as similitude-scaled replica of a full scaled building." The same approach was used in the testing and design of the test structure braced with SBCs.

Figure 5.3 shows photographs of a side elevation and an isometric view of the test structure in its final form, with braces and SBCs in place. A chevron configuration for the longitudinal bracing system was seen to be the most practical bracing configuration. The final design consisted of adding to the Clough and Tang frame twelve braces, of $3 \times 3 \times \frac{3}{16}$ inch hollow square tube section, with one SBC connecting each to gusset plates located at midspans of longitudinal beams. Figure 5.4 shows the dimensions and configuration of the bracing elements. Table 5.1 indicates the section properties of the moment frame and the bracing system. The braces resulted in six

chevrons, one per each bay of each story of the two frames. Transverse braces were also provided by $2 \times 2 \times \frac{3}{16}$ inch angle members, in double-angle form, in X-configurations in the first story and chevron configurations in the upper two stories. The chevron configuration in the upper stories was necessary to allow the ballast concrete blocks and lead packets to fit into the structure.

A typical detail of the horizontal diaphragms connecting the frames is shown in Figure 5.5. As shown in Figure 5.6, the reactive masses or ballasts rested upon the top flanges of the outer two W6×12 transverse beams of the diaphragms. It was assumed, at time of design, that the truss systems would cause the diaphragms to be stiff enough to be effectively considered rigid in the analytical model of the structure. Results will be presented in Chapter 8 indicating actual behavior very different from that assumed. The diaphragms proved to be far more flexible that originally thought. The ballast consisted, per floor, of two 4,000 pound concrete blocks and forty three 510 pound packs of lead ingots. The concrete blocks were positioned onto angle brackets welded to the transverse beams and tied down against the brackets with threaded rods going vertically through the blocks and tightened to angle sections reacting against the transverse beams below. The lead packets were individually laid over the blocks and then strapped down with tensioned steel strapping. As a measure of safety, the packets at the two ends of the blocks, extending out from the structure, were secured to the blocks by channel sections and threaded rods.

The SBCs, one at the top of each brace, were identical to the $\frac{1}{2}$ inch bolt SBCs with two bolts presented in Chapters 2 through 4. The DTIs were used as described by "Method 1" of the manufacturer's instructions. One 8-EH-112 Solon compression washer topped with hardened flat washers was placed under the nut of each bolts. As noted in Chapter 3, later experiments indicated that the use of these washers was not as beneficial to the performance of the SBCs as first thought. The shim plates were of the usual $\frac{1}{8}$ inch thick UNS-260, half hard cartridge brass. A typical detail of the brace-to-SBC-to-beam connection is shown in Figure 5.7. The $\frac{5}{8}$-th inch thick main plate of the SBCs "fish tailed" into slots cut into the $3 \times 3 \times \frac{3}{16}$ inch hollow square tube braces. The outer plates of the SBCs were then bolted onto a

$\frac{7}{8}$-th inch thick plate which was welded onto a 1 inch thick plate to form a T, the web of the T being the vertical $\frac{7}{8}$-th inch thick plate and the flange being the 1 inch thick plate. This flange was then, in turn, bolted and welded to the W6×12 longitudinal beams of the frame.

The connection presented is not necessarily an example of the way SBCs would or should be implemented in the field. Rather this connection detail was the most appropriate and convenient design for experimental purposes. The plates of the aforementioned T could have been selected to have been thinner and welding, rather than bolting, could be used to attach the outer plates of the SBCs to the T stem and the T webs to the longitudinal beams. However, the need for over-conservatism in an experimental detail and minimization of damage, such as would be cause by welding, to the moment frame dictated the necessity of a design such as that shown in Figure 5.7. Further, this design allowed for the possibility of quick dismantling of the SBCs, in case this was necessary, and it eliminated the need for any steel shims that would be needed to compensate for the difference in thickness of the gusset plates and the separations between the outer plates of the SBCs due to the thickness of the middle plates and the brass shims. The use of eight $\frac{3}{4}$ inch A325 bolts, resulted in a factor of safety of roughly 7 against static slip, relative to a maximum possible SBC slip force of 20 kips. Although, the use of such a large factor of safety in this design raised quite a few eyebrows, the author feels justified as, firstly, it was not time-efficient to use any reliable bolt tension verification methods on these bolts, and secondly, there is little data on the behavior of "slip-critical" bolts under cyclic loads of large magnitude. Needless to say, in this experimental setting it was not desirable that slips occur anywhere in the braces other than in the SBCs. The bottoms ends of the braces were connected to the moment frames as shown in the bottom plate of Figure 5.8.

Three different structural configurations were to be tested. The difference in the three consisted solely of differences in the SBC slip forces. The three configurations, with different numbers of tightened SBC bolts, are designated in this document as TS1, TS2 and TS3, with TS being acronym for "test structure."

The TS1 Configuration

This design called for 15 kip SBCs at the first level and 7.5 kip SBCs at the upper two levels. This was accommodated by using the detail already presented and leaving one of each of the two bolts of the SBCs of the upper two floors loose. That is, one of each of the two bolts of each of the SBCs in the upper two floors was only "finger tightened" and secured with two nuts to produce the effect of a lock-nut. It will be recalled, that results for the tests of such SBCs were presented in Chapter 4.

The TS2 Configuration

The TS2 design called for 15 kip SBCs at the first two levels and 7.5 kip SBCs at the third level. This was accomplished by simply tightening the "finger tight" bolts in the second levels in the usual manner. This was done on the third day of testing after tests of TS1 were completed.

The TS3 Configuration

The TS3 configuration was designed to induce torsional moments on the structure. For this purpose, one from each of the two tightened SBC bolts in the western braces of the first level of TS2 were removed. This was done approximately two weeks after the completion of the testing of TS2.

Fabrication and Assembly

The components of the SBCs and their connections to the beams, the transverse and longitudinal braces and the bottom brace connections were all fabricated at a local steel fabrication shop. The entire retrofit process took four months to complete. The process included the removal of the unnecessary additions to the frame, mementos of experimenters from the past, the straightening by heat treatment of several columns bent out-of-straight over years of subjection to various abuse, the assembly of the individual pieces of the bracing system into the structure, through drilling, bolting and welding, the loading of the ballast onto the structure, the post-tensioning of the structure onto the table and the addition of a fresh coat of bright

orange paint to the body of the moment frame. The author was assisted in these activities by an experienced and highly professional welder/ironworker.

5.4   Structure and Table Instrumentation

In addition to the work described above, eighty one strain gages were attached at various locations of the structure. For each strain gage installation, the installation surfaces were sand-blasted, smoothed with two fine grades of acid wetted sand paper, then neutralized. Each installed strain gage was coated with a special resin coating in order to protect it from the environment of the lab located adjacent to the San Francisco Bay. Also installed were twenty wire-potentiometers, for measuring various displacements, and eight accelerometers. The locations and purpose of these instruments, as well as those on the shake table, are the subject this section.

The data acquisition system at the EERC allowed for data sampling at 200 Hertz of seventy channels used in the testing of the structure. Originally sixty eight were used. After the second day of testing, two more channels were added to better monitor the behavior of the horizontal diaphragms. The channels, each of which corresponded to a reading from an instrument or a combination of instruments, were numbered 1 to 71, with channel 70 being defunct.

Table Instrumentation

Data channels 1 through 13 were devoted to the table instrumentation. Only data from channels 1 through 4 and 6 through 9 were utilized in this study. The locations and types of instruments associated with these channels are shown in Figure 5.2. Given the data from these channels, the table acceleration, displacement and pitch at any instant could be established. In this figure, and in the rest of the text of this document, "longitudinal" refers to orientation parallel to the north-south lines, while "transverse" refers to orientation parallel to east-west lines.

Structure Instrumentation

Data channels 14 through 69 and channel 71 were used to monitor the structural behavior. Of primary importance, in this monitoring, was the behavior of the SBCs. For each of the SBCs, the axial force through the SBC and the slip distance along the axis of the brace were monitored. This was accomplished by using one wire-potentiometer per SBC and a circuit of four strain gages per each brace. The wire-potentiometers were secured to the outer plates of the SBCs which were, in turn, bolted to the gusset plates. The wires were then attached to a bolts tapped into the braces below the points of attachment of the braces to the main plates of the SBC. Of the four strain gages on each brace, two measured strains coaxial with the brace while two measured Poisson strains. The wire-potentiometers and the strain gage circuits were calibrated to read force and displacement values directly. Figure 5.8 shows, in the top and middle plates, an SBC wire potentiometer and a brace strain gage circuit. The data channels corresponding to the SBC wire potentiometers and brace strain gage circuits were numbered 38 through 49 and 20 through 31 respectively. The locations of these instruments on the two longitudinal frames of the structure are shown in Figures 5.9 and 5.10. Of interest was also to monitor the bending moments in one typical brace. This was accomplished by adding a single strain gage at the bottom of the south-western brace of the first story of the structure. The data channel for this gage was channel 66, also shown in Figure 5.9.

In addition to the monitoring of the SBC behavior, certain structural response quantities such as relative story displacements, story inter-story drifts and story shear forces were also of interest. The first two of these quantities could be monitored through an array of six wire potentiometers. The six wire potentiometers, one per each level of each longitudinal frame, were secured to a stationary instrumentation wall to the south of the test structure. The wires were attached to hooks spot welded onto the structure at selected locations. Channels 15 through 20 correspond to these wire-potentiometers. The points on the structure to which the wires of the wire-potentiometers were connected are shown schematically in Figures 5.9, 5.10 and also Figure 5.11, where the locations of the instruments are given in terms of their

vertical distance from the surface of the table. For the measurement of story shear forces, instrumentation was provided for three approaches. The first two approaches consisted of measuring the acceleration of the story masses. Knowing these accelerations, inertia forces acting at each level could be calculated from the knowledge of the value of the masses. These inertia forces would then be used to approximate the shear forces at each level of the structure. For structures with low viscous damping such an approximation can be very good. Six accelerometers were devoted to this purpose. Three were positioned at each level of the western longitudinal frame of the structure. Another three were positioned on the concrete blocks at each level. Channels 32 through 37 were assigned to this set of accelerometers. The locations of these accelerometers are shown in Figures 5.9 and 5.11.

The third method for measuring story shear forces consisted of measuring the shear forces in representative columns, extrapolating the results to the rest, and adding the total shear force carried by the columns to the horizontal components of the axial forces in the braces. The instrumentation for measuring the axial forces in the braces has already been described above. To measure shear forces in columns, it was decided to measure bending moments at two sections per gaged column. Given that the columns had no external loading between the two sections, the calculated moment gradient, with respect to distance along the column, between the two sections would then be equal to the shear carried by the column. The column section bending moments were determined by measuring the axial strains on the top fibers of the flanges of the gaged sections of the columns. This was accomplished by placing a two gage circuit, one gage to each side of the centerline of the flange, on the top of each flange of each gaged section. In the first story, the two southern columns were gaged as described, while in the upper two stories only the south-western column was gaged. The data channels for the strain-gage circuits were numbered 50 through 65. The positions of these strain gage circuits are shown in Figures 5.9, 5.10 and 5.11. Two plates in Figure 5.12 show typical locations of strain-gage circuits, accelerometers and wire-potentiometer hook attachments.

Lastly, two accelerometers were attached onto the western longitudinal frame to measure any transverse accelerations. The data channels corresponding to these

were 67 and 68. The locations of the two accelerometers are indicated in Figures 5.9 and 5.11. Two additional wire-potentiometers were added after the second day of testing to quantify relative displacements between the concrete blocks and longitudinal frames due to the flexibility of the diaphragms. Channels 69 and 71 were associated with these potentiometers. Their locations are shown in Figure 5.11.

5.5   Inputs to the Table

Given a digitized acceleration history, the EERC shake table can produce shake table motions imparting an approximation of the acceleration history to table and the structure atop it. Necessarily, the requisite accelerations, velocities and displacements must be within the range of the table's limitations. Roughly speaking, the digital acceleration record is low-pass filtered, doubly integrated, then passed through a digital to analog converter to an MTS controller unit which controls the table motions. By varying the "span setting," the fraction of the amplitude of the acceleration record to be imparted to the table, an acceleration record can be reproduced on the table with the amplitudes scaled to the desired values. The EERC earthquake simulation laboratory has a library of recorded digitized acceleration histories of past significant earthquakes, as well as a number artificially synthesized records.

The shake table testing of the structure spanned over five days; 1/16/93, 1/19/93, 1/20/93, 2/3/93 and 2/4/93. The last day indicated included several tests performed as a part of a demonstration for an EERC "open house." Several runs were made on the day previous to this to preclude any embarrassing incidents during the open house. Immediately following the demonstration, the structure was converted from the TS2 configurations to the TS3 and tested. Tables 5.2, 5.3, 5.4 and 5.5 indicate the schedules of the testing of TS1, TS2 and TS3. "File Number" in these tables reflects the standard EERC format for identifying each test conducted on the shake table. The first six of the eight digits in the File Number indicate the year, month and day, respectively, on which the test was conducted. The last two digits, separated from the rest by a point, indicates the sequence of the tests conducted on the given date. "Signal Name" reflects the internal EERC naming scheme for different

File Number	Signal Name	Span Setting
930116.01	random	.4
930116.02	random	.6
930116.03	random	.8
⋆930116.04	chile.u	.491
930116.05	chile.u	.737
930116.06	chile.u	1.106
⋆930116.07	chile.u	1.1675
930119.01	ec2.h	.5
930119.02	ec2.h	1
930119.03	ec2.h	1.45
930119.04	thssr.d	0.5
930119.05	thssr.d	1
930119.06	thssr.d	1.1675
930119.07	thssr.d	1.2
930119.08	chile.u	1.1675
⋆930119.09	chile.u	1.1675
930119.10	s1	1
930119.11	s1	2
930119.12	s2	.71
930119.13	s2	.95
⋆930119.14	s3	1.1
930119.15	s4	1.498
930120.01	taft2.h	1
930120.02	taft2.h	2.5
930120.03	pacs74w.d	1
930120.04	miyagi.d	.95
⋆930120.05	pacs74w.d	1
†930120.06	miyagi.d	.95
†930120.07	miyagi.d	.95

Table 5.2: Testing schedule for the TS1 configuration of the test structure

File Number	Signal Name	Span Setting
930120.08	chile.u	1.106
⋆930120.09	chile.u	1.1675
930120.10	ec2.h	1.45
930120.11	thssr.d	1.2
930120.12	taft2.h	2.5
⋆930120.13	pacs74w.d	1
930120.14	miyagi.d	.95
†930120.15	miyagi.d	.95
930120.16	s1	2
930120.17	s2	.71
⋆930120.18	s3	1.1
930120.19	s4	1.498

Table 5.3: Testing schedule for the TS2 configuration of the test structure

File Number	Signal Name	Span Setting
930203.01	chile.u	1.1675
930203.02	s2	.71
930203.03	ec2.h	1.45
930203.04	taft2.h	1
930204.01	taft2.h	1
930204.02	ec2.h	1.45
930204.03	chile.u	1.1675
930204.04	s2	.71
†930204.05	miyagi	.95
930204.06	s3	1.1
930204.07	chile.u	1.1675
930204.08	chile.u	1.1675
930204.09	s3	1.1
930204.10	s3	1.1

Table 5.4: Testing schedule for the TS2 configuration in demonstration

File Number	Signal Name	Span Setting
930204.11	chile.u	.292
930204.12	chile.u	.584
930204.13	chile.u	.875
930204.14	chile.u	1.1675

Table 5.5: Testing schedule for the TS3 configuration of the test structure
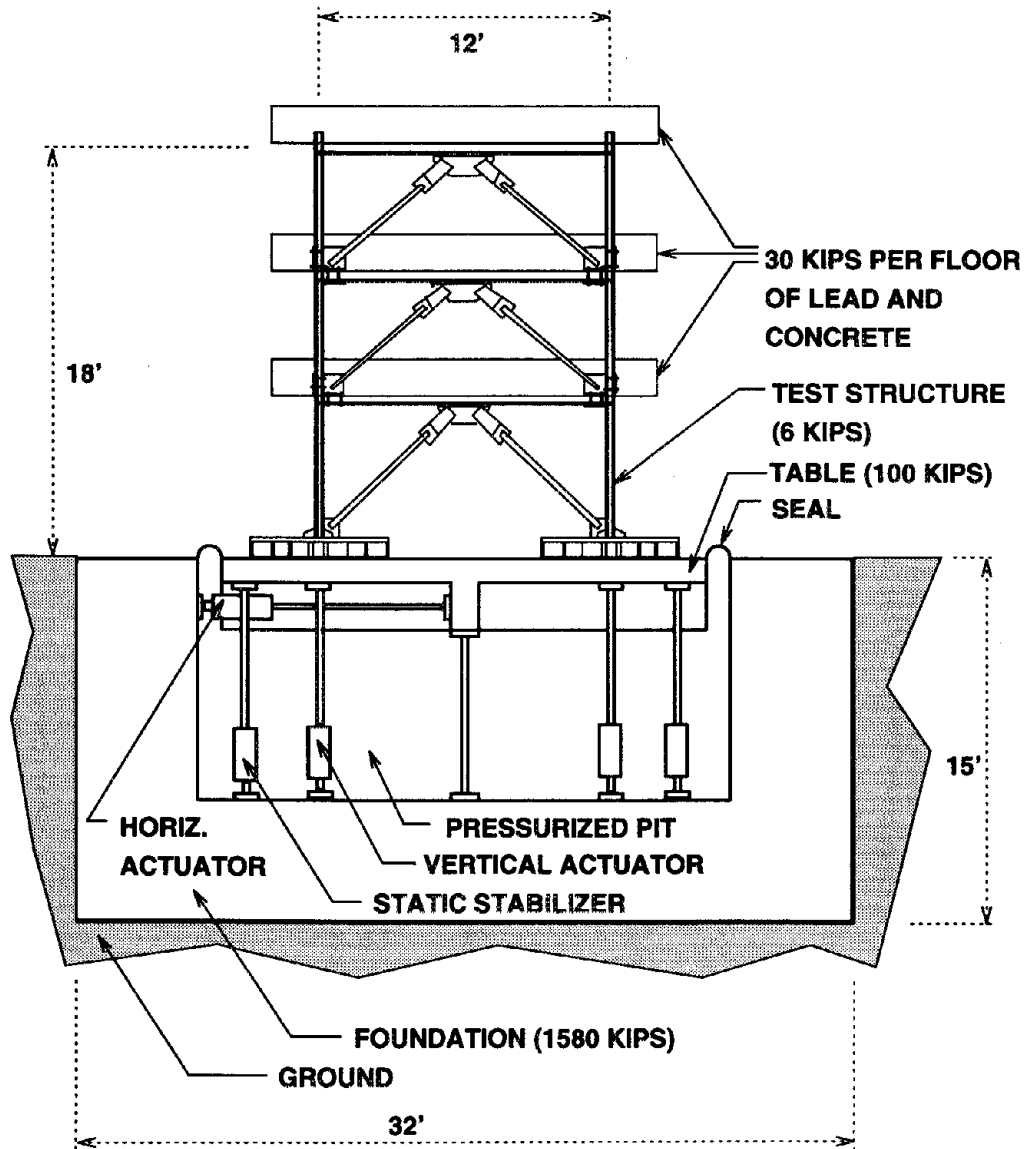
Figure 5.1: Gross dimensions and weights of table and structure.

N ⟸⟹ S
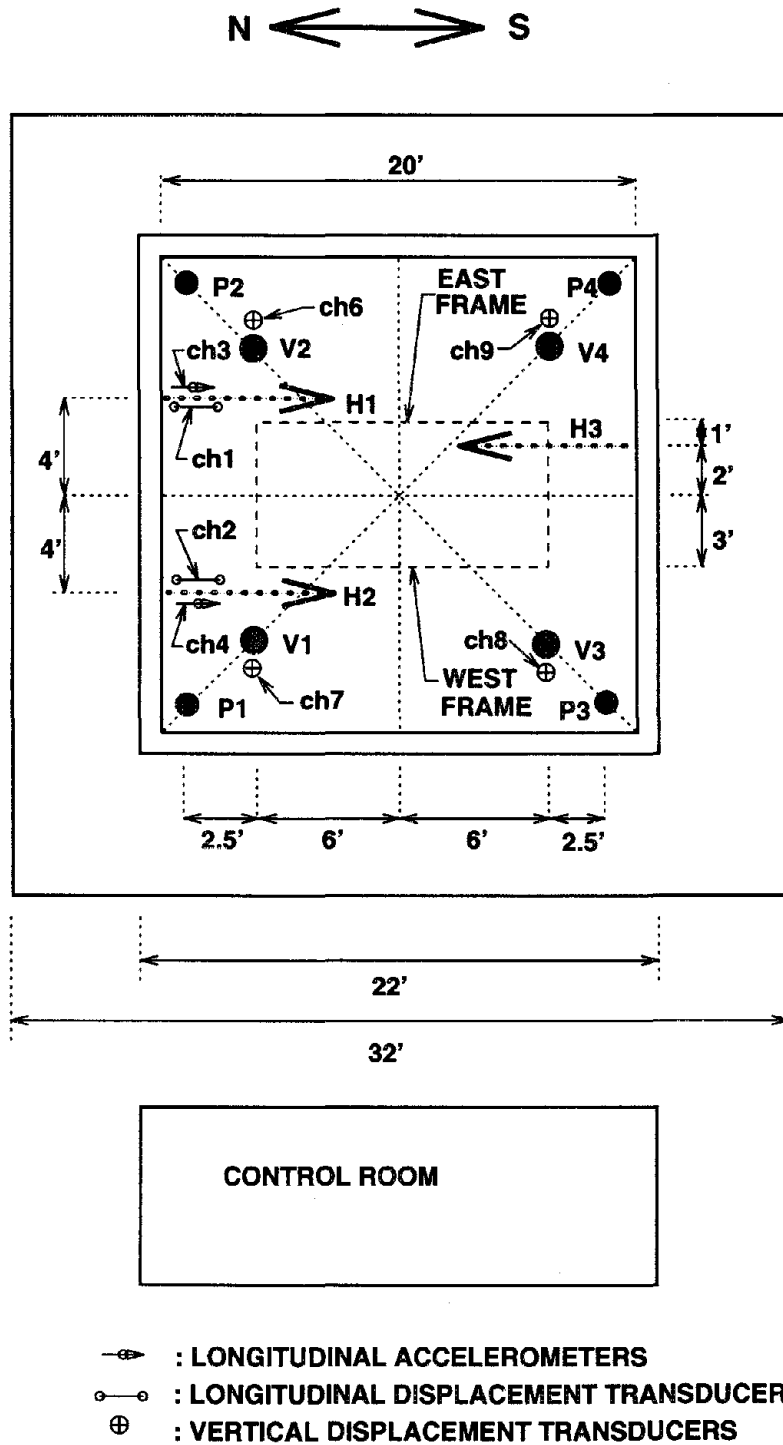
Figure 5.2: Plan view of table showing position of actuators.
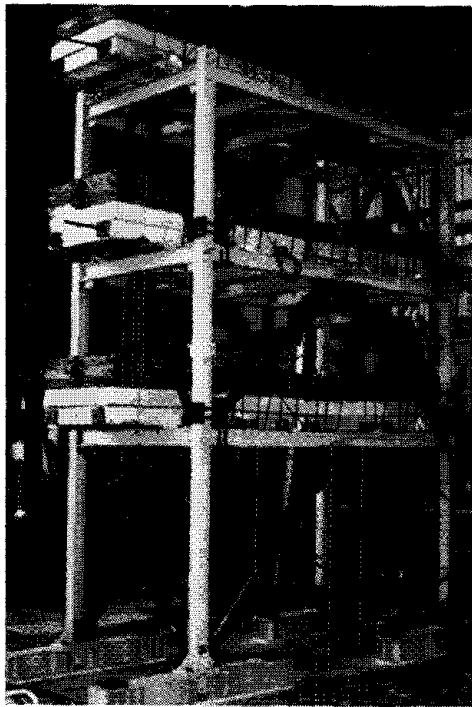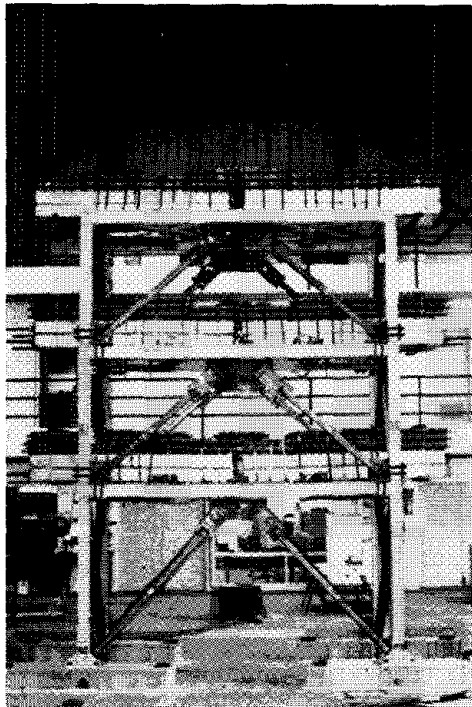
Figure 5.3: Photographs showing two views of the test structure
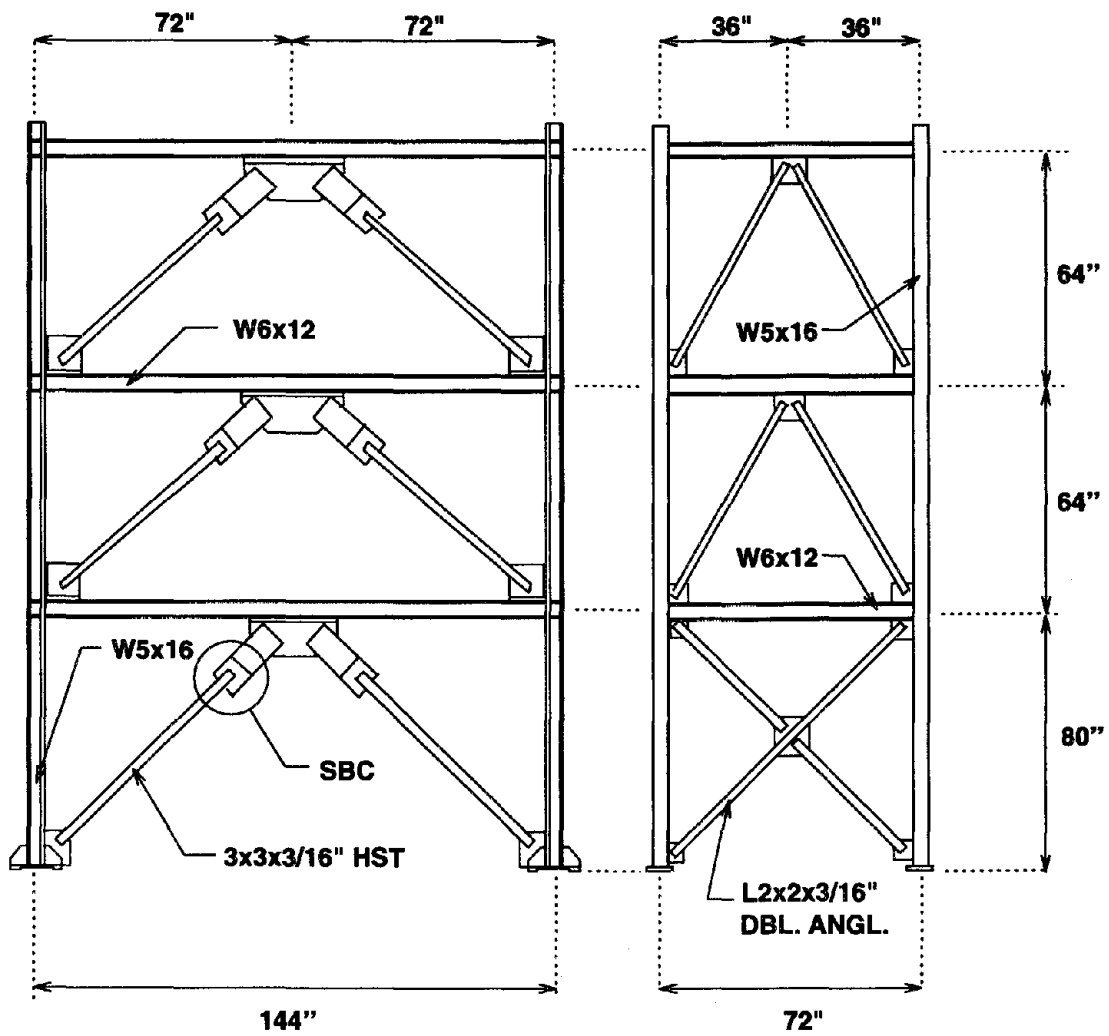
Figure 5.4: Test structure members and overall dimensions.
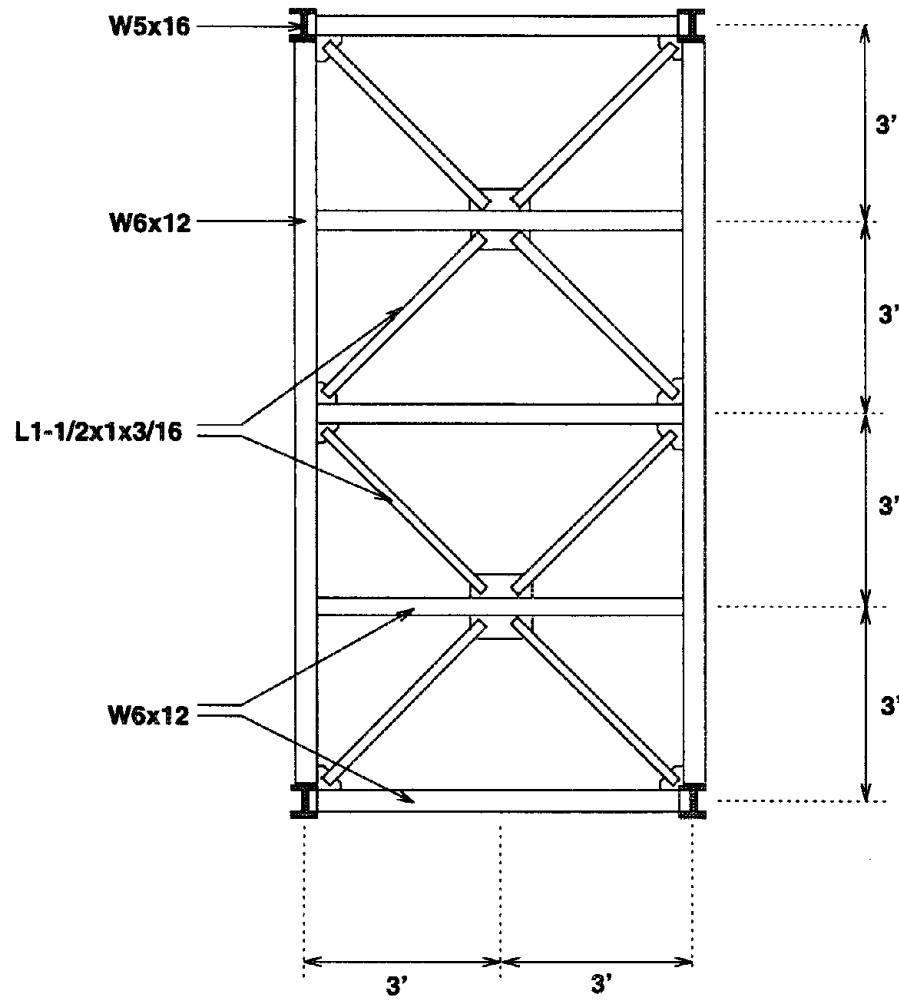
Figure 5.5: Structural detail of typical floor in structure.

93"x14"x13.5" CONCRETE BLOCKS

PACKS OF LEAD INGOTS

STEEL STRAPS SECURE
PACKS TO BLOCKS

CHANNELS AND THREADED
RODS SECURE FIRST ROW
OF PACKS TO BLOCKS

ANGLE AND THREADED
RODS SECURE BLOCKS
TO BEAMS

ANGLES BRACKET
BLOCKS IN LATERAL
DIRECTION

BEAM IS SEATED
TOP AND BOTTOM FLANGES
WELDED (TYP.)

BEAM WEB BOLTED TO
SHEAR TAB AND TOP FLANGE
WELDED (TYP.)
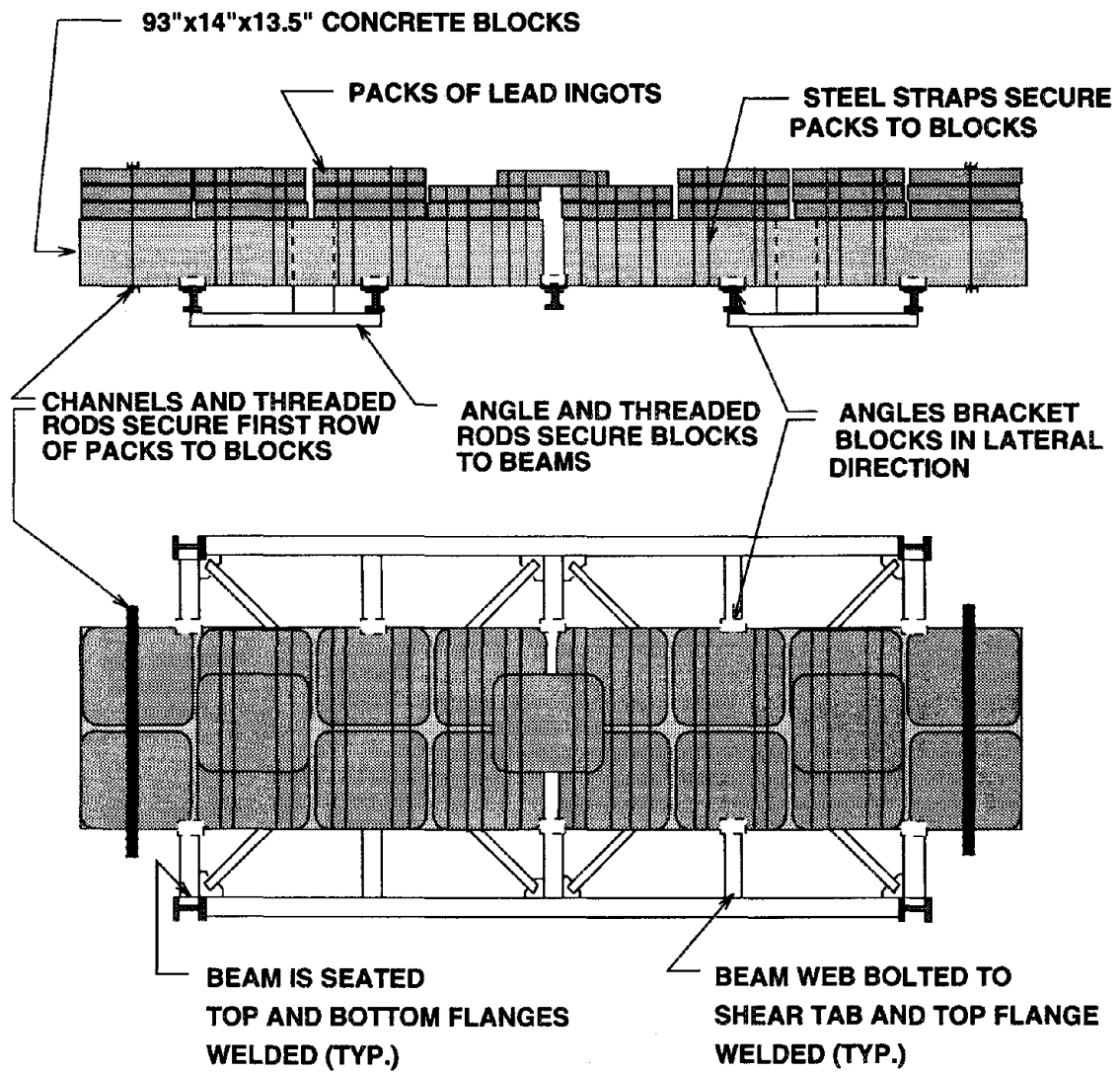
Figure 5.6: Typical detail of connection of ballast to floor
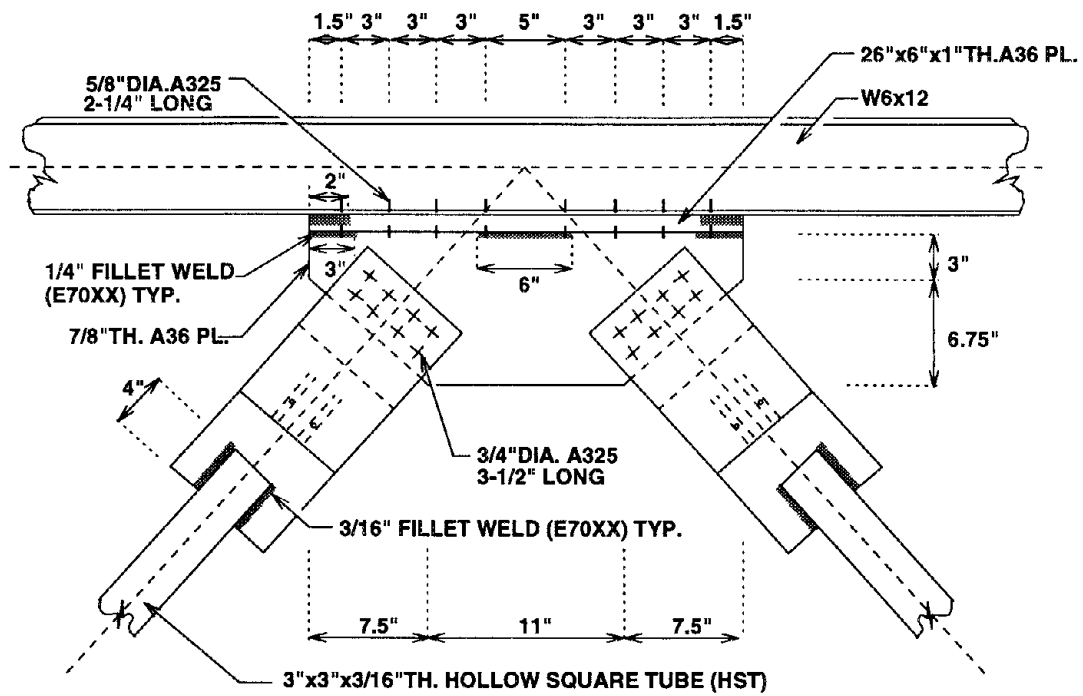
Figure 5.7: Structural detail of brace-SBC-frame assembly
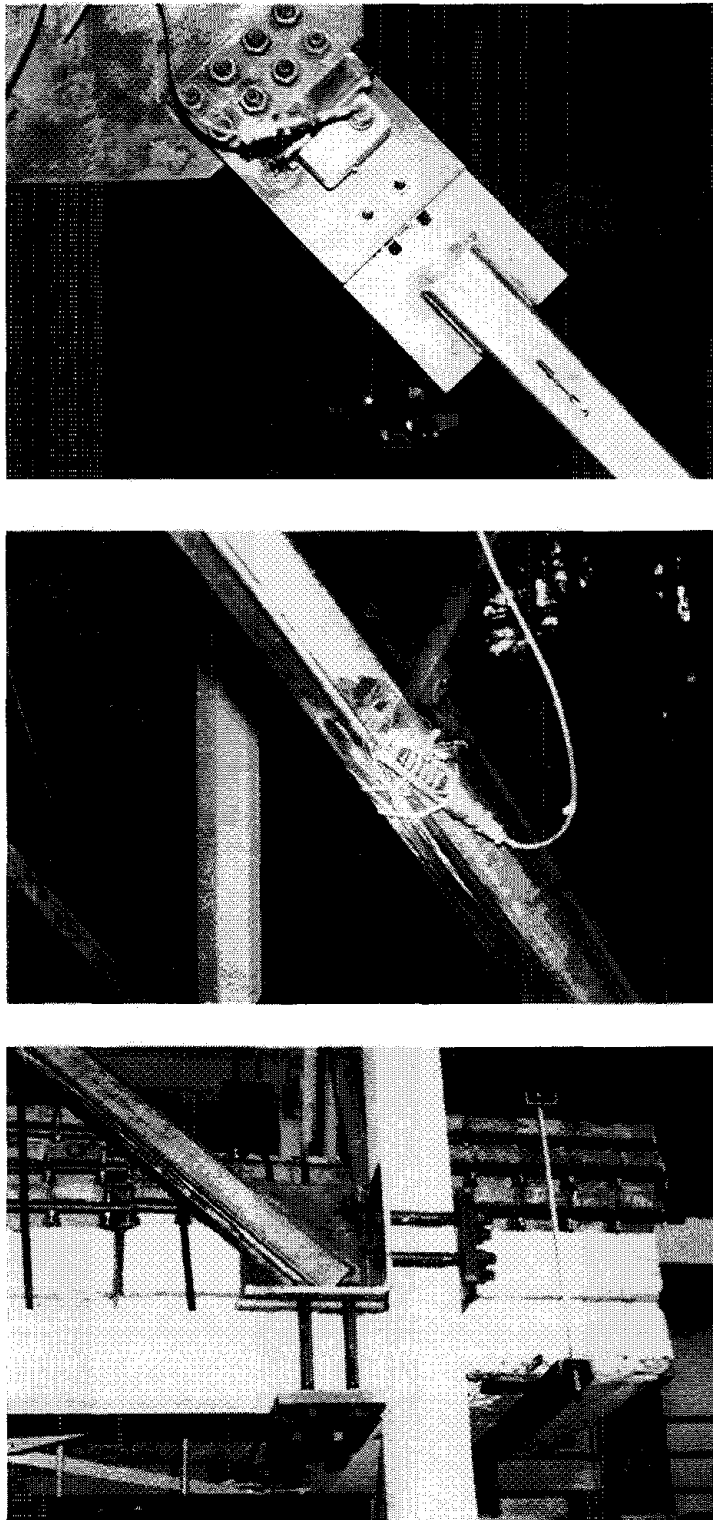
Figure 5.8: Photographs of brace/SBC and instrumentation
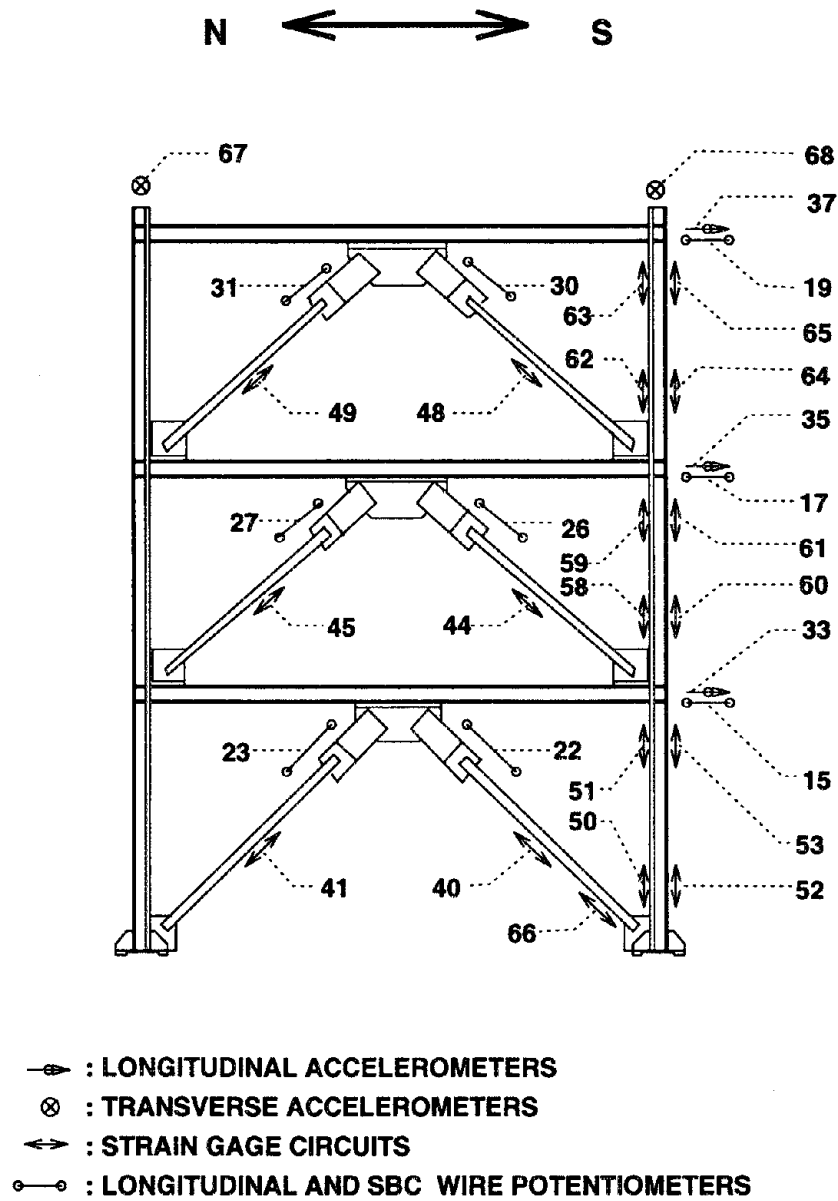
Figure 5.9: Instrumentation on western frame of structure.

N ⟵⟶ S

↔ : STRAIN GAGE CIRCUITS

o—o : LONGITUDINAL AND SBC WIRE POTENTIOMETERS
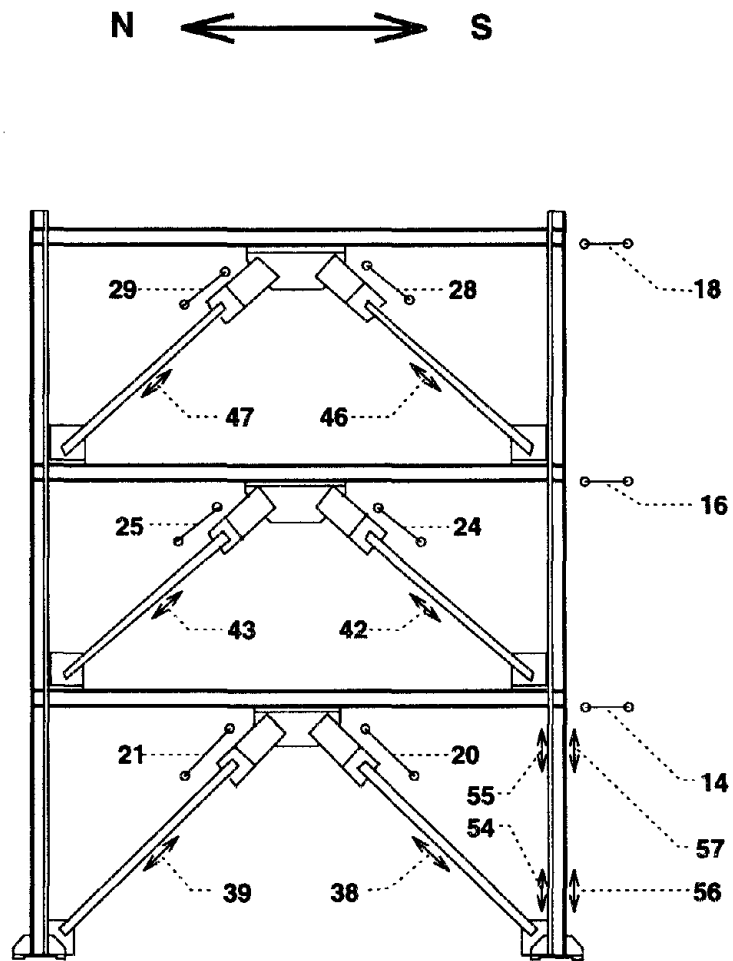
Figure 5.10: Instrumentation on eastern frame of structure.
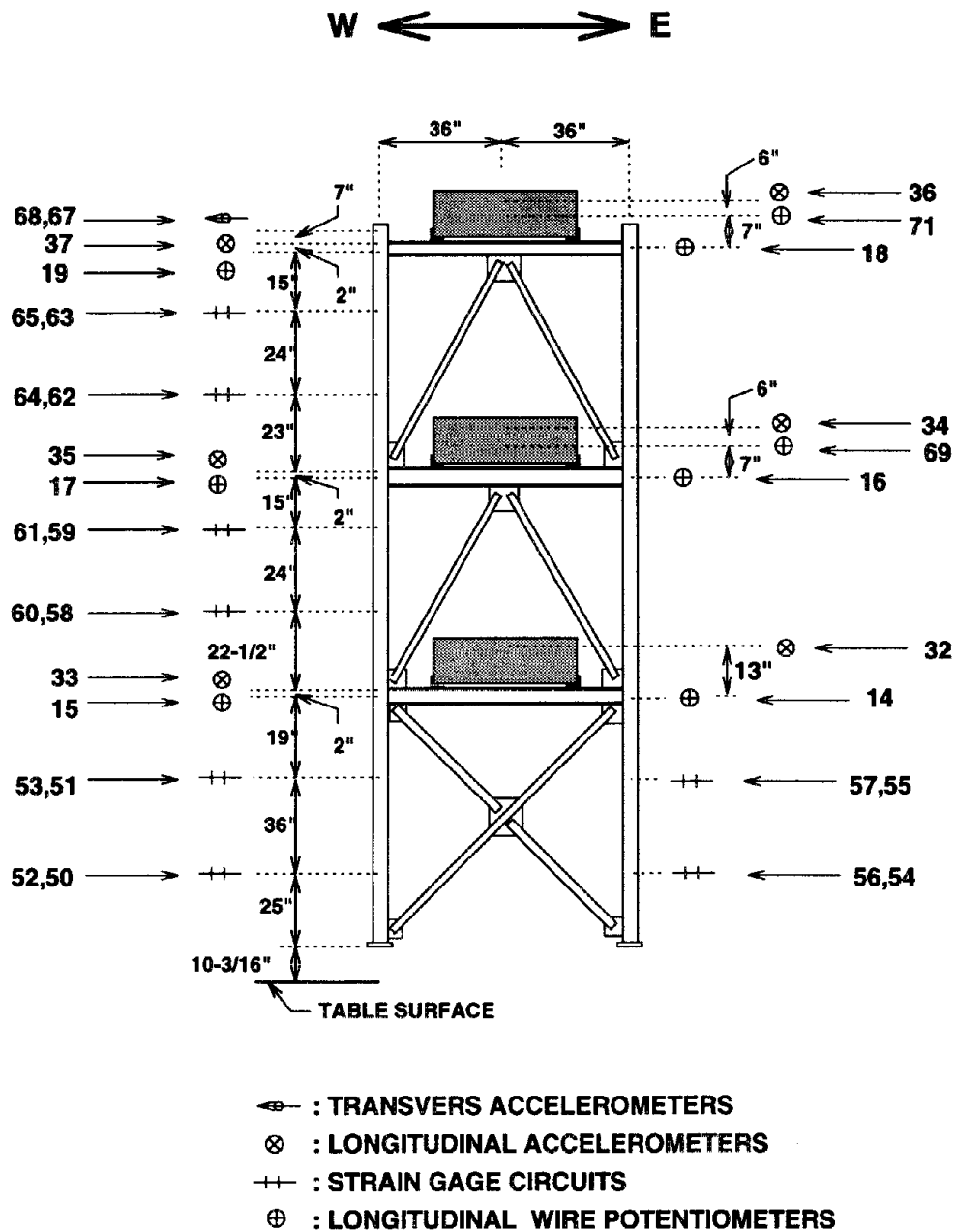
Figure 5.11: Instrument locations as viewed from South.
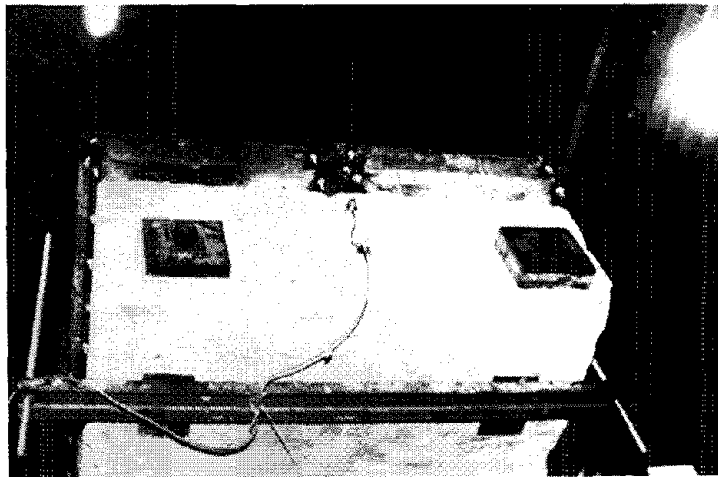
Figure 5.12: Photographs of column and block instrumentation.
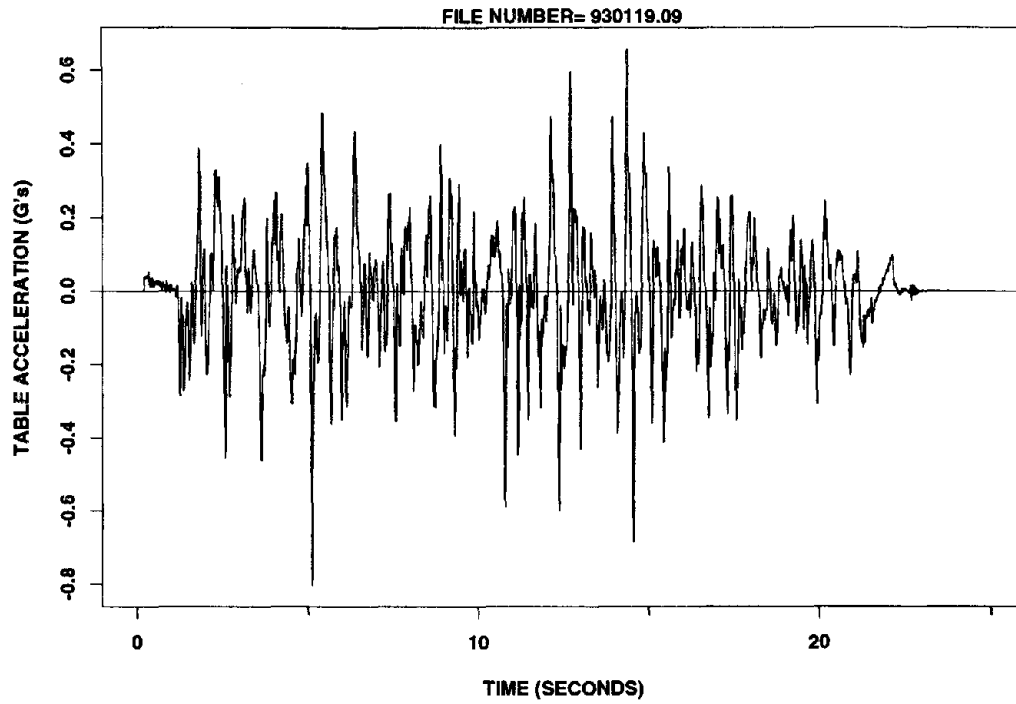
Figure 5.13: Table acceleration history for the chile.u signal.
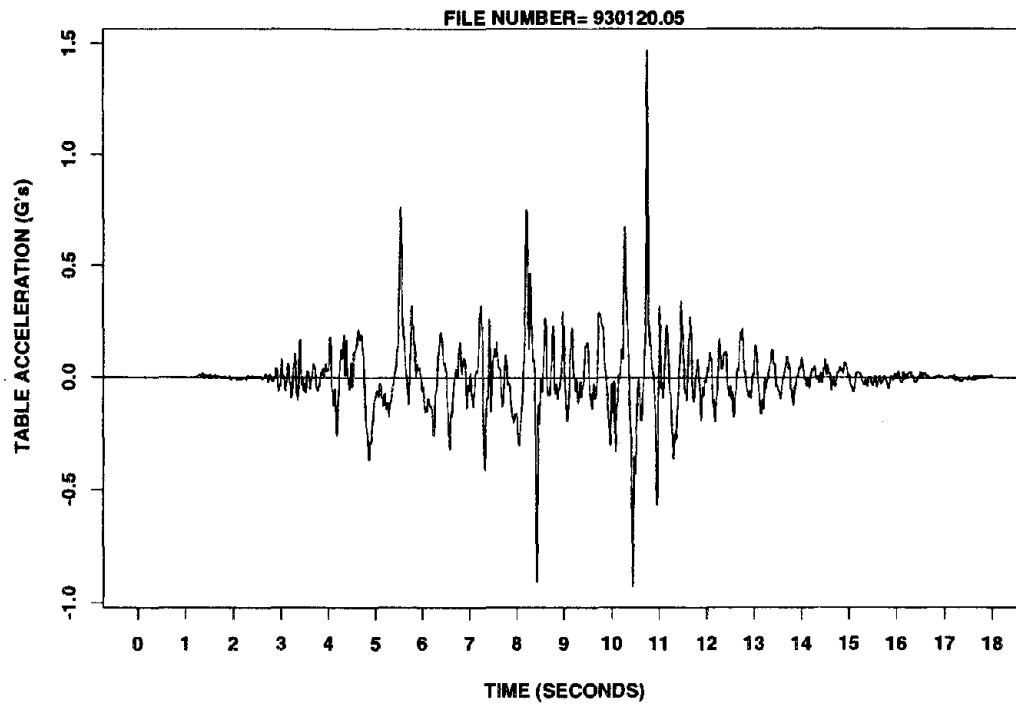
Figure 5.14: Table acceleration history for the pacs74w.d signal.
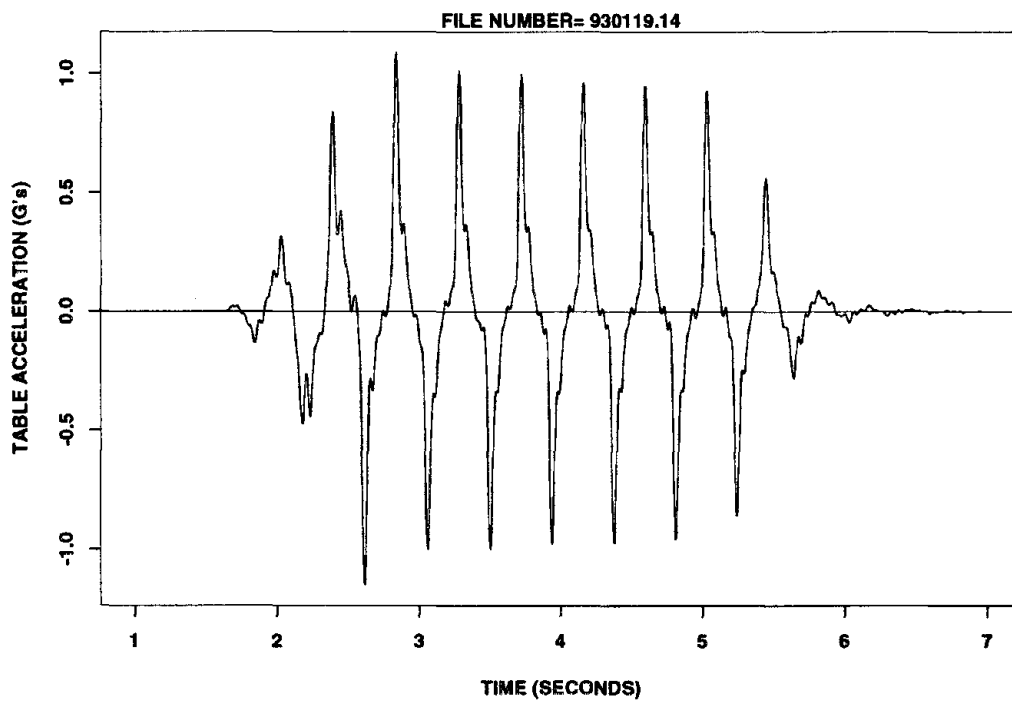
Figure 5.15: Table acceleration history for the harmonic s3 signal.

Chapter 6

Reduction Of Basic Response Quantities

6.1 Purpose

The test structure together with its instrumentation was described in the previous chapter. In the next chapter the response of the test structure, with particular attention to the behavior and effect of the SBCs, will be discussed. In this chapter a careful look is taken at the data from the instrumentation. The reduction from data of basic response quantities, referred to in next chapters, is described. This is accomplished by examining thoroughly the data from two selected tests of TS1. A narrow representative time window is selected for each of the two tests, and reduced data from all relevant channels are examined in the said time windows. This method of examination of reduced data serves dual purposes. Firstly, the formulation of various response quantities from the information from the array of instruments is established. Secondly, such a close examination, over a narrow time window and covering the response of the entire array of instruments, offers the kind of insight into the behavior of the structure that is otherwise unavailable when only selective data from specific instruments is presented.

The two selected tests are 930119.14 and 930120.15. The time window of examination for these two record were chosen to be, respectively, 2.8 to 4.0 seconds

and 7.0 to 11.0 seconds. In this chapter the two tests will simply be referred to as the harmonic and Pacoima tests. The two tests were chosen because of the strong response which they induced in the structure. The windows were chosen in such way so as to include relatively large responses while conveying enough response detail.

6.2 General Comments

In the following sections references will be made to data from various data channels. These references do not imply that the data presented are the "raw data." The data are not "raw" in the sense that high frequency noise, above 25 Hertz, has been removed through low-pass filtering and that "zero shift" or "base line drift" has been accounted for. The value of 25 Hertz was chosen as this was the cut-off frequency for the low-pass filtering used for the processing of the table input signals. The zero shift is mostly an artifact of the amplifiers used in conjunction with the data acquisition system. The structure was tested with a new data acquisition system. Due to "bugs" in this system, the first 5 seconds of data in the first few tests went unrecorded, resulting in the loss of "true zero" readings. For the most important response quantities, that is the action of the SBCs, the zero shift is inconsequential as it only results in permanent shifts in the origins of the hysteresis loops and does not effect their shape or size. For instruments such as accelerometers and table displacement transducers, the zero shift could be accounted for by subtracting from the data the post or pre-excitation values recorded for the given channels. For data channels involving structure displacements or strain in the columns, where residual permanent offsets could be physically meaningful, the practice of subtracting from the record the mean of the record was adopted. Comparison of shear forces obtained from strain gage data, zero-ed in such manner, with shear forces calculated from accelerometer data indicates simultaneous zero-crossings for both quantities. This, in turn, indicates that meaningless permanent offsets in the strain gage data channels have been eliminated successfully.

6.3 Relative Displacements and Story Drifts

Figures 6.1 and 6.2 show the table displacements and the structure relative story displacements for the harmonic and Pacoima signals mentioned above. The figures also indicate the data channels from which the data are taken. The figures present eight curves each, as four pairs of curves. The four pairs represent table, relative first, second and third level displacements. Each member of the pairs represents one instrument reading, there being two, east and west displacement transducers on the table and wire-potentiometers per each story of the structure. The relative displacements are calculated by subtracting from the wire potentiometer data the average of the two table displacement transducer readings. It is apparent from these two figures that for the case of the harmonic signal, the east and west displacement signals do not match as well as they do for that Pacoima signal. In particular it appears that the table displacements themselves do not quite coincide for this signal. Barring errors in the zero-ing of the channels, this would mean that the table undergoes a small degree of twist. However the magnitudes of this twist, are not significant enough to be of concern. It is seen that for the case of the Pacoima signal, good coincidence between the eastern and western displacements is achieved.

Figure 6.2, dealing with the Pacoima signal, indicates a behavior that is perhaps specific to structures with elastic-perfectly-plastic bracing systems. It is seen that, between roughly 8.75 and 9.75 seconds, displacement oscillations occur entirely bellow the zero axis. This behavior is interpreted as follows: Displacements involving large slip of the SBCs occur at between 8.0 and 8.5 seconds. Subsequently, temporary residual relative displacements, particularly visible in the first level, remain until about 9.75 seconds when the SBCs slip again and all relative displacement curves pass through the relative zero again. In this short period, between 8.75 and 9.75 seconds, the braces are in strained condition forcing the residual deformations on the moment frame. The oscillations seen in this period are due to mostly elastic vibrations, but also include some very small slips in the SBCs. This short period will be referred to again in the rest of the chapter, where more evidence for the explanations given here will be presented.

Relative story displacements shown in Figures 6.1 and 6.2 include in them contributions to story displacements from the pitching of the table. In the chapters following this one, the term "relative displacement" will mean relative displacements corrected so as to not include table pitch contributions. Where confusion may occur, the term "corrected" will describe the quantities in question. Where this correction is not made, it will be explicitly indicated that quantities in question include table pitch. The relative story displacements are corrected by subtracting from them the displacement contributions due to the table pitch. The table pitch causes, effectively, a rigid body rotation of the entire structure. Knowing the magnitude of these rotations, this magnitude can be multiplied by the vertical distance between the axis of rotation of the table and a given wire-potentiometer, measuring displacement at that story, to arrive at the contribution to that displacement reading due to the table pitch. The pitch magnitude can be calculated from displacement transducer data from vertical actuators V1, V2, V3 and V4. The positions of these actuators and channel numbers for the transducers attached to them were given in Figure 5.2. Figures 6.3 and 6.4 indicate contributions to the relative story displacements due to the table pitch for the harmonic and Pacoima signals. By subtracting from the uncorrected relative story displacements indicated in these Figures 6.1 and 6.2 the corresponding displacements indicated in Figures 6.3 and 6.4, the corrected relative story displacements are found.

6.4 Story Shear Forces

The instrumentation on the test structure provided for three independent means of calculating the story shear forces. These three methods were described in the last chapter. In this section the story shear forces calculated by the three methods are compared for the two mentioned signals over the time-windows of discussion.

Story Shears From Strain Gages

The first method for calculation of story shears discussed here is based on data from strain gages on columns and braces. This method also allows for the

separate examination of the components of story shear carried by the braces and that carried by the columns.

As mentioned in the previous chapter, strain gage circuits on each of the twelve braces in the structure allowed for the monitoring of the axial forces in the braces. The story shear force component carried by braces can be calculated by summing the horizontal components of these brace axial forces. Such calculated forces for the two signals in discussion are shown in Figures 6.5 and 6.6. At this point in should be recalled that, for TS1, SBC design slip forces were chosen to be 15 kips at the first story and 7.5 kips at the second and third stories. Then, the story shear force components carried by the braces would be expected to be "chopped off" at the nominal values of $4 \times 15 \times 0.669 = 40.14$ kips, at the first level, and $4 \times 7.5 \times 0.7474 = 22.44$ kips at the second and third levels. The values 0.669 and 0.7474 are the cosines of the first and upper level brace angles with the horizon. It is seen in Figures 6.5 and 6.6 that this expectation is nearly perfectly realized. In carrying lateral forces, the SBCs effectively regulate the magnitude of the force to be carried by individual SBCs and therefore the lateral force resisted by the bracing system. This effect is emphatically demonstrated in Figure 6.5. The horizontal portions of the curves in the two figure correspond to slippage occurring in all SBCs of the stories corresponding to the curves. At this point, it should be pointed out that for the case of the Pacoima signal, in the period between 8.75 and 9.75 seconds, the story shear component carried by the braces at the first level is particularly small relative to the nominal value of 22.44 kips mentioned above. This indicates that no, or little, slips occur over this period at the first story.

Figures 6.7 and 6.8 show the story shear components carried by the columns. As mentioned in the previous chapter, two columns at the first story and one column in each of the second and third stories were gaged. To extrapolate from these columns the story shear components carried by the columns, the sum of the shears carried by two columns in the first story was multiplied by 2.0, while the shear carried by the columns of the second and third stories were each multiplied by 4.0. Two sections per column were gaged with two strain gage circuits per section, one circuit per external face of each of the two flanges of each I-section. The strain gage circuits measured

the average top fiber axial strains. The shear force carried by each column was calculated by calculating the gradient, with respect to distance along the column, of the bending moment between of the two gaged sections. There being no external loads on the column between the gaged sections, this gradient was theoretically linear and its calculation required only knowledge of the bending moment at each gaged section. Given top fiber axial strains, ϵ_1 and ϵ_2, for the two flanges of a section, the bending moment at the section is given by $(\frac{\epsilon_1 - \epsilon_2}{2})ES$, where E and S are the Young and the section moduli. Simplified reduction formulas based on the principles described above are given for each of the curves in Figures 6.7 and 6.8. In these formulae, the factors 24 and 36 reflect the axial distance, in inches, between the gaged sections. These factors are used in calculating the bending moment gradients between the two sections. The factor 10^6 is present in the formulae to indicate conversion of units of micro-strain, reported by the channels, to non-dimensional strain units. In multiplying the sum of the first story shears by a factor of 2.0, the denominator in the above given bending formula is cancelled. While in multiplying the single column shear forces in the second and third levels by 4.0, a factor of 2.0 remains in the numerators as indicated in the figures. It is also noted from Figure 6.8 that in the period between 8.75 and 9.75 seconds the components of story shear carried by the columns of the first and third stories are relatively constant, while some oscillations occur in this quantity for the second story. At this point, a more refined explanation of the behavior in this period is possible. What can be concluded from this figure is that in this time period the SBCs of the third and first stories are "locked," keeping the columns in these stories in fixed deformed configuration leading to constant shear components carried by the columns in these stories. It should be pointed out the total story shear of the first and third stories is not constant. Oscillations of this quantity are due to oscillations occurring in the brace shear components as shown in Figure 6.6. While the story shear components carried by the columns for these two stories is constant, the same quantity is not constant for the second story implying that columns undergo deformations in time. This, in turn indicates that the SBCs of the second story are active, i.e. not "locked," in this time period. In later sections in this chapter, it will be seen that the above described explanations indeed correlate well with the data

from the SBC wire-potentiometer data.

Story Shears from Accelerometers

Given the column and brace story shear components as presented above, it is clear that the sum of the two components results in the total story shear forces calculated from strain gage data from the braces and columns. Before the total story shears calculated based on strain gage data is presented, the two other methods for calculating the total story shear components are discussed. These two methods involve measuring the accelerations of the story masses. Given these accelerations, the inertial forces acting at each level of the structure can be calculated by multiplying accelerations at each level by the magnitude of the reactive mass at the level. For structures with little true viscous damping, the inertial forces are almost completely equilibrated by the actions of the displacement dependent portion of the lateral force resisting system, i.e. the the story forces due to the deformations in the columns and braces. This then allows for the calculation of story shear forces by measuring accelerations of the levels of the structure. Total story shear forces are calculated from this method by summing for each story the inertial forces above it.

As explained in the previous chapter, accelerometers measuring longitudinal accelerations were placed on the south concrete blocks at each level and also on the south-west column at beam centerlines of each story. The locations for these were given in Figure 5.11. By themselves, the set of accelerometers on the concrete blocks should in theory be adequate for the purpose explained above. However, the second set of three accelerometers were provided on the south-west column as a means of verification. Given rigid or very stiff diaphragms, the two sets of instrumentation would be expected to produce very similar results. As hinted at in the previous chapter, the diaphragms proved to be rather flexible, and also non-linear, in behavior. This subject will be more elaborated on in Chapter 8. Figures 6.9 and 6.10 show the readings of the two sets of accelerometers for the three levels, in conjunction with the table accelerometer readings, for the two signals in the time window of discussion. It is seen that, for the case of the harmonic signal, the acceleration readings in the

upper two levels between the two sets of accelerometers match each other poorly. For the case of the Pacoima signal much better results are achieved. This is due to the non-linearities in the behavior of the diaphragms. For the case of the Pacoima signal, in the time window shown, the excitations are small compared to the harmonic signal. This causes the diaphragms to to remain stiff. As will be seen in Chapter 8, the diaphragms become very flexible under larger loads. Also of interest is that the two table accelerometer readings do not entirely match each other. This hints at the existence at some twist causing forces acting on the table.

Comparison of Three Methods

Having given the above explanations, comparisons can be made between the resulting total story shears from each of the three methods. Figures 6.11 and 6.12 show the total story shears computed using the data already presented in previous figures. In these two figures the solid curves indicate the total story shears calculated through the strain gages on the braces and columns, while the dashed and dash-dotted lines indicate total story shears calculated from accelerometers on the south west column and the concrete blocks respectively. Story weights of 32 kips were used in calculation of the accelerometer based total story shears. As expected the accelerometer based calculations match each other extremely well for the case of the Pacoima signal, while for the case of the harmonic signal the result are not as close. Comparison of the accelerometer based total story shears versus those calculated from strain gage data reveals a similar trend. Results between the two, strain gage based and accelerometer based, calculations match each other extremely well for the case of the Pacoima signal while for the harmonic signal results tend to not coincide as well. Given the explanation regarding the flexibility of the diaphragms, one would expect the results based on the accelerometers on the blocks to be, while different from that based on the frame accelerometers, more representative of the real behavior. Indeed, the results from the block accelerometers are closer, particularly if only peaks are considered, to the results for the strain gage data. Some distortion of the block accelerometer data is possible, as the blocks were observed to rock under some of

the stronger, in particular harmonic, excitations. This rocking occurs due to the vertical movements of the midpoints of the longitudinal beams. The causes of such movements are explained in the next chapter.

In light of the above discussions, it is concluded that the more appropriate method for story shear force calculations for the test structure is the methods based on the strain gage data. No evidence exists thus far indicating that the results based on this method may be distorted. That this method relies on a much larger number of instruments (thirty two strain gages in all) rather than the few instruments (three accelerometers in each method) indicates reduced sensitivity to instrumental error. Further, from an intuitive point of view, it is expected that given sinusoidal type displacements, sinusoid like shear force histories be present. The shear force histories calculated from strain gage data resemble sinusoids the most as seen in Figure 6.11. Where references will be made in the next chapters to shear forces, unless indicated explicitly, the term references will be to shear forces calculated from strain gage data.

6.5   Slip Distances and Brace Forces of SBCs

The most central and important response quantities of interest, in the discussion of the behavior of the test structure, are the slip distances and the axial forces of the twelve SBCs in the structure. As explained in the previous chapter, one wire potentiometer per each SBC was dedicated to reporting the relative movements or slips between the main plates and the outer plates of the SBCs. The SBCs being in series with braces, the force through each SBC was necessarily equal to the axial force in the brace connected to the SBC. Each brace was gaged with a strain gage circuit to report axial forces in units of kips. The story shear force components carried by the braces, discussed earlier, were calculated by considering the sums of the force readings from these circuits. In this section, the brace forces and slip distances for each SBC are examined individually.

Slip Distances

Figures 6.13 and 6.14 show twelve plots each, one plot for each SBC, indicating the slip distance histories for the harmonic and Pacoima signals in the time windows of discussion. Channel numbers indicating the origins of each curve and an alphanumeric designation for each SBC in question are given in each plot. The designations are self-explanatory; the integer in the designation indicates the story in which the SBC is located, while the two following letters designate the compass quadrants of the location in the story. The points of the compass in relation to the position of the structure were identified in Figure 5.2. The plots are arranged in each page such that the top six plots correspond to SBCs of the western longitudinal frame, while the bottom six plots correspond to the SBC of the easter longitudinal frame. Plots to the left of the pages correspond to northern SBCs, while those to the right correspond to the southern SBCs. For each frame, the SBCs of the first second and third stories are naturally positioned from bottom page half to top page half. This arrangement and designation scheme will be used again in the next chapter where a flock of similar curves will be presented. In the plots of the figures currently in discussion, the horizontal portions of the curves correspond to no slip occurring (or "lockage") at the SBCs. Conversely, the non-horizontal segments of the curves indicate occurrence of slippage (or "activity") at the SBCs. Most interestingly, for the case of the Pacoima signal, Figure 6.14, it is seen that the hypothesis thus far given regarding behavior of the SBCs in the period between 8.75 and 9.75 seconds has been to large extent correct. That is, in this period the SBCs of the first and third stories are "locked", while those of the second story slip. In the same figure, it is also seen that SBCs at a given floor do not necessarily undergo identical slips. It will be explained in the next chapter that the SBCs with the smallest slip force in a story will be the most active under small excitations. For large acceleration pulses however it is expected that all SBCs of a story slip almost simultaneously. This is indeed seen to be the case throughout the plots of Figure 6.13, and also in Figure 6.14 at roughly 8.33 and 10.75 seconds. Indeed, at these two instances in the Pacoima signal large table acceleration pulses appear as indicated in Figure 6.10.

Brace Forces

Figures 6.15 and 6.16 show the brace forces for each of the twelve SBCs in the structure. The plots in the figures are arranged in the same scheme as used in the presentation of the SBC slip distances. As expected, it is seen that for the upper two stories the brace forces are "chopped off" at roughly 7.5 kips while for the braces of the first level the same phenomenon occurs at roughly 15.0 kips.

SBCs Hysteresis Loops

Plotting the displacement quantities presented in Figures 6.13 and 6.14 against the force quantities presented in Figures 6.15 and 6.16 results in the hysteresis loops for each of the twelve SBCs of the structure for the two signals over the time windows of discussion. Plots of these hysteresis loop are given in Figures 6.17 and 6.18.

6.6 Brace Bending Moment

As mentioned in Chapter 5, a single strain gage (channel 66) was installed near the fixed end of the south-western brace of the first level (1SW), in addition to the force measuring strain gage circuit (channel 40), to monitor the brace bending moment near the fixed end. The strain gage was positioned on the top flange, with respect to bending in the plane of the frame, and calibrated to measure strain directly. The axial top fiber strain measured by this strain gage is due to two actions: the bending moment on the brace and the axial force on the brace. The axial force is measured by the strain gage circuit used for monitoring the SBC axial force. Given that the strain gage measures a top fiber axial strain of ϵ_t, and that the strain gage circuit measure an axial brace force of P, the strain component due to bending at the gaged section is given by $(\epsilon_t - \frac{P}{AE})$. Then the bending moment at the section is given by $ES(\epsilon_t - \frac{P}{AE})$. In these expressions, A, S and E are respectively the cross-sectional area, the section modulus and the elastic modulus for steel. Figures 6.13 and 6.14 show the SW1 brace bending moments calculated, from the measured data according

to the given formula, for the two signals in discussion and over the time windows of interest. As noted before, the factor 10^6 indicates conversion of micro-strains to strains. It is seen that the magnitudes of the brace bending moments are relatively small, the yield moment for the section in discussion being 80 kip-inches. For both figures, it is noted that the bending moments oscillate in-step with the first story drifts, as can be recognized by comparing the two figures with Figures 6.1 and 6.2.

6.7 Transverse Accelerations of Test Structure

Figures 6.21 and 6.22 show the measured transverse accelerations of the test structure at the third level's south and north extremes. As before the two figures correspond to the harmonic and Pacoima signals, and are given for the time-windows discussed throughout this chapter. As a reminder, the locations of these two accelerometers were given in Figure 5.9 (channels 67 and 68). The two accelerometers were oriented in the same direction and obeyed identical sign conventions, yet as can be seen in these two figures the readings from the two accelerometers appear to have opposite signs throughout the periods shown in the time-windows. Such readings can only be explained as being the result of torsional moments on the structure. Some of these torsional moments can be ascribed to the small degrees of twist exhibited by the table. However, comparison of the two figures with Figures 6.9 and 6.10, in which the table accelerations are indicated in the bottom plots, indicates that the phenomenon associated with the transverse accelerations shown in Figures 6.21 and 6.22 involves much higher frequencies than those observed in Figures 6.9 and 6.10. It is believed that the observed phenomenon is due to the fact that at any given level four SBCs have the tendency to slip, or activate, at different points in time. Indeed, given a large impulse, it would be rationally expected that the four SBCs of a given floor slip in succession, with the SBC with the smallest slip force slipping first and the SBC with the largest slip force slipping last. With the activation of each SBC at a given floor, the center of stiffness at that floor shifts. Each time this shift moves the center of stiffness to a new position, the moment arm between the center of mass of the level and the center of stiffness of the level causes a different torsional moment

on the structure. Given the symmetry of the test structure and roughly identical slip forces in the braces of a given story, the center of mass at a given level coincides with the center of stiffness at that level prior to the occurrence of any SBC slip at that story, and also while all SBCs are concurrently slipping. However between the occurrence of these two states, wild variations in torsional moments on the structure are possible. The lateral bracing system of the test structure was consciously designed to resist such torsional moments and, as such, performed flawlessly.

FILE NUMBER= 930119.14

Table Displacements:ch1,ch2

ch14,ch15 (less avg. of ch1,ch2)

ch16,ch17 (less avg. of ch1,ch2)

ch18,ch19 (less avg. of ch1,ch2)

DISPLACEMENT (INCHES)

TIME (SECONDS)
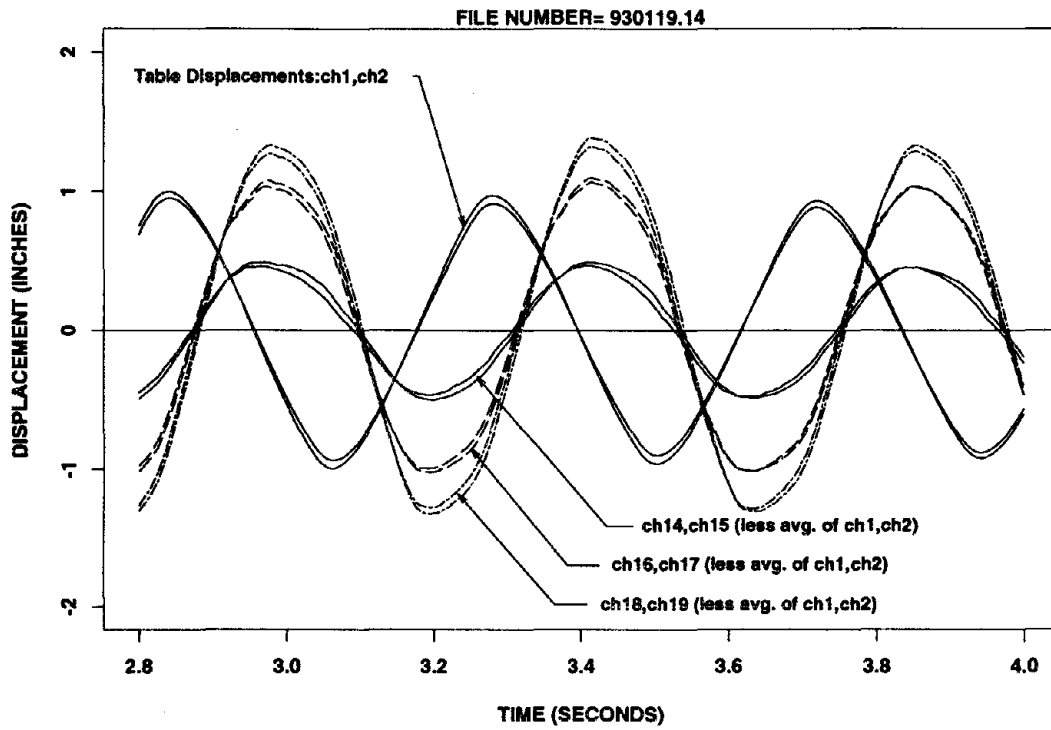
Figure 6.1: Table and relative structure displacements due to the harmonic signal.

FILE NUMBER= 930120.05

ch14,ch15 (less avg.of ch1,ch2)

ch16,ch17 (less avg. of ch1,ch2)

ch18,ch19 (less avg. of ch1,ch2)

DISPLACEMENT (INCHES)

Table Displacements:ch1,ch2

TIME (SECONDS)
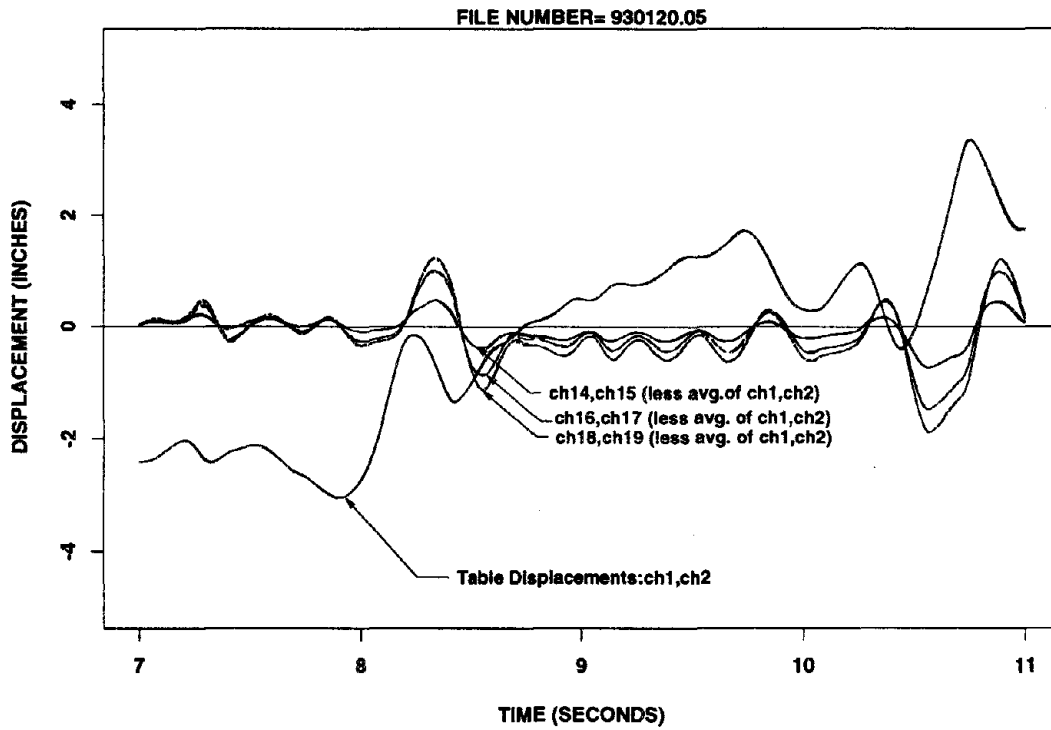
Figure 6.2: Table and relative structure displacements due to the Pacoima signal.

FILE NUMBER= 930119.14

Disp at lev. 3 due tbl. pitch: 217.6875xTable pitch
Disp at lev. 2 due tbl. pitch: 153.6875xTable pitch
Disp at lev. 1 due tbl. pitch: 90.1875xTable pitch

Table pitch: avg(atan((ch8-ch6)/144),atan((ch9-ch7)/144)) radians.

TIME (SECONDS)
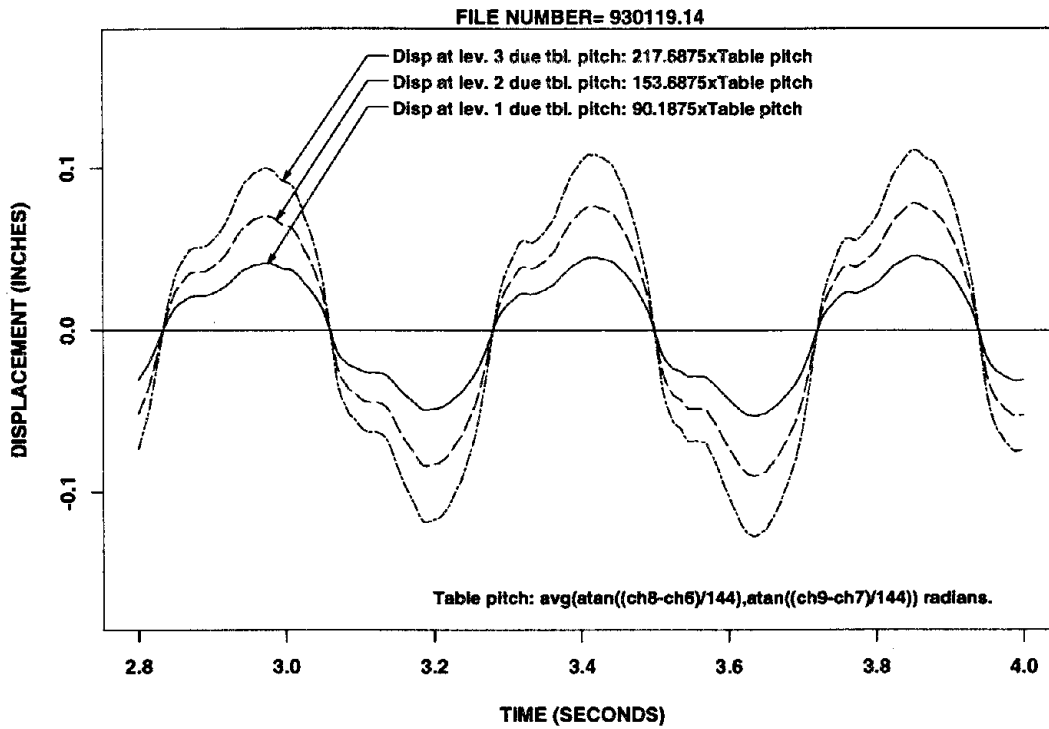
Figure 6.3: Pitch components of story displacements due to the harmonic signal.

FILE NUMBER= 930120.05

Disp at lev. 3 due tbl. pitch: 217.6875xTable pitch
Disp at lev. 2 due tbl. pitch: 153.6875xTable pitch
Disp at lev. 1 due tbl. pitch: 90.1875xTable pitch

Table pitch: avg(atan((ch8-ch6)/144),atan((ch9-ch7)/144)) radians.

TIME (SECONDS)
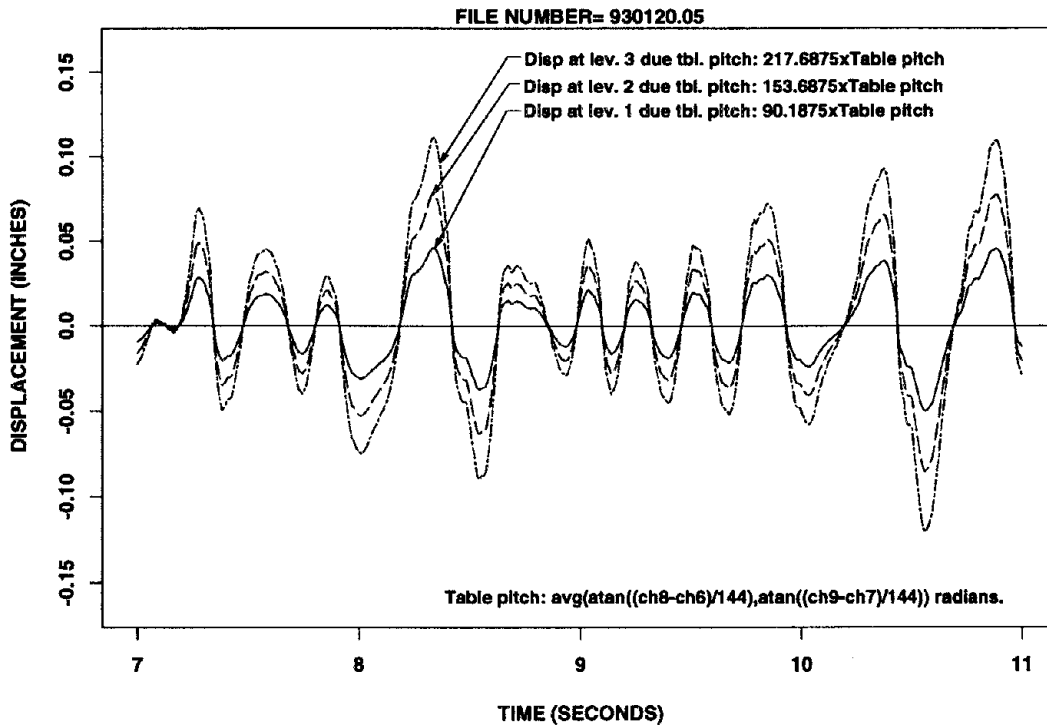
Figure 6.4: Pitch components of story displacements due to the Pacoima signal.

FILE NUMBER= 930119.14

Brace Shear, 1st story:(ch40+ch38-ch41-ch39)x0.669

Brace Shear, 2nd story:(ch44+ch42-ch45-ch43)x0.7474

Brace shear, 3rd story:(ch48+ch46-ch49-ch47)x.7474
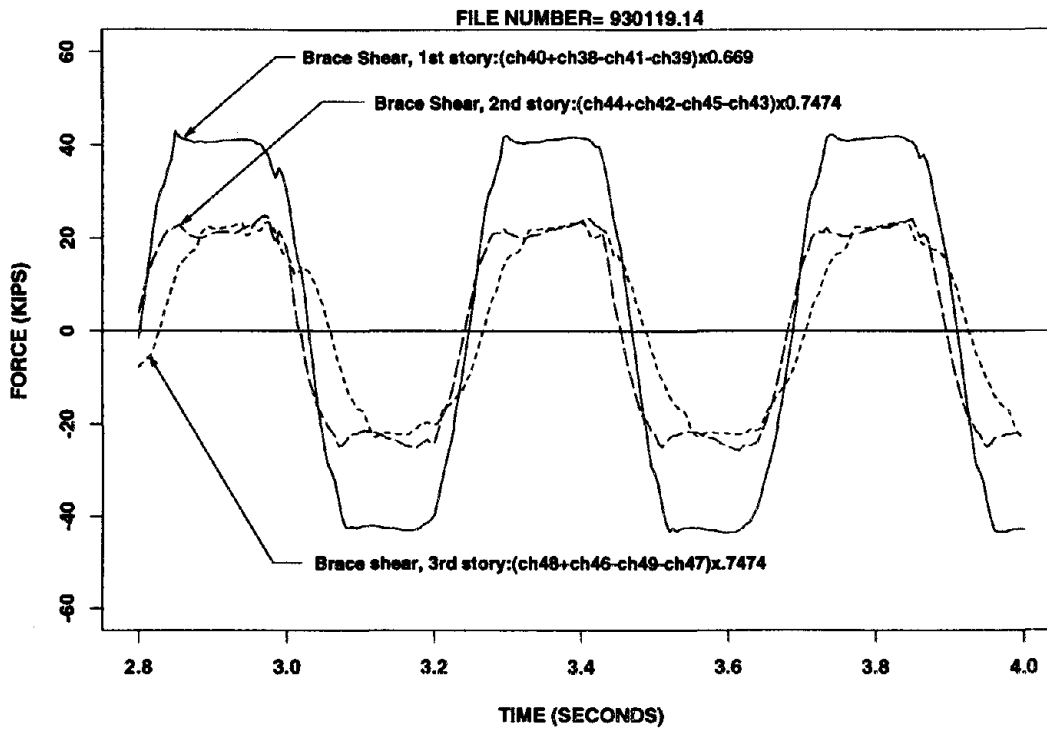
Figure 6.5: Story shear components carried by braces due to the harmonic signal.

FILE NUMBER= 930120.05

Brace Shear, 1st story:(ch40+ch38-ch41-ch39)x0.669

Brace Shear, 2nd story:(ch44+ch42-ch45-ch43)x0.7474

Brace shear, 3rd story:(ch48+ch46-ch49-ch47)x.7474
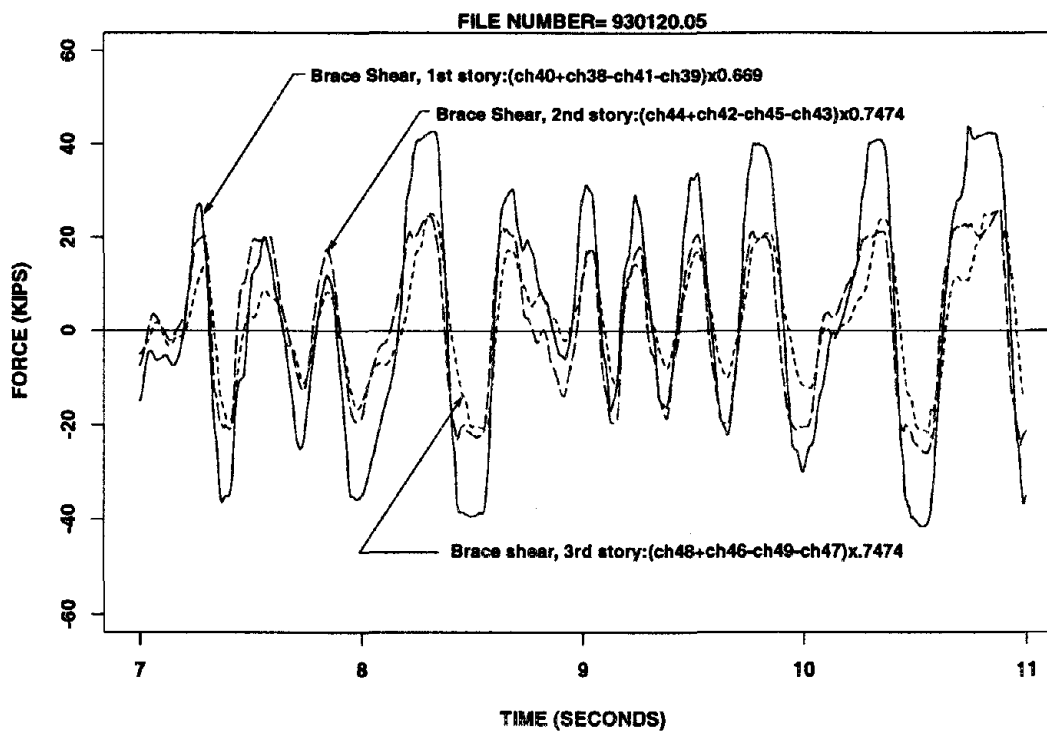
Figure 6.6: Story shear components carried by braces due to the Pacoima signal.

FILE NUMBER= 930119.14

Col. shear, 2nd story:(2/10^6)ES(ch61-ch59-ch60+ch58)/24

Col. Shear, 1st story:(1/10^6)ES(ch53-ch51-ch52+ch50+ch57-ch55-ch56+ch54)/36

Col. Shear, 3rd story:(2/10^6)ES(ch65-ch63-ch64+ch62)/24

TIME (SECONDS)
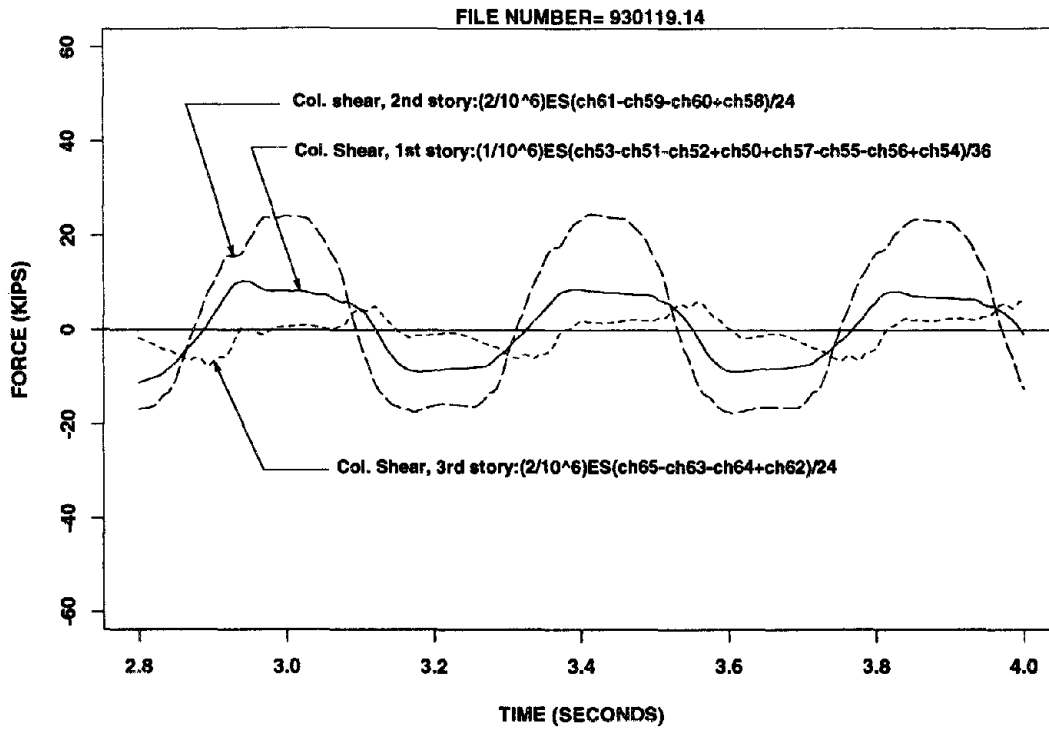
Figure 6.7: Story shear components carried by columns due to the harmonic signal.

FILE NUMBER= 930120.05

Col. Shear, 1st story:(1/10^6)ES(ch53-ch51-ch52+ch50+ch57-ch55-ch56+ch54)/36

Col. shear, 2nd story:(2/10^6)ES(ch61-ch59-ch60+ch58)/24

Col. Shear, 3rd story:(2/10^6)ES(ch65-ch63-ch64+ch62)/24

TIME (SECONDS)
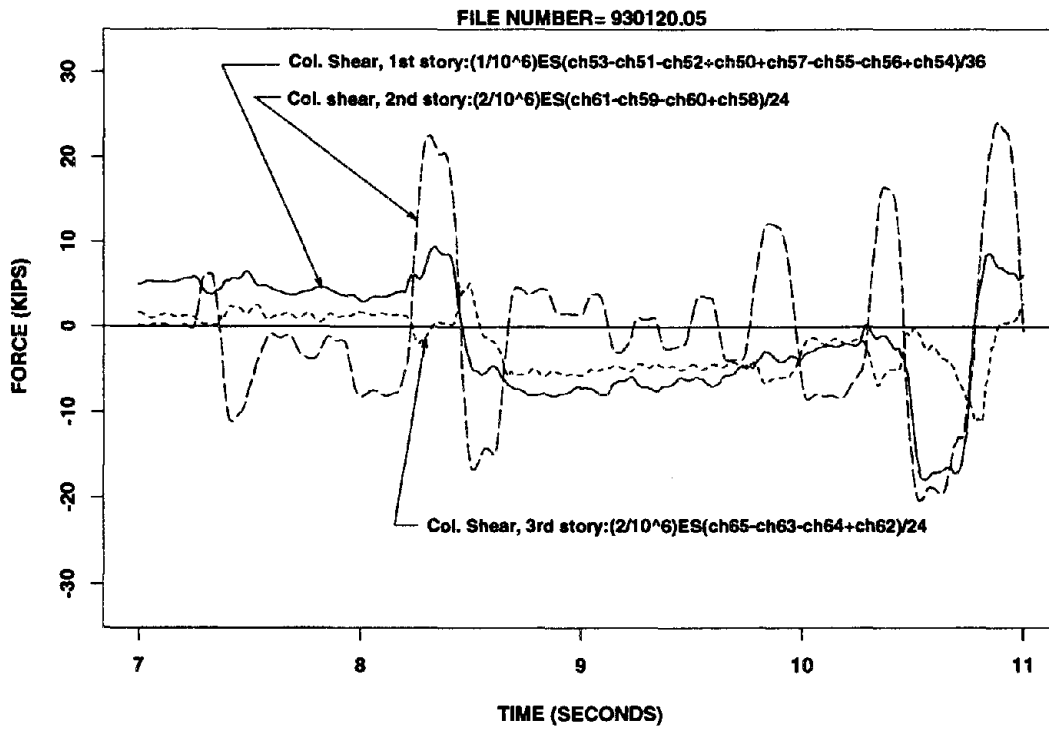
Figure 6.8: Story shear components carried by columns due to the Pacoima signal.
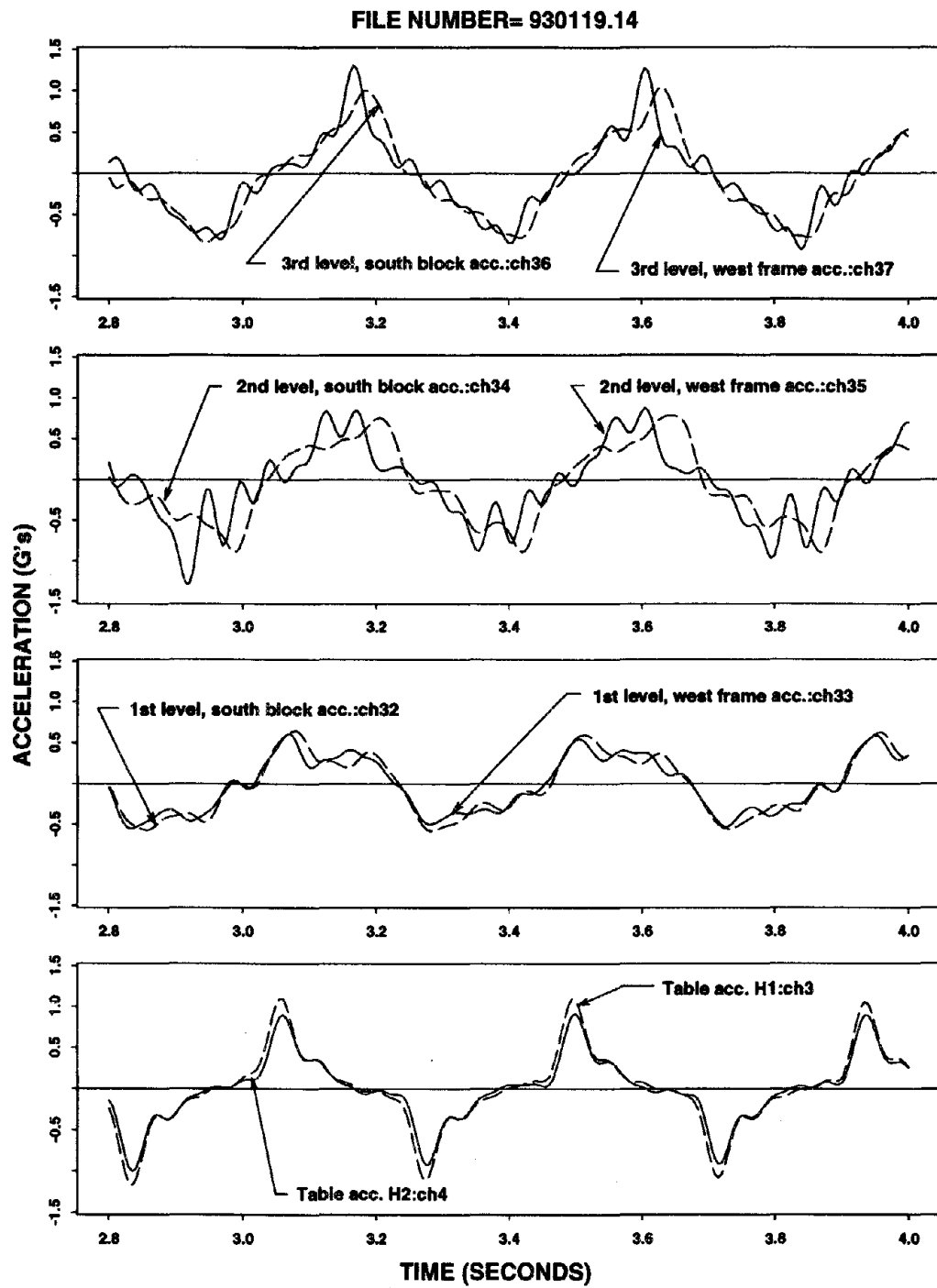
Figure 6.9: Accelerometer reading at various levels due to the harmonic signal

FILE NUMBER= 930120.05
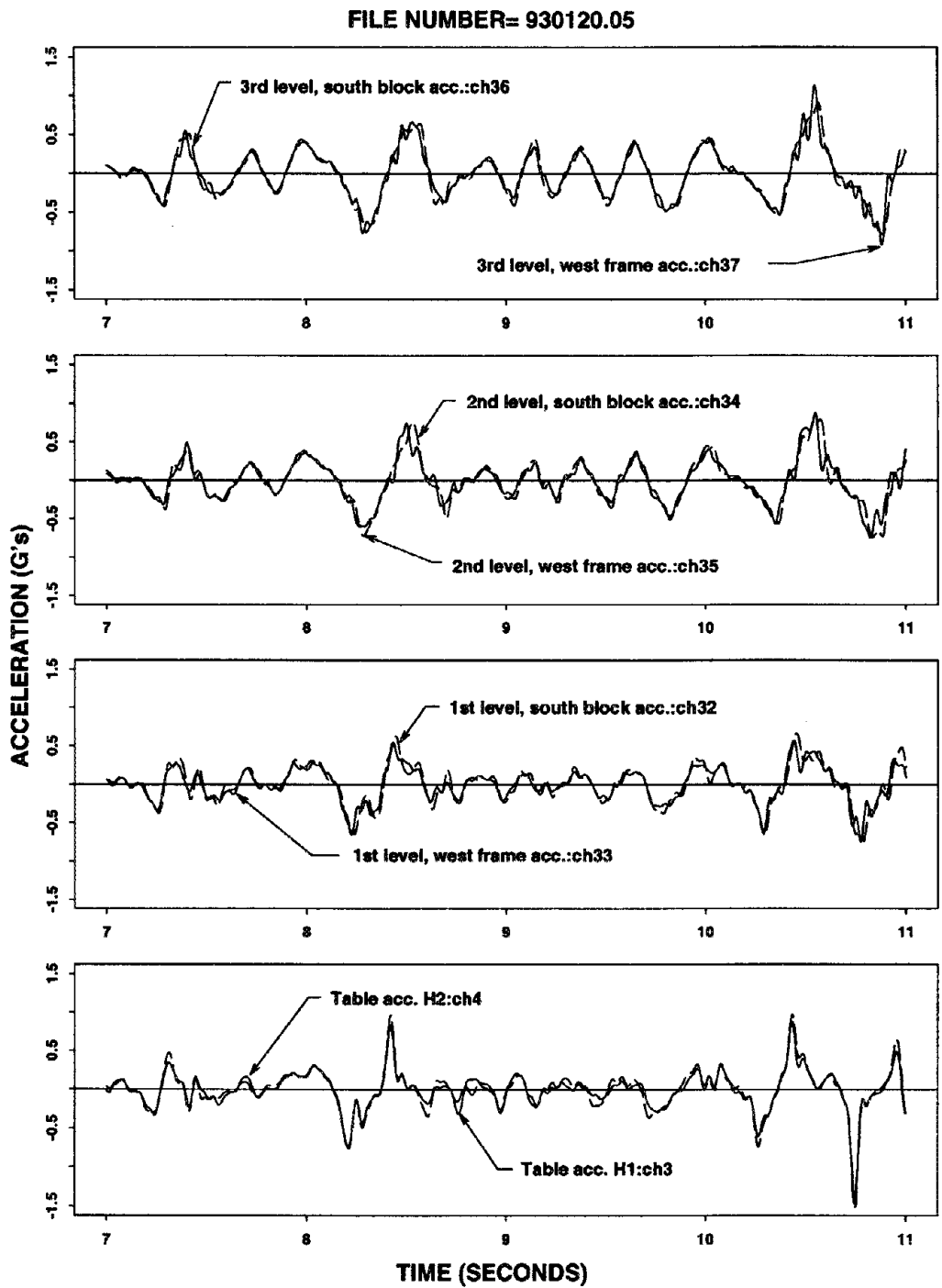
Figure 6.10: Accelerometer reading at various levels due to the Pacoima signal

FILE NUMBER= 930119.14
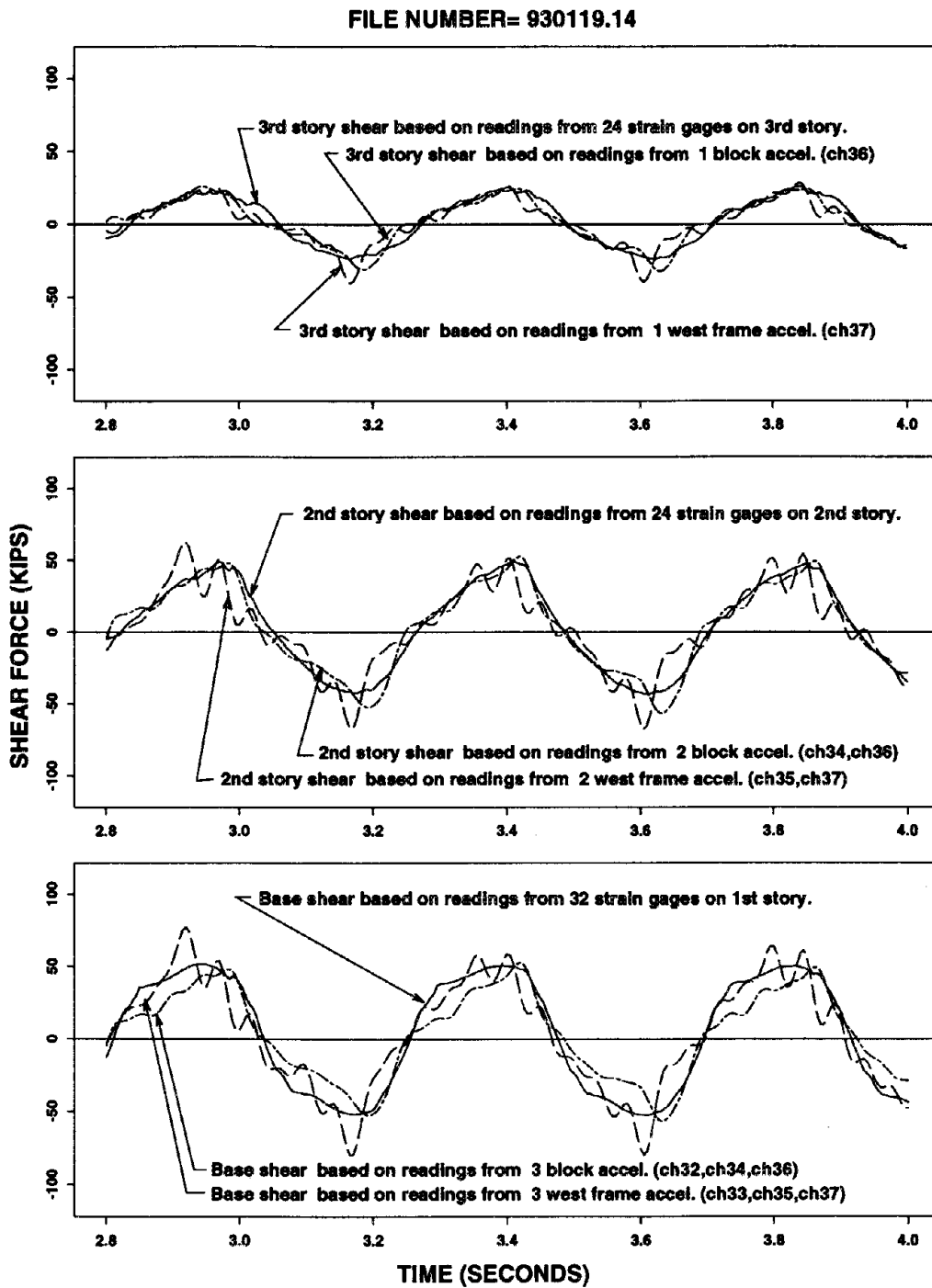
Figure 6.11: Three calculations of story shear forces due to the harmonic signal.

FILE NUMBER= 930120.05
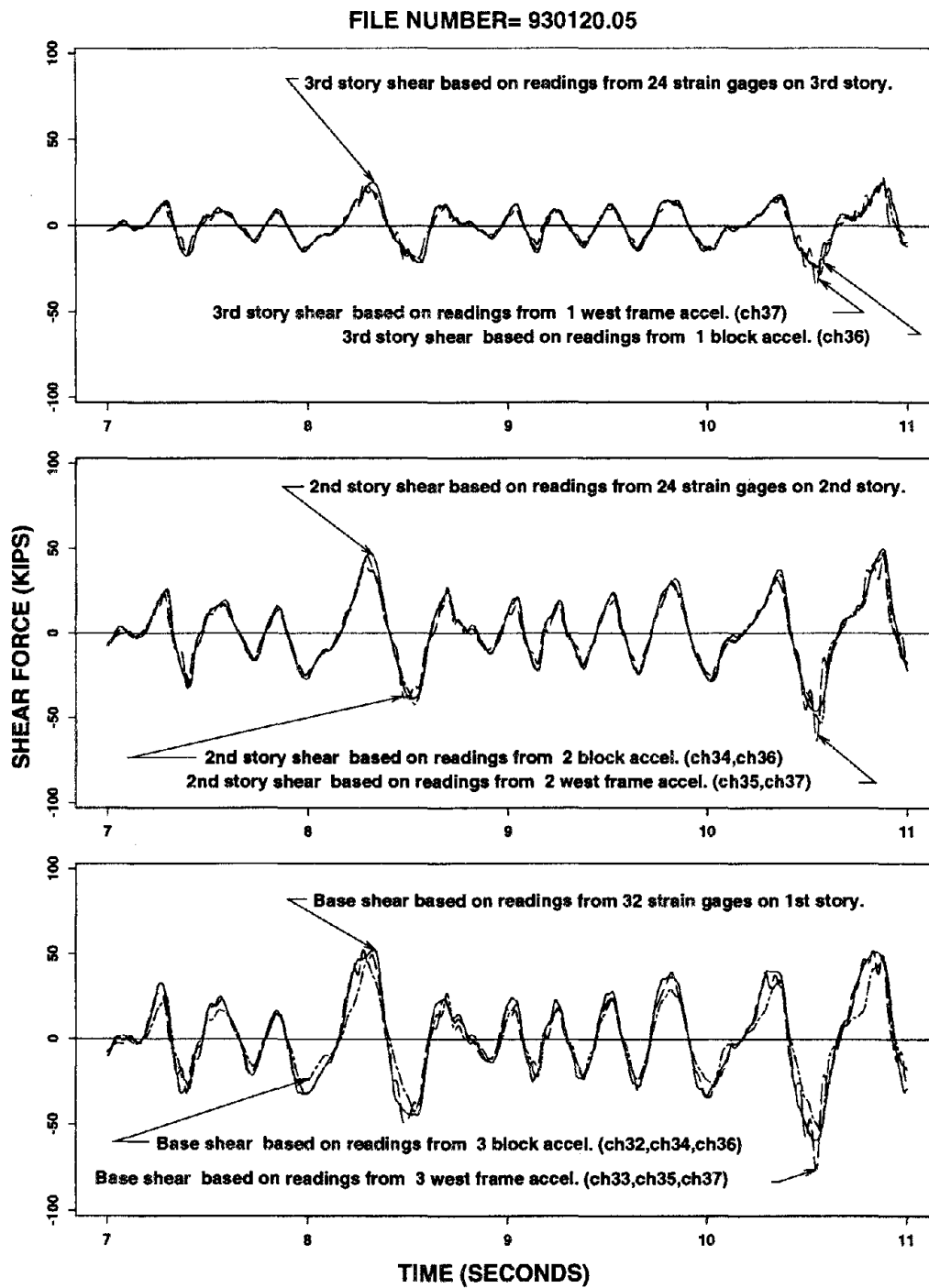
Figure 6.12: Three calculations of story shear forces due to the harmonic signal.
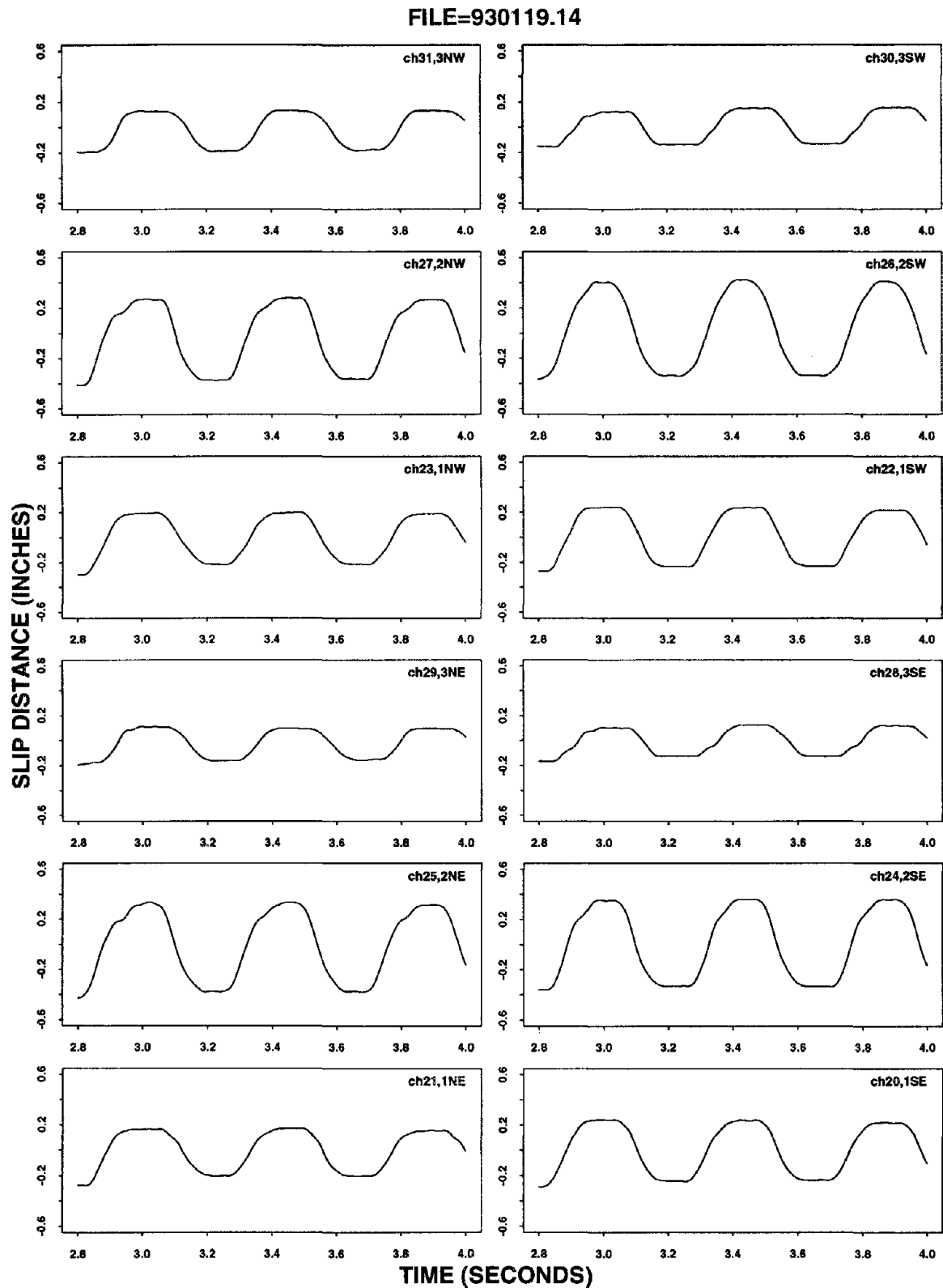
FILE=930119.14

Figure 6.13: Brace slip histories due to the harmonic signal.
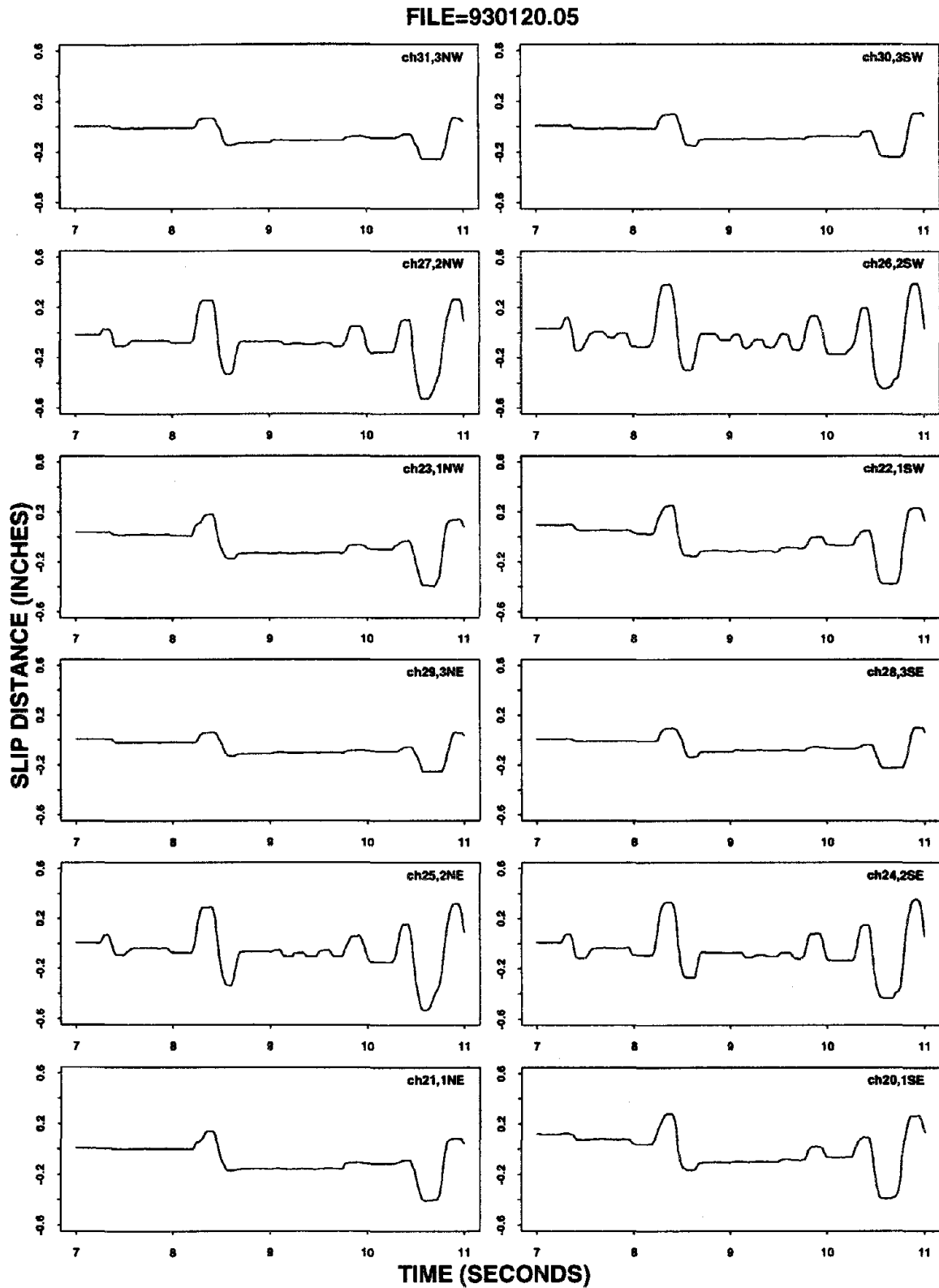
FILE=930120.05

Figure 6.14: Brace slip histories due to the Pacoima signal.
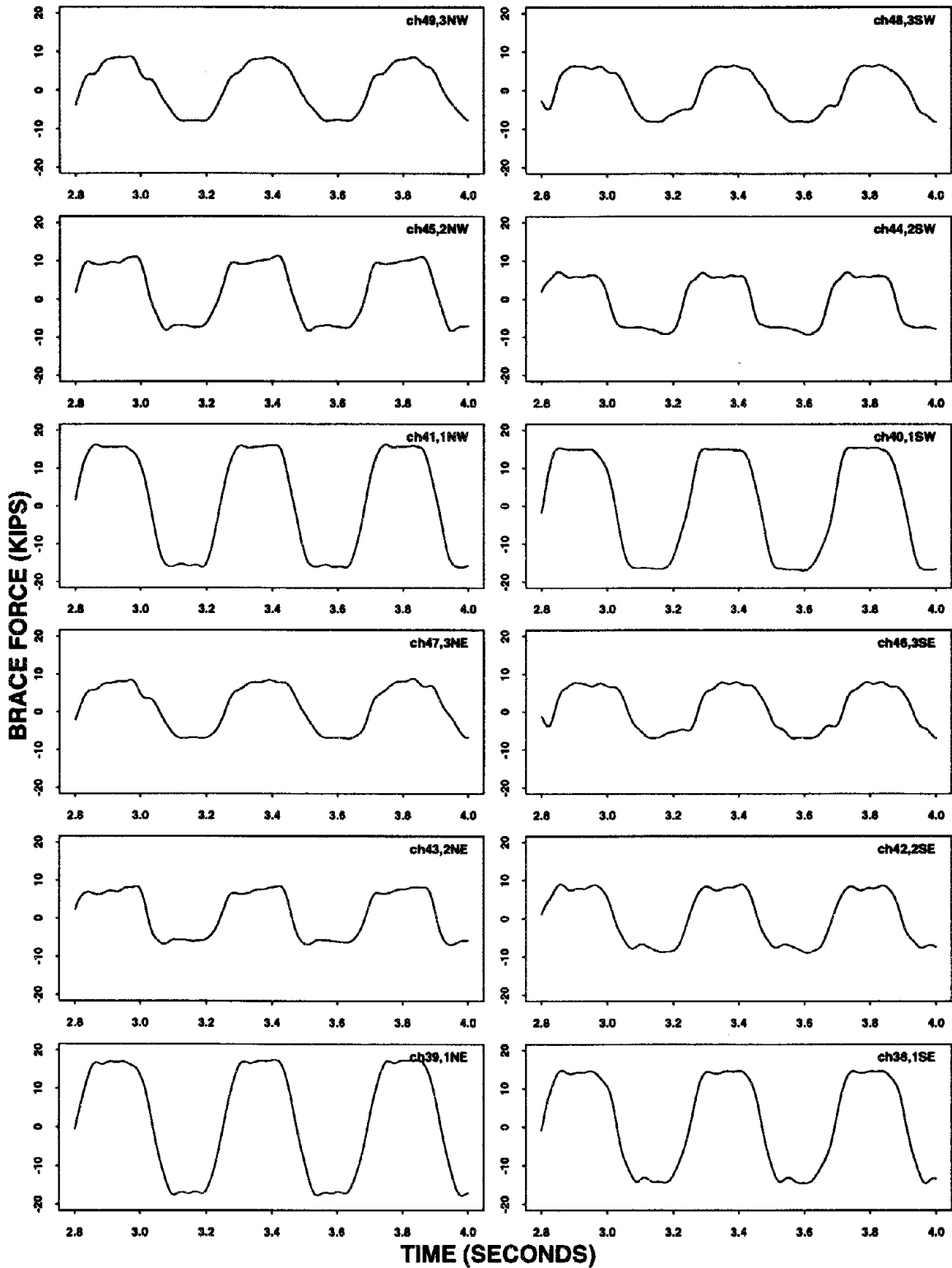
FILE=930119.14

Figure 6.15: Brace force histories due to the harmonic signal.
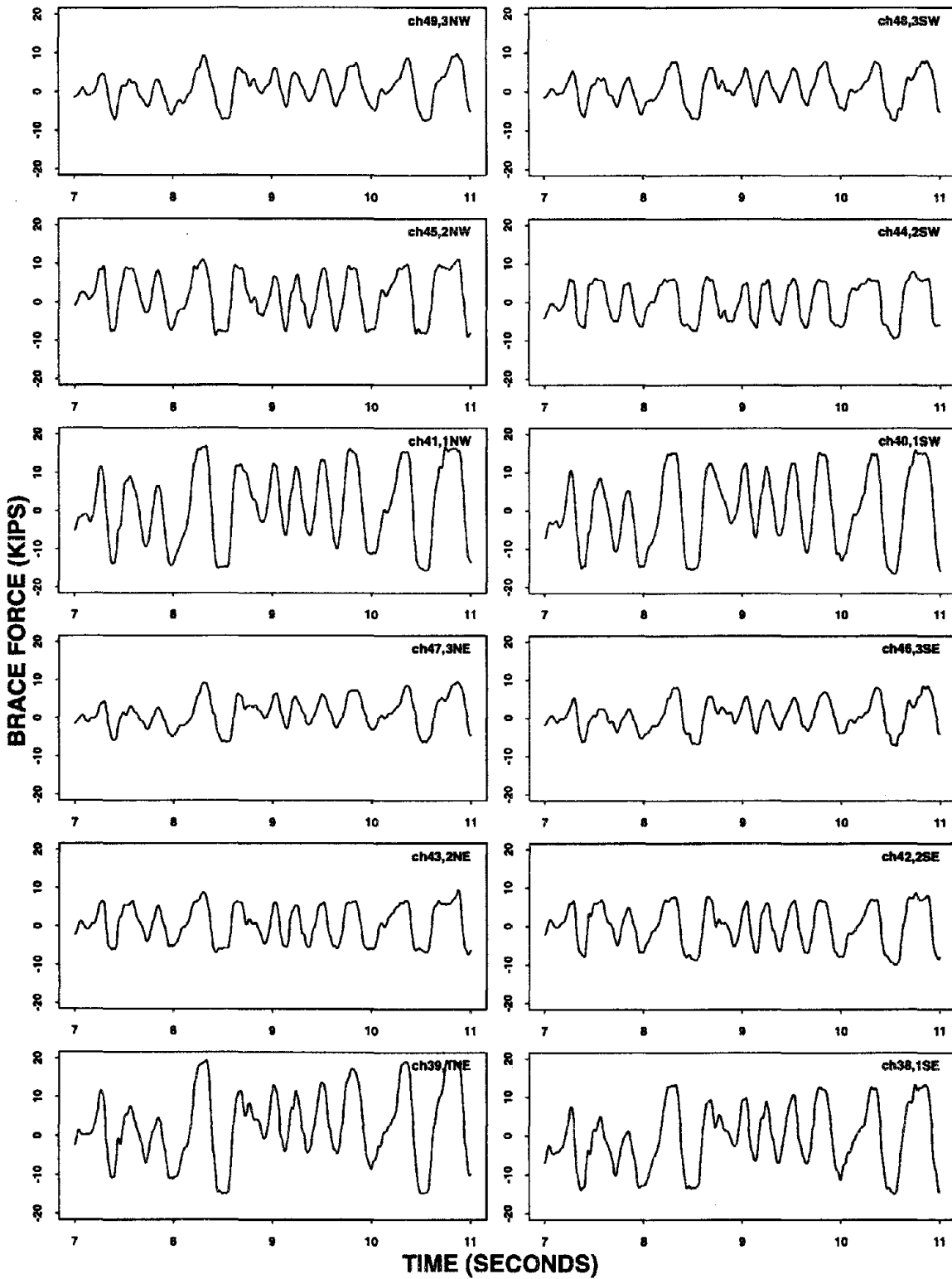
FILE=930120.05

Figure 6.16: Brace force histories due to the Pacoima signal.

FILE=930119.14
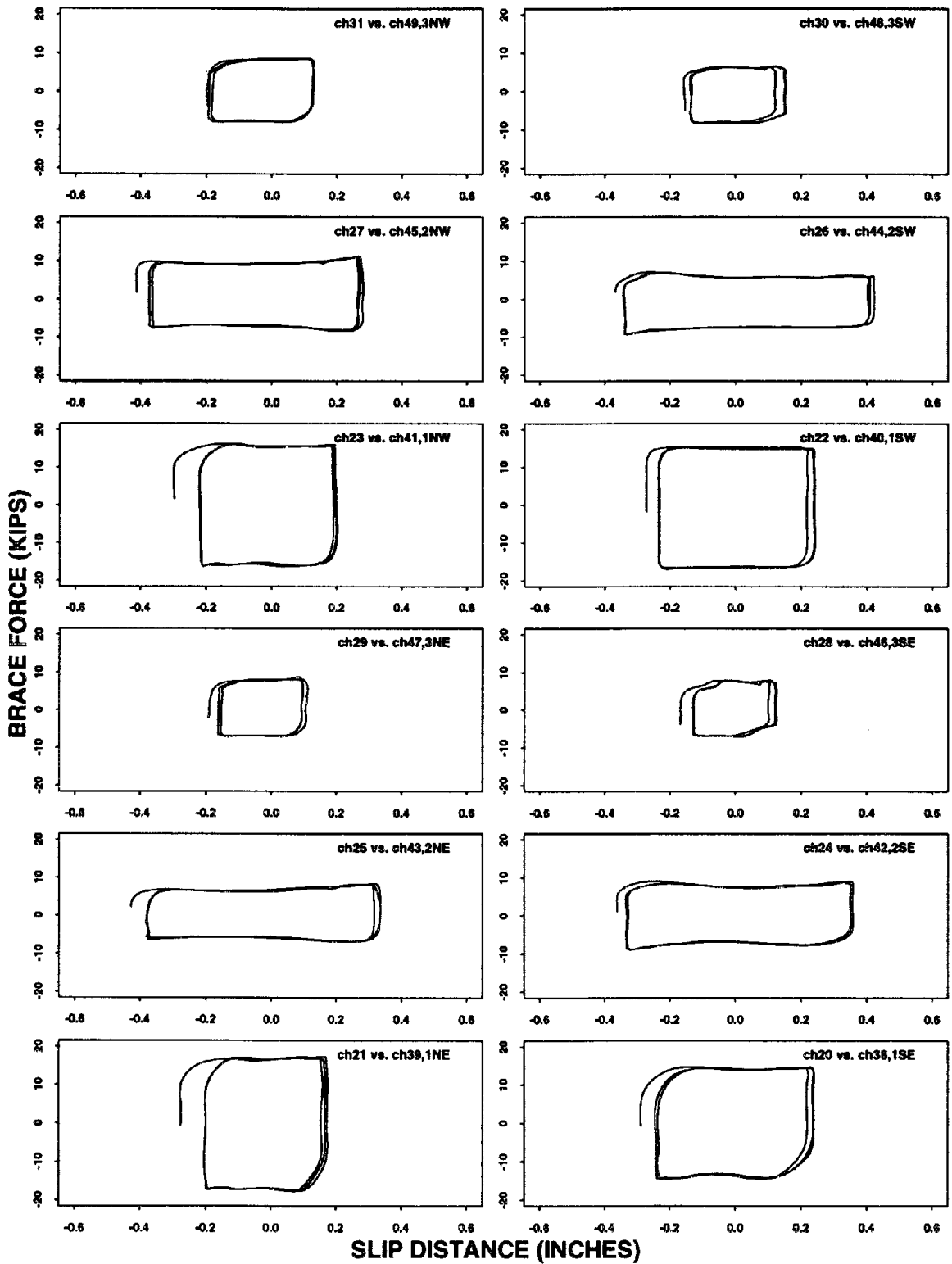
Figure 6.17: Hysteresis at SBCs due to the harmonic signal.

FILE=930120.05
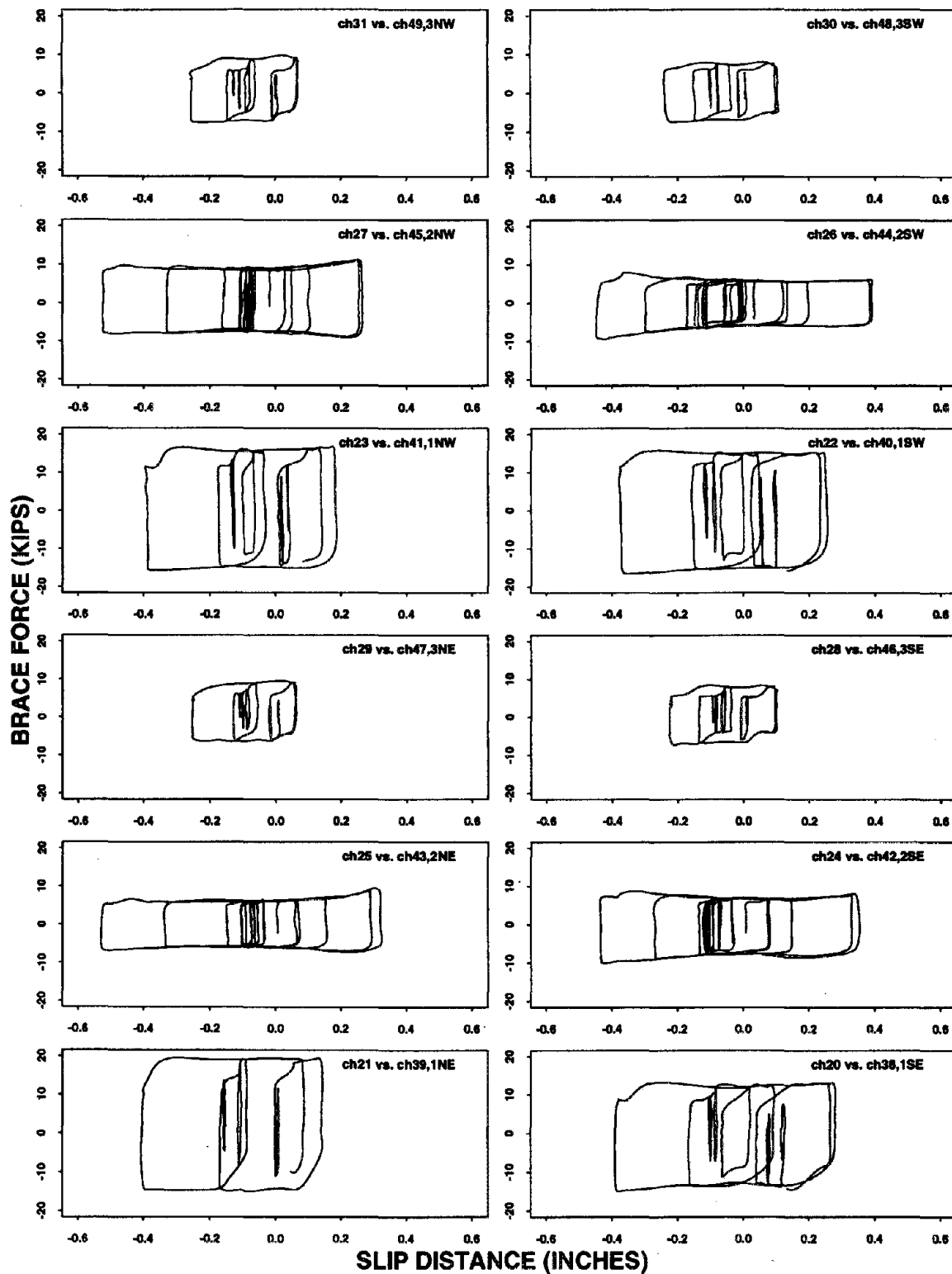
Figure 6.18: Hysteresis at SBCs due to the Pacoima signal.
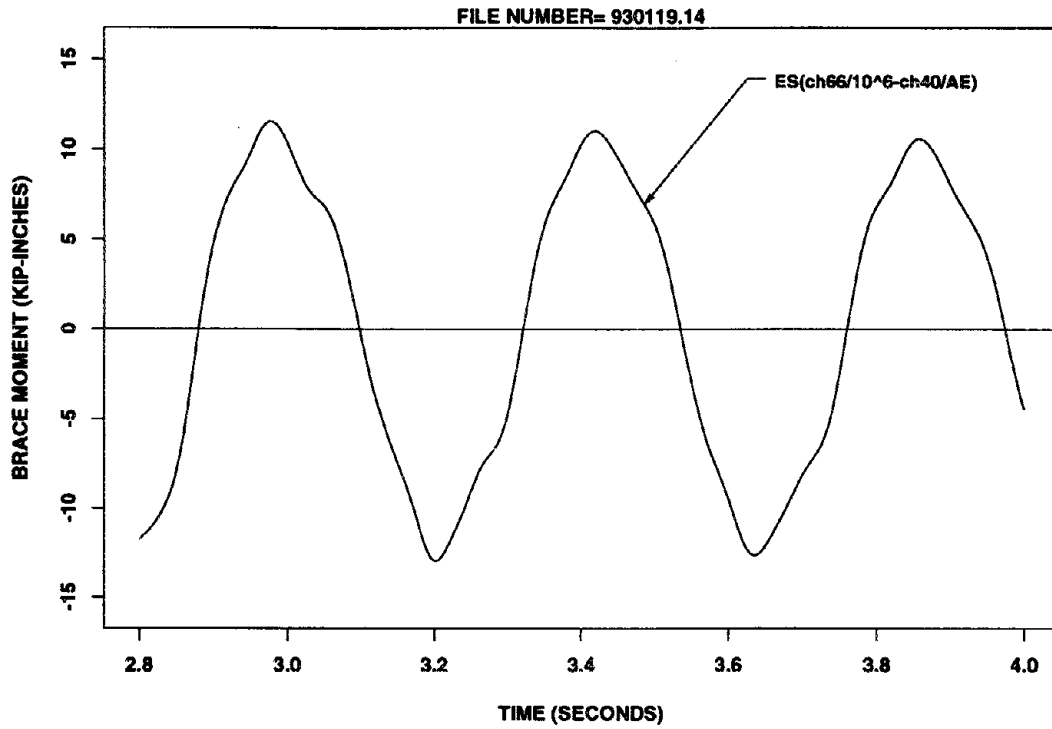
Figure 6.19: Brace moments due to the harmonic signal.
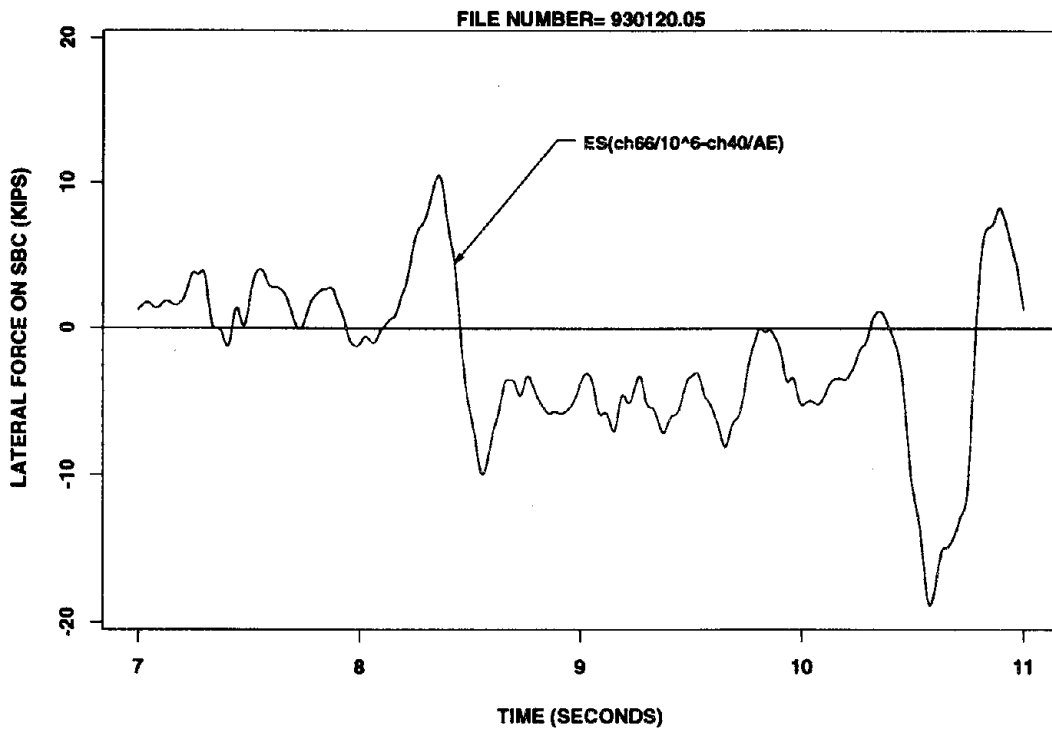
Figure 6.20: Brace moments due to the Pacoima signal.
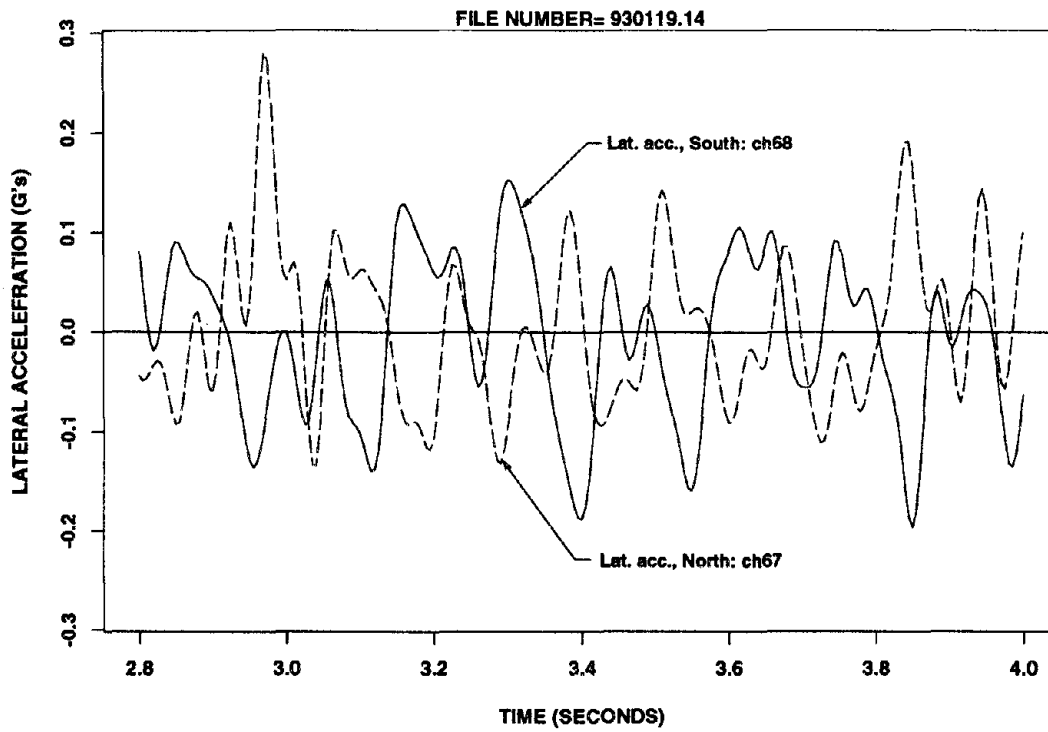
Figure 6.21: Transverse frame accelerations due to the harmonic signal.
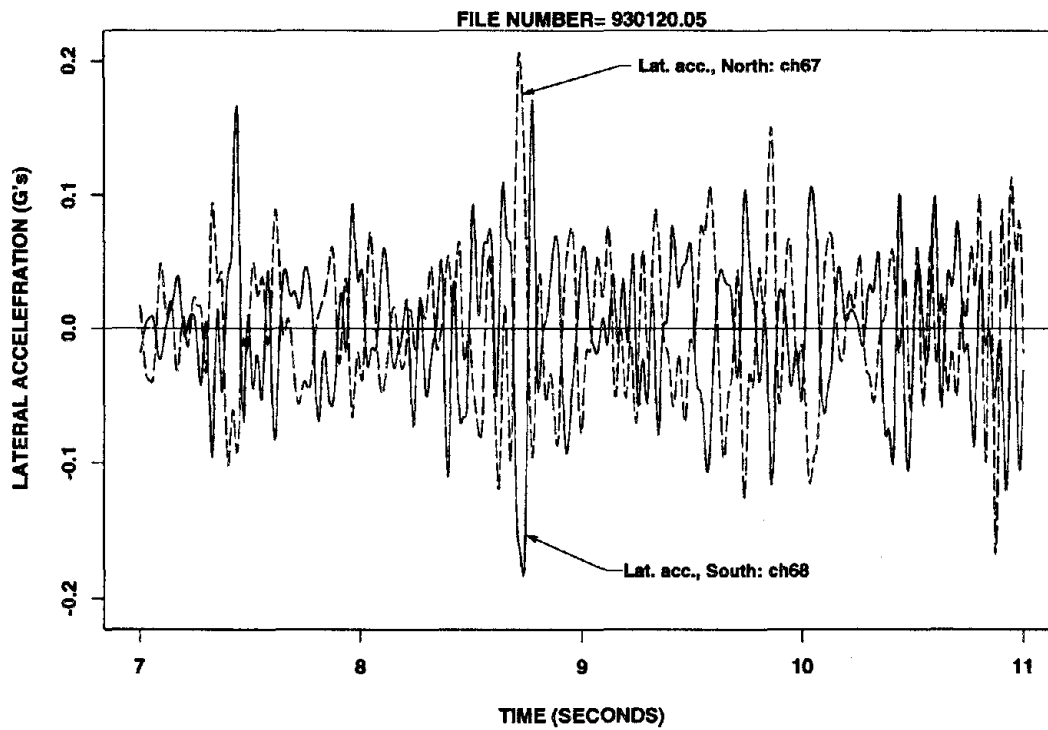
Figure 6.22: Transverse frame accelerations due to the Pacoima signal.

Chapter 7

Response of Test Structure with SBCs

7.1 General

Chapters 2 and 3 described the experimental results from the testing of individual SBCs in the C/T machine and subjected to harmonic imposed axial displacements. Chapter 4 described experimental results from the testing of individual SBCs, in the C/T machine, subjected to analytically derived imposed axial displacements simulating response of SBCs in structures subjected to various seismic excitations. Having described the test structure, in Chapter 5, and the general procedures of data reduction from instrumentation readings in Chapter 6, this is the point in this document at which the central subject regarding SBC behavior is examined; that is, the in-situ behavior of the connections, in the test structure subjected to real and devastatingly large accelerations, and their effect on response of the structure.

Both the local behavior of the SBCs and their effects on the global response of the structure are examined. The behavior of SBCs of the test structure is compared with that described in Chapters 2 through 4. The effects of the addition of extra bolts to the SBCs of the second level are noted. The global effect of the SBCs on the lateral force resisting system of structure is discussed. The effects of the choice of a chevron configuration are considered. The bending moments induced in the bracing

members due to the slip in the SBCs are considered and suggestions for predicting these moments are made. The effect of the twelve SBCs in the structure is evaluated in terms of the energy input and dissipation histories. These histories are then compared for the TS1 and TS2 configurations. Finally, the extrema of the responses of TS1 and TS2 are compared to each other and also the response of another energy dissipation system, the ADAS, tested on the same frame with the same masses and with similar table inputs.

7.2 Hysteresis at SBCs

As described in Chapter 4, unworn SBCs go through a "break-in" process which generally occurs in the course of the first few inches of cumulative travel. During this "break-in" the slip force of the connections increases and reaches a plateau, marking the end of the "break-in" phase. This same behavior would be expected to occur in the SBCs of the test structure. This was indeed the case. To see this, the very first tests of the structure are examined.

The Chilean signal was chosen to be the first strong earthquake signal to be applied. The shake table, at its maximum capacity, would be capable of delivering this acceleration history with an amplification of 1.1675 times that of the original recorded acceleration history. That amplification would result in a peak acceleration of roughly 0.8 Gs. The structure was designed with SBCs to withstand the said signal with an amplification of 1.5. Despite analytical results indicating an indestructible design (that is, relative to the capacity of the table), the thought of a 96,000 pound structure accelerating horizontally at 0.8 Gs convinced the experimenters to delay "the moment of truth" by increasing the amplitude of the signal to its maximum in four steps. Figure 7.1 shows the hysteresis of the SBCs of the structure due to the first of the said signals. The peak table acceleration was 0.34 Gs, corresponding to an amplification of 0.491. Corresponding hysteresis loops for the fourth signal are shown in Figure 7.2. The peak table acceleration was 0.81 Gs. The apparent large slips of the SBC of brace 3SE in Figure 7.2 do not reflect real displacements. The true slip distances of this SBC should be nearly identical to that of 3NE. It is suspected that

a lose data cable must have collided with the wire of the wire potentiometer causing the apparent large displacements.

Comparison of Figures 7.1 and 7.2 reveals that not only have the hysteresis loops increased in width, but that they have also increased in height. The increases in heights correspond to increase of the slip forces. This increase is attributed to the "break-in" phenomenon. As the test structure was rather strong, even in comparison to the capacity of the shake table, slips at SBCs were small, contributing to slow gradual increase of the cumulative slip distance. This also meant that the test structure could be tested over and over again without any appreciable loss of slip force at the SBCs. Nearly sixty tests strong enough to cause slip at SBCs were conducted on the structure without any significant reduction in the value of slip forces of SBCs being observed.

Effect of Change of Configuration from TS1 to TS2

As noted in Chapter 5, three structural configurations, TS1, TS2 and TS3, were tested successfully. Two of these, TS1 and TS2, are described in this chapter and then again in Chapter 8. Three sample table inputs applied to each of the two configurations have been chosen for this presentation. These table inputs are the Chilean signal, amplified by a factor of 1.1675, the un-amplified Pacoima signal and a harmonic signal applied at 2.27 Hertz. Accordingly, six representative shake table tests are presented. The three pairs, in the order of the above mentioned signals, and identified in testing schedule Tables 5.2 and 5.3, are 930119.09/930120.09, 930120.05/930120.13 and 930119.14/930120.18. Two of these, 930119.14 and 930120.05, are familiar from discussions in Chapter 6 in regards to data reduction. Test 930119.09 is also, in a way, familiar. The table input for this test is the same as the one causing the hysteresis at SBCs shown in Figure 7.2. Figure 7.3 shows the hysteresis loops for test 930119.09 with a different scale used in plotting. The scale has been altered so as to make comparison with the other five sample cases easier. However, accounting for the difference in plotting scale, it seen that the loops shown Figure 7.2 are almost identical to those of Figure 7.3. Both tests are of TS1. The two tests, with identical inputs signals,

were separated by three days and nine tests. Such repeatability speaks well of the consistency of the behavior of SBCs. From this point on in the presentation, the six representative tests mentioned above will be referred to by the name of the associated table input signal in conjunction with the name of the structural configuration. For example, test 930120.05 will be referred to as "TS1 subjected to the Pacoima signal."

Figure 7.4 shows hysteresis loops of TS2 subjected to the Chilean signal. A dramatic change is seen in the shape of the hysteresis loops. As expected, the hight of the hysteresis loops of the second level is increased. This being due to the addition of one extra bolt to each of the SBCs of the second level. The magnitudes of the slip forces are in accordance with the slip forces of the specimens tested in the C/T machine and presented in Chapters 2 through 4. However, the most striking feature of this change is the decrease in the width of the hysteresis loops of the second story SBCs and a corresponding increase in the widths of the hysteresis loops of the the first story SBCs. This change in response is seen again in the responses of TS1 and TS2 due to the Pacoima and harmonic signals. The hysteresis loops of the SBCs of TS1 and TS2 due to the Pacoima signal are shown respectively in Figures 7.5 and 7.6. Similar hysteresis loops for the responses of TS1 and TS2 due to the harmonic signal are shown in Figures 7.7 and 7.8. It is seen that for all six cases presented, the SBC behave as one would expect given the results of Chapters 2, 3 and 4. The behavior of the connections is seen to be elastic-perfectly-plastic. The magnitudes of the slip force are within range of that indicated by C/T testing. And, even, the "chewed off corners", due to bolt hole tolerances and deformation of the holes in the shims, are present and particularly noticeable for smaller slips.

It should be noted that the increase or decrease in the width of the hysteresis loops corresponds directly to the increase or decrease of the story drifts at the level of the SBCs in question. It is seen then that the change in the slip forces, due to the addition of the extra bolts, in a single story of the structure, changes the entire behavior of the structure and, in particular, drastically effects the magnitude of the story drifts. It is shown in Chapter 8 that this difference in behavior between TS1 and TS2 can be predicted by non-linear dynamic analyses of the two configurations. Indeed, as of the time of the writing of this document, this is the only reliable method

of predicting the behavior of structures with SBCs.

Hysteresis of Bracing System at Story Level

In order to appreciate better the role of the bracing system with SBCs in the lateral force resisting system of the structure, it is best to examine the the combined effect of the four braces and SBCs at each level. Figures 7.9 and 7.10 show the sums of the horizontal components of the brace forces at each level plotted against the average corrected story drifts of the two longitudinal frames at those levels. By corrected story drifts, it is meant that the contribution of the table pitch to displacements of the stories has been taken to account and is not reflected in the drifts. The two figures show the hysteresis of the bracing systems at each story for, respectively, TS1 and TS2 due to the harmonic signal. It is seen that the same trends that were observed in the plots of the individual SBCs are also apparent in these two plots. The figures represent the hysteretic behavior of the bracing system in resisting lateral loads, as such they attest to stability of the hysteretic mechanism provided by the SBCs. That hysteresis loops in these figures are so close to ideal linearly-elastic-perfectly-plastic (LEPP) behavior suggests also that, under right circumstances, a whole array of SBCs may be modelled as a single LEPP spring.

From a conceptual point of view, the forces indicated in Figures 7.9 and 7.10 can be thought of as drag forces of constant magnitude acting on the three levels of the un-braced frame. With movement of the un-braced frame, the products of the the drag forces with the story displacements represent energy dissipated by non-conservative work done by the the drag forces going through the displacements.

7.3   Compliance with Small Angle Geometry

In classical analysis of structures, small angle geometry is used for calculating components of displacements. Accordingly, given story drift d at any level of the test structure, and assuming the beams and columns to be axially rigid and the midpoint of the beam restrained vertically, the slip of the brace would be $d \cos \theta$, less the

elastic stretch of the brace due to the slip force. θ is the angle of the brace with the horizontal. Similarly, the displacement of the brace perpendicular to its own axis and in the plane of the frame would be given by $d \sin \theta$. These relations are shown in Figure 7.11 parts (a) and (b). Part (c) of the figure shows the forces that may be acting at the brace at the point of its connection with the SBC. FS is a force parallel to the un-deformed axis of the brace and can at most be equal to the slip force of the SBC. F is a force acting perpendicular to the un-deformed axis of the brace. Determination of the approximate magnitude of F is necessary for the design of the brace to withstand bending moments. It is noted that in this figure, the angles between the braces and beams in the deformed geometry are different from those in the un-deformed geometry. This is so because the standard slot widths of the two and one bolt SBCs used in the structure were such that the SBCs allowed a considerable amount of rotation of the middle plates of the SBCs with respect to the outer plates. As such the SBCs of the test structure could be considered to be hinges. Part (c) of Figure 7.11 shows a cantilever-ed braced. For a case where SBCs are allowed no rotations, the SBC ends of the braces would be shown restrained in rotation but free to move horizontally. The relative deformations would be the same.

Relationship of Slip to Drift

Figures 7.12 and 7.13 show, for each brace, plots of the corrected story drifts at the story of the braces versus the slip of the braces. The plots are arranged in the same positions in the figures as those for the hysteresis loops described earlier in this chapter. The two figures are respectively for TS1 and TS2 subjected to the harmonic signal. In these plots, the diagonal lines represent the relation given by small deformation theory, assuming a slip force of zero. The lines go through the origin and have slopes of $\frac{1}{\cos \theta}$. Accounting for the elastic stretch and shortening of the braces before slip in tension and compression, under cyclic loading as is the case here, theory would predict parallelogram shaped loops. The sides of the parallelogram would be vertical and of twice the length of the elastic stretch, while the top and bottom of the parallelogram would be parallel to the described line. As seen in Figures 7.12 and 7.13

the behavior can indeed be described as tracing roughly parallelograms. A puzzling feature of these plots is that the heights of the plots for several adjacent braces seem to be unequal. As an example consider the cases of the bottom two plots in each of the two figures. As in the case of the hysteresis loops the two plots are associated, left to right, with respectively the North and South braces of the East frame at the first level, i.e. 1SE and 1NE. It is seen that the vertical legs of the parallelograms of the northern brace, 1NE, are larger than that of the southern. Looking back at the hysteresis loops of these two braces it will be noticed that the northern brace has the larger slip force of the two. The correlation is also observed to be true for other adjacent braces. This phenomenon is best explained in conjunction with a discussion of the behavior, in particular, of chevron bracing connected with SBCs.

Peculiarities of Chevron Bracing with SBCs

Figure 7.14 is used as a visual aid in the discussion of behavior of chevron bracing with SBCs. Part (a) shows the schematic diagram of a chevron braced frame. The braces are designated 1 and 2. The angle of the braces with the horizon is indicated as θ. The point of the concentric connection of the braces to the beam is marked with a heavy dot. $F1$ and $F2$ are the slip forces of the SBCs of the two braces. Only the braces are assumed to be non-rigid axially in this qualitative presentation. The beams and the columns are assumed to be axially rigid. The assumption is not far from the reality. In the diagrams, external force is shown by solid arrows while internal force is shown by dashed arrows. Assuming that the slip forces of the braces are of equal magnitude, slip occurs in the two braces simultaneously. As slipping is equivalent to having zero stiffness, then (b) is representative of the behavior of the braced system while slippage continues at the SBCs of the braces. That is the braces are replaced with forces of magnitude equal to the slip forces of the SBC and acting at the midpoint of the beam in directions parallel to the axes of the braces. Given that the forces are of equal magnitude, their vectorial resolution results in no vertical forces, while their horizontal resolution results in a force of $(F1 + F2)\cos\theta$ acting as a drag force in direction opposite to the externally applied force F. (d) shows the

force-deformation curve resulting from the above description. Branch (a) of this curve indicates force-deformation relation before the occurrence of simultaneous slip in both braces. This branch has a slope indicative of the stiffness of the braced frame. Branch (b) indicates behavior while sliding occurs at SBCs. The slope of the branch indicates the stiffness of the frame without the bracing. Δ indicates the deformation of the braced frame before simultaneous slip occurs in the braces. Slip is indicated in this figure to occur at $(F1 + F2)\cos\theta$. This is not absolutely correct as this would only be true if the frame itself were to not resist any lateral deformation. However, given that the braces are far stiffer then the beams and columns in flexure again the assumption is good. Relating Δ to Figures 7.12 and 7.13, it is seen that Δ would ideally indicate half the height of the vertical legs of the parallelograms. The vertical legs indicate increase of drift with no increase in slip distance. That is Δ by definition. Reversal of loads results in 2Δ for the heights of the parallelograms. Equal slip forces then would result in equal heights for the parallelograms of adjacent braces. As we have seen, for a number of brace pairs this is not true, as it is also not true that the slip force of the pairs are equal. Suppose $F1$ to be larger than $F2$, then applying the external force F will cause brace 2 to slip first. This results in the situation portrayed in (e). While sliding occurs at the SBC of 2 and the SBC of 1 is locked, the structure has the stiffness and behavior of an eccentric braced frame with a very long shear link. As the external force increases, brace 1 also slips resulting in the situation shown in (f). Note that unlike (b), in which the center point of the beam remained vertically stationary, here the midpoint of the beam moves downward due to the imbalance of the slip forces of the SBCs. This displacement is indicated by δ. (g) shows the horizontal and vertical resolution of forces at the midpoint of the beam. The horizontal drag force is calculated as before, while a vertical force of magnitude $(F1 - F2)\sin\theta$ is seen also to act at the midpoint of the beam. This vertical force causes the displacement δ mentioned above. With reversal of load, a displacement of magnitude δ above the original position would result in similar manner. Upon cyclic loading then, the midpoint of the beam would oscillates vertically. Such movements, although of small magnitude, were indeed observed in the test structure during testing. The behavior described above results in a tri-linear force-displacement curve shown in (h). Branch

(a) in this curve has the the same slope as branch (a) in (d). Branch (f) has the same slope as branch (b) in (d). Branch (e) has a slope of the stiffness of the eccentric brace in (e). $\Delta 2$ is the drift of the frame at at which the weaker brace 2 slips, while $\Delta 1$ is the drift of the frame when the stronger brace 1 joins brace 2 in slipping. As in the case with $F1$ equal to $F2$, the Δs are related to the heights of the vertical legs of the parallelograms in Figures 7.12 and 7.13. $\Delta 1$ indicates the drift of the structure while no slippage occurs at at the stronger brace, while $\Delta 2$ indicates the same for the weaker brace. Then, whenever $F1$ is greater than $F2$, $\Delta 1$ is greater than $\Delta 2$. Examination of Figures 7.12 and 7.13, while recalling that the vertical sides of the parallelograms are related to the Δs by a factor of 2, shows this statement to be in accord with experimental results.

Bending Moments of Brace Connected with SBC

An issue of concern that arose during the design phase of the bracing system was the estimation of the moments induced in the braces due to slip of SBC and the associated story drifts. As mentioned above, small angle geometry dictates that a unit story drift gives rise to a displacement at the SBC connected tip of the brace perpendicular to brace, and in the plane of the frame, of magnitude $\sin \theta$. Assuming the other end of the brace to be fixed, it is seen that the brace must flex to accommodate this displacement. Given that the SBC end is assumed to be hinged, this bending is due to two orthogonal force vectors acting through the position of the bolts of the SBC. These two are F and FS shown in part (c) of Figure 7.11. The bending moment to be resisted is the given by $M = FL + FSd \sin \theta$. Letting slip distance to be designated l and assuming no vertical movements of the midpoint of the beam, and recalling that $l = d \sin \theta$, the moment, M, shown in part (c) of Figure 7.11 can be approximated by $M = [3\frac{EI}{L^2}(1 - \frac{FS}{P_{cr}}) + FS] \tan \theta \times l$. P_{cr} is the Euler buckling load of a simply supported pin of flexural rigidity EI and length $2L$. FS is considered positive in this relation when it causes compression in the member. This equation implies that under compression the brace is more flexible than an axially unloaded cantilever. Similarly it can be shown that in tension the brace will have

larger flexural stiffness. It would be much more convenient in design, however, to use the assumption that the bending moments can be approximated by treating the brace as a cantilever without the consideration of the contribution of the axial force to the bending moment. For small deformations encountered in the test of the Test structure this assumption is reasonable. Given this assumption, the bending moment in the brace would be given by $M = \frac{EI}{L^2} \tan \theta \times l$. The experimental measurement of the brace moment, M, for the south-western brace, SW1, of the first level of the structure was described in Chapter 6. This moment is plotted against the slip distance of the brace for TS1 and TS2 subjected to the harmonic signal in Figures 7.15 and 7.16. A line through the origin with slope $\frac{EI}{L^2} \tan \theta$ is superimposed over these two plots. Extension is indicated as positive in these figures. It is seen that for both figures the magnitude of the brace moment is rather small, on the order of 15 kip-inches. Further, it is seen the the equation $M = \frac{EI}{L^2} \tan \theta \times l$ does rather well as a design tool to estimate the bending moments on the brace. The equation appears to overestimate the moments over most of the range of the slip distance. This happens, perhaps, because the end of the brace is not truly fixed. The hollow tube of the brace "fish tails" into a gusset plate, and it is possible for the flanges of the tube to flex.

7.4 Energy Input and Dissipation Histories

It will be recalled that in Chapter 1 the "Sink Analogy" was used to describe the energy balance equation for a SDOF structure with an Coulomb friction-type connection. The concepts presented in Chapter 1 regarding the energy quantities can be extended to a multi-degree-of-freedom structure like the structure tested [28]. The quantities relevant to the discussion here and indexed to represent the test structure and are given as;

$$E_i = \int \sum_{i=1}^{3} m_i \ddot{v}_{t_i} dv_g$$

$$E_k = \frac{1}{2} \sum_{i=1}^{3} m_i \dot{v}_{t_i}^2$$

$$E_s = \frac{1}{2} \mathbf{v}^\mathrm{T} \mathbf{K_{frame}} \mathbf{v} + \frac{1}{2} \sum_{j=1}^{12} \frac{f_{brcae_j}^2}{k_{brace_j}}$$

Here, m_i , v_g, $\dot{v}_{t_i}$, and $\ddot{v}_{t_i}$ refer to the story masses, ground displacements, absolute velocities and absolute accelerations. $\mathbf{v}$ is the vectorial representation of the structure relative displacements. $\mathbf{K_{frame}}$ is the stiffness matrix for the test structure without the braces. For the present case, the rotational and vertical degrees of freedom of stiffness matrix were condensed out so that $\mathbf{K_{frame}}$ was a 3×3 matrix. In calculation, the East and West frames were treated separately. f_{brcae_j} and k_{brace_j} are the instantaneous axial brace force and axial stiffness of the j-th brace, there being 12 braces in the structure. E_h is assigned here entirely to the SBCs. This quantity is calculated as the sum of the integrals of the brace forces with respect to the slips of the SBCs for the twelve braces with SBCs. To E_{vd} is assigned all the remaining energy, viscous damping being an abstract quantity.

The more interesting energy quantities calculated from the experimental data are E_k and E_s. Although these quantities were found to be small in terms of the magnitude of E_i, they provide some interesting insight into the behavior of the structure. Figures 7.17 and 7.18 show histories for $E_k + E_s$ for TS1 subjected to the harmonic and Pacoima signals. E_s is also shown so that relative proportions become apparent. Both curves are very unlike what one would expect for a conventional structure. Most impressive is the large difference in magnitude between the peaks and valleys of the $E_k + E_s$ curves. A drop from a peak to a valley in $E_k + E_s$ represents loss of instantaneous energy in a quarter cycle of vibration. It is apparent that the structure is shedding energy at a very a high rate in time. The curves are interestingly different from those for linear-elastic structures in that in such structures the tendency is for E_s to vanish concurrent with E_k reaching its maximum. It is seen in Figure 7.17 that, except for the beginning and end of the record, E_s is continuously positive. This is so because for the harmonic motion slippage at SBCs occurred from the extreme displaced position of the structure in one direction to the extreme in the opposite directions, i.e., when the structure passes through the zero displacement position where E_k is at its maximum, the brace are loaded due to the slipping at SBCs. The strain energy of the braces then is maximum through out the range of the motion, excepting the end extremes of the motion. At the end extremes, the frame is at its peak strain energy state. Therefore, for continuous motion causing slippage

at the SBCs, the strain energy is continuously positive.

The most important energy quantity of interest relating to the subject of this document is E_h. In the present discussion, the energy dissipated by the SBCs is the E_h. All other source of dissipation, some of which are no doubt hysteretic, are assigned to be "viscously" damped. The sources of such damping could be the internal friction of materials, sliding and deformation of the lead and concrete blocks, non-linearities in the structural systems of the decks, etc. In the present discussion attention is confined to hysteretic energy dissipated by the SBCs. Some researchers have considered the ratio of $\frac{E_h}{E_i}$, where E_h indicates only the hysteretic energy dissipated by energy dissipators, as a performance index for the dissipators. That trend is not followed here. With an energy dissipating system like the SBCs, a structure experiencing a long-duration excitation of intensity small enough, relative to the SBCs, not to cause slip in the SBCs would cause a large E_i while E_h would remain zero. On the other hand a strong jolt causing all SBCs to slip would cause a near unity $\frac{E_h}{E_i}$. The use of this ratio as a performance index would identify the first case as a case of poor performance, while in fact the SBCs would have done their job as designed, that is not slip under small amplitude excitation. Nevertheless, E_i curves are presented in conjunction with E_h as are E_k and E_s.

For each of the six representative experiments mentioned in the section on the hysteresis at SBCs, a pair of figures is presented. One plot in the pair indicates the relative displacement history of the structure levels due to the excitation, while the other immediately below it presents the energy input and dissipation histories. The twelve plots are the Figures 7.19 through 7.30. The displacement time history figures are presented for qualitative comparison with energy time histories. Given the high frequencies of oscillations in some of the plots, it is difficult to read the displacements of the second and first levels. However, the maxima of drift and displacement at each level and for each of the records is presented in tabulated form in the next section. Further, these plots will be compared with analytical simulation results in the next chapter, in which the plots will be examined more clearly about the points of maximum response.

The six energy input and dissipation history figures are interpreted as fol-

lows: The top curve in each figure is the absolute input energy. This curve was calculated by integrating the base shear force with respect to the table displacements. The base shear force used was that calculated by the array of strain gages, as explained in Chapter 6. Then starting from the bottom and coming up, each "layer" is the hysteretic energy dissipated by a single SBC. The twelve layers represent respectively, from the bottom up, the hysteretic energies for SBCs 1SE, 1NE, 1SW, 1NW, 2SE, 2NE, 2SW, 2NW, 3SE, 3NE, 3SW and 3NW. The naming scheme is the same as that used in the plots of the hysteresis loops. Then, immediately above the twelve-th layer are two curves representing the addition of E_k and E_s to the total hysteretic energy of the SBCs. As indicated earlier the magnitudes are rather small when presented in the same scale as E_i and E_h. However, it is noted that the contours generated by the addition of these energies to the hysteretic energies of the SBCs match, rather well, the contours of E_i and further near time zero the two curves coincide. This indicates that the energy difference between E_i and the sum of E_h, E_k and E_s is monotonically, and almost linearly, increasing with time. This quantity is assigned to E_{vd} discussed in Chapter 1 and indicated in the figures as "dissipated viscously." That the difference is nearly zero early in the record is good indication that the numerical methods in generating the plots and the instrumentation readings are consistent with theory demanding energy balance.

Several trends are present for the energy histories. In all figures, it is seen that large jumps in E_h are coincident with large displacements of the stories of the structure. This is expected. Large deformations occur when the SBCs slip. The slipping of SBCs is tantamount to increase in E_h. It also appears from the figures that there are cases where SBCs on the same level of the structure dissipate very different quantities of total hysteretic energy. For example, in Figure 7.20 at the first level the first layer, 1SE, has almost twice the thickness of the second layer, 1NE. This trend repeated in Figure 7.22. However, the same two structural configurations, TS1 for Figure 7.20 and TS2 for Figure 7.22, when subjected to the harmonic input behave differently as seen in Figures 7.28 and 7.30. The same two SBCs appear to have dissipated nearly equal amounts of energy. There is a simple explanation for this behavior. An examination of Figures 7.3 through 7.8 reveals that brace 1SE has

a noticeably lower slip force than brace 1NE. This was also observed in the discussion regarding the effects of unequal slip forces on chevron bracing. Clearly, given the symmetry of the test structure, with an increasing lateral load at a given story the first SBC to slip is the one with the smallest slip force. Now, if one were to imagine a harmonic excitation just intense enough to cause the weak SBC to slip, but not the next weakest, at the end of the excitation only the weakest SBC will have dissipated any energy. Then, it is no surprise that for an excitation like the Chilean, with long duration high frequency excitations of various amplitudes, the weaker braces dissipate the larger portion of the energies per floor. Now, if one were to imagine the same harmonic excitation to have large enough intensity to cause all SBCs to slip every cycle, the result would be that the SBCs would dissipate roughly equal amounts of energy, that is if the slip forces were relatively close. The weaker SBCs would slip slightly larger distances as they activate slightly earlier and stop slipping slightly later than the stronger braces. The last case described with the hypothetical strong harmonic load is exactly that of the cases shown in Figures 7.28 and 7.30. A re-examination of Figures 7.7 and 7.8 reveals indeed that the SBC with lower slip forces have the larger slip distances.

In a similar manner to the behavior of the individual SBCs, it is seen that in the comparison of per level hysteretic energy dissipation for the Chilean signal, the levels with the smaller ratio of combined SBCs slip load to shear force dissipate more energy than the ones with the larger ratio for the Chilean earthquake. For TS1, the weaker level is the second, while for TS2 it is the the first. It is seen in Figures 7.20 and 7.22 that the second level dissipates the larger portion of the hysteretic energy for TS1 while for TS2 the largest portion of the dissipation occurs in the first level. Examination of Figures 7.28 and 7.30 shows that for the strong harmonic excitation the distribution of hysteretically dissipated energy becomes more uniform for the two levels for both TS1 and TS2. The same explanation given for the change in proportions of energies dissipated amongst the SBCs of the same floor for the two excitations, the Chilean and harmonic, accounts for the change in proportions of hysteretic energy dissipated per floor for the same two excitations. Figures 7.24 and 7.26 indicate the proportions of hysteretic energy distribution for the Pacoima signal

per level and per SBCs of the same levels to be rather similar to those for TS1 and TS2 subjected to the harmonic signal. This occurs because the Pacoima signal was composed of mostly small amplitude acceleration pulses with a few magnificently large pulses (as large 1.5 Gs). The small accelerations tend not to cause any major slips in the weaker SBCs or levels, while the larger pulses cause the majority of SBCs to slip. This results in a similar effect as that observed for the harmonic excitations.

7.5 Comparison of Response Extrema for TS1, TS2, ADAS3 and ADAS1

The discussions and comparisons of the responses of TS1 and TS2 have thus far been focused on the behavior of the SBCs, both locally and as a part of the structural system. The structure itself has, effectively, been used as a tool for the testing of the SBCs in-situ as a part of a structural system. The main criterion for the design of the bracing system with the SBCs, was to get maximum response from SBCs in a safe and controlled manner. With the restriction of using $\frac{1}{2}$ inch diameter A325 bolts tightened to their specific bolt tension, the TS1 and TS2 configurations were the two natural designs for a symmetric structure. The two designs were by no means optimal. That is, given non-discrete choices for the slip forces of the SBCs, a design to, say, result in minimal and uniformly distributed story drifts could have been achieved (this has been shown by analyses, not presented in this document). It is however interesting to examine the two designs to discern whether either design had any clear superiority over the other. This is accomplished here by comparing tabulated response extrema for the two configurations for each of the discussed signals.

Tables 7.1, 7.2 and 7.3 show the extrema for response quantities of interest of TS1 and TS2 due to the Chilean, Pacoima and harmonic signals respectively. In addition, Table 7.1 compares the performances of TS1 and TS2 to the performance of another energy dissipation system, the ADAS, which was tested in the same frame and using the Chilean signal [31]. The tables are organized as follows: The columns represent the different structural configurations, the rows indicate from top to bottom,

the experiment identification number, configuration name, peak accelerations and pitch of the table, relative story displacements, inter-story drift indices, third story transverse accelerations, longitudinal story accelerations, bending moment at brace 1SW and the story shear forces. Two table accelerations are given, one for each of the table accelerometers. The letter "B" indicates that the acceleration and shear force quantities are due to the accelerometer data from the blocks. Letters "E" and "W" indicate the quantities to be in relation to the East and West frames. "NA" indicates that the data was either not available or not applicable. The letter "G" indicates, for the story shear forces, that the data used were from the strain gages on the braces and columns rather than from accelerometers. As mentioned in Chapter 6, the shear force data based on the strain gages is thought to be more reliable than those based on the accelerometers. Only the shear forces based on the gage data are shown in Tables 7.2 and 7.3. Accelerometer shear force extrema are shown in Table 7.1 so that fair comparison can be made with structure shear forces of the ADAS systems, as the for the ADAS system shears forces appear to be based on accelerometer data for the structure masses.

First, the TS1 and TS2 responses are compared to each other. Certain trends can be discerned from the tables. Comparison of relative displacement and story drift extrema shows that for the Chilean and harmonic signals, in particular, these quantities are smaller in TS2 at the second and third levels. However the same quantities are smaller in TS1 at the first level. On the other hand, for the Pacoima signal the first level drifts are rather similar for the two configurations while again in the second and third stories TS2 displays better control of the drifts and relative displacements. These trends are consistent with the observed differences in the widths of the hysteresis loops discussed earlier. On the whole, it appears that TS2 is the better of the two designs as far as limiting of the drifts is concerned. Average drifts for this configuration are consistently smaller. Lateral acceleration appear to be smaller for TS1 in the case of the Chilean signal, while they are the smaller in TS2 for the Pacoima and harmonic signals. These accelerations are related to torsional response, the consideration of which is outside the scope of this document. No clear advantage is apparent in either configuration from the comparison of longitudinal

accelerations. However, the clear trend is that, with the exception of a single reading for the harmonic record, the structure attenuates the applied accelerations. This is to be expected from a structure like this capable of shedding energy at a high rate. Brace bending moments appear to be comparable for the two configurations. Comparison of shear forces reveals that in the three cases either the shear forces are very close, or the smaller values occur in TS1. Indeed, in summary it can be said that the gains made in reducing drifts and displacements by TS2 are paid for by an increase in the shear forces. Both structures are considered however to have performed as designed, that is the designs allowed for the study of the SBC characteristics studied as an integral part of a structure. It should be noted that the inter-story drifts of the structure compare rather well with code requirements for both configurations. The UBC, for example, implicitly limits ultimate drifts to 1.5 % for structures with R_w of 8. It is seen that for the three signals which by far exceed in intensity the excitations considered by codes, the largest drift index is of magnitude 1.11 %.

Comparisons with the ADAS system

Tests were conducted in 1988, using the same ductile moment resisting frame used for the testing of the SBC connections, to test the performance of the ADAS [31] energy dissipating elements. The ADAS elements dissipate energy by causing yield due to flexure over the entire lengths of links specially profiled so as to match bending moments to section moment capacities. ADAS elements have been shown to have extremely well behaved energy dissipation characteristics. Tests have indicated that no strength degradation occurs over large numbers of inelastic excursions. The ADAS elements have predictable and consistent force deformation characteristics, and by increasing the size and numbers of links different combinations of strength and stiffness can be obtained. The ADAS elements were installed into the test frame in an inverted Y bracing scheme, where the vertical stem of the Y consisted of the ADAS elements. The diagonal arms of the inverted Y consisted of $4" \times 4" \times \frac{1}{4}"$ hollow square tube sections. Two configurations were tested, ADAS3 and ADAS1. Six ADAS elements, two per floor, were used in the testing of ADAS3. For the testing

of ADAS1, the units of the upper two floors were locked. The masses with which the structure was loaded were identical to those used for the testing of the SBCs. Furthermore, amongst the table inputs used in the testing of ADAS3 and ADAS1 was the same Chilean signal discussed throughout this chapter. Although it has not been the objective of the experimental program of the testing of TS1 and TS2, to make comparisons with the performance of other systems, the similarity of the two experimental programs requires that at least a cursory comparison be made.

The Chilean signal with the largest amplification used for the testing of ADAS3, registered a peak acceleration reading, from the average of table accelerometers, of 0.56 Gs. The response extrema of ADAS3 are shown in Table 7.1 together with the extrema for TS1 and TS2 due to the same signal but amplified to peak accelerations of 0.81 Gs and 0.86 Gs respectively. A cursory examination reveals that despite the fact that the signal was significantly weaker than those used for the testing of TS1 and TS2, the magnitudes of the base shear forces are roughly equal, while the inter-story drifts of TS1 and TS2 are smaller by at least a factor of two. ADAS1 was tested with the same signal amplified to a peak acceleration of 0.84 Gs. For this case it is seen that the inter-story drifts in the upper two stories, where the ADAS elements were locked, are smaller than those observed for TS1 but comparable with those of TS2. Drifts of the first level however are larger by a factor four than those for TS1 and TS2, while the base shear is also larger.

The above comparison does not purport to demonstrate superiority of one system over the other, only that for the given frame and the given signal the bracing system with SBCs performs more efficiently. The two systems are mainly different in that while the SBC connection is inherently rigid before slipping, an ADAS of an equivalent yield force to the slip force of the SBC, will inherently be flexible. This means that the systems will cause different dynamic characteristics in the structures in which they are used and so one system or the other may be more appropriate depending on the design requirements.

7.6 Conclusions and Remarks

The shake table testing of the test structure equipped with SBCs in a braced chevron configuration was a success in that it demonstrated that the performance observed in the testing of SBCs in the C/T machine could be repeated in-situ in a structural system. The behavior of the SBCs of the test structure were entirely consistent with that observed in the testing of identical connections in the C/T machine. The same "break-in" phenomenon was observed in the testing of SBCs in the C/T machine observed in the SBCs of the test structure. The slip forces were also of the magnitudes indicated by the C/T machine testing.

Of the three configurations tested, the results for two have been presented. The third configuration, TS3, indicated that a successful design with SBCs was possible even with the presence of large torsional moment causing eccentricities. Due to limitations of both scope and space, the result for tests of this configuration are not included in this document. In the two configurations presented, the SBCs were shown to result in highly effective hysteretic behavior in the lateral force resisting bracing systems. Despite the structure being the first structure of its kind, fitted with SBCs and tested on a shake table, the design procedure used to design the structure produced two rather robust design solutions even with the given limitation of using $\frac{1}{2}$ inch standard A325 bolts. The use of $\frac{1}{2}$ inch A325 bolts were only a limitation in that they resulted in too large a slip force, for example in the third level where single bolts were used in each SBC. In realistic structures where larger slip forces would be necessary this would not be a problem.

Small displacement geometry was seen to adequately approximate the relationship between inter-story drifts and slip distances in the SBCs. Peculiarities of chevron bracing systems with SBCs of unequal slip force were discussed. Such unequal slip forces are seen to cause vertical forces acting at the midpoints of the beams above the chevron brace. This is an issue that should be considered when designing chevron braced systems with SBCs placed in the braces rectilinear with the brace axes. Small geometry assumptions, in conjunction with assuming braces to act as cantilevers, were seen to adequately estimate the small moments produced in the

braces in conjunction with the slipping of the SBCs.

The kinetic and strain energy histories indicated rapid shedding of energy by the structural system. This is attributed to the efficiency of the SBCs as energy dissipators. Examination of the hysteretic energy dissipation history curves for individual SBC and individual stories indicated that under long duration excitations with lower acceleration amplitudes weaker individual SBCs and stories with smaller ratios of reactive mass above to total SBC horizontal slip force were likely to dissipate the larger proportion of energy. For larger acceleration amplitudes capable of causing all SBCs to slip the proportions of total hysteretic energy dissipated were more uniform for SBCs of the same story and also per individual story.

Tabulated response extrema for the TS1 and TS2 configurations showed that the TS2 design was only marginally superior to the TS1 configuration, in that it resulted in smaller average inter-story drifts. However, TS2 experienced slightly larger base shear forces. The responses of both configurations were also compared with the performance of the ADAS3 and ADAS1 designs subjected to the Chilean signal. It was seen that for the test structure, in particular, the two configurations with SBCs were competitive with the structural configurations fitted with the ADAS.

File Number	930119.09	930120.09	880719.10	880725.28
Configuration	TS1	TS2	ADAS3	ADAS1
Table Acc. 1 (G's)	0.86	0.91	.56	.84
Table Acc. 2 (G's)	0.75	0.81	.56	.84
Table Pitch (Rad.)	0.00053	0.00063	NA	NA
Rel. Disp 1E (Inch)	0.36	0.44	1.6	1.98
Rel. Disp 1W (Inch)	0.35	0.42	1.6	1.98
Rel. Disp 2E (Inch)	0.75	0.62	2.65	2.22
Rel. Disp 2W (Inch)	0.76	0.63	2.65	2.22
Rel. Disp 3E (Inch)	0.93	0.75	3.17	2.26
Rel. Disp 3W (Inch)	0.92	0.74	3.17	2.26
Int. Drift. 1E (%)	0.45	0.54	2.0	2.48
Int. Drift. 1W (%)	0.44	0.53	2.0	2.48
Int. Drift. 2E (%)	0.62	0.31	1.69	0.38
Int. Drift. 2W (%)	0.64	0.33	1.69	0.38
Int. Drift. 3E (%)	0.28	0.21	1.03	0.19
Int. Drift. 3W (%)	0.27	0.19	1.03	0.19
Trans. Acc. 3S (G's)	0.12	0.15	NA	NA
Trans. Acc. 3N (G's)	0.12	0.18	NA	NA
Tot. Acc. 1B (G's)	0.59	0.56	.48	.64
Tot. Acc. 1W (G's)	0.49	0.59	NA	NA
Tot. Acc. 2B (G's)	0.83	0.66	.68	.67
Tot. Acc. 2W (G's)	0.70	0.65	NA	NA
Tot. Acc. 3B (G's)	0.66	0.85	.78	.71
Tot. Acc. 3W (G's)	0.70	0.77	NA	NA
Brace Moment (Kip-inch)	8.28	8.28	NA	NA
Lev. 3 Shear-G (Kip)	21	24	NA	NA
Lev. 3 Shear-B (Kip)	21	26	24	22
Lev. 2 Shear-G (Kip)	43	45	NA	NA
Lev. 2 Shear-B (Kip)	46	46	41	43
Base Shear-G (Kip)	50	61	NA	NA
Base Shear-B (Kip)	52	54	54	64

Table 7.1: Extrema for TS1 and TS2 subjected to the Chilean signal with similar data for ADAS3 and ADAS1.

File Number	930120.05	930120.13
Configuration	TS1	TS2
Table Acc. 1 (G's)	1.5	1.5
Table Acc. 2 (G's)	1.4	1.4
Table Pitch (Rad.)	0.00055	0.00065
Rel. Disp 1E (Inch)	0.68	0.71
Rel. Disp 1W (Inch)	0.68	0.67
Rel. Disp 2E (Inch)	1.4	1.1
Rel. Disp 2W (Inch)	1.4	1.1
Rel. Disp 3E (Inch)	1.8	1.4
Rel. Disp 3W (Inch)	1.8	1.3
Int. Drift. 1E (%)	0.86	0.89
Int. Drift. 1W (%)	0.85	0.84
Int. Drift. 2E (%)	1.11	0.69
Int. Drift. 2W (%)	1.09	0.67
Int. Drift. 3E (%)	0.59	0.33
Int. Drift. 3W (%)	0.60	0.35
Trans. Acc. 3S (G's)	0.21	0.20
Trans. Acc. 3N (G's)	0.22	0.16
Tot. Acc. 1B (G's)	0.78	0.82
Tot. Acc. 1W (G's)	0.75	0.86
Tot. Acc. 2B (G's)	0.80	0.81
Tot. Acc. 2W (G's)	0.88	0.82
Tot. Acc. 3B (G's)	0.91	0.92
Tot. Acc. 3W (G's)	1.14	0.99
Brace Moment (Kip-inch)	18.63	17.25
Lev. 3 Shear-G (Kip)	26	24
Lev. 2 Shear-G (Kip)	50	49
Base Shear-G (Kip)	59	69

Table 7.2: Extrema for TS1 and TS2 subjected to the Pacoima signal

File Number	930119.14	930120.18
Configuration	TS1	TS2
Table Acc. 1 (G's)	1.2	1.2
Table Acc. 2 (G's)	1.1	1.1
Table Pitch (Rad.)	0.00063	0.00066
Rel. Disp 1E (Inch)	0.52	0.68
Rel. Disp 1W (Inch)	0.54	0.66
Rel. Disp 2E (Inch)	1.1	1.0
Rel. Disp 2W (Inch)	1.1	1.0
Rel. Disp 3E (Inch)	1.3	1.2
Rel. Disp 3W (Inch)	1.4	1.2
Int. Drift. 1E (%)	0.65	0.85
Int. Drift. 1W (%)	0.67	0.82
Int. Drift. 2E (%)	0.89	0.58
Int. Drift. 2W (%)	0.90	0.59
Int. Drift. 3E (%)	0.46	0.30
Int. Drift. 3W (%)	0.47	0.32
Trans. Acc. 3S (G's)	0.30	0.17
Trans. Acc. 3N (G's)	0.20	0.19
Tot. Acc. 1B (G's)	0.65	0.98
Tot. Acc. 1W (G's)	0.68	0.87
Tot. Acc. 2B (G's)	0.9	0.9
Tot. Acc. 2W (G's)	1.29	0.95
Tot. Acc. 3B (G's)	1.05	0.86
Tot. Acc. 3W (G's)	1.4	1.2
Brace Moment (Kip-inch)	15.18	17.94
Lev. 3 Shear-G (Kip)	26	26
Lev. 2 Shear-G (Kip)	49	53
Base Shear-G (Kip)	57	68

Table 7.3: Extrema for TS1 and TS2 subjected to the harmonic signal

FILE=930116.04
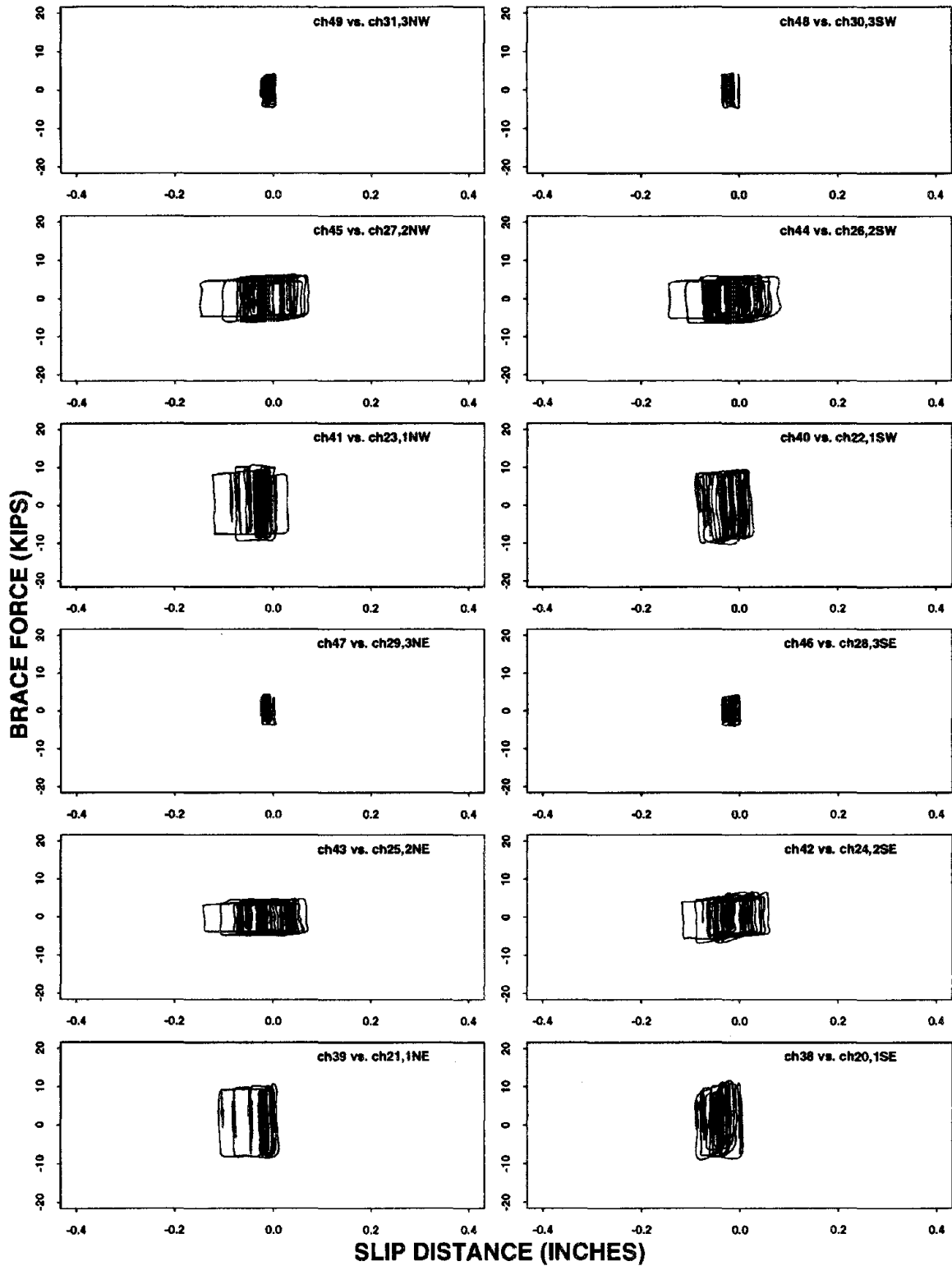
Figure 7.1: Hysteresis at SBCs of TS1 due to the first signal causing slip (Chile, 0.34 Gs)

FILE=930116.07
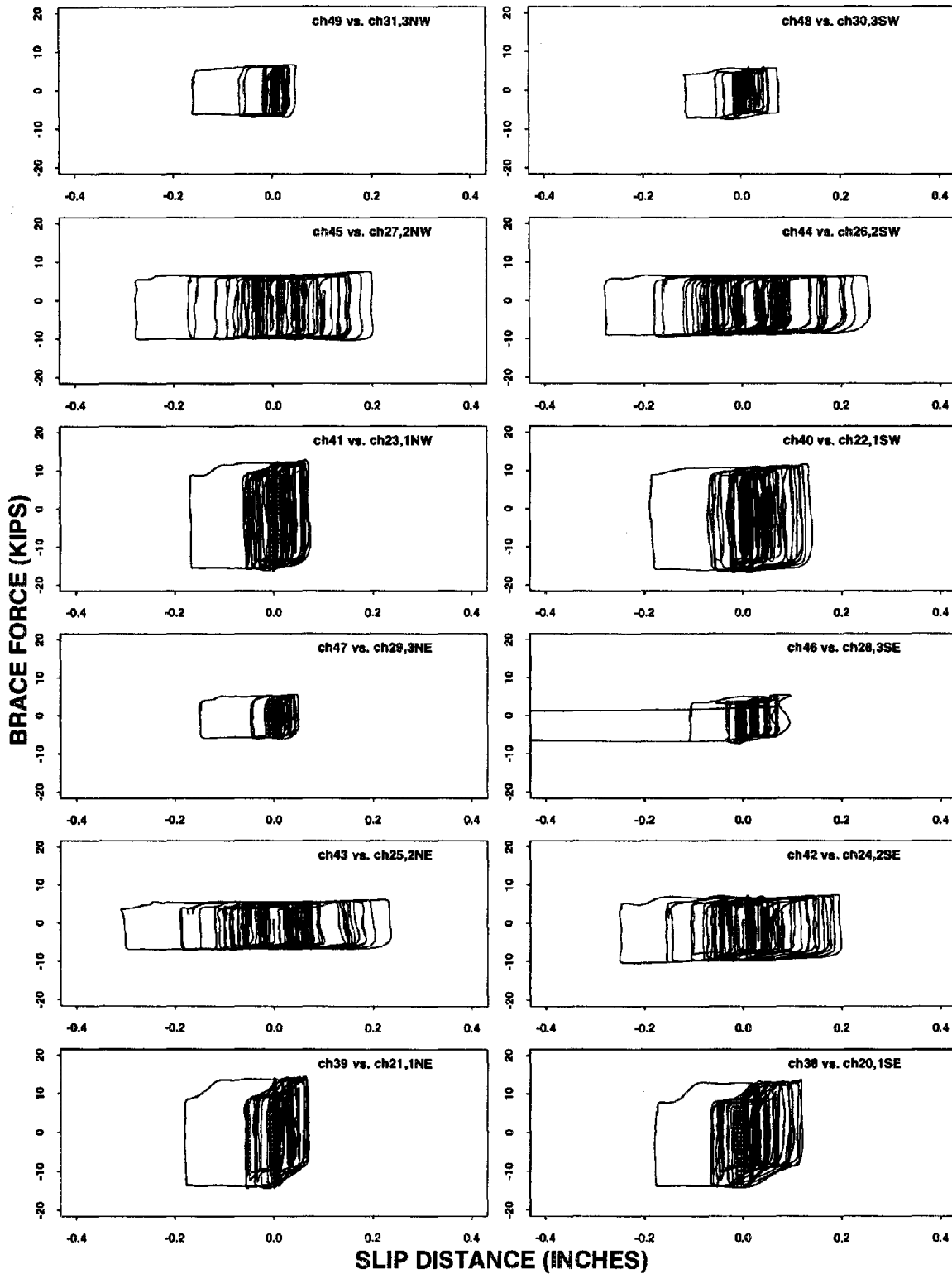
Figure 7.2: Hysteresis at SBCs of TS1 due to the fourth signal causing slip (Chile, 0.81 Gs)

FILE=930119.09
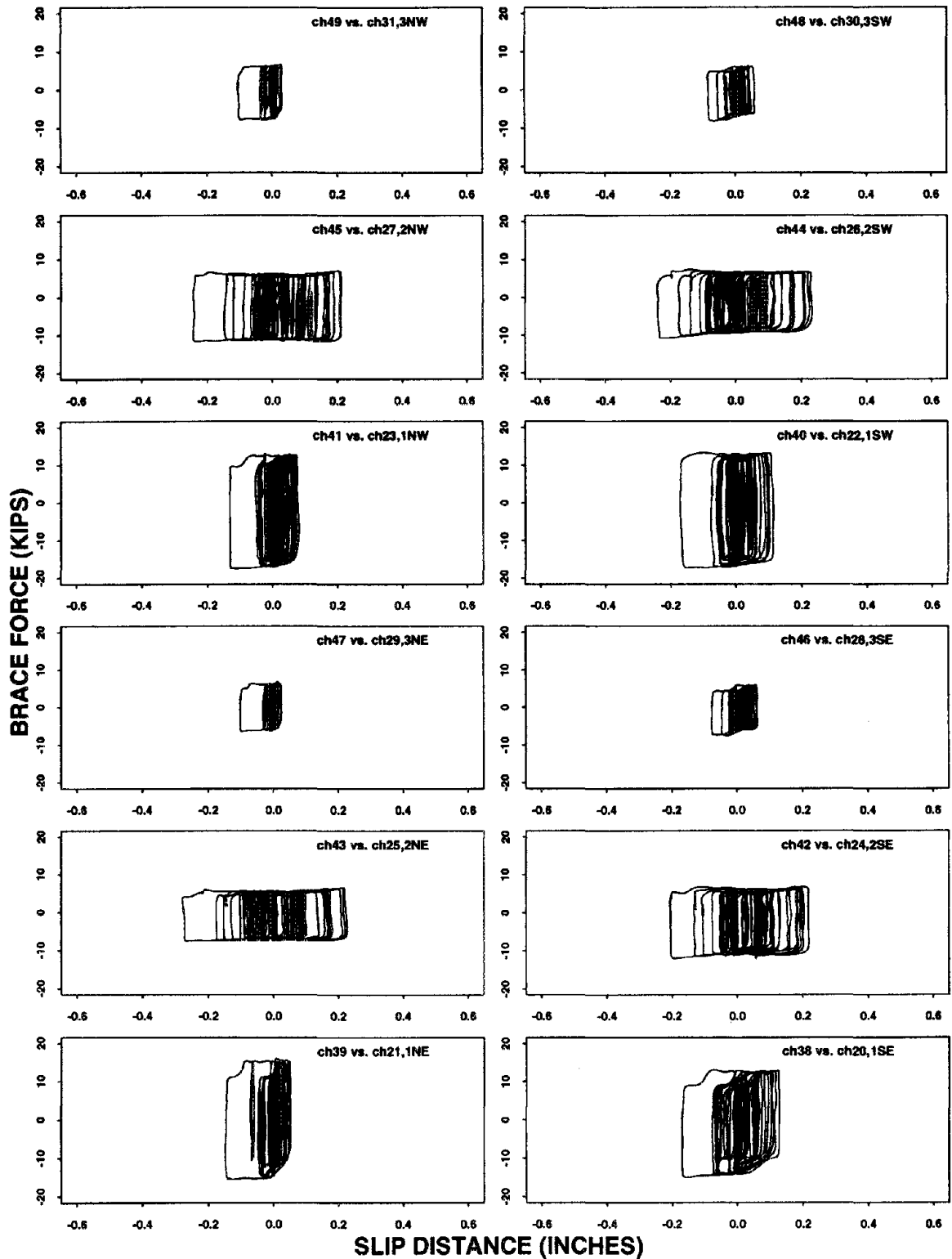
Figure 7.3: Hysteresis at SBCs of TS1 due to the Chilean signal
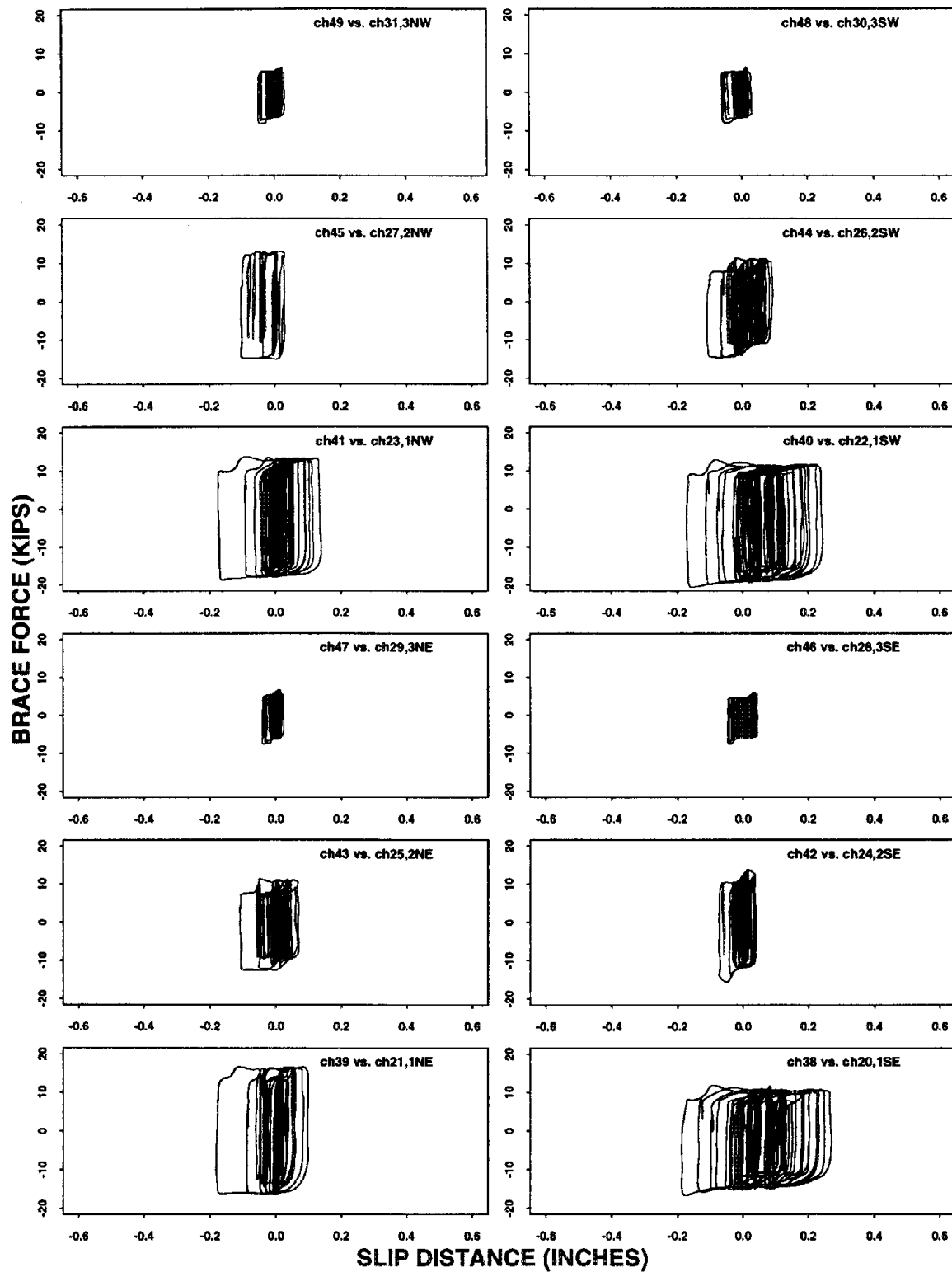
FILE=930120.09

Figure 7.4: Hysteresis at SBCs of TS2 due to the Chilean signal
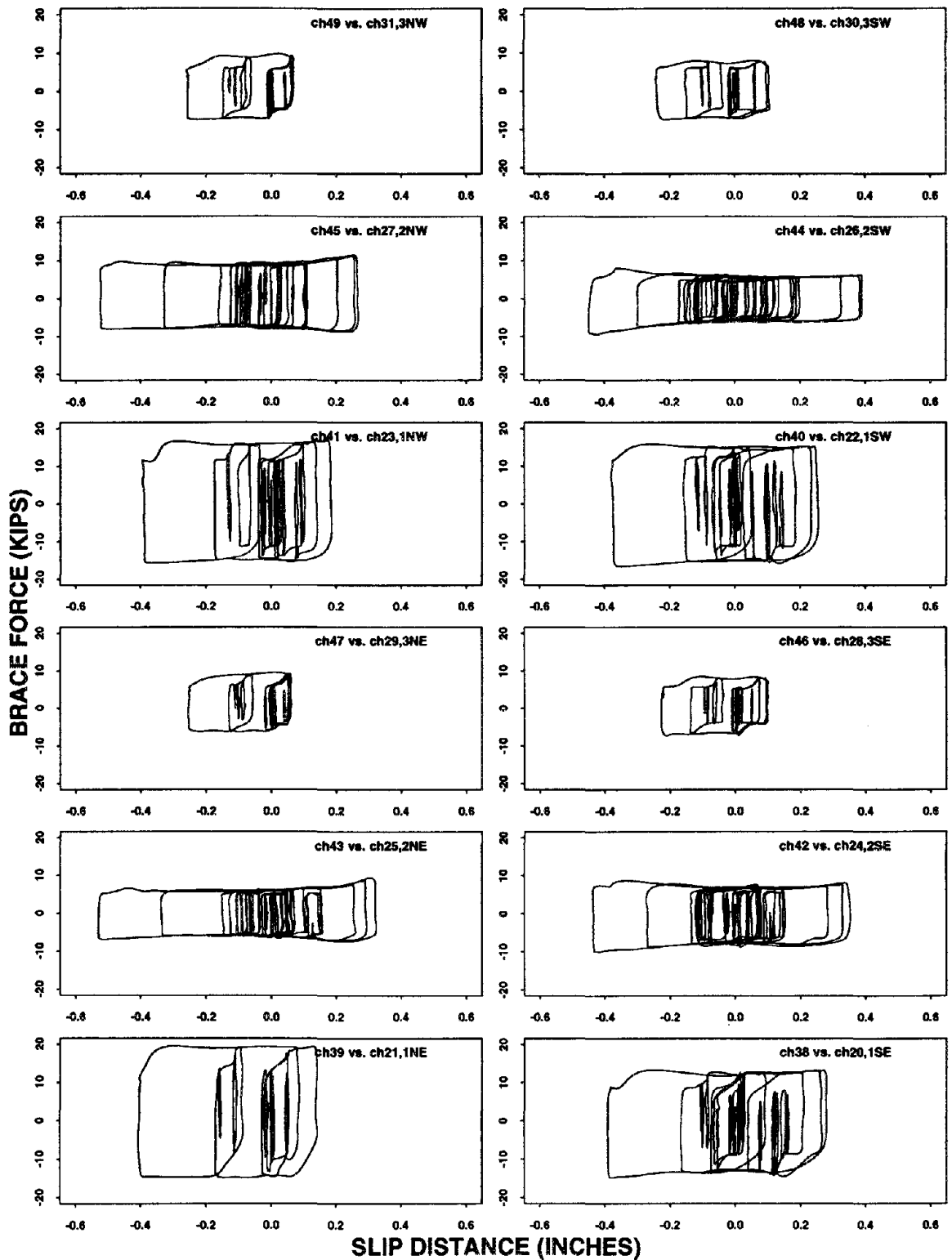
FILE=930120.05

Figure 7.5: Hysteresis at SBCs of TS1 due to the Pacoima signal
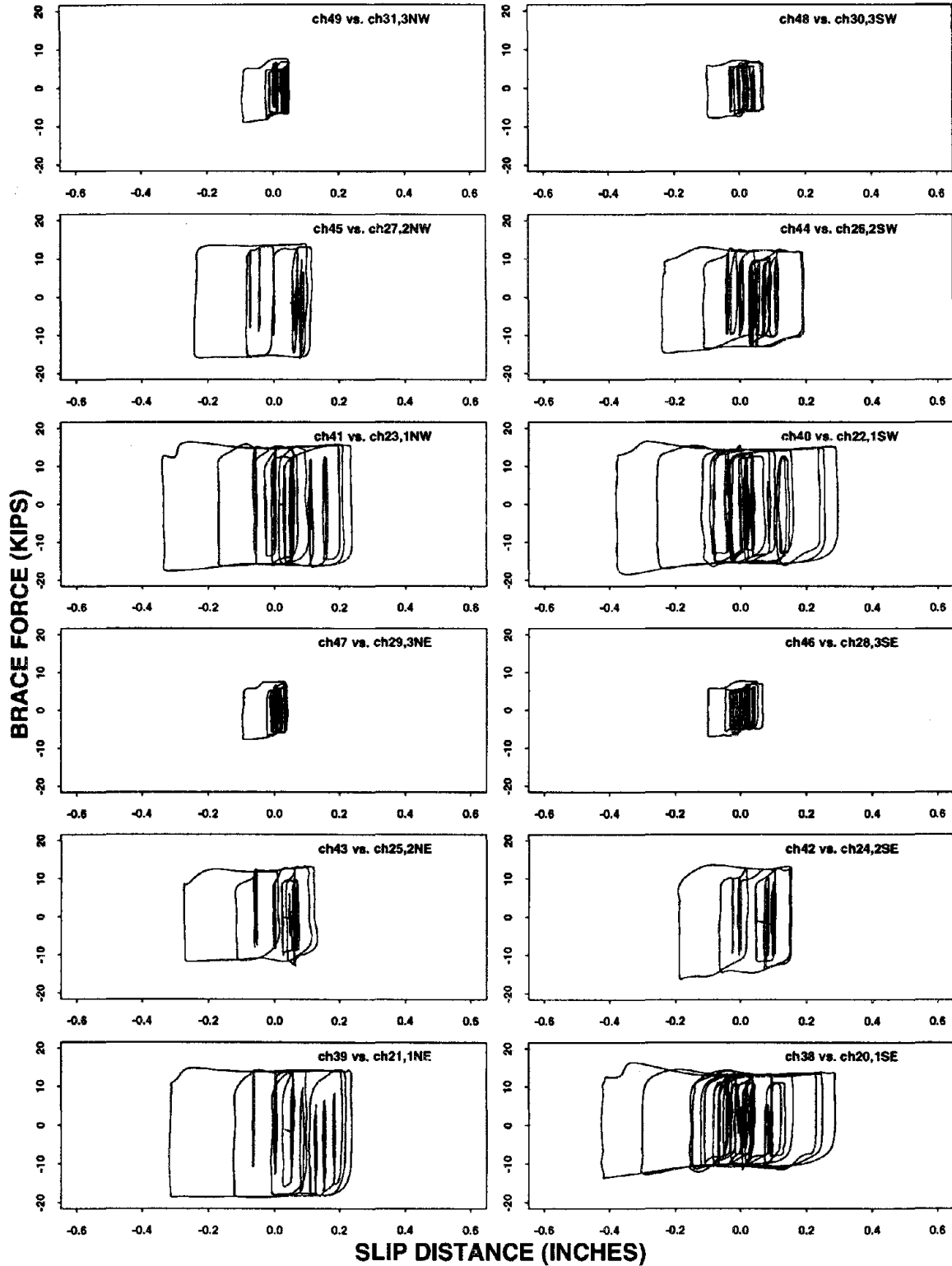
FILE=930120.13

Figure 7.6: Hysteresis at SBCs of TS2 due to the Pacoima signal

FILE=930119.14
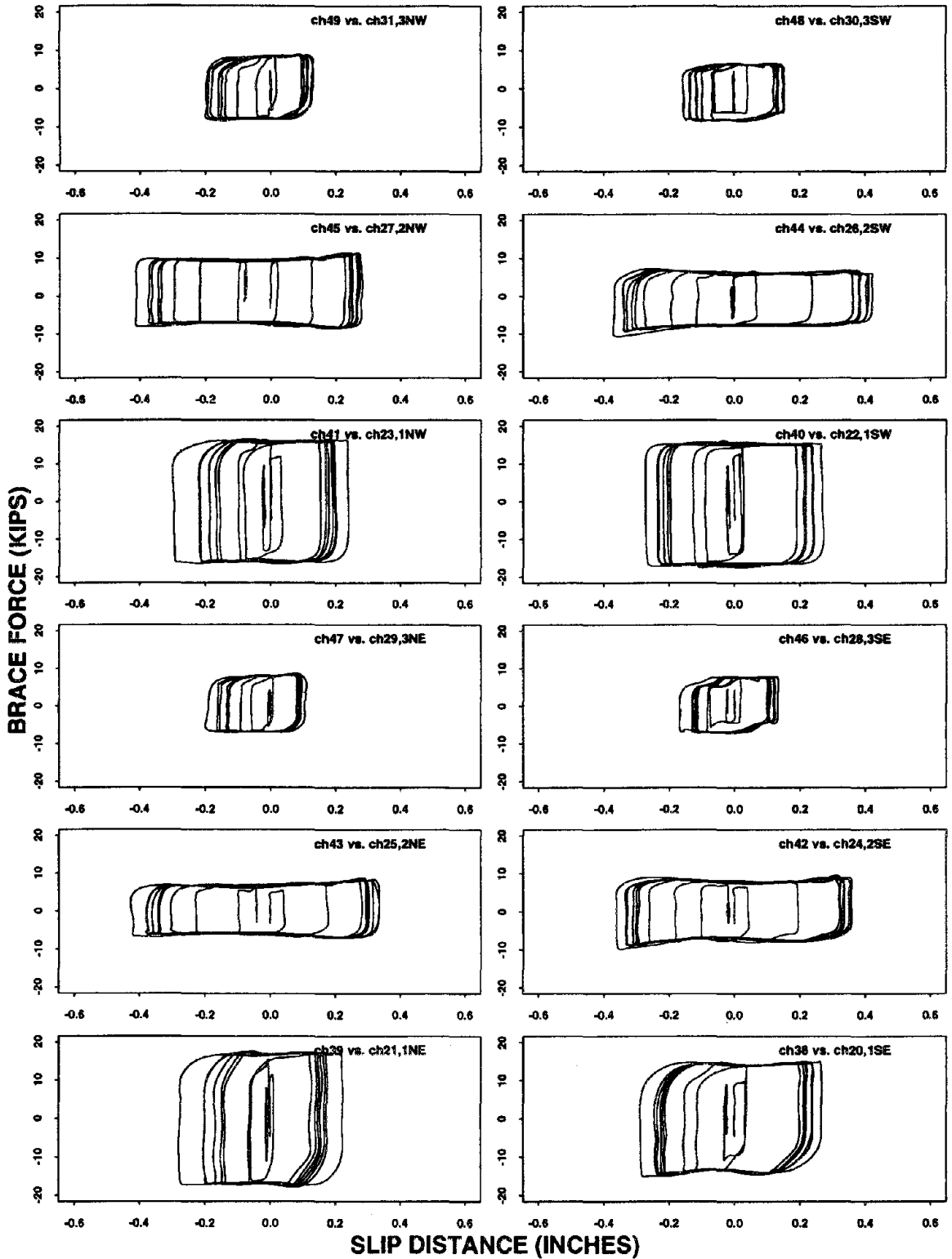
Figure 7.7: Hysteresis at SBCs of TS1 due to the harmonic signal

FILE=930120.18
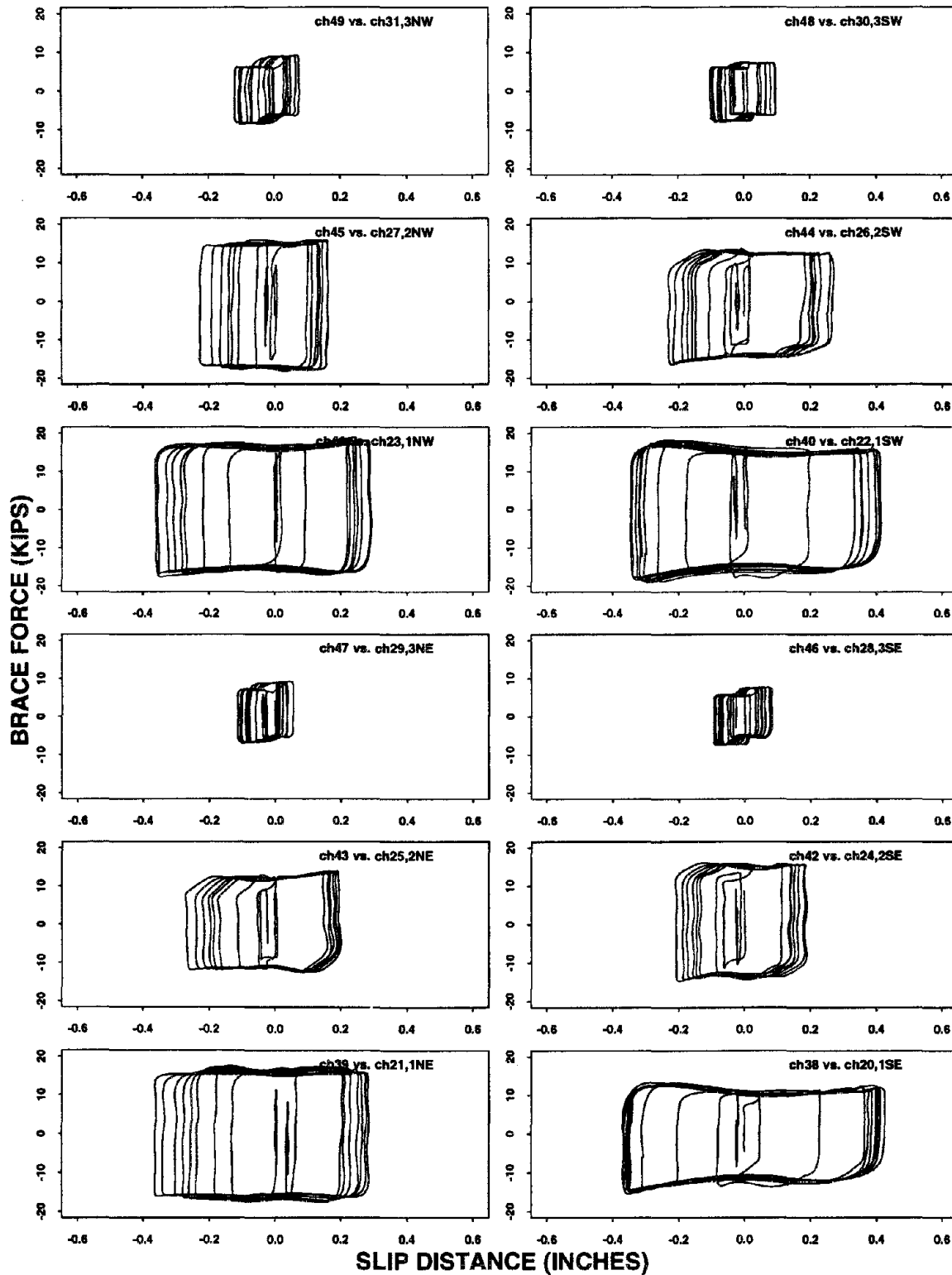
Figure 7.8: Hysteresis at SBCs of TS2 due to the harmonic signal

FILE=930119.14
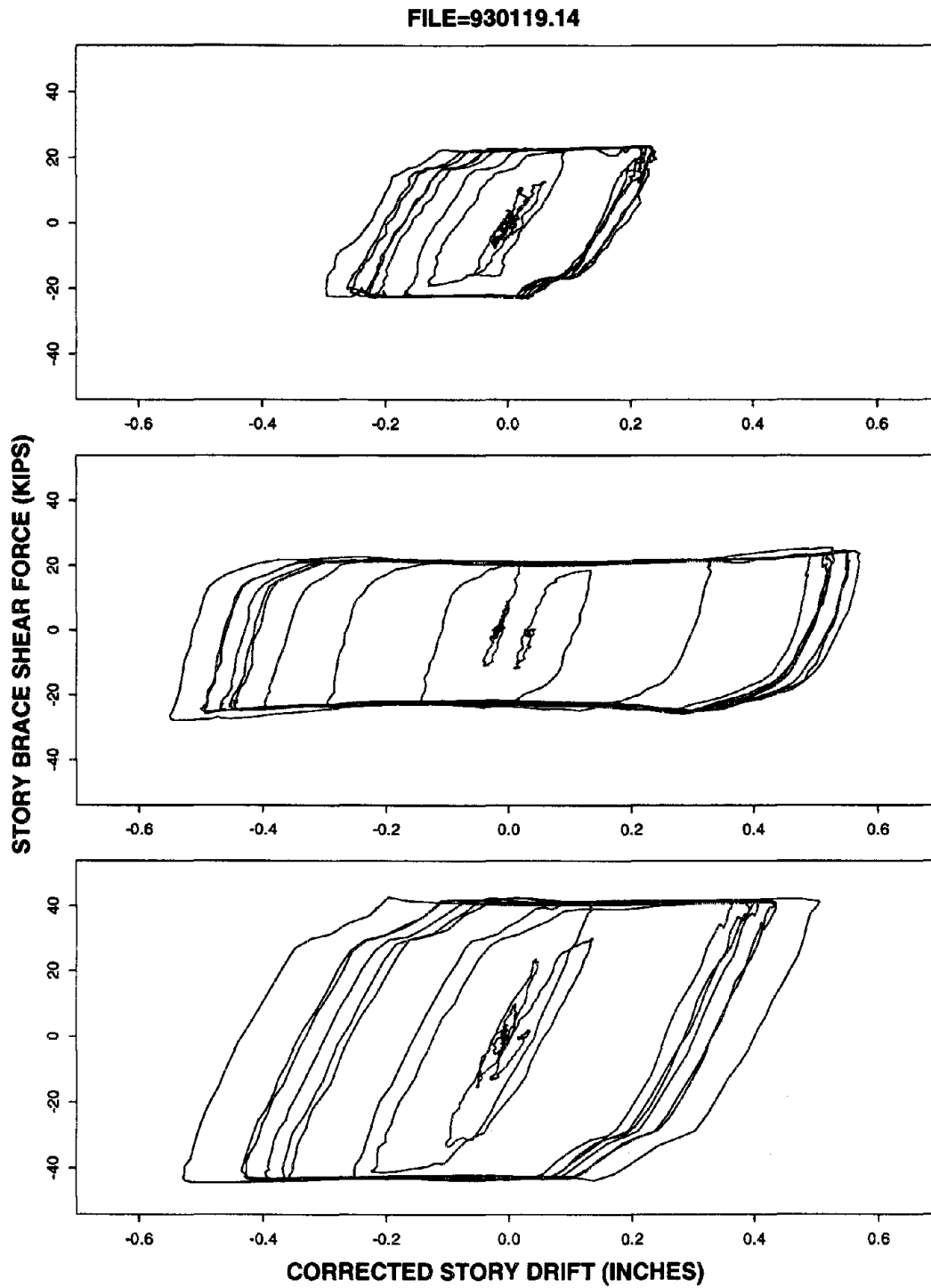
Figure 7.9: Hysteresis of bracing system at three levels of the TS1 due to the harmonic signal

FILE=930120.18
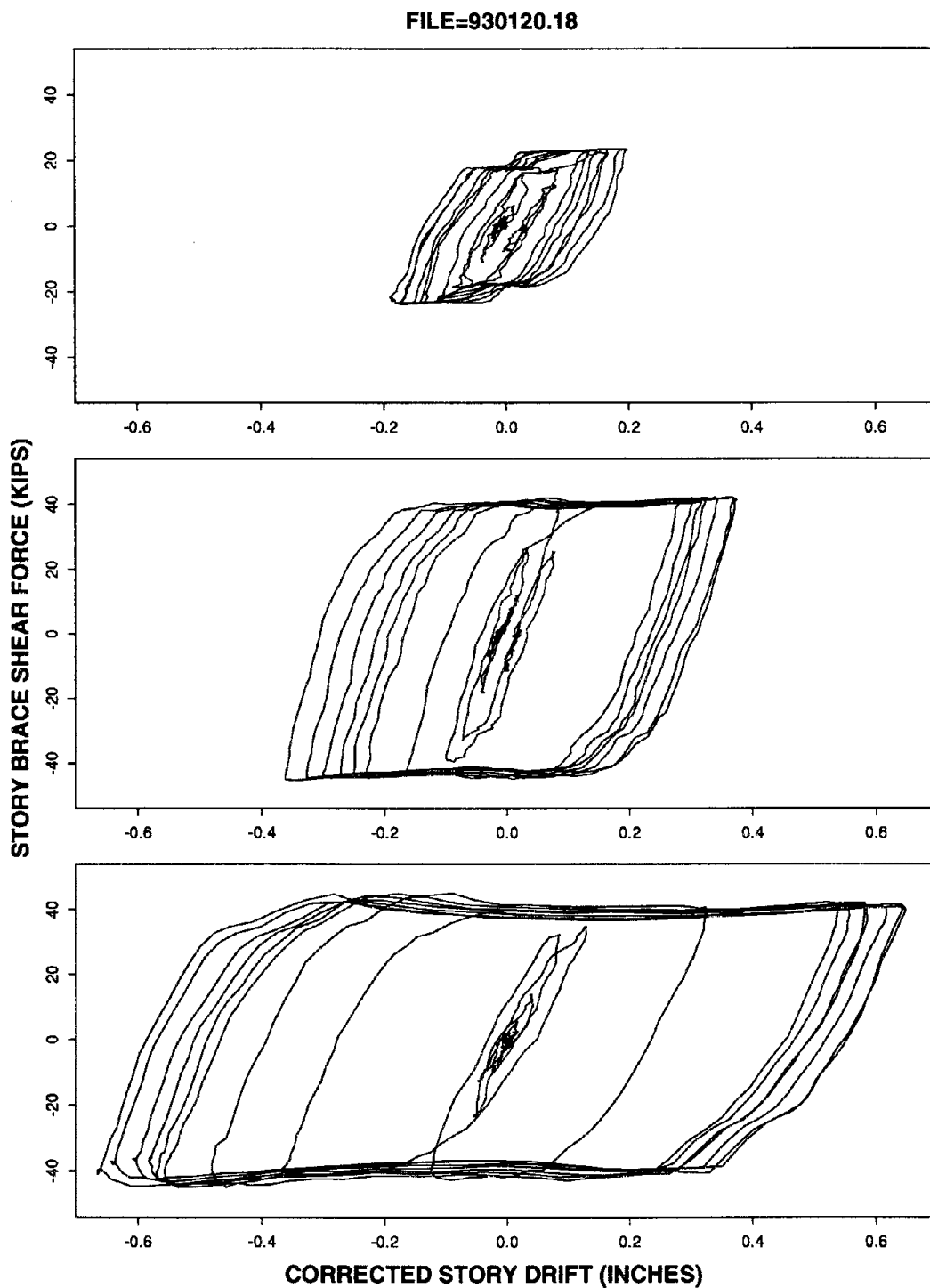
Figure 7.10: Hysteresis of bracing system at three levels of the TS2 due to the harmonic signal
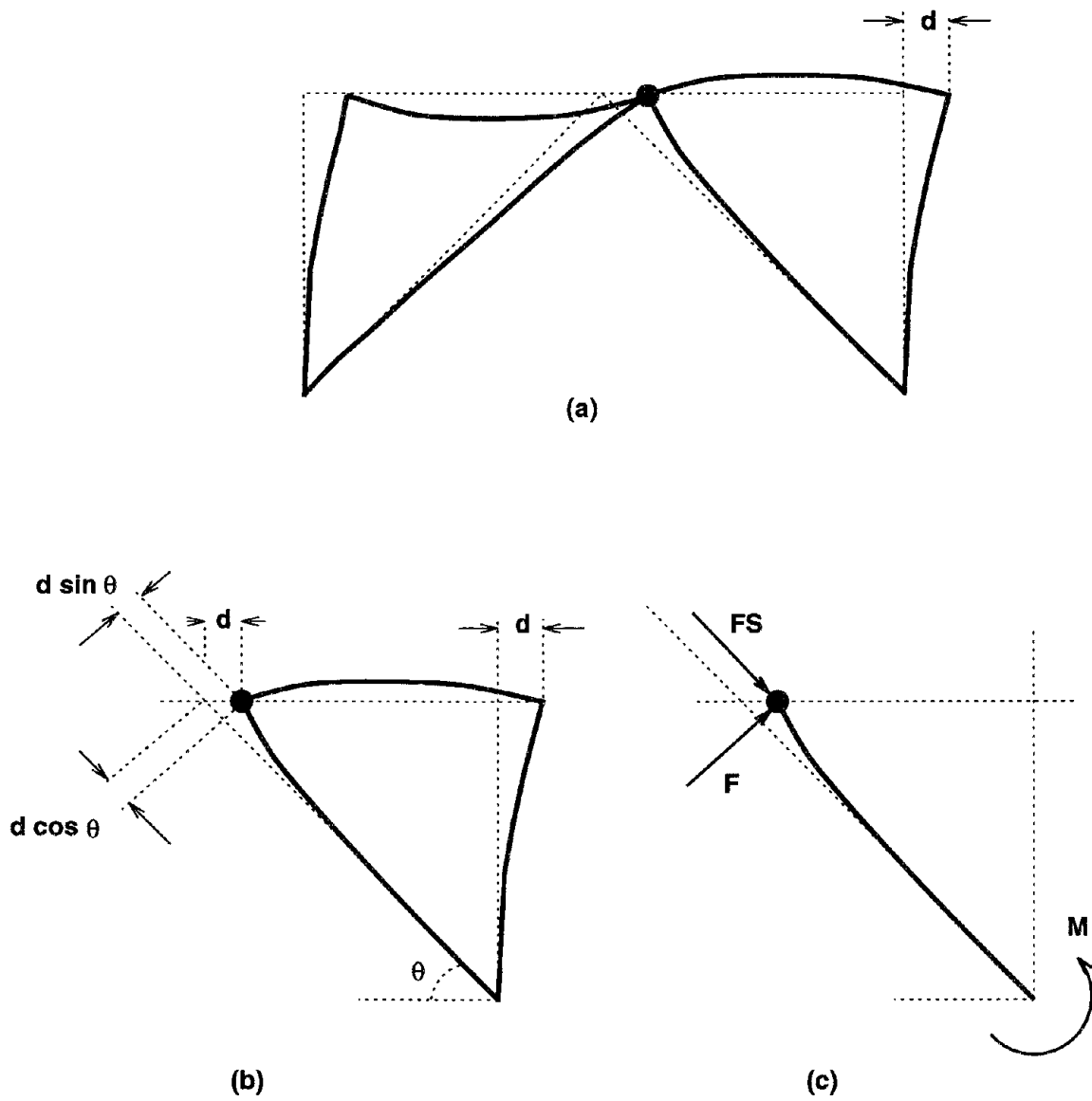
Figure 7.11: Relations of small geometry for displacement of braces and forces acting at SBC

FILE=930119.14
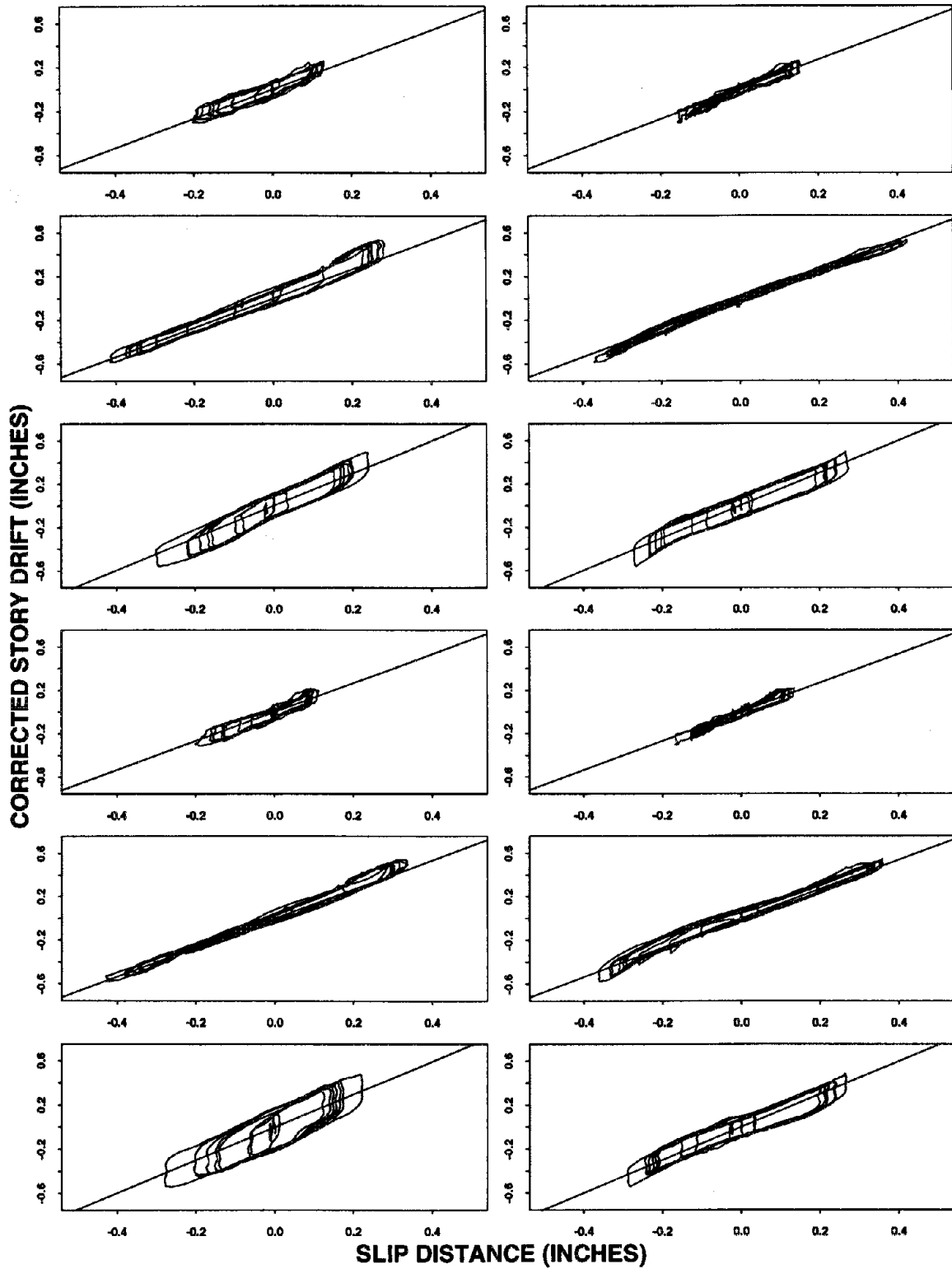
Figure 7.12: Inter-story drifts versus SBC slip (TS1, harmonic)

FILE=930120.18
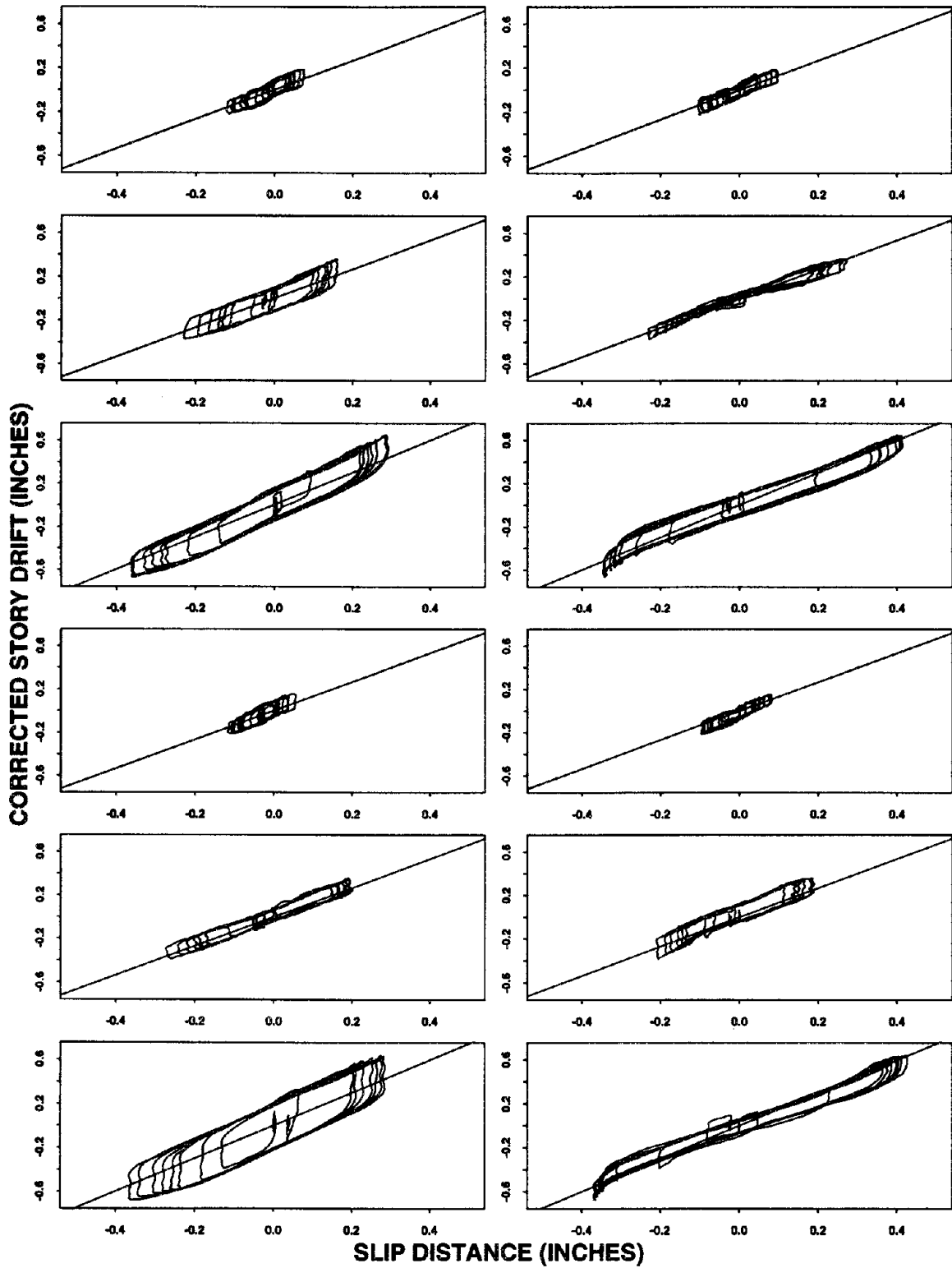
Figure 7.13: Inter-story drifts versus SBC slip (TS2, harmonic)
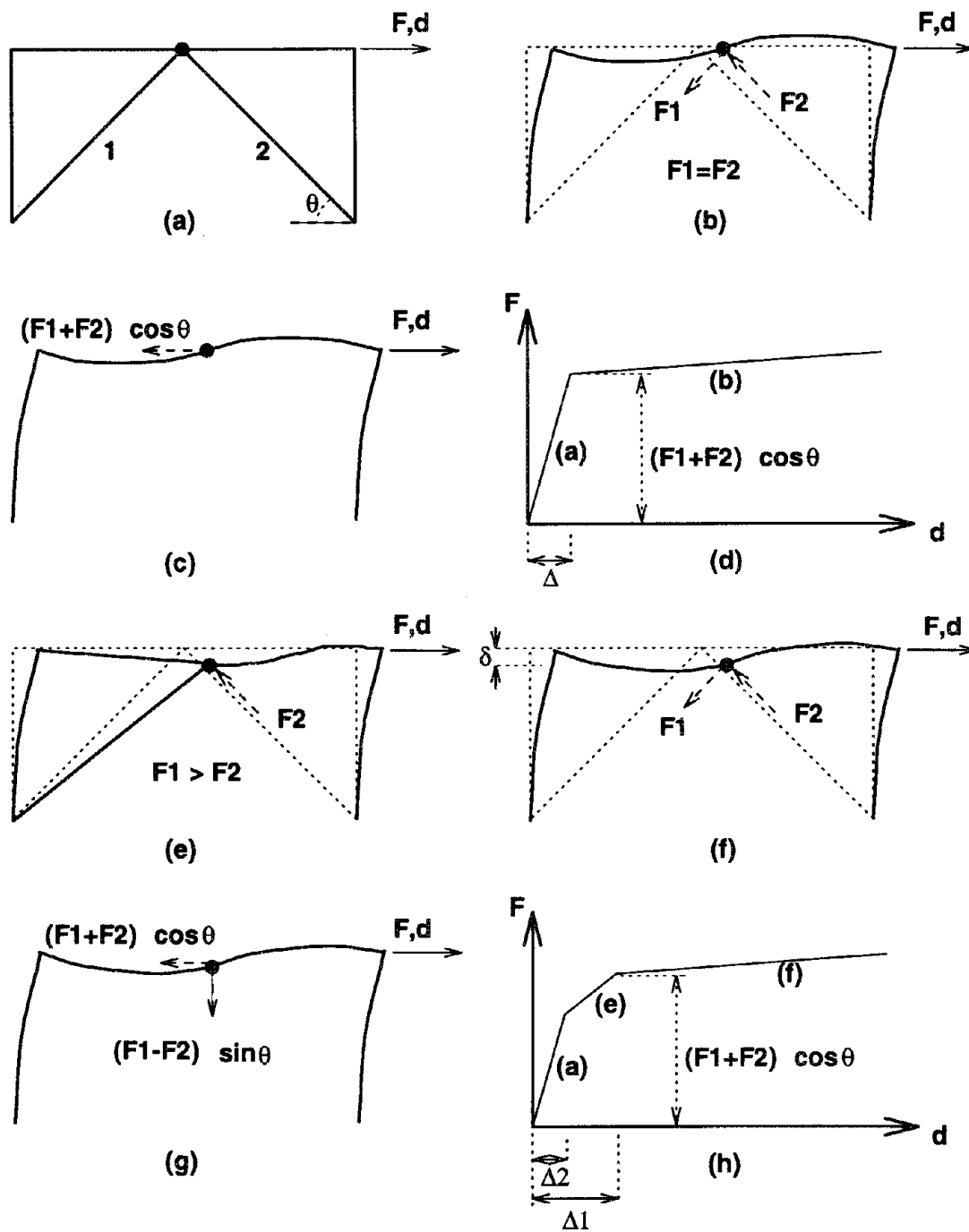
Figure 7.14: Schematic description of effect of unequal slip forces on chevron bracing
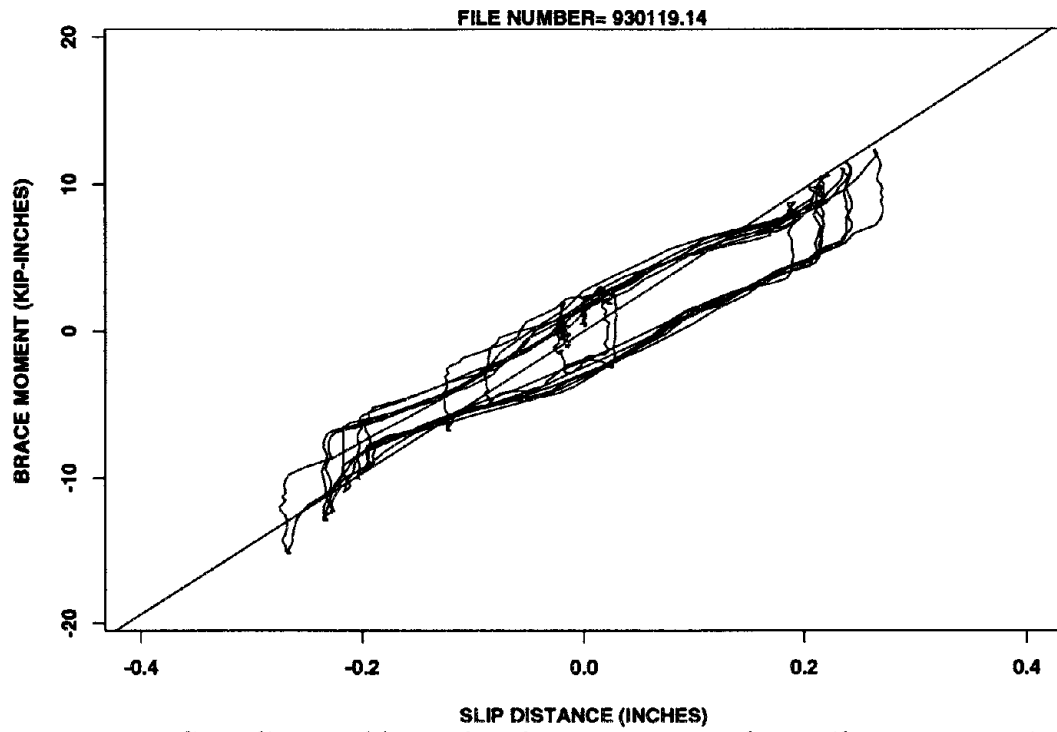
Figure 7.15: Compliance of brace bending moment with cantilever assumption.
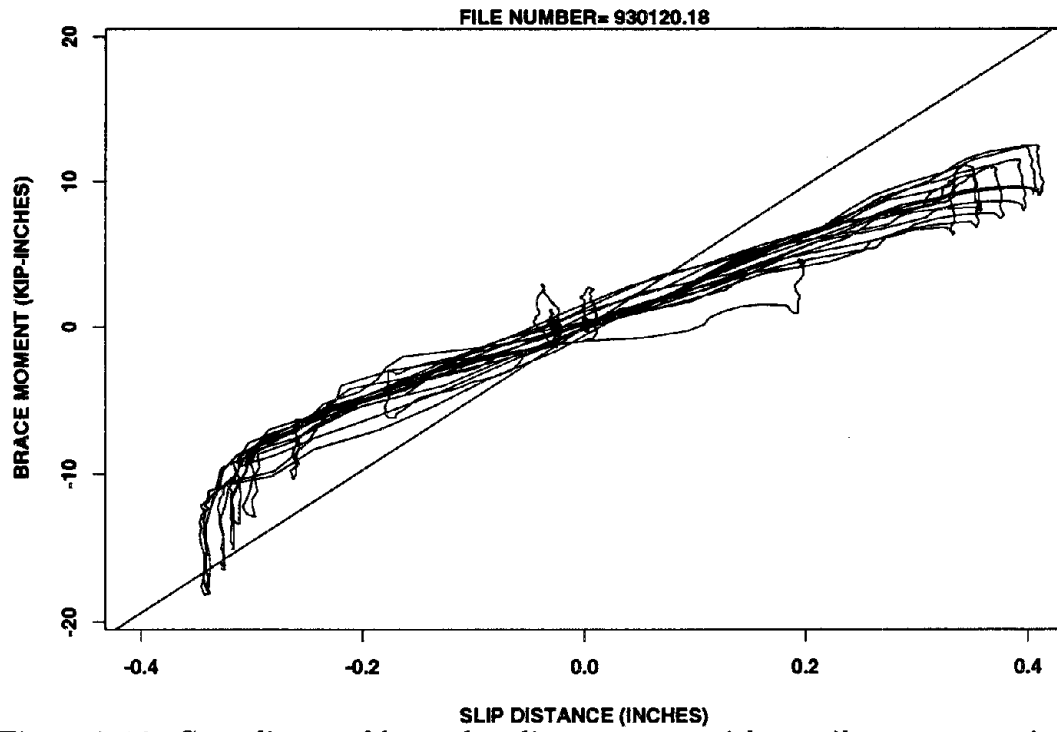
Figure 7.16: Compliance of brace bending moment with cantilever assumption.

FILE NUMBER= 930119.14
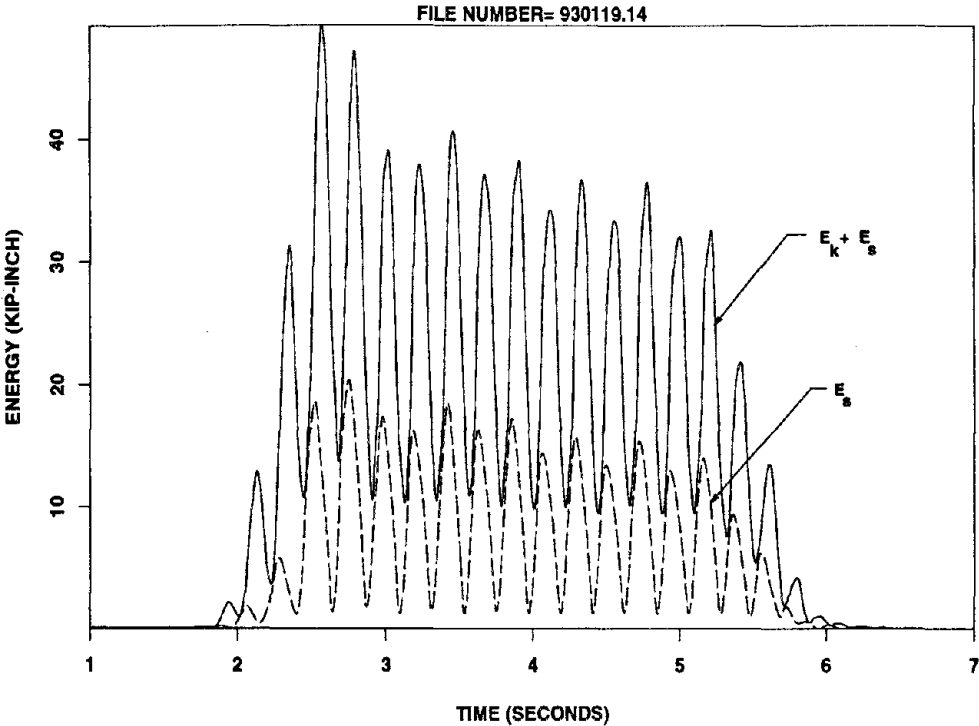
Figure 7.17: Kinetic and strain energies of TS1 in response to the harmonic signal

FILE NUMBER= 930120.05
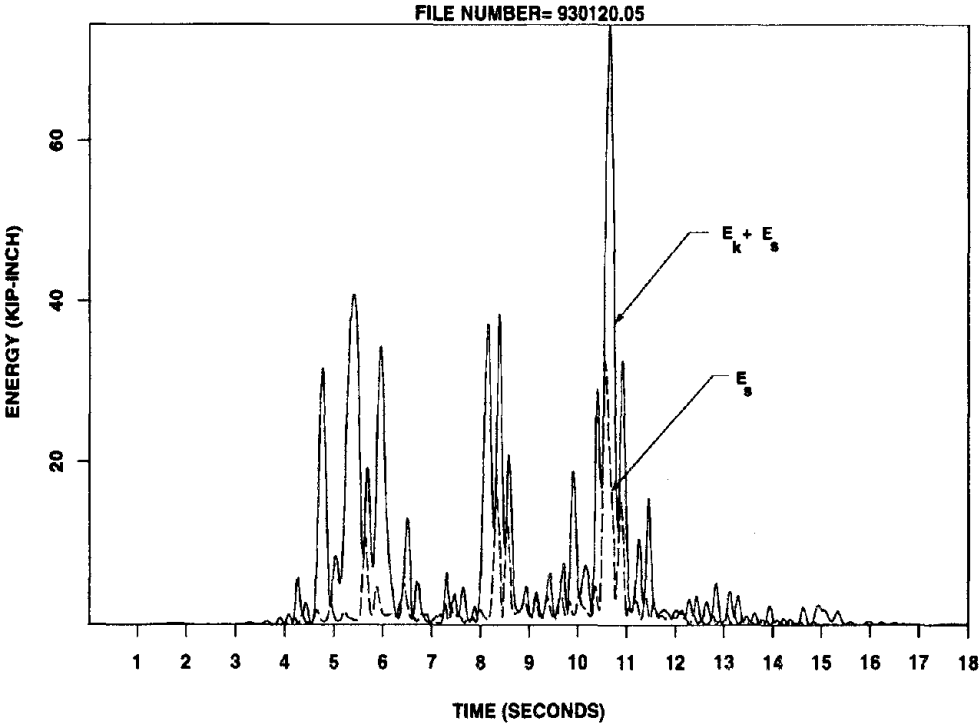
Figure 7.18: Kinetic and strain energies of TS1 in response to the Pacoima signal

FILE NUMBER= 930119.09
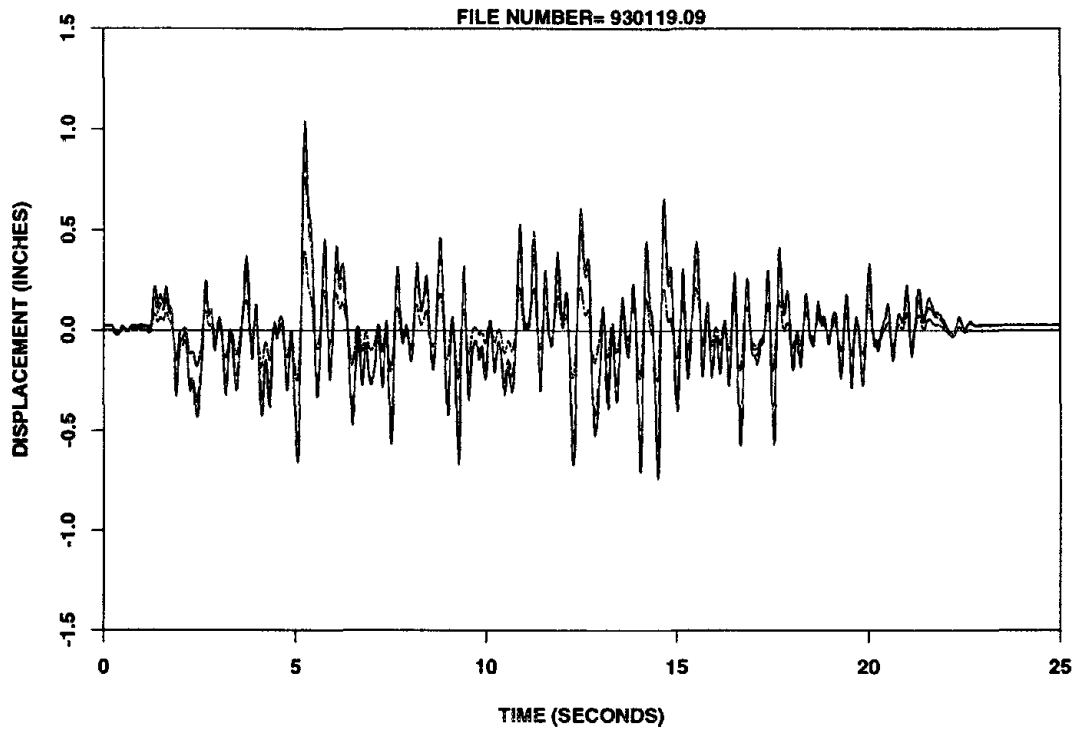
Figure 7.19: Relative displacements for TS1 subjected to the Chilean signal

FILE=930119.09
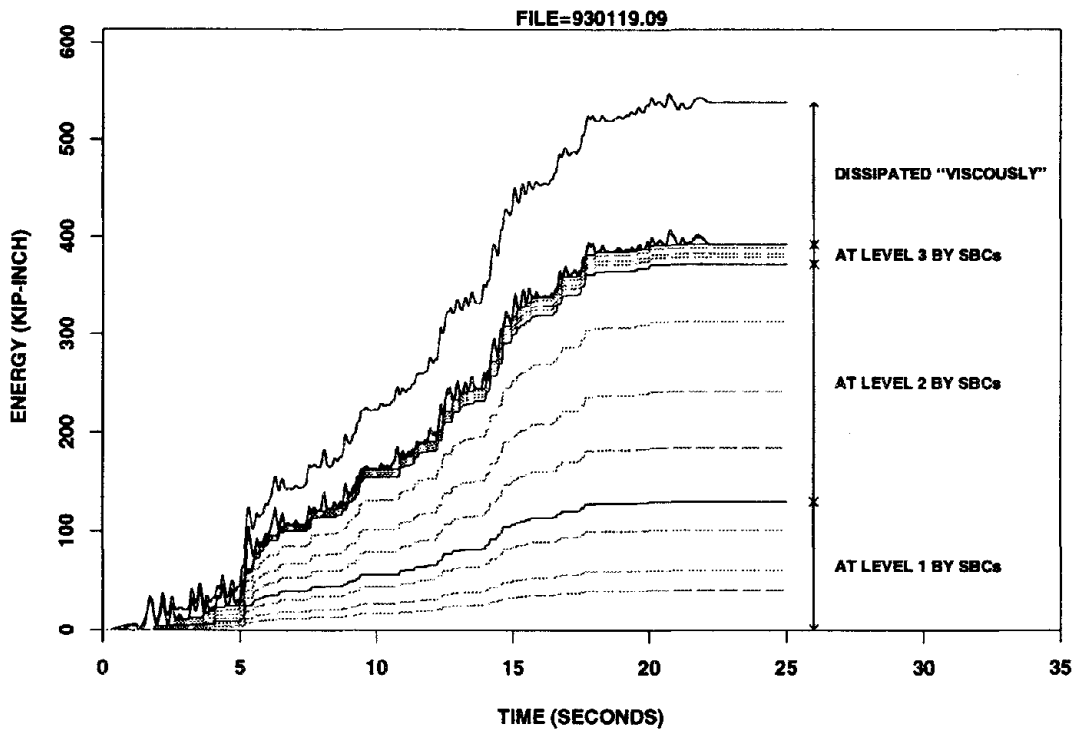
Figure 7.20: Energy history for TS1 subjected to the Chilean signal

FILE NUMBER= 930120.09
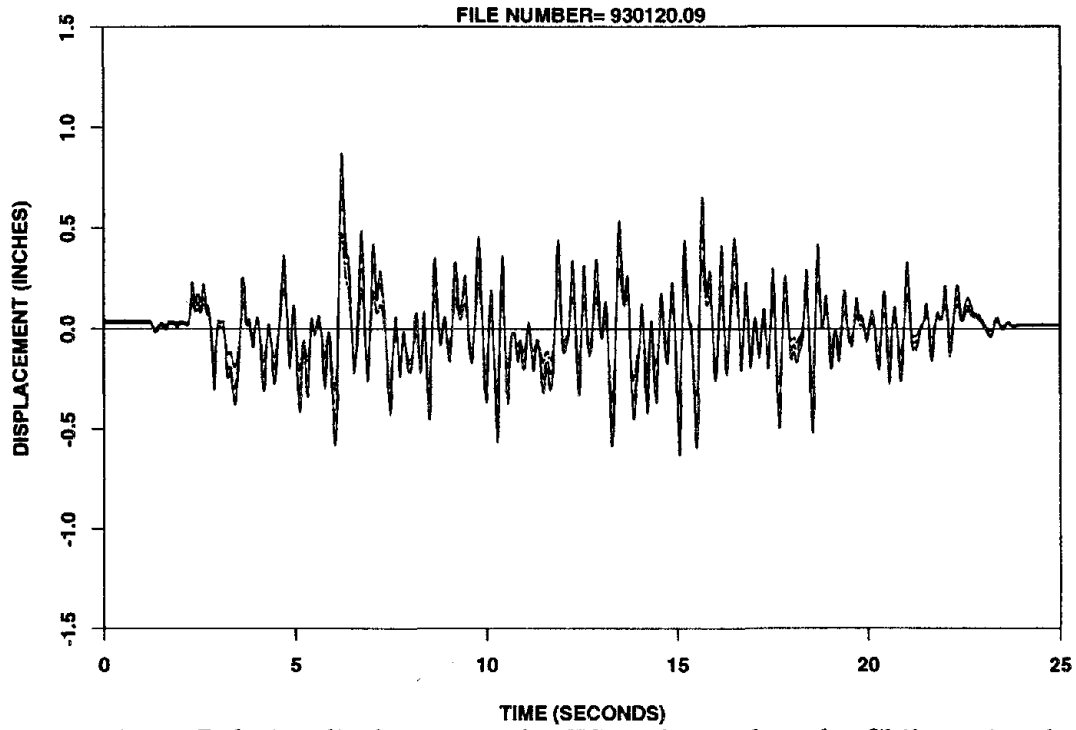
Figure 7.21: Relative displacements for TS2 subjected to the Chilean signal

FILE=930120.09

DISSIPATED "VISCOUSLY"

AT LEVEL 3 BY SBCs

AT LEVEL 2 BY SBCs

AT LEVEL 1 BY SBCs
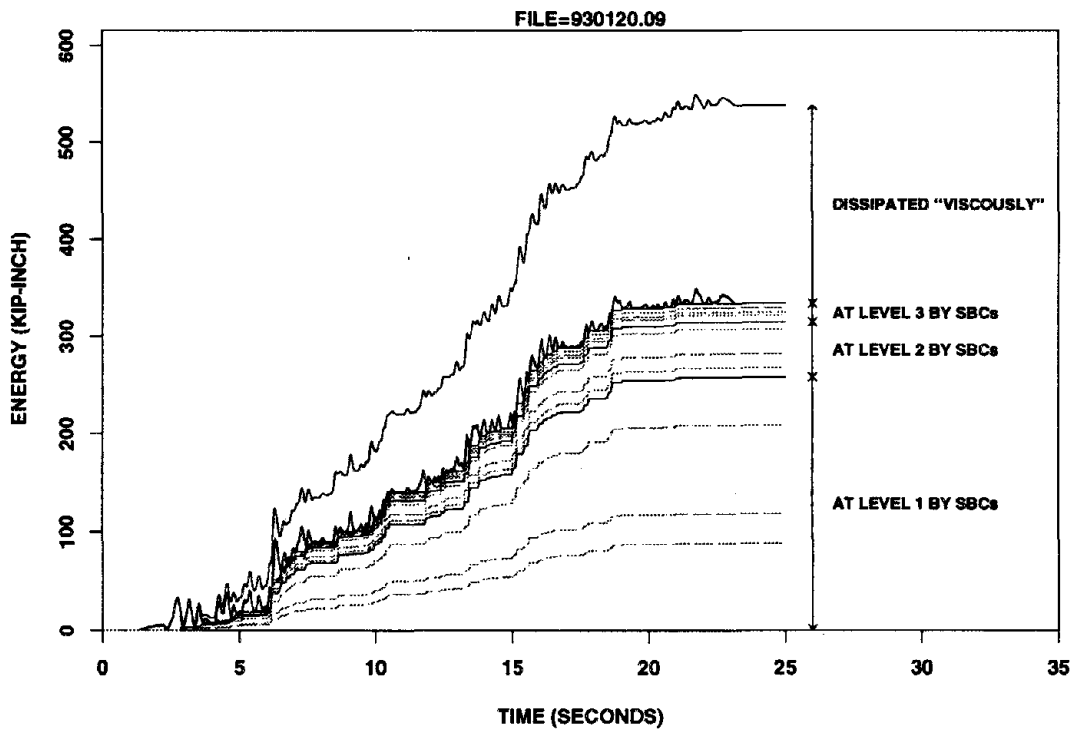
Figure 7.22: Energy history for TS2 subjected to the Chilean signal

FILE NUMBER= 930120.05
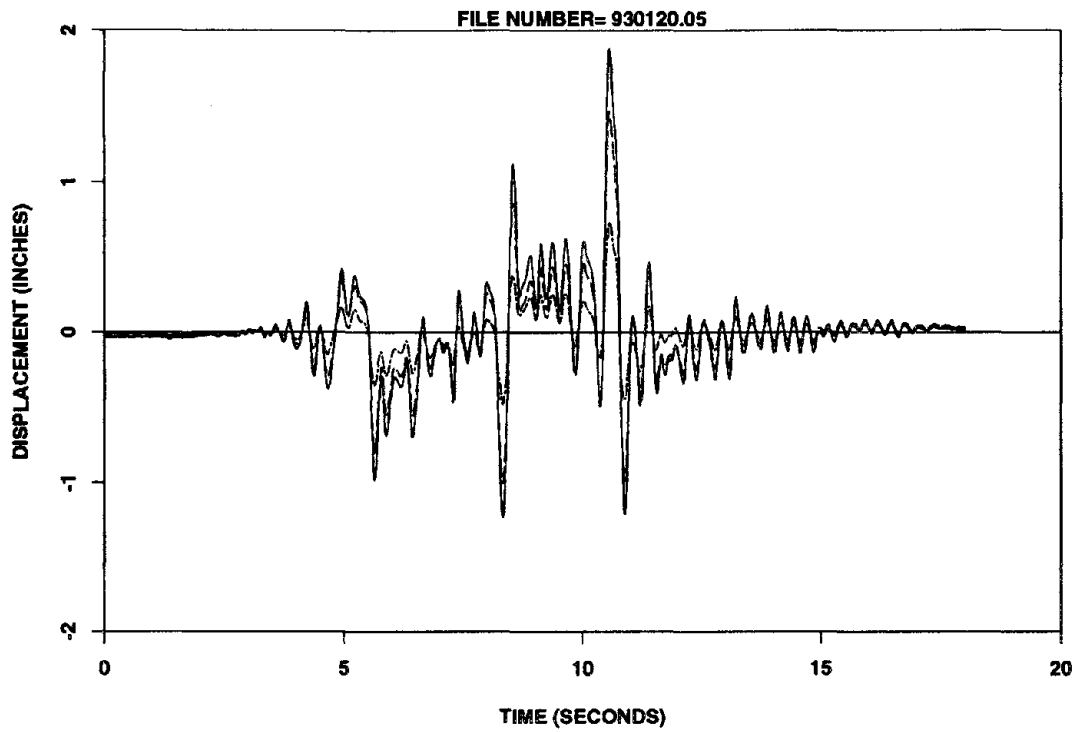
Figure 7.23: Relative displacements for TS1 subjected to the Pacoima signal

FILE=930120.05
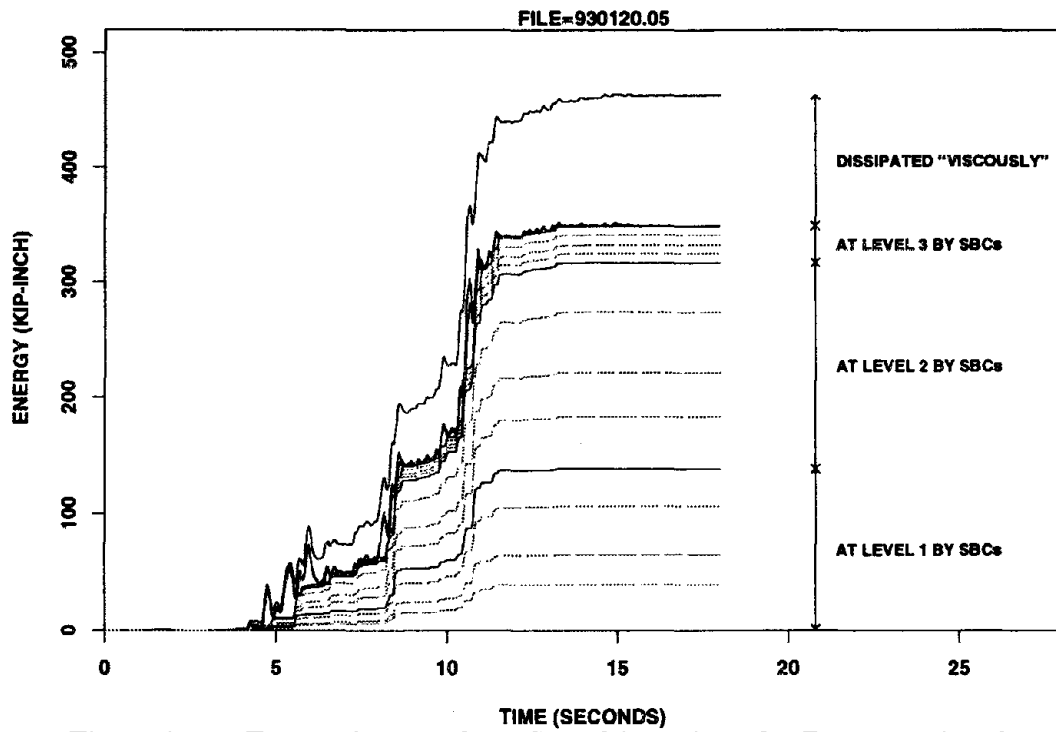
Figure 7.24: Energy history for TS1 subjected to the Pacoima signal

FILE NUMBER= 930120.13
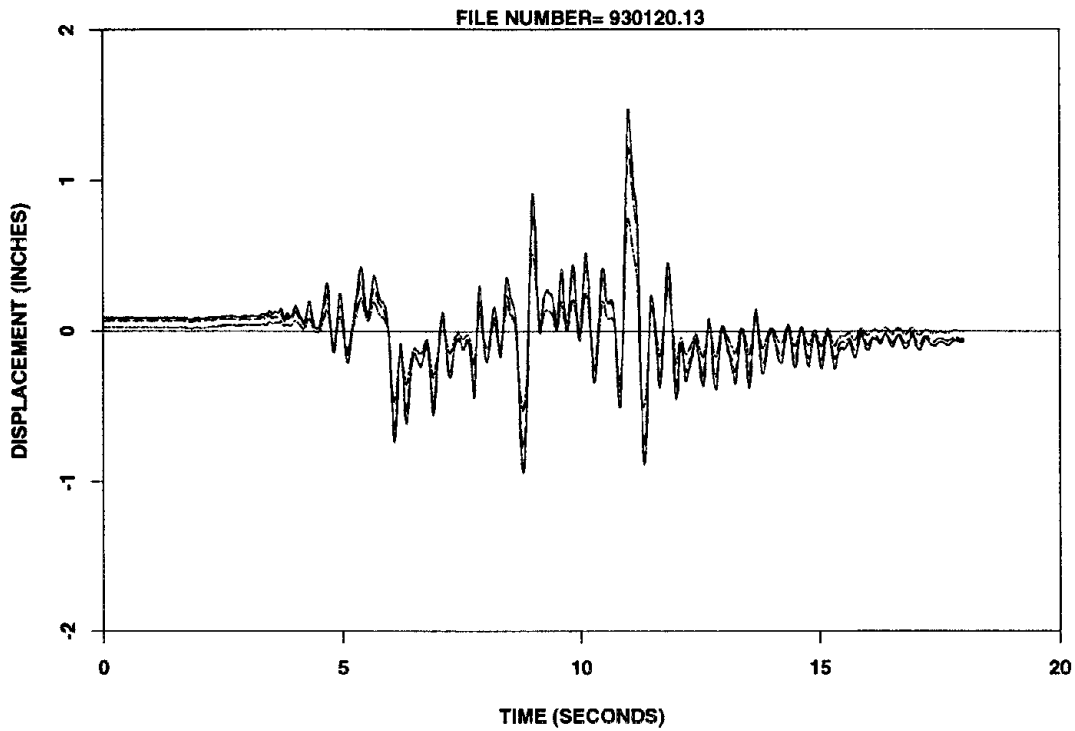
Figure 7.25: Relative displacements for TS2 subjected to the Pacoima signal

FILE=930120.13
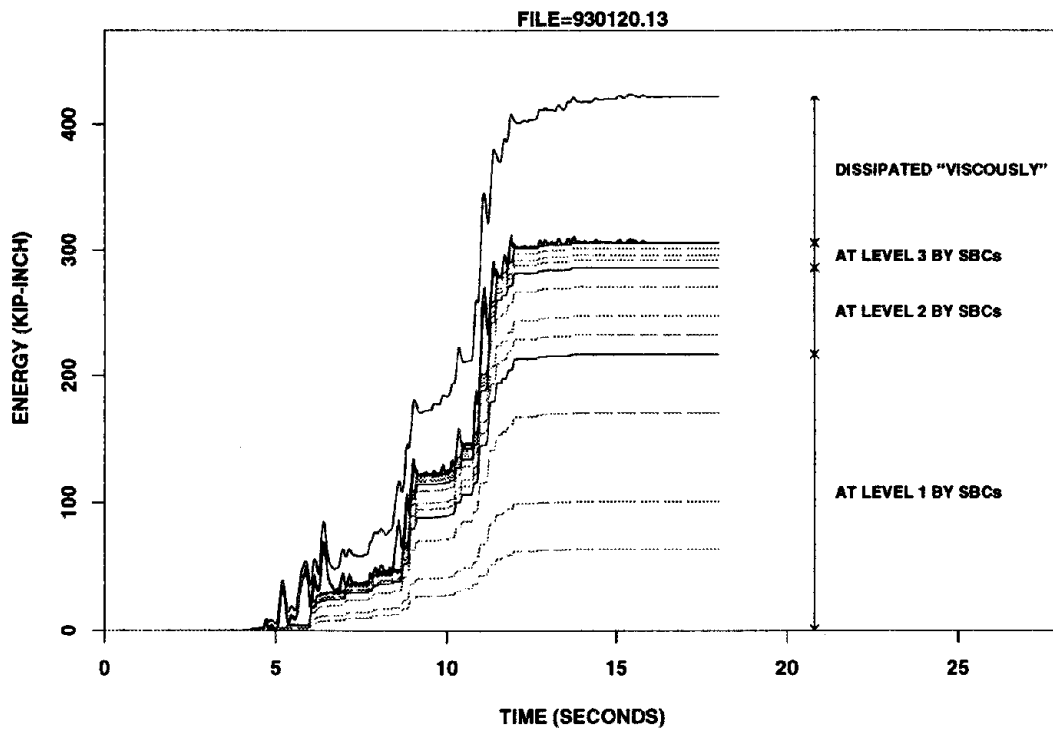
Figure 7.26: Energy history for TS2 subjected to the Pacoima signal

FILE NUMBER= 930119.14
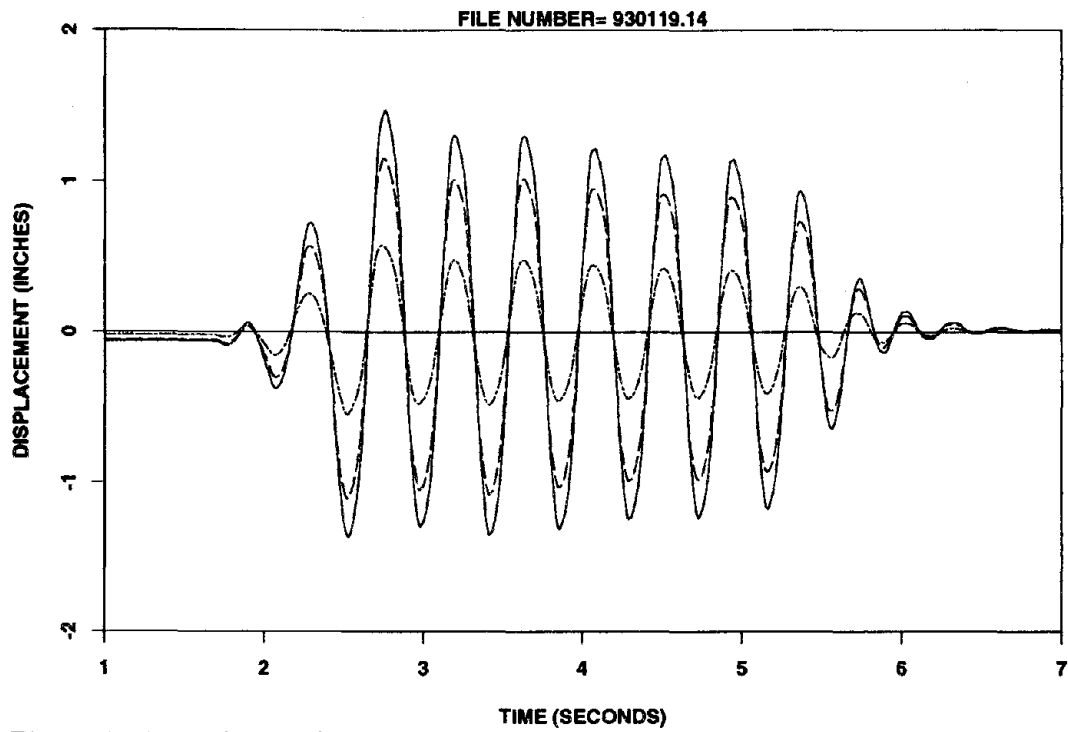
Figure 7.27: Relative displacements for TS1 subjected to the harmonic signal

FILE= 930119.14

DISSIPATED "VISCOUSLY"

AT LEVEL 3 BY SBCs

AT LEVEL 2 BY SBCs

AT LEVEL 1 BY SBCs
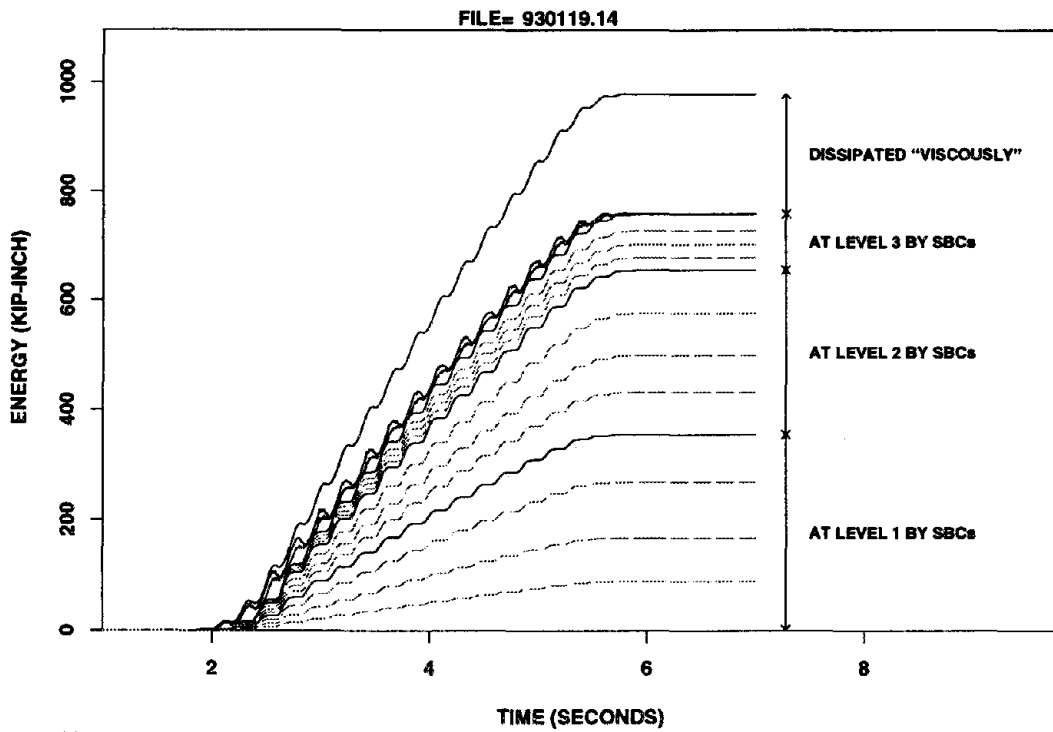
Figure 7.28: Energy history for TS1 subjected to the harmonic signal

FILE NUMBER= 930120.18
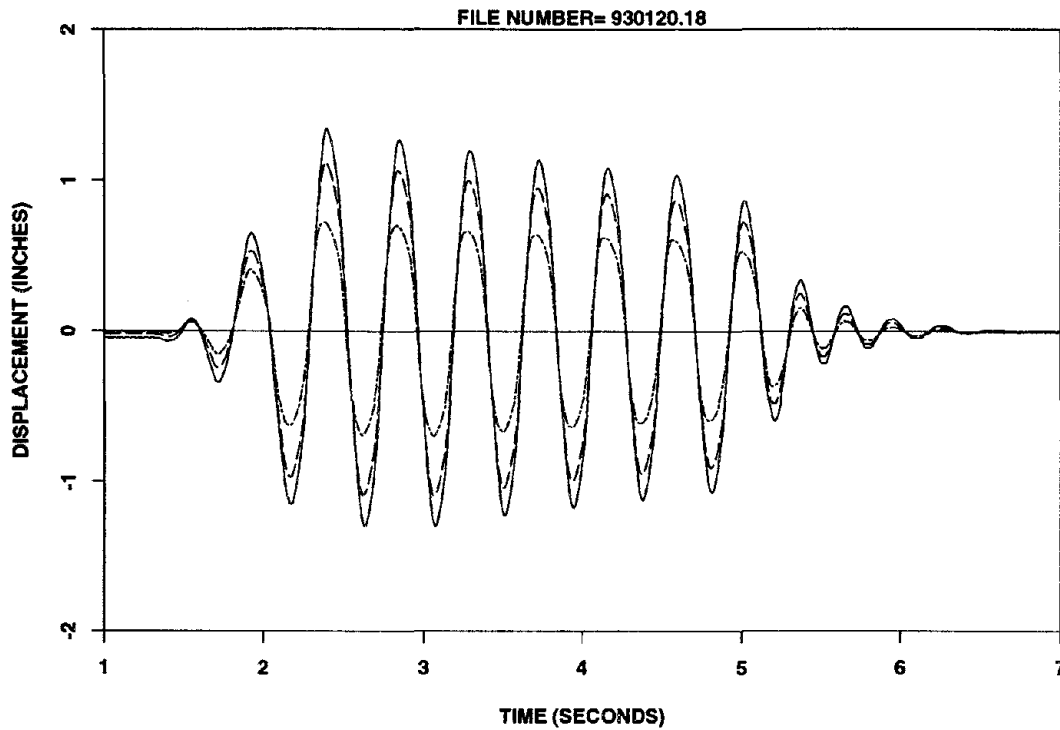
Figure 7.29: Relative displacements for TS2 subjected to the harmonic signal

FILE= 930120.18
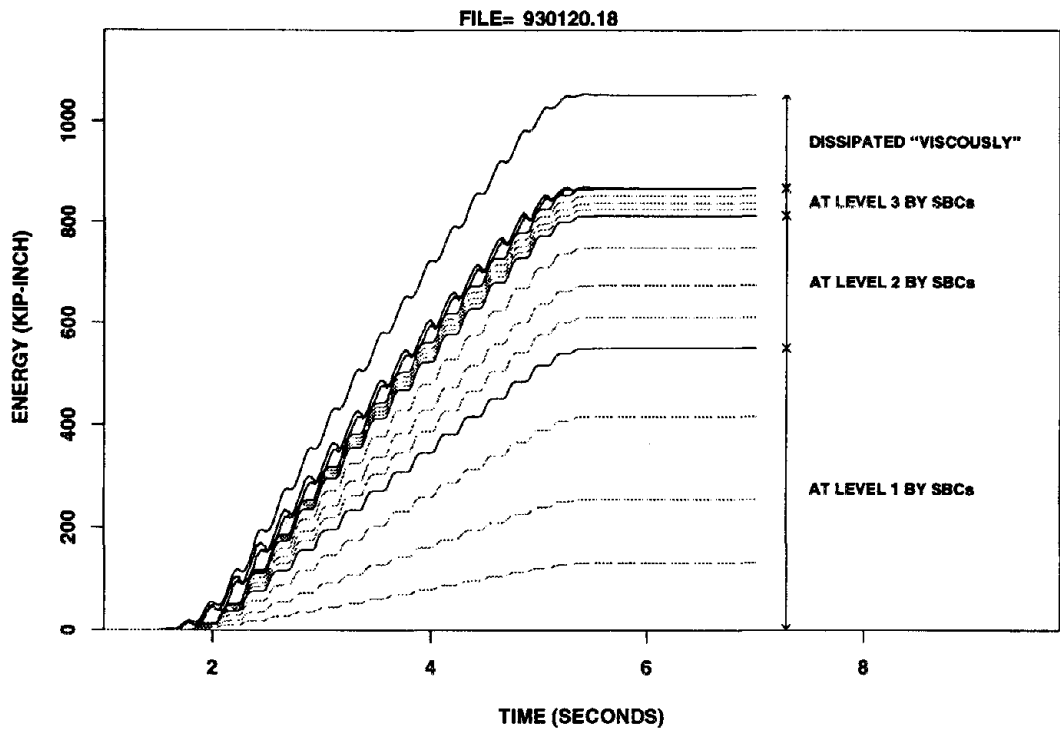
Figure 7.30: Energy history for TS2 subjected to the harmonic signal

Chapter 8

Analytical Simulations

8.1 Purpose

A particularly attractive feature of bracing elements with linearly-elastic-perfectly-plastic (LEPP) force-deformation behavior, such as is the case with a brace connected with an SBC, is the ease with which they lend themselves to numerical modeling. Dynamic analysis software capable of including such elements in the structural model have been available since the early 1970s. One such family of programs is the Drain-2D family, the current representative of which is Drain-2DX [4], has been widely used by both researchers and practitioners.

The simplest non-linear element which this program models is the LEPP truss element. This element has traditionally been used to approximate yielding in tension and buckling in compression of truss type elements. This approximation is generally accomplished by assigning appropriate yield stresses in tension and compression. Generally, very small yield stresses are assigned in compression to account for the sudden loss of strength accompanied by buckling. Although this model is a poor representation of a real truss member undergoing buckling, as it does no take into account strength and stiffness degeneration, it is ideal for representing a truss member connected with a Coulomb type frictional connection such as the SBC.

To model a truss member with a Coulomb-type frictional connection with this mathematical model, it suffices to assign to the member the actual EA of the

physical brace, to model the stiffness of the brace, and equal tension and compression yield stresses of a magnitude such that their product with the area, A, of the brace results in the expected slip force of the connection.

Clearly, if one can accurately model the behavior of a structure equipped with SBCs and predict its response given an acceleration history, then one can design that structure to withstand that acceleration history. In general, an analytical model is sufficient for design purposes if it can, within reason, predict the peak response of a structure. Given that the brace elements connected with SBCs exhibit behavior very similar to the mathematical model of a LEPP truss, it is reasonable to expect to be able to simulate the response both quantitatively and qualitatively, i.e. to be able to get a simulated history of, say, the displacement of the structure which closely resembles the experimental displacement history. Having obtained a very clear picture of the response of the test structure through the monitoring instrumentation, an ideal opportunity presents itself to see indeed how closely analytical simulation can match the experimentally obtained behavior. That is the purpose of this chapter.

8.2   Analytical Model of Test Structure

The test structure was modeled with the program Drain-2DX, version 0.01. At the time of the writing of this document, version 1.10 was being released. This and other later versions following version 0.01 produce identical results when the only non-linear elements used are the LEPP truss elements. The later releases are capable of modeling more complex non-linear elements that are neither used nor necessary for modeling of brace elements with SBCs.

As mentioned in Chapter 4, this program was used in the preliminary design stage of the test structure to obtain analytically derived slip displacement histories which were then imposed, in the C/T machine, to SBC connections identical to those which were eventually installed in the test structure. This testing was done to verify the performance of the connections under loading similar to that expected for such connections to undergo in the test structure during testing. Although, by all measures, that design process produced a successful design, the analytical model used lacked

certain refinements which are used in the analytical model used for the simulations presented in this chapter. That finalized analytical model is shown schematically in Figure 8.1.

The final analytical model is different from the initial model in mainly three aspects. These are the inclusion of the deck stiffnesses and the pithing stiffness and inertia of the shake table into the analytical model, and the use of effective, as measured, slip forces for the brace yield forces of the model. At the time of the initial design, it was thought that the decks on which the concrete blocks rest were stiff enough as to be modeled as rigid. Linear-elastic analysis of the decks indicated a conservative stiffness of 660 kips/inch provided by the decks between the points of contact with the blocks and the longitudinal frames. On the second day of testing it was observed that some relative deformations were present between the concrete blocks and the end columns of the longitudinal frame. To quantify these two additional wire potentiometers, channels 69 and 71, were installed to monitor the displacements of the blocks relative to the reference wall. The position of these instruments is indicated in Figure 5.11. With these additions it was possible to get an idea of the force-deformation characteristics of the decks. Referring to Figure 5.11, by subtracting from channel 69 the average of the channels 16 and 17 one gets the relative deformation of the level 2 deck between the point of contact of the blocks with the deck and the end columns of the longitudinal frames. Given the data from channel 34, the accelerations of the level 2 blocks, and knowing the mass of the concrete blocks and lead ingots, the value of the force going through the decks can be established. Then, plotting this force value versus the relative deformations described above results in the force-deformation curve for the level 2 deck. Figure 8.2 shows this curve from data taken from TS2 subjected to the harmonic signal. It is seen from this figure that the behavior of the decks is rather non-linear, with two distinct slopes apparent for this particular test. Indeed this behavior is almost suggestive of a frictional/yielding mechanism. The two slopes appear parallel to those of the two lines shown in the figure, first of which with a value of 660 kips/inch , as mentioned above, represents the analytical linear-elastic stiffness of the decks at the points of contact with the blocks. The second slope with a value of 112 kips/inch represents a similar analytical

linear-elastic stiffness but calculated with the assumption that the truss elements in the decks do not contribute to the stiffness. It then appears that the truss elements in the decks contribute little to the stiffness of the decks beyond a certain load. This may be attributed to the fact that the connections of the trusses to the beams were rather flexible and due to the combined effects of slenderness and lack of straightness of the trusses causing them to buckle in compression. In either case, the smaller stiffness indicated by this plot is used to model the decks in the two dimensional analytical model, that is half of 112 kips/inch. Where as in the initial model, the story masses were distributed to the outer two nodes of the longitudinal beams, e.g., nodes 1, 2, 4 and 5 in Figure 8.1. In the final model, the beam nodes are slaved together horizontally and the total story masses are concentrated at nodes, having only horizontal freedom, separated from the slaved nodes by springs representing the deck stiffnesses, e.g., nodes 20,21 and 22 separated from slaved nodes by springs 9, 10 and 11.

The test structure was possibly the stiffest structure of such height and mass tested on the shake table. Previous researchers have noted the considerable shake table-structure interaction possible during the testing of such a structure. Elaborate schemes for modeling of this interaction have been proposed [21]. However, these schemes are appropriate for elastic structures and have not been used here. The method used here, is one that has been commonly preferred by researchers [32, 2] due to its simplicity. The method consists of including the table in the analytical model of the structure by attaching the structure to a stiff beam pivoted at the center and stabilized by springs giving it an equivalent pitching stiffness to that effectively applied by the vertical actuators and stabilizers and by adding masses to this beam to account for the pitching inertia of the table. The values of pitching inertia and stiffness used to model the table are based on values suggested by [21], and are respectively 1251 kips-sec^2-inch and 2.27x10^7 kip-inches/radian. Figure 8.3 shows a plot of the overturning moment versus the table pitch for the test of TS2 subjected to the harmonic signal. Overturning moment is calculated by summing the product of story shear forces and story heights for the three stories, while table pitch rotation is calculated in the same way as explained in Chapter 5. It is seen that the stiffness

suggested by [21] is rather reasonable. The table pitching inertia and stiffness are included in the analytical model by assigning appropriate vertical masses to nodes 16 and 17, shown in Figure 8.1, and connecting these nodes to the fixed reference frame through appropriate springs, shown as springs 7 and 8.

The analytical model used a mass damping of $\alpha = 1.0$. This is equivalent to a critical damping ratio of 2 %. The damping value was arrived at by trial and error. Actual table acceleration histories were used as inputs for the simulation . These were arrived at by taking the averages of the accelerations read by channels 3 and 4 for each of the tests simulated. Such acceleration histories were shown in Chapter 5. Lastly, the yield/slip forces for the braces of the model were determined individually for each simulation from the experimentally measured slip forces associated with each simulation. Such measurements were made by measuring the heights of combined story hysteresis loops for a given story, such as those presented in Figure 7.9 and 7.10, increasing the measured value by $\frac{1}{\cos\theta}$, θ being the angle of the braces at that story, accounting for the slope of the braces and then assigning equally an eighth of this force to each of the two braces of the analytical model at that story. The factor of one eighth is necessary as measuring the height of the hysteresis loop results in measuring double the story slip force and because the hysteresis is due to four braces per story. Where slips were so small as to cause the "chewed off corners" of the hysteresis loops to distort significantly the rectangular shape of the loops, somewhat smaller slip forces were used. These slip forces were in all case within 5 % of that determined by measuring the full height of the loops.

Section properties given by Table 5.1 were used to model the structural elements. The springs shown in Figure 8.1 were modeled as simple truss elements with $\frac{EA}{L}$ assigned to produce the necessary stiffnesses.

8.3   Analytical Results

The simulation results presented here correspond to test results presented in Chapter 7. Namely, simulation results are given for two structural configurations, TS1 and TS2, each subjected to three acceleration inputs; the Chilean, Pacoima and

CHAPTER 8. ANALYTICAL SIMULATIONS   198

the harmonic input. For each case, the analytically derived displacement history is presented for each level. Then, the analytical displacement histories of each structure level are compared with the experimental over the time-window in which the critical response occurs. In addition, analytical hysteresis loops are presented for the braces at each level for each case. These may be compared with the experimental hysteresis loops presented for each case in Chapter 7.

It should be noted here that the analytical model represents at each structure level four braces, each of which has a different and non-unique slip force, with two braces of identical and constant slip forces. Therefore, the analytical hysteresis loops are representative of a sort of average effect of the hysteresis of the real braces.

Simulated Responses to the Chilean Signal

Figures 8.4 and 8.5 show the simulated displacement time histories of the three levels of, respectively, TS1 and TS2 due to the Chilean signal. The general characteristics of these are to be compared with the experimental results shown in Figures 7.19 and 7.21. The comparison of these two sets of figures indicates that with the exception of the presence of a, roughly, 0.1 inch offset between the analytical experimental displacement histories, the two sets of figures match each other rather well. At this point it is noted that, as indicated in Chapter 6, the value of absolute zero is an unknown in the experimental data due to zero shifts in the instrumentation, residual deformations in the structure after each test and the loss of the original true zero due to malfunction of the data acquisition system. The data from the instruments is best judged in terms of relative changes from an assumed zero. In most cases this assumed zero was calculated by subtracting the mean from the record. This technique appears to have worked well in most cases. However an erroneous offset of say 0.1 inches, in particular in the record of the displacement of the first story where residual displacements are most likely due to the smaller ratio of the stiffnesses of the columns to the story slip forces of the SBCs, is not unlikely.

The left hand sides of Figures 8.6 and 8.7 show plots of the experimental and simulated displacement histories of the three levels of the structure in a time-window

about the peak displacement response and adjusting the analytical record by shifting the analytical values by 0.1 inches. It is seen that with this offset taken into account, rather good correlation between the analytical and experimental results is achieved for both the TS1 and TS2 responses.

The right hand side of Figures 8.6 and 8.7 show plots of the analytical hysteresis loops for typical braces at each level. These are to be compared with their experimental counterparts shown in Figures 7.3 and 7.4. It is seen that, again counting for zero-shifts, correspondence is rather good.

Simulated Responses to the Pacoima Signal

As mentioned previously, this signal produced one of the severest responses in the test structure. Figures 8.8 and 8.9 show the analytical displacement histories for TS1 and TS2. The experimental counterparts of these are the Figures 7.23 and 7.25. No zero corrections were necessary for these simulations. Simulations matched experimental results surprisingly well. Direct comparisons of the analytical and experimental displacements at the three levels are shown in the left hand sides of Figures 8.10 and 8.11 respectively for TS1 and TS2. The right hand sides of the figures show the analytical hysteresis loops. The experimental counterparts of these are shown in Figures 7.5 and 7.6.

Simulated Responses to the Harmonic Signal

Figures 8.12, 8.13, 8.14 and 8.15 show, as for the last two cases, the analytically derived responses of TS1 and TS2 this time to the harmonic signal. The experimental counterparts of these response quantities are found in Figures 7.27, 7.29, 7.7 and 7.6. Again, no zero corrections are made for these response quantities. The correlation between experimental and analytical results is again seen to be excellent.

8.4   Discussion and Conclusions

As mentioned at the beginning of this chapter, the goal of dynamic analysis of a structure, from the designers point of view, is to approximately quantify the maximum response of the structure given a particular input. Data presented in this chapter indicates that with proper modeling the response of a structure with SBCs can be approximately determined not only in terms of peak response, but also in terms of general behavior.

Proper modeling of SBCs consists mainly of determining the correct equivalent slip force. As indicated in Chapter 2 this slip force initially varies with the cumulative slip distance; increasing rapidly to a constant plateau and then remaining effectively constant. Given the information in Chapter 2, one can determine the effective slip force by a trial-and-error procedure. If analysis shows that the cumulative slip distance is significantly larger than that required to "wear in" the SBCs, then the nominal slip force should be used. However, for the case of very weak excitations or over-designed SBCs where analysis indicates cumulative slip distances smaller than that necessary for "wear in", an effective slip force, possibly based on the equal energy principle, is more appropriate. If slip displacements are small during an excitation, regardless of the value of the cumulative slip distance, the effects of the "chewed off corners" of the hysteresis loops must be taken into account in determination of the slip force.

That changes in the response between the different configurations of the structure, e.g. TS1 and TS2, can so well be represented analytically indicates the feasibility of a trial-and-error design approach for the design of structures with SBCs. Such an approach would consist of selecting an SBC configuration, executing the analysis, judging the results in terms of the design criteria and repeating the analysis with a new design until the criteria are satisfied. It must be noted that the results presented in this chapter are for 2-dimensional simulations of a 3-dimensional symmetric structure tested in one horizontal direction. Correct modeling of a 3-dimensional structure, in particular one with a new technology such as the SBCs, is contingent on reasonable assumptions regarding the coupling and interaction of orthogonal lateral

force resisting systems.

For completeness of presentation a sample Drain-2DX input file, that for the simulation of the response of TS1 to the Pacoima signal has been included in Appendix B. This input file follows the conventions and specifications indicated in Figure 8.1.
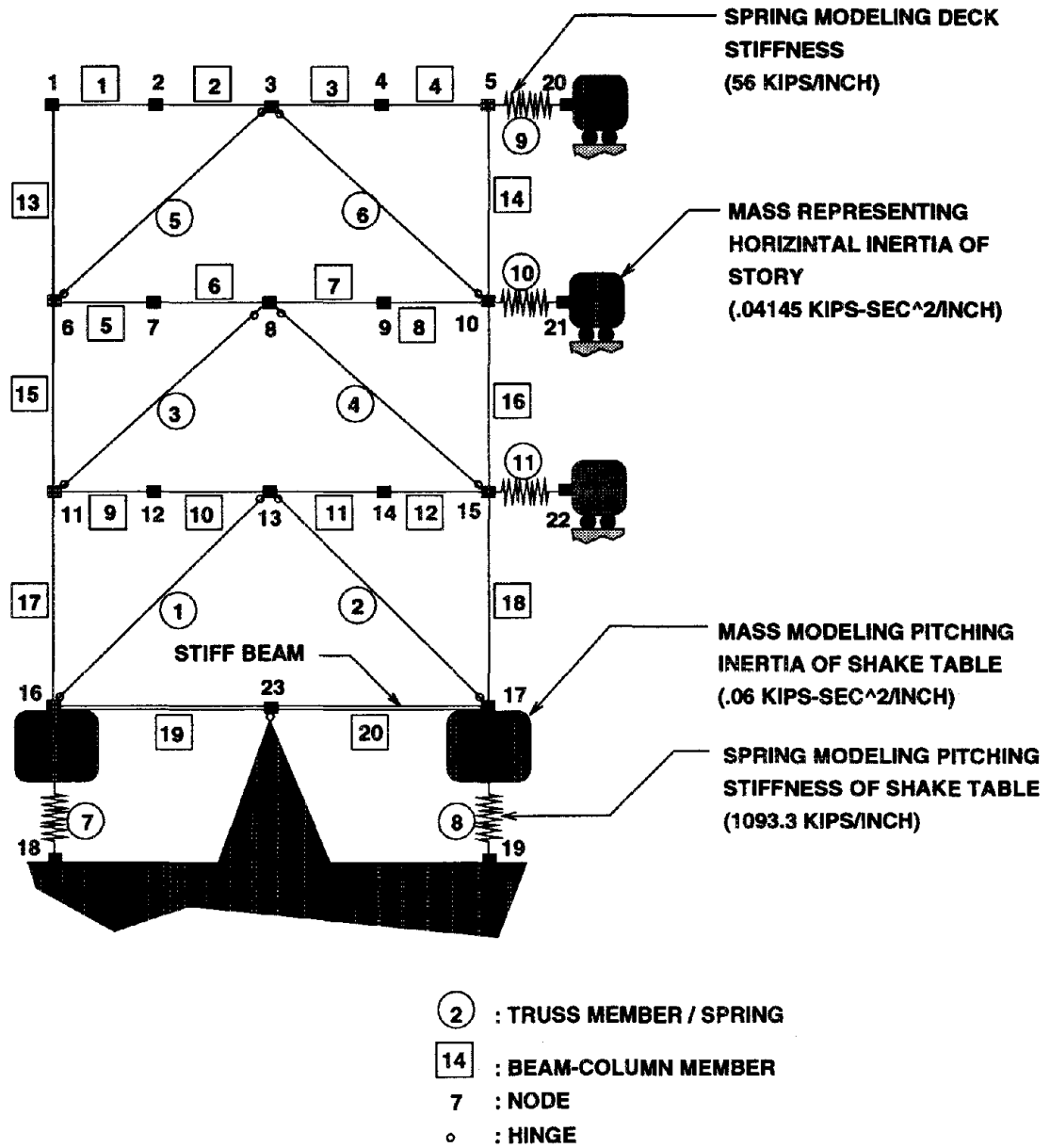
Figure 8.1: Schematic representation of the analytical model of the test structure.
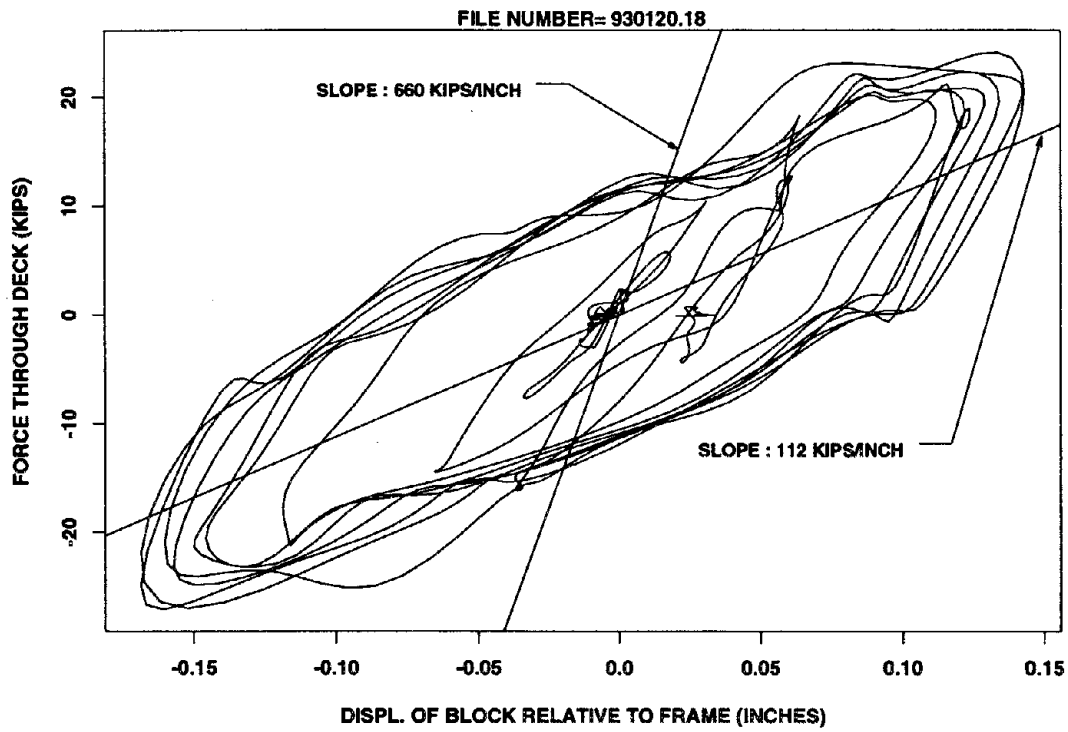
Figure 8.2: Force-deformation characteristics of level 2 deck.
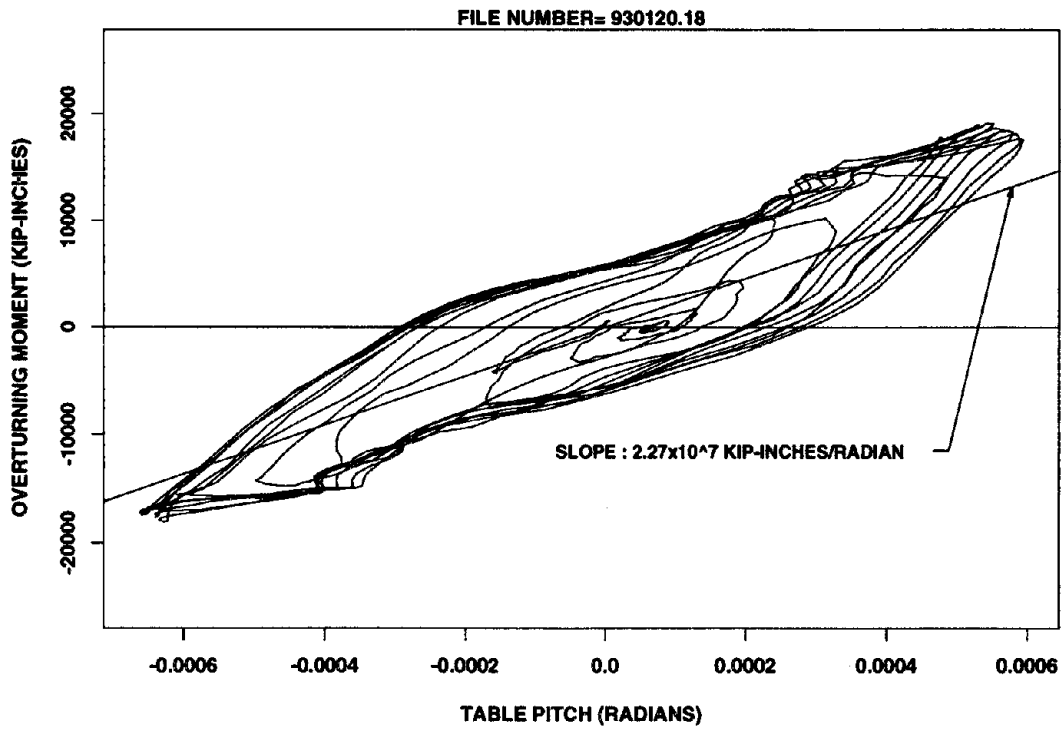
Figure 8.3: Overturning moment-pitch characteristics of table.
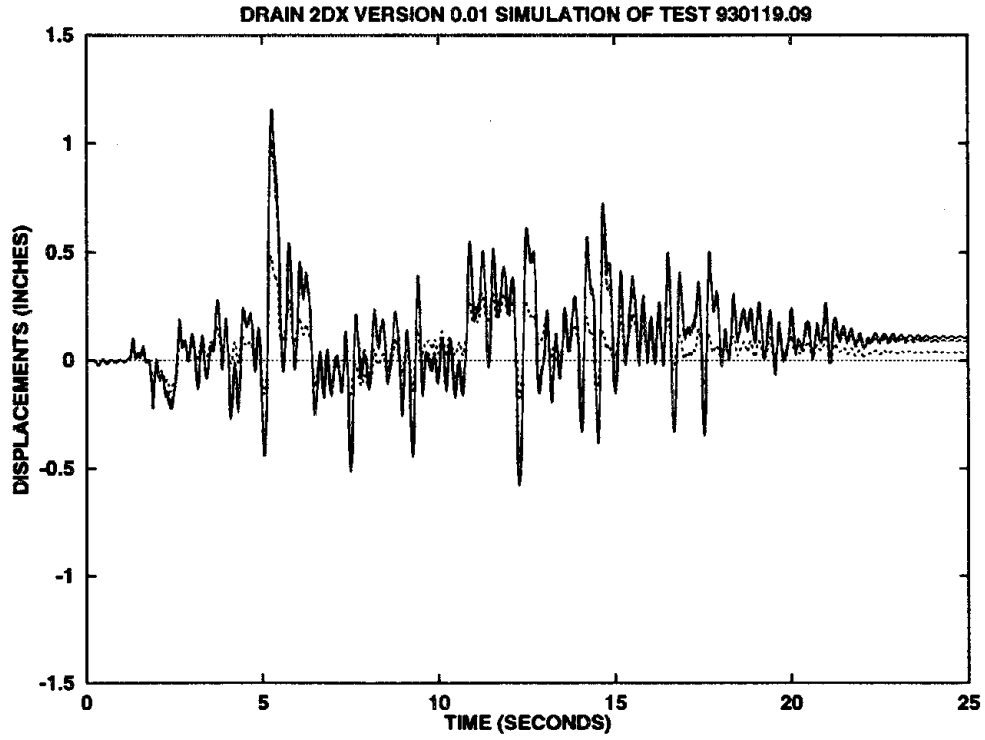
Figure 8.4: Simulated displacement history of TS1 due to the Chilean signal.
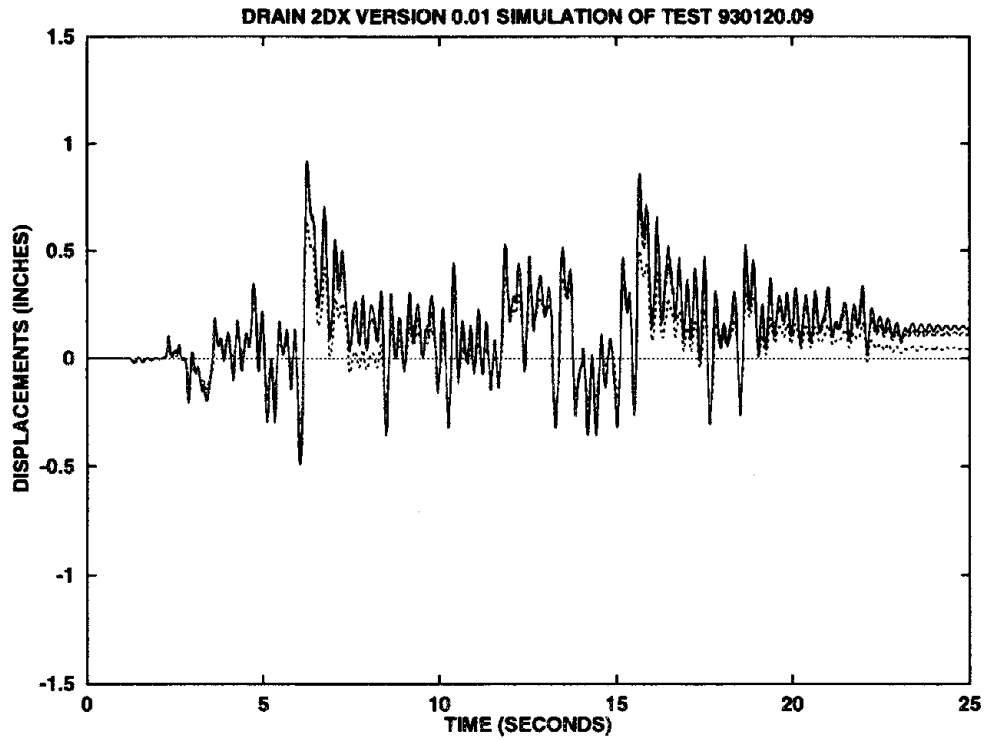
Figure 8.5: Simulated displacement history of TS2 due to the Chilean signal.
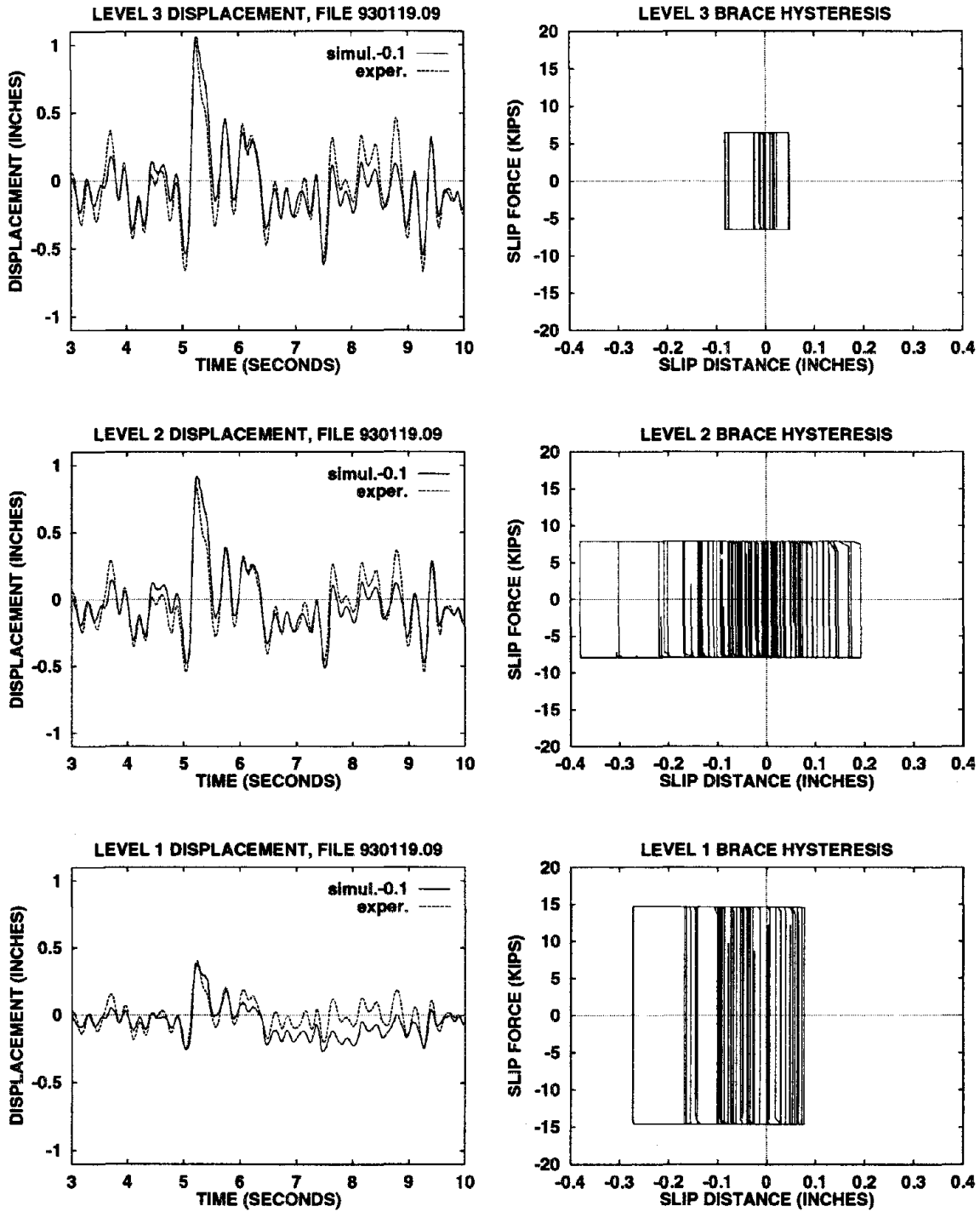
Figure 8.6: Analytical and experimental story displacements and analytical brace hystereses of TS1 due to the Chilean signal.
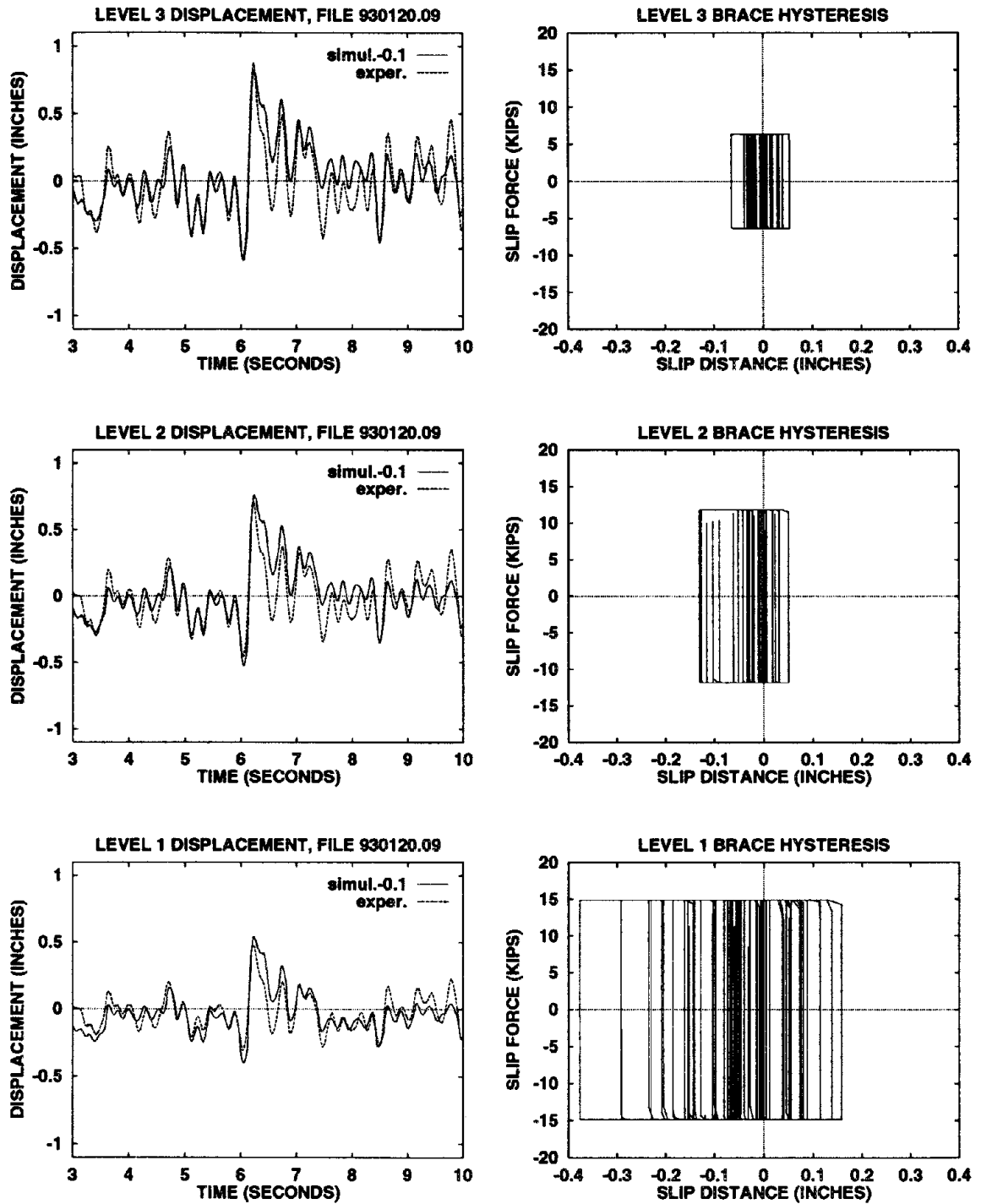
Figure 8.7: Analytical and experimental story displacements and analytical brace hystereses of TS2 due to the Chilean signal.
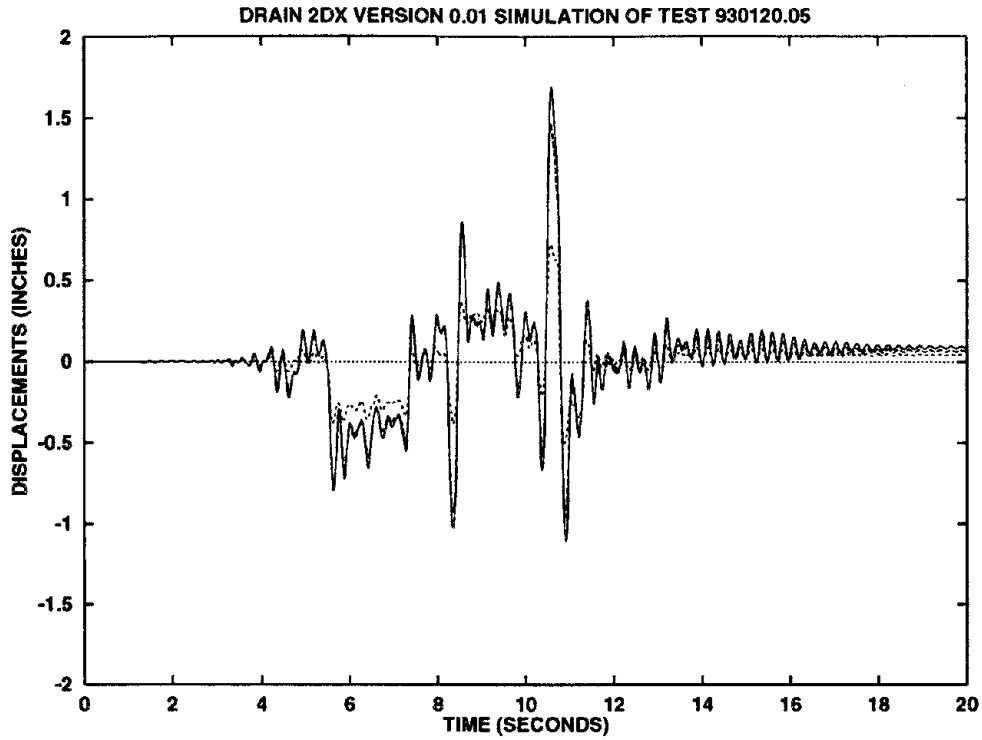
Figure 8.8: Simulated displacement history of TS1 due to the Pacoima signal.
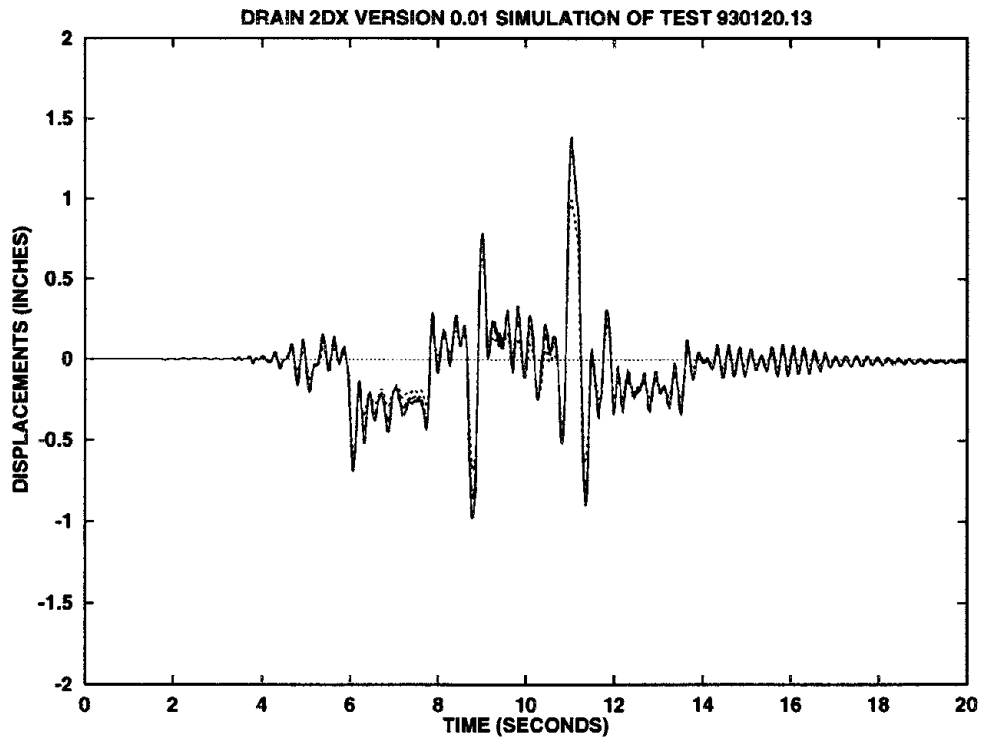
Figure 8.9: Simulated displacement history of TS2 due to the Pacoima signal.
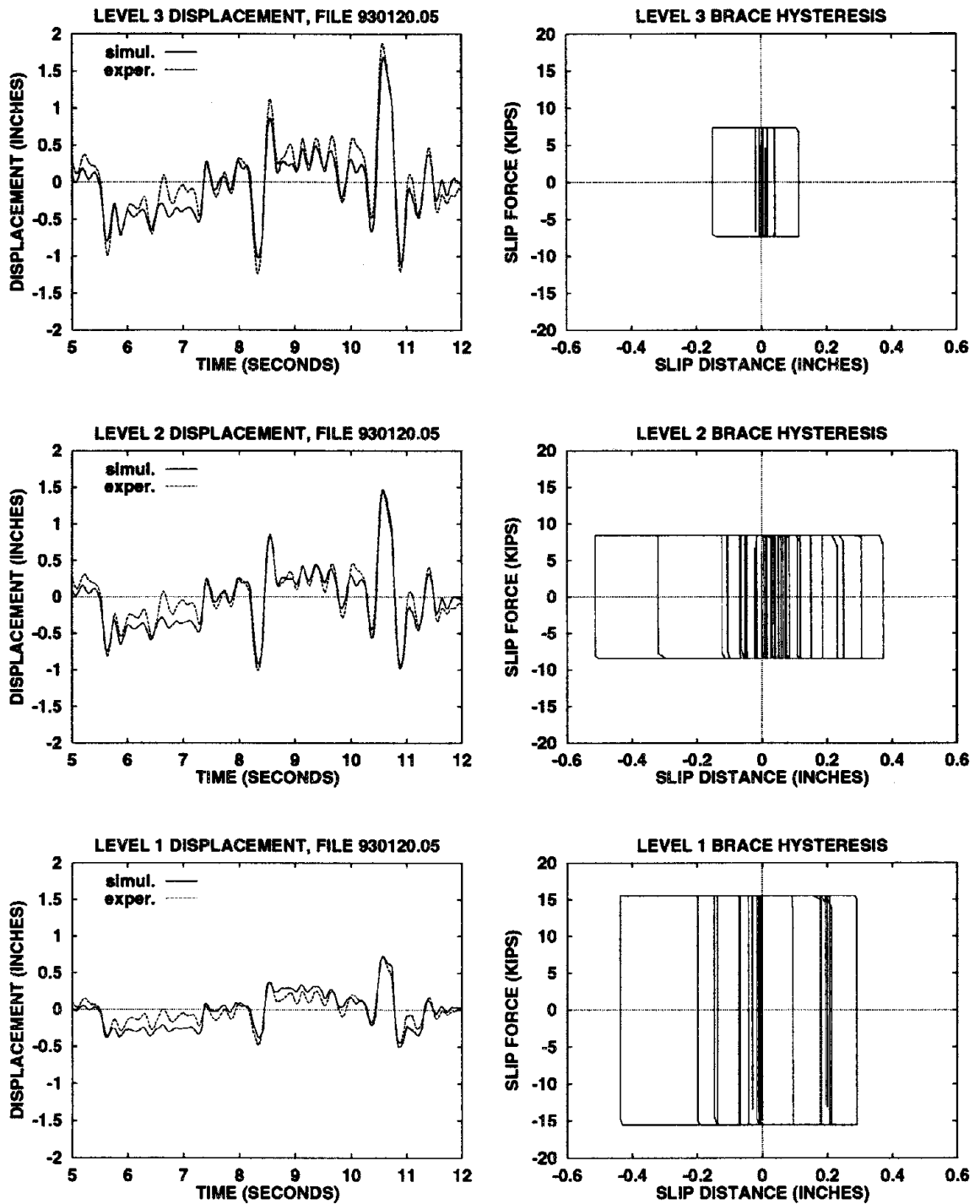
Figure 8.10: Analytical and experimental story displacements and analytical brace hystereses of TS1 due to the Pacoima signal.
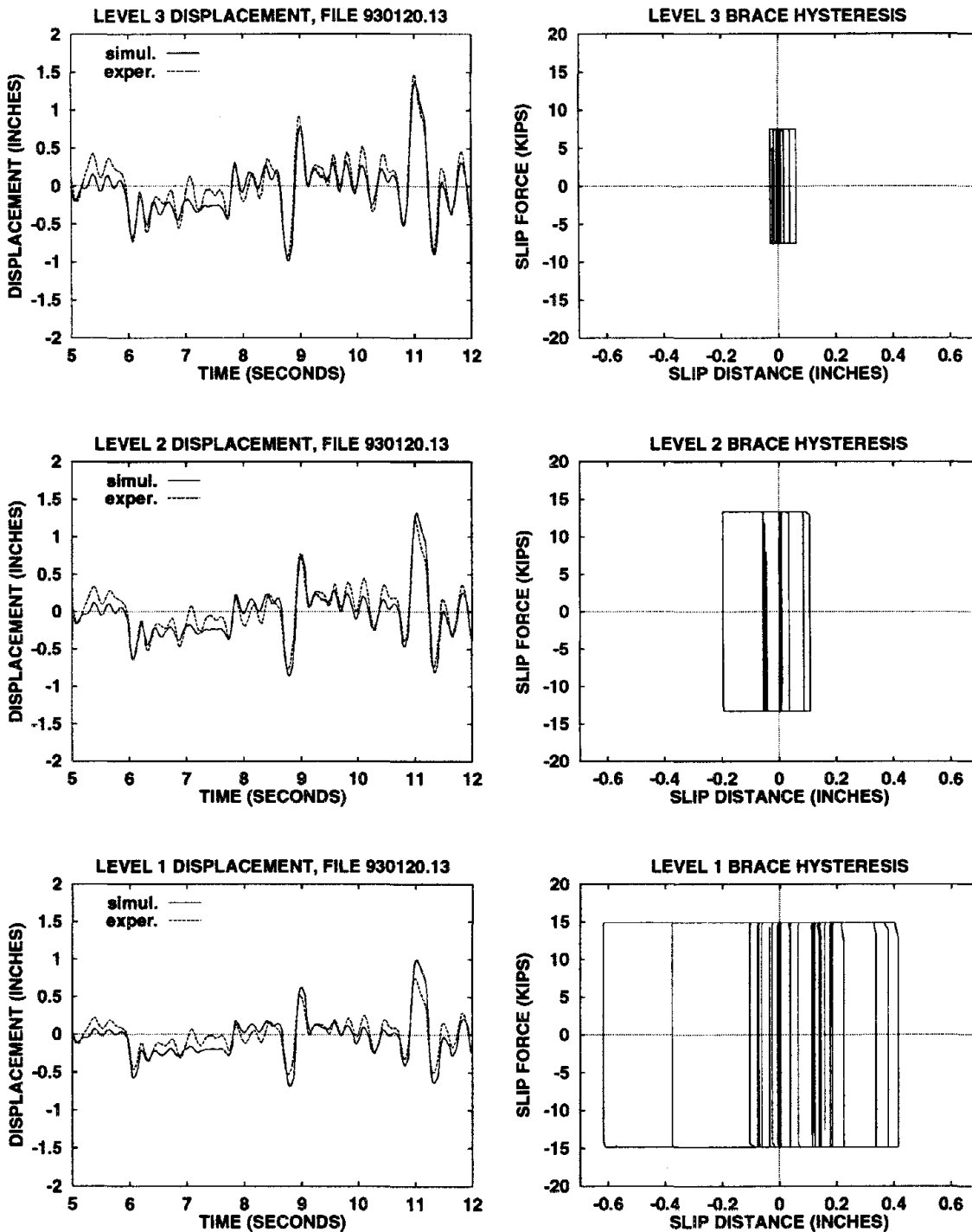
Figure 8.11: Analytical and experimental story displacements and analytical brace hystereses of TS2 due to the Pacoima signal.

DRAIN 2DX VERSION 0.01 SIMULATION OF TEST 930119.14
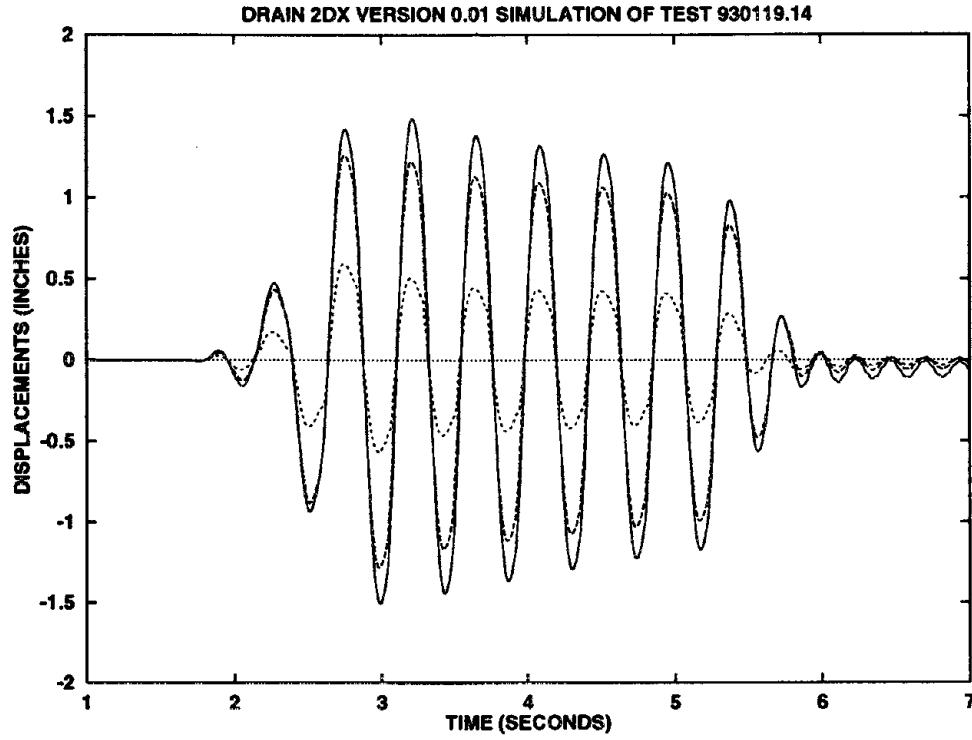
Figure 8.12: Simulated displacement history of TS1 due to the harmonic signal.

DRAIN 2DX VERSION 0.01 SIMULATION OF TEST 930120.18
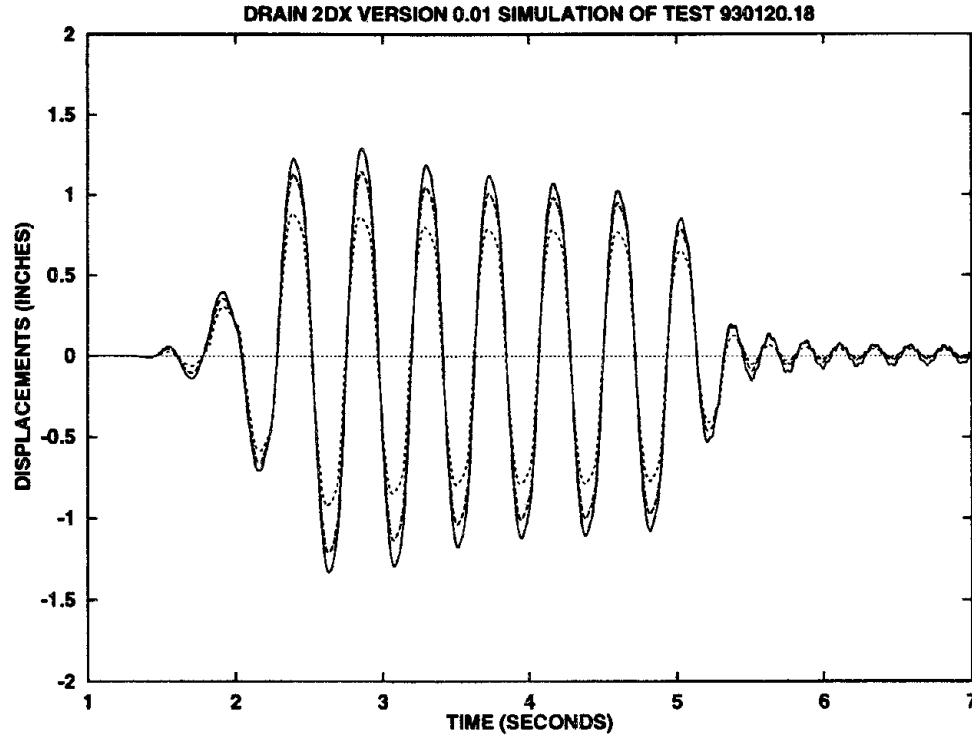
Figure 8.13: Simulated displacement history of TS2 due to the harmonic signal.
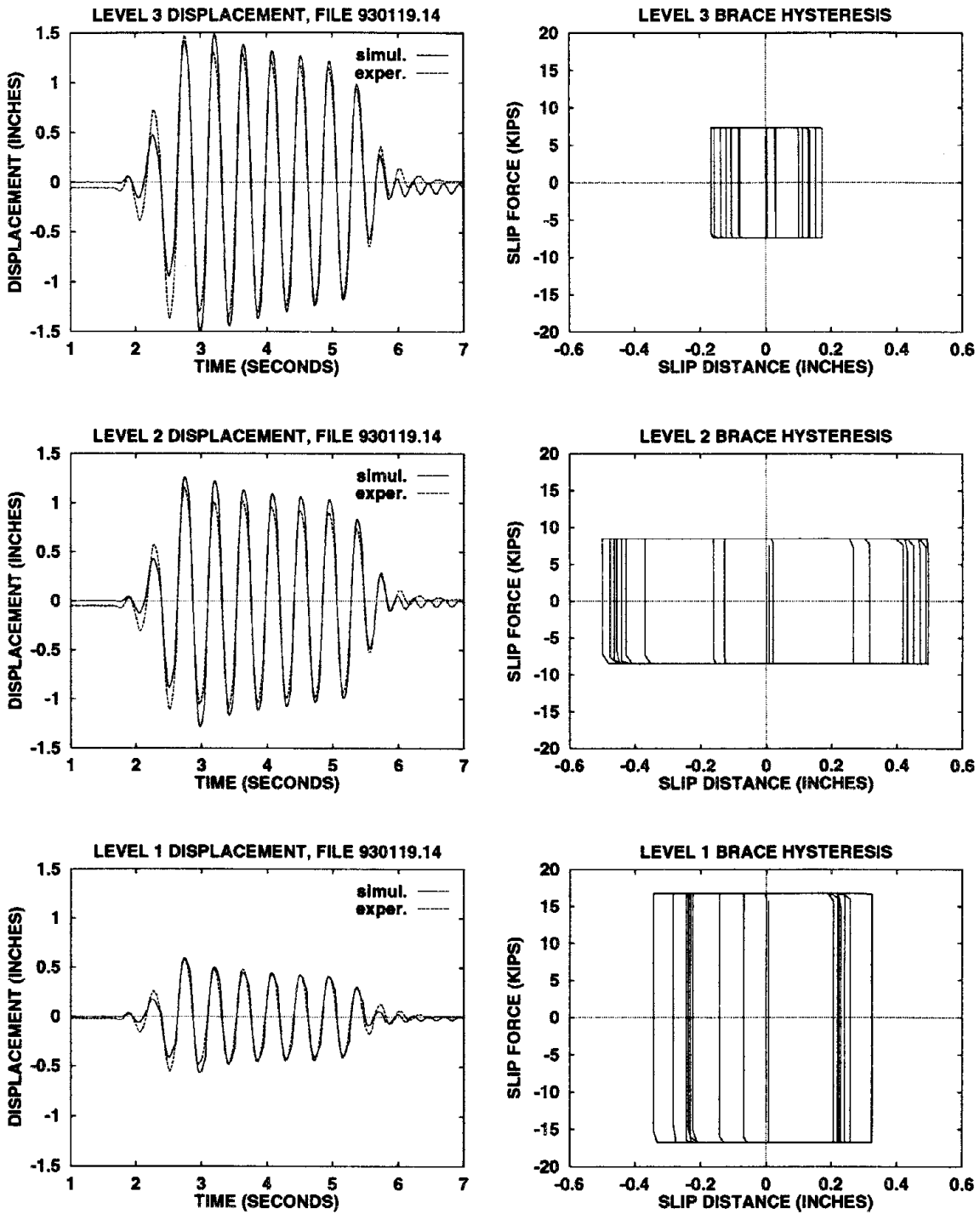
Figure 8.14: Analytical and experimental story displacements and analytical brace hystereses of TS1 due to the harmonic signal.
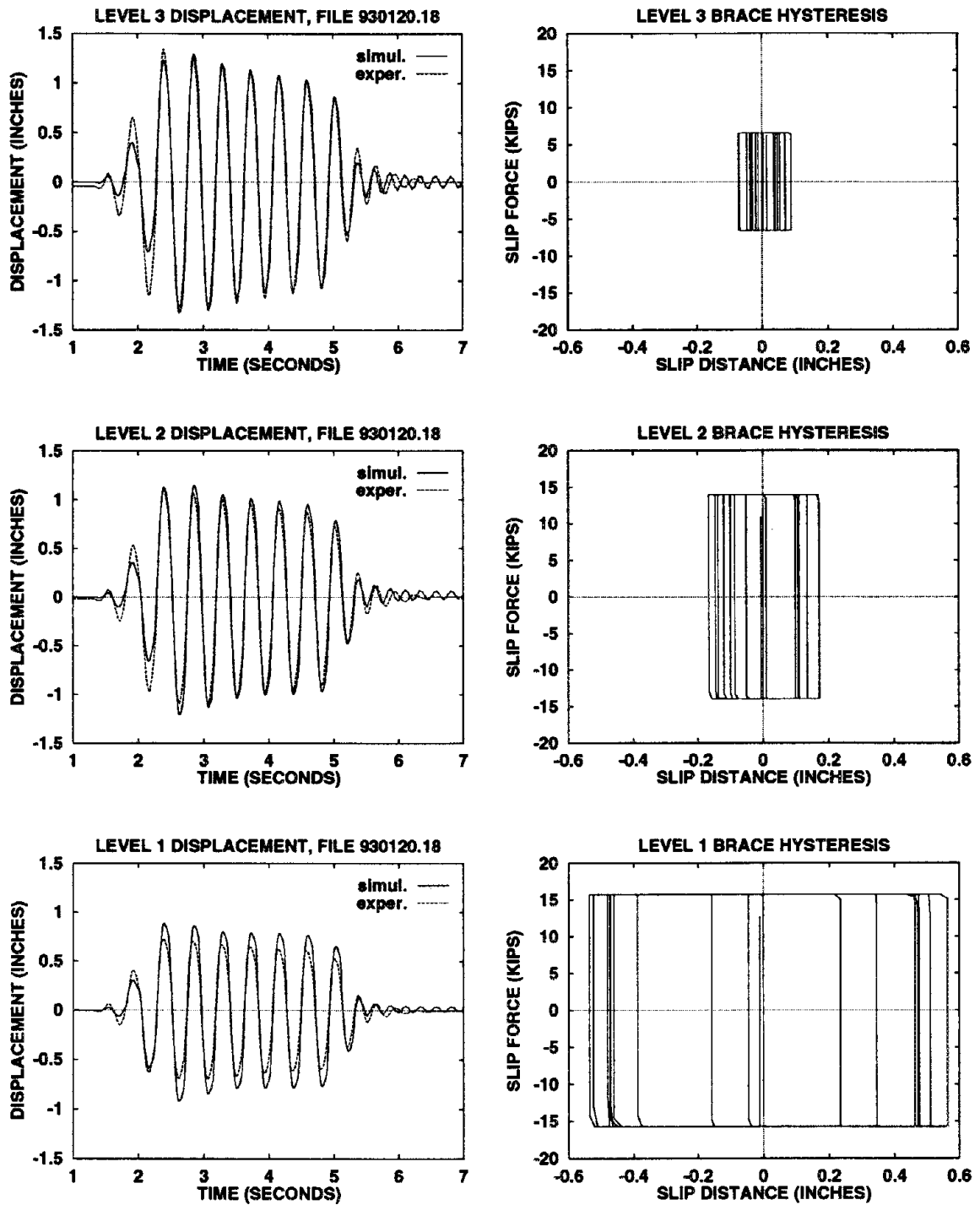
Figure 8.15: Analytical and experimental story displacements and analytical brace hystereses of TS2 due to the harmonic signal.

Chapter 9

Conclusions

9.1 Summary and Conclusions

The experimental and analytical investigation of the potential utility of SBCs for seismic energy dissipation, the major findings of which have been presented in the first eight chapters of this document, demonstrate that properly designed SBCs can be utilized in structural systems as highly effective means for energy dissipation in seismic events. The lessons learned from this investigation can be broadly divided into two categories: those dealing with the SBCs themselves and those dealing with structural systems utilizing SBCs as their primary source for energy dissipation.

Tests of a number of individual SBCs on the C/T machine have demonstrated that relatively stable hysteretic behavior can be achieved in SBCs by, primarily, providing dissimilar coupling frictional surfaces for the structural steel surfaces used. This has been achieved successfully in this study by use of very simple brass shims of half-hard cartridge variety. The use of these shims, in conjunction with de-greased clean-mill-scaled steel surfaces, with appropriate and properly tightened high-strength bolts, results in slip forces with stable characteristics.

DTI washers were found to be sufficiently good indicators for assuring proper tightening of SBC bolts. For all except for three connections tested, the manufacturer's recommended "Method 1" of using DTIs was followed. For three SBCs with $\frac{1}{2}$ inch diameter A325 bolts "Method 2" was used. It was found that these SBCs

exhibited distinctly different behavior from the rest. All connections tested, those with $\frac{1}{2}$ inch diameter bolts and those with $\frac{3}{4}$ inch diameter bolts, in which bolts were tightened by "Method 1" exhibited roughly identical behavior. Assuming that DTIs provided exactly the RCSC bolt preloads (respectively 12 and 28 kips for $\frac{1}{2}$ and $\frac{3}{4}$ inch diameter A325 bolts), initial static slip for these connections occurred at a mean slip coefficient of 0.30, then the sliding slip coefficient increased from an initial value of 0.21 to 0.31 within a cumulative travel of roughly 10 inches of the bolt. This coefficient was then maintained for up to 50 inches of cumulative travel, well beyond that demanded by most any earthquake for a code designed structure. The connections in which "Method 2" was used for tightening of the bolts, exhibited static and dynamic slip coefficients 30 to 50 % larger than the rest with a much shorter cumulative travel required to reach peak dynamic slip forces. It is believed that this difference in behavior is due to the over-conservatism inherent in "Method 2". This method appears to cause bolt preloads well beyond the specified bolt preload, possibly causing full yield of the bolts.

The connections were tested with and without Belleville washers and also with different numbers of Belleville washers. It was found that although some benefit may be gained by their use in maintaining bolt tension, and therefore the slip forces of the SBCs, in the range of cumulative bolt travel of interest, the connections in which brass shims were used were rather insensitive to the presence of the washers. However, it is thought that the use of these washers may be of some benefit in reducing loss, due to creep, of bolt tension.

Tests on the shake table of the three story chevron braced test structure equipped with twelve SBCs demonstrated that implementation of SBCs into a real structural system is feasible both in terms of practicality of physical fabrication and installation and in terms of the analytical design concepts and tools available. The components of the bracing system and SBCs were fabricated at a local steel fabrication shop and assembled into the structure by a two man team composed of the author and an experienced welder/ironworker. Only standard fabrication shop technology was used in fabrication and assembly. By adding and removing bolts to and from SBCs, it was possible to, in effect, test three different structures, data for two of which has

been presented in this document. Results for all three configurations indicate SBCs to be extremely effective in controlling story drifts and therefore controlling associated damage. It was found that behavior of the SBCs in the structure complied well with that observed of SBCs tested in the C/T machine. Slip forces in the SBCs were of the same magnitude as those of similar SBCs tested in the C/T machine.

The test structure results indicate that small deformation theory relates well the relationship between story drifts and slip distance in the braces. Moreover, results show that, given that the slip force in the two braces of the chevron are close to each other in magnitude, the braces can be designed as cantilever beams undergoing deformations calculated based on small deformation theory.

Most importantly, it is shown that the popular non-linear analysis program Drain-2DX, using an analytical model of the structure based on experimental results and modeling braces with SBCs as truss members with equal yield stresses in compression and tension, can adequately characterize the response of the test structure both quantitatively and qualitatively. This indicates that given proper two dimensional idealization of a structure, the structure may be designed with SBCs using such software.

9.2 Necessary Future Research

This document has presented a detailed picture of one working type of SBC and its unidirectional implementation into a test structure and its effects thereupon. Although the SBC with brass shims has been shown to have desired characteristics, the choice of brass as a suitable frictional surface is not necessarily the only choice providing such behavior. It is possible that a number of other shim materials may result in the suitable behavior. It is also possible that treatments of the steel surfaces, such as nitriding and carborization, may eliminate the need for a dissimilar metal shim. In addition, it may be possible to combine the two methods, i.e. use a non-steel shim against a case-hardened steel surface. These possibilities need to be explored, possibly with collaboration of Tribologists.

Although all indications point to galvanic corrosion not being a hazard to

steel-brass SBCs in non-corrosive environments, its is felt that this issue needs further investigation. If possible, test specimens should be assembled and put through environments conducive to accelerated corrosion. These specimens should then be tested in a C/T machine and results compared with those of un-corroded specimens. The use of different protective coatings should also be investigated.

It is necessary that large SBCs such as those that would be necessary in the retrofit of large industrial structures be tested not only in the C/T machine, but also integrally in conjunction with the braces and frame which they connect. It is felt that this is particularly important for the case of chevron bracing, in which imbalances in the slip forces of the braces cause vertical forces to act upon the beams of the frames at the points of intersection of braces. A mild form of this phenomenon was observed to occur in the test structure.

This study has shown that the design of structures with SBCs is possible, given appropriate idealizations, with non-linear dynamic analysis software through a process of trial and error. However, there is reason to believe that computationally non-intensive methods for preliminary design of structures may be possible to derive. Development of such methods would make the option of using SBCs available to a broader sector of the profession. It is necessary that investigations aimed at developing such design methods be pursued.

Another topic that needs further exploration and that may play a fundamental role in the propagation of and acceptance by industry of the use SBCs is the subject of the method of providing the necessary normal forces to the sliding surfaces of the SBCs. A large number of SBCs utilizing DTIs, applied by "Method 1", have been shown to have excellent behavior. Three SBCs with bolts tightened with DTIs and using "Method 2" have also been tested and shown to have possibly superior performance to those tightened by "Method 1". An experimental investigation of characteristics of SBCs tightened with DTIs using "Method 2" would greatly increase the versatility of SBCs, in particular as in some situations the use of "Method 1" is rather difficult. Furthermore, there are now available a number of alternative fasteners that may be used in place of conventional high-strength nuts and bolts. In particular, the use of lock pin and collar or blind bolts of structural grade may prove

to be of great advantage both in terms of speed of assembly and in terms of the reliability afforded by the installation method for these fasteners.

Lastly, and perhaps most importantly, both experimental and analytical studies need be undertaken in the 3-dimensional design of structures with SBCs. Although, it is tempting to follow the traditional method of designing 3-dimensional structures by idealizing them into two 2-dimensional structures, it may be the case that in some structures with braces with SBCs not in a line going through the center of stiffness of the structure at a given floor, large torsional forces may be generated. These force may be the result of an inappropriate choice of design slip forces or be due to accidentally large or small slip forces resulting from careless assembly. Although of small magnitude, such torsional forces were observed to be present in the test structure. These torsional forces must be resisted in part by the lateral force resisting system orthogonal to the said SBCs. If this lateral system also includes SBCs and these are under-designed, undesirable displacements could follow. Given that non-linear analysis programs for dynamic analysis of 3-dimensional structures are available, such problems can be analyzed purely analytically at first, and the conclusions then verified by shake table or pseudo-dynamic tests. It is felt that although common engineering sense may be adequate to handle the consideration of torsional forces induced by SBCs for simple low-rise structural systems, for more complicated and high-rise structures this subject needs to be further studied.

9.3 Impact on Industry

As of the time of the writing of this document, two San Francisco Bay area engineering firms have expressed interest in using SBCs in retrofit projects. In the case of one of these, the decision has been finalized to go ahead with the retrofit, with 64 SBCs, of a large steel structure with existing chevron bracing rather similar to those of the test structure. Moreover, there is strong indication that, at the suggestion of the author and the P.I., this firm is willing to test, in the C/T machine, a full-sized SBC identical to those to be implemented in the field as a means of verification. Such strong interest expressed by professionals in the industry, manifested at so short a

time after the completion of the project, is due mainly to the attractiveness of SBCs as an inexpensive, inherently simple and technologically readily available option for energy dissipation.

It is foreseen that, with continued research on the subject of SBCs, the use of SBCs in retrofit of existing structures and the design of new structures may become an option competitive with proprietary marketed energy dissipation devices currently available. Once accepted by industry as a viable design option, the use of these connections may simultaneously significantly contribute to the safety of structures while at the same time reduce the general cost of construction.

Bibliography

[1] I. D. Aiken, J. M. Kelley, and A. S. Pall. Seismic response of a nine story frame with damped cross bracing. In *Proceedings of Ninth World Conference on Earthquake Engineering*, Tokyo-Kyoto, Japan, August 1988.

[2] I. D. Aiken and J. M. Kelly. Earthquake simulator testing and analytical studies of two energy-absorbing systems for multistory structures. *Report no. UCB/EERC-90/03*, Earthquake Engineering Research Center, University of California, Berkeley, October 1990.

[3] H. Akiyama. *Earthquake-Resistant Limit-State Design for Buildings*. University of Tokyo Press, 1985.

[4] R. Allahabadi and G. H. Powell. Drain-2dx users guide. *Report no. EERC-88/06*, Earthquake Engineering Research Center, University of California, Berkeley, March 1988.

[5] J. O. Almen and A. Laszlo. The uniform-section disk spring. *Transactions of the American Society of Mechanical Engineers*, 58, 1936.

[6] American Institute of Steel Construction, Chicago, Illinois. *Allowable Stress Design (ASD), Manual of Steel Construction*, 1989.

[7] P. J. Blau. *Friction and Wear Transitions of Materials*. Noyes Publications, 1989.

[8] R. W. Clough and D. T. Tang. Earthquake simulator study of a steel frame structure, vol. i: Analytical results. *Report no. EERC-75/6*, Earthquake Engineering Research Center, University of California, Berkeley, April 1975.

[9] T. F. Fitzgerald, T. A. Anagnos, M. Goodson, and T. Zsutty. Slotted bolted connections in aseismic design for concentrically braced connections. *Earthquake Spectra*, 5(2), 1989.

[10] C. E. Grigorian and E. P. Popov. Slotted bolted connections for energy dissipation. In *Proceedings of Seminar on Seismic Isolation, Passive Energy Dissipation, and Active Control*, San Francisco, California, March 1993.

[11] C. E. Grigorian, T. S. Yang, and E. P. Popov. Slotted bolted connection energy dissipators. *Report no. UCB/EERC-92/10*, Earthquake Engineering Research Center, University of California, Berkeley, October 1992.

[12] Intenational Conference of Building Officicals, Whittier, California. *Uniform Building Code*, 1988.

[13] G. L. Kulak, J. W. Fisher, and J. H. A. Struik. *Guide to Design Criteria for Bolted and Riveted Joints*. John Wiley and Sons, second edition, 1987.

[14] A. S. Pall and C. Marsh. Energy dissipation in panelized buildings using limited slip bolted joints. In *Proceedings of AICAP-CEB Conference*, Rome, Italy, May 1979.

[15] A. S Pall and C. Marsh. Response of friction damped braced frames. *Journal of the Structural Division of ASCE*, 108(ST6), 1982.

[16] A. S. Pall, C. Marsh, and P. Fazio. Friction joints for seismic control of large panel structures. *Journal of the Prestressed Concrete Institute*, 25(6), 1980.

[17] E. P. Popov, T. S. Yang, and C. E. Grigorian. New directions in structural seismic designs. *Earthquake Spectra*, 9(4), 1993.

[18] E. Rabinowicz. *Friction and Wear of Materials*. John Wiley and Sons, Inc., 1965.

[19] E. Rabinowicz. Wear coefficients - metals. In M. B. Peterson and W. O. Winer, editors, *Wear Control Handbook*. American Society of Mechanical Engineers, 1980.

[20] D. Rea and J. Penzien. Dynamic response of 20ft by 20ft shaking table. In *Proceedings of Fifth World Conference on Earthquake Engineering*, Rome, Italy, 1974.

[21] A. M. Rinawi and R. W. Clough. Shaking table - structure interaction. *Report no. EERC-91/13*, Earthquake Engineering Research Center, University of California, Berkeley, October 1991.

[22] K. Roik, U. Dorka, and P. Dechent. Vibration control of structures under earthquake loading by three-stage friction-grip elements. *Earthquake Engineering and Structural Dynamics*, 16, 1988.

[23] D. T. Tang. Earthquake simulator study of a steel frame structure, vol. ii: Analytical results. *Report no. EERC-75/36*, Earthquake Engineering Research Center, University of California, Berkeley, October 1975.

[24] D. T. Tang and R. W. Clough. Shake table tests of a steel frame - a progress report. *Report no. EERC-74/8*, Earthquake Engineering Research Center, University of California, Berkeley, July 1974.

[25] R. Tremblay and S. F. Steimer. Energy dissipation through friction bolted connections in concentrically braced frames. In *Proceedings of Seminar on Seismic Isolation, Passive Energy Dissipation, and Active Control*, San Francisco, California, March 1993.

[26] C. M. Uang. On esatablishing R (or R_w) and C_d factors for building seismic provisions. *Journal of the Structural Division of ASCE*, 117(1), 1991.

[27] C. M. Uang and V. V. Bertero. Implications of recorded earthquake ground motions on seismic building structures. *Report no. UCB/EERC-88/13*, Earthquake Engineering Research Center, University of California, Berkeley, November 1988.

[28] C. M. Uang and V. V. Bertero. Use of energy as a design criterion in earthquake-resistant design. *Report no. UCB/EERC-88/18*, Earthquake Engineering Research Center, University of California, Berkeley, November 1988.

[29] C. M. Uang, A. Whittaker, and V. V. Bertero. Earthquake simulation tests and associated studies of a 0.3 scale model of a six-story concentrically braced steel structure. *Report no. UCB/EERC-86/10*, Earthquake Engineering Research Center, University of California, Berkeley, December 1986.

[30] W. J. Venuti. Energy absorbtion of high strength bolted connections. Test report for the Structural Steel Educational Council, Department of Civil Engineering, San Jose State University, San Jose, California, May 1976.

[31] A. Whittaker, V. V. Bertero, J. Alonso, and C. Thompson. Earthquake simulator testing of steel plate added damping and stiffness elements. *Report no. UCB/EERC-89/02*, Earthquake Engineering Research Center, University of California, Berkeley, January 1989.

[32] A. Whittaker, C. M. Uang, and V. V. Bertero. Earthquake simulation tests and associated studies of a 0.3 scale model of a six-story eccentrically braced steel structure. *Report no. UCB/EERC-87/02*, Earthquake Engineering Research Center, University of California, Berkeley, July 1987.

[33] T. S. Yang. DANS, A computer program for the dynamic analysis of nonlinear shear buildings. *CE 299 Project*, University of California, Berkeley, 1991.

Appendix A

Abbreviations and Nomenclature

Although the body of this document defines the abbreviation used and describes the conventions on which its nomenclature is based, this appendix is provided for ease of reference.

Abbreviations

The following list gives the definitions of the common abbreviations encountered in the text.

SBC - Slotted Bolted Connection
RPP - Rigid-perfectly-plastic
SDOF - Single degree of freedom
LEPP - Linearly-elastic-perfectly-plastic
AISC - American Institute of Steel Construction
ASD - Allowable Stress Design
UBC - Uniform Building Code
NYR - Number of yield returns
SJSU - San Jose State University
UCB - University of California at Berkeley
EERC - Earthquake Engineering Research Center
DTI - Direct Tension Indicator

RCSC - Research Council on Structural Connections

C/T - Compression/Tension (testing machine)

LVDT - Linearly variable displacement transducer

ADAS - Added damping and stiffness (device)

Nomenclature

Conventions for the nomenclature relating to individual SBC test specimens, such as 2B1WBR2, 2A3WBR1, etc., are given on page 25 (Chapter 2).

Three configuration of the test structure, tested on the shake table, are named TS1, TS2 and TS3. These are described on page 94 (Chapter 5).

Conventions relating to the file numbers of individual shake table tests, such as 930119.14, 930120.05, etc., are given on page 98 (Chapter 5).

Appendix B

Sample Drain-2DX Input File

Below is the input file for Drain-2DX version 0.01 for the simulation of test 930120.05, i.e. TS1 response to the Pacoima signal.

```
DAC           new    0              D7 CARM
    23    23    0     3      3    2     2    1
     1     0        0.0    208.0
     2     1       36.0      0.0
     3     2       36.0      0.0
     4     3       36.0      0.0
     5     4       36.0      0.0
     6     0        0.0    144.0
     7     6       36.0      0.0
     8     7       36.0      0.0
     9     8       36.0      0.0
    10     9       36.0      0.0
    11     0        0.0     80.0
    12    11       36.0      0.0
    13    12       36.0      0.0
    14    13       36.0      0.0
    15    14       36.0      0.0
    16     0        0.0      0.0
```

17	16	144.0	0.0		
18	16	0.0	-10.0		
19	17	0.0	-10.0		
20	5	10.0	0.0		
21	10	10.0	0.0		
22	15	10.0	0.0		
23	16	72.0	0.0		
23	1	1	0	23	
18	1	1	0	19	
20	0	1	0	22	
1	5	1	2	3	4	5
1	5	6	7	8	9	10
1	5	11	12	13	14	15

20	16.0	16.0	0.0	22	1	386.0	1.0
16	23.3	23.3	0.0	17	1	386.0	0.0

1	11	1	0	.0000	TRUSS EL.(SBC)
7					

1	2.9e4	2.02	7.680	7.680	0
2	2.9e4	2.02	4.170	4.170	0
3	2.9e4	2.02	3.640	3.640	0
4	2.9e3	3.77	1.0e9	1.0e9	0
5	2.9e3	.193	1.0e9	1.0e9	0
6	2.9e3	.193	1.0e9	1.0e9	0
7	2.9e3	.193	1.0e9	1.0e9	0

1	16	13	1	1
2	17	13	1	1
3	11	8	1	2
4	15	8	1	2
5	6	3	1	3
6	10	3	1	3
7	18	16	1	4

```
 8   19   17    1    4
 9    5   20    1    5
10   10   21    1    6
11   15   22    1    7
 2   20    0    0 .0000      BEAM-COLUMN EL.
 3    6    3
 1      2.9e4       0.02       3.61       22.2  4.0  4.0  2.0
 2      2.9e4       0.02       4.70       21.0  4.0  4.0  2.0
 3      2.9e4       0.02       1000       1000  4.0  4.0  2.0
 1        7.5        0.0        0.0        0.0
 2        0.0       -7.5        0.0        0.0
 3        0.0        0.0        3.0       -7.5
 4        0.0        0.0        3.0       -5.0
 5        2.5        0.0        0.0        0.0
 6        0.0       -2.5        0.0        0.0
 1    1      1.0e9      1.0e9
 2    1      1.0e9      1.0e9
 3    1      1.0e9      1.0e9
 1    1    2    1    1    5    2    2
 2    2    3    1    1    0    2    2
 3    3    4    1    1    0    2    2
 4    4    5    1    1    6    2    2
 5    6    7    1    1    1    2    2
 6    7    8    1    1    0    2    2
 7    8    9    1    1    0    2    2
 8    9   10    1    1    2    2    2
 9   11   12    1    1    1    2    2
10   12   13    1    1    0    2    2
11   13   14    1    1    0    2    2
12   14   15    1    1    2    2    2
13    1    6    5    2    3    1    1
```

```
14    5   10    5    2    3    1    1
15    6   11    5    2    3    1    1
16   10   15    5    2    3    1    1
17   11   16    5    2    4    1    1
18   15   17    2    2    4    1    1
19   16   23    0    3    0    3    3
20   17   23    0    3    0    3    3
 0
 0
 0    0    0    0    0    0
 3    0    0    0    0    3
 5   10   15
 1    1    3    5
 0    0    1
FILE  3601 930120.05
      .005        1.0  386.0        1
      0.0    1  (F13.10)                    120.05av
eign     0MODE SHAPE AND PERIOD ANALYSIS
    3     0.001
accn     0 WITH EVENT CALCULATION
    0       0.0    0       0.0    1      0.0    0       0.0
    0    1   10    1    1    0.005 25000      25.0
FILE      1.00
stop
```

EARTHQUAKE ENGINEERING RESEARCH CENTER REPORT SERIES

EERC reports are available from the National Information Service for Earthquake Engineering (NISEE) and from the National Technical Information Service (NTIS). Numbers in parentheses are Accession Numbers assigned by the National Technical Information Service; these are followed by a price code. Contact NTIS, 5285 Port Royal Road, Springfield Virginia, 22161 for more information. Reports without Accession Numbers were not available from NTIS at the time of printing. For a current complete list of EERC reports (from EERC 67-1) and availablity information, please contact University of California, EERC, NISEE, 1301 South 46th Street, Richmond, California 94804.

UCB/EERC-84/01　"Pseudodynamic Test Method for Seismic Performance Evaluation: Theory and Implementation," by Shing, P.-S.B. and Mahin, S.A., January 1984, (PB84 190 644)A08.

UCB/EERC-84/02　"Dynamic Response Behavior of Kiang Hong Dian Dam," by Clough, R.W., Chang, K.-T., Chen, H.-Q. and Stephen, R.M., April 1984, (PB84 209 402)A08.

UCB/EERC-84/03　"Refined Modelling of Reinforced Concrete Columns for Seismic Analysis," by Kaba, S.A. and Mahin, S.A., April 1984, (PB84 234 384)A06.

UCB/EERC-84/04　"A New Floor Response Spectrum Method for Seismic Analysis of Multiply Supported Secondary Systems," by Asfura, A. and Der Kiureghian, A., June 1984, (PB84 239 417)A06.

UCB/EERC-84/05　"Earthquake Simulation Tests and Associated Studies of a 1/5th-scale Model of a 7-Story R/C Frame-Wall Test Structure," by Bertero, V.V., Aktan, A.E., Charney, F.A. and Sause, R., June 1984, (PB84 239 409)A09.

UCB/EERC-84/06　"Unassigned," by Unassigned, 1984.

UCB/EERC-84/07　"Behavior of Interior and Exterior Flat-Plate Connections Subjected to Inelastic Load Reversals," by Zee, H.L. and Moehle, J.P., August 1984, (PB86 117 629/AS)A07.

UCB/EERC-84/08　"Experimental Study of the Seismic Behavior of a Two-Story Flat-Plate Structure," by Moehle, J.P. and Diebold, J.W., August 1984, (PB86 122 553/AS)A12.

UCB/EERC-84/09　"Phenomenological Modeling of Steel Braces under Cyclic Loading," by Ikeda, K., Mahin, S.A. and Dermitzakis, S.N., May 1984, (PB86 132 198/AS)A08.

UCB/EERC-84/10　"Earthquake Analysis and Response of Concrete Gravity Dams," by Fenves, G.L. and Chopra, A.K., August 1984, (PB85 193 902/AS)A11.

UCB/EERC-84/11　"EAGD-84: A Computer Program for Earthquake Analysis of Concrete Gravity Dams," by Fenves, G.L. and Chopra, A.K., August 1984, (PB85 193 613/AS)A05.

UCB/EERC-84/12　"A Refined Physical Theory Model for Predicting the Seismic Behavior of Braced Steel Frames," by Ikeda, K. and Mahin, S.A., July 1984, (PB85 191 450/AS)A09.

UCB/EERC-84/13　"Earthquake Engineering Research at Berkeley - 1984," by EERC, August 1984, (PB85 197 341/AS)A10.

UCB/EERC-84/14　"Moduli and Damping Factors for Dynamic Analyses of Cohesionless Soils," by Seed, H.B., Wong, R.T., Idriss, I.M. and Tokimatsu, K., September 1984, (PB85 191 468/AS)A04.

UCB/EERC-84/15　"The Influence of SPT Procedures in Soil Liquefaction Resistance Evaluations," by Seed, H.B., Tokimatsu, K., Harder, L.F. and Chung, R.M., October 1984, (PB85 191 732/AS)A04.

UCB/EERC-84/16　"Simplified Procedures for the Evaluation of Settlements in Sands Due to Earthquake Shaking," by Tokimatsu, K. and Seed, H.B., October 1984, (PB85 197 887/AS)A03.

UCB/EERC-84/17　"Evaluation of Energy Absorption Characteristics of Highway Bridges Under Seismic Conditions - Volume 1 (PB90 262 627)A16 and Volume II (Appendices) (PB90 262 635)A13," by Imbsen, R.A. and Penzien, J., September 1986.

UCB/EERC-84/18　"Structure-Foundation Interactions under Dynamic Loads," by Liu, W.D. and Penzien, J., November 1984, (PB87 124 889/AS)A11.

UCB/EERC-84/19　"Seismic Modelling of Deep Foundations," by Chen, C.-H. and Penzien, J., November 1984, (PB87 124 798/AS)A07.

UCB/EERC-84/20　"Dynamic Response Behavior of Quan Shui Dam," by Clough, R.W., Chang, K.-T., Chen, H.-Q., Stephen, R.M., Ghanaat, Y. and Qi, J.-H., November 1984, (PB86 115177/AS)A07.

UCB/EERC-85/01　"Simplified Methods of Analysis for Earthquake Resistant Design of Buildings," by Cruz, E.F. and Chopra, A.K., February 1985, (PB86 112299/AS)A12.

UCB/EERC-85/02　"Estimation of Seismic Wave Coherency and Rupture Velocity using the SMART 1 Strong-Motion Array Recordings," by Abrahamson, N.A., March 1985, (PB86 214 343)A07.

UCB/EERC-85/03　"Dynamic Properties of a Thirty Story Condominium Tower Building," by Stephen, R.M., Wilson, E.L. and Stander, N., April 1985, (PB86 118965/AS)A06.

UCB/EERC-85/04　"Development of Substructuring Techniques for On-Line Computer Controlled Seismic Performance Testing," by Dermitzakis, S. and Mahin, S., February 1985, (PB86 132941/AS)A08.

UCB/EERC-85/05　"A Simple Model for Reinforcing Bar Anchorages under Cyclic Excitations," by Filippou, F.C., March 1985, (PB86 112 919/AS)A05.

UCB/EERC-85/06　"Racking Behavior of Wood-framed Gypsum Panels under Dynamic Load," by Oliva, M.G., June 1985, (PB90 262 643)A04.

UCB/EERC-85/07   "Earthquake Analysis and Response of Concrete Arch Dams," by Fok, K.-L. and Chopra, A.K., June 1985, (PB86 139672/AS)A10.

UCB/EERC-85/08   "Effect of Inelastic Behavior on the Analysis and Design of Earthquake Resistant Structures," by Lin, J.P. and Mahin, S.A., June 1985, (PB86 135340/AS)A08.

UCB/EERC-85/09   "Earthquake Simulator Testing of a Base-Isolated Bridge Deck," by Kelly, J.M., Buckle, I.G. and Tsai, H.-C., January 1986, (PB87 124 152/AS)A06.

UCB/EERC-85/10   "Simplified Analysis for Earthquake Resistant Design of Concrete Gravity Dams," by Fenves, G.L. and Chopra, A.K., June 1986, (PB87 124 160/AS)A08.

UCB/EERC-85/11   "Dynamic Interaction Effects in Arch Dams," by Clough, R.W., Chang, K.-T., Chen, H.-Q. and Ghanaat, Y., October 1985, (PB86 135027/AS)A05.

UCB/EERC-85/12   "Dynamic Response of Long Valley Dam in the Mammoth Lake Earthquake Series of May 25-27, 1980," by Lai, S. and Seed, H.B., November 1985, (PB86 142304/AS)A05.

UCB/EERC-85/13   "A Methodology for Computer-Aided Design of Earthquake-Resistant Steel Structures," by Austin, M.A., Pister, K.S. and Mahin, S.A., December 1985, (PB86 159480/AS)A10 .

UCB/EERC-85/14   "Response of Tension-Leg Platforms to Vertical Seismic Excitations," by Liou, G.-S., Penzien, J. and Yeung, R.W., December 1985, (PB87 124 871/AS)A08.

UCB/EERC-85/15   "Cyclic Loading Tests of Masonry Single Piers: Volume 4 - Additional Tests with Height to Width Ratio of 1," by Sveinsson, B., McNiven, H.D. and Sucuoglu, H., December 1985, (PB87 165031/AS)A08.

UCB/EERC-85/16   "An Experimental Program for Studying the Dynamic Response of a Steel Frame with a Variety of Infill Partitions," by Yanev, B. and McNiven, H.D., December 1985, (PB90 262 676)A05.

UCB/EERC-86/01   "A Study of Seismically Resistant Eccentrically Braced Steel Frame Systems," by Kasai, K. and Popov, E.P., January 1986, (PB87 124 178/AS)A14.

UCB/EERC-86/02   "Design Problems in Soil Liquefaction," by Seed, H.B., February 1986, (PB87 124 186/AS)A03.

UCB/EERC-86/03   "Implications of Recent Earthquakes and Research on Earthquake-Resistant Design and Construction of Buildings," by Bertero, V.V., March 1986, (PB87 124 194/AS)A05.

UCB/EERC-86/04   "The Use of Load Dependent Vectors for Dynamic and Earthquake Analyses," by Leger, P., Wilson, E.L. and Clough, R.W., March 1986, (PB87 124 202/AS)A12.

UCB/EERC-86/05   "Two Beam-To-Column Web Connections," by Tsai, K.-C. and Popov, E.P., April 1986, (PB87 124 301/AS)A04.

UCB/EERC-86/06   "Determination of Penetration Resistance for Coarse-Grained Soils using the Becker Hammer Drill," by Harder, L.F. and Seed, H.B., May 1986, (PB87 124 210/AS)A07.

UCB/EERC-86/07   "A Mathematical Model for Predicting the Nonlinear Response of Unreinforced Masonry Walls to In-Plane Earthquake Excitations," by Mengi, Y. and McNiven, H.D., May 1986, (PB87 124 780/AS)A06.

UCB/EERC-86/09   "EACD-3D: A Computer Program for Three-Dimensional Earthquake Analysis of Concrete Dams," by Fok, K.-L., Hall, J.F. and Chopra, A.K., July 1986, (PB87 124 228/AS)A08.

UCB/EERC-86/10   "Earthquake Simulation Tests and Associated Studies of a 0.3-Scale Model of a Six-Story Concentrically Braced Steel Structure," by Uang, C.-M. and Bertero, V.V., December 1986, (PB87 163 564/AS)A17.

UCB/EERC-86/11   "Mechanical Characteristics of Base Isolation Bearings for a Bridge Deck Model Test," by Kelly, J.M., Buckle, I.G. and Koh, C.-G., November 1987, (PB90 262 668)A04.

UCB/EERC-86/12   "Effects of Axial Load on Elastomeric Isolation Bearings," by Koh, C.-G. and Kelly, J.M., November 1987.

UCB/EERC-87/01   "The FPS Earthquake Resisting System: Experimental Report," by Zayas, V.A., Low, S.S. and Mahin, S.A., June 1987, (PB88 170 287)A06.

UCB/EERC-87/02   "Earthquake Simulator Tests and Associated Studies of a 0.3-Scale Model of a Six-Story Eccentrically Braced Steel Structure," by Whittaker, A., Uang, C.-M. and Bertero, V.V., July 1987, (PB88 166 707/AS)A18.

UCB/EERC-87/03   "A Displacement Control and Uplift Restraint Device for Base-Isolated Structures," by Kelly, J.M., Griffith, M.C. and Aiken, I.D., April 1987, (PB88 169 933)A04.

UCB/EERC-87/04   "Earthquake Simulator Testing of a Combined Sliding Bearing and Rubber Bearing Isolation System," by Kelly, J.M. and Chalhoub, M.S., December 1990.

UCB/EERC-87/05   "Three-Dimensional Inelastic Analysis of Reinforced Concrete Frame-Wall Structures," by Moazzami, S. and Bertero, V.V., May 1987, (PB88 169 586/AS)A08.

UCB/EERC-87/06   "Experiments on Eccentrically Braced Frames with Composite Floors," by Ricles, J. and Popov, E., June 1987, (PB88 173 067/AS)A14.

UCB/EERC-87/07   "Dynamic Analysis of Seismically Resistant Eccentrically Braced Frames," by Ricles, J. and Popov, E., June 1987, (PB88 173 075/AS)A16.

UCB/EERC-87/08   "Undrained Cyclic Triaxial Testing of Gravels-The Effect of Membrane Compliance," by Evans, M.D. and Seed, H.B., July 1987, (PB88 173 257)A19.

UCB/EERC-87/09   "Hybrid Solution Techniques for Generalized Pseudo-Dynamic Testing," by Thewalt, C. and Mahin, S.A., July 1987, (PB 88 179 007)A07.

UCB/EERC-87/10   "Ultimate Behavior of Butt Welded Splices in Heavy Rolled Steel Sections," by Bruneau, M., Mahin, S.A. and Popov, E.P., September 1987, (PB90 254 285)A07.

UCB/EERC-87/11   "Residual Strength of Sand from Dam Failures in the Chilean Earthquake of March 3, 1985," by De Alba, P., Seed, H.B., Retamal, E. and Seed, R.B., September 1987, (PB88 174 321/AS)A03.

UCB/EERC-87/12   "Inelastic Seismic Response of Structures with Mass or Stiffness Eccentricities in Plan," by Bruneau, M. and Mahin, S.A., September 1987, (PB90 262 650/AS)A14.

UCB/EERC-87/13   "CSTRUCT: An Interactive Computer Environment for the Design and Analysis of Earthquake Resistant Steel Structures," by Austin, M.A., Mahin, S.A. and Pister, K.S., September 1987, (PB88 173 339/AS)A06.

UCB/EERC-87/14   "Experimental Study of Reinforced Concrete Columns Subjected to Multi-Axial Loading," by Low, S.S. and Moehle, J.P., September 1987, (PB88 174 347/AS)A07.

UCB/EERC-87/15   "Relationships between Soil Conditions and Earthquake Ground Motions in Mexico City in the Earthquake of Sept. 19, 1985," by Seed, H.B., Romo, M.P., Sun, J., Jaime, A. and Lysmer, J., October 1987, (PB88 178 991)A06.

UCB/EERC-87/16   "Experimental Study of Seismic Response of R. C. Setback Buildings," by Shahrooz, B.M. and Moehle, J.P., October 1987, (PB88 176 359)A16.

UCB/EERC-87/17   "The Effect of Slabs on the Flexural Behavior of Beams," by Pantazopoulou, S.J. and Moehle, J.P., October 1987, (PB90 262 700)A07.

UCB/EERC-87/18   "Design Procedure for R-FBI Bearings," by Mostaghel, N. and Kelly, J.M., November 1987, (PB90 262 718)A04.

UCB/EERC-87/19   "Analytical Models for Predicting the Lateral Response of R C Shear Walls: Evaluation of their Reliability," by Vulcano, A. and Bertero, V.V., November 1987, (PB88 178 983)A05.

UCB/EERC-87/20   "Earthquake Response of Torsionally-Coupled Buildings," by Hejal, R. and Chopra, A.K., December 1987.

UCB/EERC-87/21   "Dynamic Reservoir Interaction with Monticello Dam," by Clough, R.W., Ghanaat, Y. and Qiu, X-F., December 1987, (PB88 179 023)A07.

UCB/EERC-87/22   "Strength Evaluation of Coarse-Grained Soils," by Siddiqi, F.H., Seed, R.B., Chan, C.K., Seed, H.B. and Pyke, R.M., December 1987, (PB88 179 031)A04.

UCB/EERC-88/01   "Seismic Behavior of Concentrically Braced Steel Frames," by Khatib, I., Mahin, S.A. and Pister, K.S., January 1988, (PB91 210 898/AS)A11.

UCB/EERC-88/02   "Experimental Evaluation of Seismic Isolation of Medium-Rise Structures Subject to Uplift," by Griffith, M.C., Kelly, J.M., Coveney, V.A. and Koh, C.G., January 1988, (PB91 217 950/AS)A09.

UCB/EERC-88/03   "Cyclic Behavior of Steel Double Angle Connections," by Astaneh-Asl, A. and Nader, M.N., January 1988, (PB91 210 872)A05.

UCB/EERC-88/04   "Re-evaluation of the Slide in the Lower San Fernando Dam in the Earthquake of Feb. 9, 1971," by Seed, H.B., Seed, R.B., Harder, L.F. and Jong, H.-L., April 1988, (PB91 212 456/AS)A07.

UCB/EERC-88/05   "Experimental Evaluation of Seismic Isolation of a Nine-Story Braced Steel Frame Subject to Uplift," by Griffith, M.C., Kelly, J.M. and Aiken, I.D., May 1988, (PB91 217 968/AS)A07.

UCB/EERC-88/06   "DRAIN-2DX User Guide.," by Allahabadi, R. and Powell, G.H., March 1988, (PB91 212 530)A12.

UCB/EERC-88/07   "Theoretical and Experimental Studies of Cylindrical Water Tanks in Base-Isolated Structures," by Chalhoub, M.S. and Kelly, J.M., April 1988, (PB91 217 976/AS)A05.

UCB/EERC-88/08   "Analysis of Near-Source Waves: Separation of Wave Types Using Strong Motion Array Recording," by Darragh, R.B., June 1988, (PB91 212 621)A08.

UCB/EERC-88/09   "Alternatives to Standard Mode Superposition for Analysis of Non-Classically Damped Systems," by Kusainov, A.A. and Clough, R.W., June 1988, (PB91 217 992/AS)A04.

UCB/EERC-88/10   "The Landslide at the Port of Nice on October 16, 1979," by Seed, H.B., Seed, R.B., Schlosser, F., Blondeau, F. and Juran, I., June 1988, (PB91 210 914)A05.

UCB/EERC-88/11   "Liquefaction Potential of Sand Deposits Under Low Levels of Excitation," by Carter, D.P. and Seed, H.B., August 1988, (PB91 210 880)A15.

UCB/EERC-88/12   "Nonlinear Analysis of Reinforced Concrete Frames Under Cyclic Load Reversals," by Filippou, F.C. and Issa, A., September 1988, (PB91 212 589)A07.

UCB/EERC-88/13   "Implications of Recorded Earthquake Ground Motions on Seismic Design of Building Structures," by Uang, C.-M. and Bertero, V.V., November 1988, (PB91 212 548)A06.

UCB/EERC-88/14   "An Experimental Study of the Behavior of Dual Steel Systems," by Whittaker, A.S. , Uang, C.-M. and Bertero, V.V., September 1988, (PB91 212 712)A16.

UCB/EERC-88/15   "Dynamic Moduli and Damping Ratios for Cohesive Soils," by Sun, J.I., Golesorkhi, R. and Seed, H.B., August 1988, (PB91 210 922)A04.

UCB/EERC-88/16   "Reinforced Concrete Flat Plates Under Lateral Load: An Experimental Study Including Biaxial Effects," by Pan, A. and Moehle, J.P., October 1988, (PB91 210 856)A13.

UCB/EERC-88/17   "Earthquake Engineering Research at Berkeley - 1988," by EERC, November 1988, (PB91 210 864)A10.

UCB/EERC-88/18   "Use of Energy as a Design Criterion in Earthquake-Resistant Design," by Uang, C.-M. and Bertero, V.V., November 1988, (PB91 210 906/AS)A04.

UCB/EERC-88/19   "Steel Beam-Column Joints in Seismic Moment Resisting Frames," by Tsai, K.-C. and Popov, E.P., November 1988, (PB91 217 984/AS)A20.

UCB/EERC-88/20   "Base Isolation in Japan, 1988," by Kelly, J.M., December 1988, (PB91 212 449)A05.

UCB/EERC-89/01   "Behavior of Long Links in Eccentrically Braced Frames," by Engelhardt, M.D. and Popov, E.P., January 1989, (PB92 143 056)A18.

UCB/EERC-89/02   "Earthquake Simulator Testing of Steel Plate Added Damping and Stiffness Elements," by Whittaker, A., Bertero, V.V., Alonso, J. and Thompson, C., January 1989, (PB91 229 252/AS)A10.

UCB/EERC-89/03   "Implications of Site Effects in the Mexico City Earthquake of Sept. 19, 1985 for Earthquake-Resistant Design Criteria in the San Francisco Bay Area of California," by Seed, H.B. and Sun, J.I., March 1989, (PB91 229 369/AS)A07.

UCB/EERC-89/04   "Earthquake Analysis and Response of Intake-Outlet Towers," by Goyal, A. and Chopra, A.K., July 1989, (PB91 229 286/AS)A19.

UCB/EERC-89/05   "The 1985 Chile Earthquake: An Evaluation of Structural Requirements for Bearing Wall Buildings," by Wallace, J.W. and Moehle, J.P., July 1989, (PB91 218 008/AS)A13.

UCB/EERC-89/06   "Effects of Spatial Variation of Ground Motions on Large Multiply-Supported Structures," by Hao, H., July 1989, (PB91 229 161/AS)A08.

UCB/EERC-89/07   "EADAP - Enhanced Arch Dam Analysis Program: Users's Manual," by Ghanaat, Y. and Clough, R.W., August 1989, (PB91 212 522)A06.

UCB/EERC-89/08   "Seismic Performance of Steel Moment Frames Plastically Designed by Least Squares Stress Fields," by Ohi, K. and Mahin, S.A., August 1989, (PB91 212 597)A05.

UCB/EERC-89/09   "Feasibility and Performance Studies on Improving the Earthquake Resistance of New and Existing Buildings Using the Friction Pendulum System," by Zayas, V., Low, S., Mahin, S.A. and Bozzo, L., July 1989, (PB92 143 064)A14.

UCB/EERC-89/10   "Measurement and Elimination of Membrane Compliance Effects in Undrained Triaxial Testing," by Nicholson, P.G., Seed, R.B. and Anwar, H., September 1989, (PB92 139 641/AS)A13.

UCB/EERC-89/11   "Static Tilt Behavior of Unanchored Cylindrical Tanks," by Lau, D.T. and Clough, R.W., September 1989, (PB92 143 049)A10.

UCB/EERC-89/12   "ADAP-88: A Computer Program for Nonlinear Earthquake Analysis of Concrete Arch Dams," by Fenves, G.L., Mojtahedi, S. and Reimer, R.B., September 1989, (PB92 139 674/AS)A07.

UCB/EERC-89/13   "Mechanics of Low Shape Factor Elastomeric Seismic Isolation Bearings," by Aiken, I.D., Kelly, J.M. and Tajirian, F.F., November 1989, (PB92 139 732/AS)A09.

UCB/EERC-89/14   "Preliminary Report on the Seismological and Engineering Aspects of the October 17, 1989 Santa Cruz (Loma Prieta) Earthquake," by EERC, October 1989, (PB92 139 682/AS)A04.

UCB/EERC-89/15   "Experimental Studies of a Single Story Steel Structure Tested with Fixed, Semi-Rigid and Flexible Connections," by Nader, M.N. and Astaneh-Asl, A., August 1989, (PB91 229 211/AS)A10.

UCB/EERC-89/16   "Collapse of the Cypress Street Viaduct as a Result of the Loma Prieta Earthquake," by Nims, D.K., Miranda, E., Aiken, I.D., Whittaker, A.S. and Bertero, V.V., November 1989, (PB91 217 935/AS)A05.

UCB/EERC-90/02   "Javid's Paradox: The Influence of Preform on the Modes of Vibrating Beams," by Kelly, J.M., Sackman, J.L. and Javid, A., May 1990, (PB91 217 943/AS)A03.

UCB/EERC-90/03   "Earthquake Simulator Testing and Analytical Studies of Two Energy-Absorbing Systems for Multistory Structures," by Aiken, I.D. and Kelly, J.M., October 1990, (PB92 192 988)A13.

UCB/EERC-90/05   "Preliminary Report on the Principal Geotechnical Aspects of the October 17, 1989 Loma Prieta Earthquake," by Seed, R.B., Dickenson, S.E., Riemer, M.F., Bray, J.D., Sitar, N., Mitchell, J.K., Idriss, I.M., Kayen, R.E., Kropp, A., Harder, L.F., Jr. and Power, M.S., April 1990, (PB 192 970)A08.

UCB/EERC-90/07   "A Unified Earthquake-Resistant Design Method for Steel Frames Using ARMA Models," by Takewaki, I., Conte, J.P., Mahin, S.A. and Pister, K.S., June 1990.

UCB/EERC-90/08   "Soil Conditions and Earthquake Hazard Mitigation in the Marina District of San Francisco," by Mitchell, J.K., Masood, T., Kayen, R.E. and Seed, R.B., May 1990, (PB 193 267/AS)A04.

UCB/EERC-90/09   "Influence of the Earthquake Ground Motion Process and Structural Properties on Response Characteristics of Simple Structures," by Conte, J.P., Pister, K.S. and Mahin, S.A., July 1990, (PB92 143 064)A15.

UCB/EERC-90/10   "Experimental Testing of the Resilient-Friction Base Isolation System," by Clark, P.W. and Kelly, J.M., July 1990, (PB92 143 072)A08.

UCB/EERC-90/11   "Seismic Hazard Analysis: Improved Models, Uncertainties and Sensitivities," by Araya, R. and Der Kiureghian, A., March 1988.

UCB/EERC-90/12   "Effects of Torsion on the Linear and Nonlinear Seismic Response of Structures," by Sedarat, H. and Bertero, V.V., September 1989, (PB92 193 002/AS)A15.

UCB/EERC-90/13   "The Effects of Tectonic Movements on Stresses and Deformations in Earth Embankments," by Bray, J. D., Seed, R. B. and Seed, H. B., September 1989.

233

UCB/EERC-90/14   "Inelastic Seismic Response of One-Story, Asymmetric-Plan Systems," by Goel, R.K. and Chopra, A.K., October 1990, (PB93 114 767)A11.

UCB/EERC-90/17   "Behavior of Peak Values and Spectral Ordinates of Near-Source Strong Ground-Motion over a Dense Array," by Niazi, M., June 1990, (PB93 114 833)A07.

UCB/EERC-90/19   "Cyclic Behavior of Steel Top-and-Bottom Plate Moment Connections," by Harriott, J.D. and Astaneh-Asl, A., August 1990, (PB91 229 260/AS)A05.

UCB/EERC-90/20   "Seismic Response Evaluation of an Instrumented Six Story Steel Building," by Shen, J.-H. and Astaneh-Asl, A., December 1990, (PB91 229 294/AS)A04.

UCB/EERC-90/21   "Observations and Implications of Tests on the Cypress Street Viaduct Test Structure," by Bollo, M., Mahin, S.A., Moehle, J.P., Stephen, R.M. and Qi, X., December 1990, (PB93 114 775)A13.

UCB/EERC-91/02   "Displacement Design Approach for Reinforced Concrete Structures Subjected to Earthquakes," by Qi, X. and Moehle, J.P., January 1991, (PB93 114 569/AS)A09.

UCB/EERC-91/03   "A Long-Period Isolation System Using Low-Modulus High-Damping Isolators for Nuclear Facilities at Soft-Soil Sites," by Kelly, J.M., March 1991, (PB93 114 577/AS)A10.

UCB/EERC-91/04   "Dynamic and Failure Characteristics of Bridgestone Isolation Bearings," by Kelly, J.M., April 1991, (PB93 114 528)A05.

UCB/EERC-91/05   "Base Sliding Response of Concrete Gravity Dams to Earthquakes," by Chopra, A.K. and Zhang, L., May 1991, (PB93 114 544/AS)A05.

UCB/EERC-91/06   "Computation of Spatially Varying Ground Motion and Foundation-Rock Impedance Matrices for Seismic Analysis of Arch Dams," by Zhang, L. and Chopra, A.K., May 1991, (PB93 114 825)A07.

UCB/EERC-91/07   "Estimation of Seismic Source Processes Using Strong Motion Array Data," by Chiou, S.-J., July 1991, (PB93 114 551/AS)A08.

UCB/EERC-91/08   "A Response Spectrum Method for Multiple-Support Seismic Excitations," by Der Kiureghian, A. and Neuenhofer, A., August 1991, (PB93 114 536)A04.

UCB/EERC-91/09   "A Preliminary Study on Energy Dissipating Cladding-to-Frame Connection," by Cohen, J.M. and Powell, G.H., September 1991, (PB93 114 510)A05.

UCB/EERC-91/10   "Evaluation of Seismic Performance of a Ten-Story RC Building During the Whittier Narrows Earthquake," by Miranda, E. and Bertero, V.V., October 1991, (PB93 114 783)A06.

UCB/EERC-91/11   "Seismic Performance of an Instrumented Six-Story Steel Building," by Anderson, J.C. and Bertero, V.V., November 1991, (PB93 114 809)A07.

UCB/EERC-91/12   "Performance of Improved Ground During the Loma Prieta Earthquake," by Mitchell, J.K. and Wentz, Jr., F.J., October 1991, (PB93 114 791)A06.

UCB/EERC-91/13   "Shaking Table - Structure Interaction," by Rinawi, A.M. and Clough, R.W., October 1991, (PB93 114 917)A13.

UCB/EERC-91/14   "Cyclic Response of RC Beam-Column Knee Joints: Test and Retrofit," by Mazzoni, S., Moehle, J.P. and Thewalt, C.R., October 1991, (PB93 120 277)A03.

UCB/EERC-91/15   "Design Guidelines for Ductility and Drift Limits: Review of State-of-the-Practice and State-of-the-Art in Ductility and Drift-Based Earthquake-Resistant Design of Buildings," by Bertero, V.V., Anderson, J.C., Krawinkler, H., Miranda, E. and The CUREe and The Kajima Research Teams, July 1991, (PB93 120 269)A08.

UCB/EERC-91/16   "Evaluation of the Seismic Performance of a Thirty-Story RC Building," by Anderson, J.C., Miranda, E., Bertero, V.V. and The Kajima Project Research Team, July 1991, (PB93 114 841)A12.

UCB/EERC-91/17   "A Fiber Beam-Column Element for Seismic Response Analysis of Reinforced Concrete Structures," by Taucer, F., Spacone, E. and Filippou, F.C., December 1991.

UCB/EERC-91/18   "Investigation of the Seismic Response of a Lightly-Damped Torsionally-Coupled Building," by Boroschek, R. and Mahin, S.A., December 1991, (PB93 120 335)A13.

UCB/EERC-92/01   "Studies of a 49-Story Instrumented Steel Structure Shaken During the Loma Prieta Earthquake," by Chen, C.-C., Bonowitz, D. and Astaneh-Asl, A., February 1992, (PB93 221 778)A08.

UCB/EERC-92/02   "Response of the Dumbarton Bridge in the Loma Prieta Earthquake," by Fenves, G.L., Filippou, F.C. and Sze, D.T., January 1992, (PB93 120 319)A09.

UCB/EERC-92/03   "Models for Nonlinear Earthquake Analysis of Brick Masonry Buildings," by Mengi, Y., McNiven, H.D. and Tanrikulu, A.K., March 1992, (PB93 120 293)A08.

UCB/EERC-92/04   "Shear Strength and Deformability of RC Bridge Columns Subjected to Inelastic Cyclic Displacements," by Aschheim, M. and Moehle, J.P., March 1992, (PB93 120 327)A06.

UCB/EERC-92/05   "Parameter Study of Joint Opening Effects on Earthquake Response of Arch Dams," by Fenves, G.L., Mojtahedi, S. and Reimer, R.B., April 1992, (PB93 120 301)A04.

UCB/EERC-92/06   "Seismic Behavior and Design of Semi-Rigid Steel Frames," by Nader, M.N. and Astaneh-Asl, A., May 1992.

UCB/EERC-92/09   "Evaluation of Code Accidental-Torsion Provisions Using Earthquake Records from Three Nominally Symmetric-Plan Buildings," by De la Llera, J.C. and Chopra, A.K., September 1992, (PB94 117 611)A08.

UCB/EERC-92/10   "Slotted Bolted Connection Energy Dissipators," by Grigorian, C.E., Yang, T.-S. and Popov, E.P., July 1992, (PB92 120 285)A03.

UCB/EERC-92/11   "Mechanical Characteristics of Neoprene Isolation Bearings," by Kelly, J.M. and Quiroz, E., August 1992, (PB93 221 729)A07.

UCB/EERC-92/12   "Application of a Mass Damping System to Bridge Structures," by Hasegawa, K. and Kelly, J.M., August 1992, (PB93 221 786)A06.

UCB/EERC-92/13   "Earthquake Engineering Research at Berkeley - 1992," by EERC, October 1992.

UCB/EERC-92/14   "Earthquake Risk and Insurance," by Brillinger, D.R., October 1992, (PB93 223 352)A03.

UCB/EERC-92/15   "A Friction Mass Damper for Vibration Control," by Inaudi, J.A. and Kelly, J.M., October 1992, (PB93 221 745)A04.

UCB/EERC-92/16   "Tall Reinforced Concrete Buildings: Conceptual Earthquake-Resistant Design Methology," by Bertero, R.D. and Bertero, V.V., December 1992, (PB93 221 695)A12.

UCB/EERC-92/17   "Performance of Tall Buildings During the 1985 Mexico Earthquakes," by Terán-Gilmore, A. and Bertero, V.V., December 1992, (PB93 221 737)A11.

UCB/EERC-92/18   "Dynamic Analysis of Nonlinear Structures using State-Space Formulation and Partitioned Integration Schemes," by Inaudi, J.A. and De la Llera, J.C., December 1992.

UCB/EERC-93/02   "Evaluation of an Active Variable-Damping-Structure," by Polak, E., Meeker, G., Yamada, K. and Kurata, N., 1993, (PB93 221 711)A05.

UCB/EERC-93/03   "An Experimental Study of Flat-Plate Structures under Vertical and Lateral Loads," by Hwang, S.-H. and Moehle, J.P., February 1993.

UCB/EERC-93/04   "Seismic Performance of a 30-Story Building Located on Soft Soil and Designed According to UBC 1991," by Teran-Gilmore, A. and Bertero, V.V., 1993, (PB93 221 703)A17.

UCB/EERC-93/05   "Multiple-Support Response Spectrum Analysis of the Golden Gate Bridge," by Nakamura, Y., Der Kiureghian, A. and Liu, D., May 1993, (PB93 221 752)A05.

UCB/EERC-93/06   "On the Analysis of Structures with Viscoelastic Dampers," by Inaudi, J.A., Zambrano, A. and Kelly, J.M., August 1993.

UCB/EERC-93/07   "Earthquake Analysis and Response of Concrete Gravity Dams Including Base Sliding," by Chávez, J.W. and Fenves, G.L., December 1993.

UCB/EERC-93/08   "Model for Anchored Reinforcing Bars under Seismic Excitations," by Monti, G., Spacone, E. and Filippou, F.C., December 1993.

UCB/EERC-93/09   "A Methodology for Design of Viscoelastic Dampers in Earthquake-Resistant Structures," by Abbas, H. and Kelly, J.M., December 1993.

UCB/EERC-93/10   "Tuned Mass Dampers Using Viscoelastic Dampers," by Inaudi, J.A., Lopez-Almansa, F. and Kelly, J.M., December 1993.

UCB/EERC-93/11   "Nonlinear Homogeneous Dynamical Systems," by Inaudi, J.A. and Kelly, J.M., December 1993.

UCB/EERC-93/12   "Synthesized Strong Ground Motions for the Seismic Condition Assessment of the Eastern Portion of the San Francisco Bay Bridge," by Bolt, B.A. and Gregor, N.J., December 1993.

UCB/EERC-94/01   "Preliminary Report on the Seismological and Engineering Aspects of the January 17, 1994 Northridge Earthquake," by EERC, January 1994.

UCB/EERC-94/02   "Energy Dissipation with Slotted Bolted Connections," by Grigorian, C.E. and Popov, E.P., February 1994.